Federal Aviation Administration

Flight Safety Analysis Handbook

Version 1.0

Federal Aviation Administration
Associate Administrator for Commercial Space Transportation
800 Independence Avenue, Room 331
Washington, DC 20591

Version 1.0 **September 2011**

NOTICE

Use of trade names or names of manufacturers in this document does not constitute an official endorsement of such products or manufacturers, either expressed or implied, by the Federal Aviation Administration.

TABLE OF CONTENTS

LIST OF FIGURES

LIST OF TABLES

1.0 INTRODUCTION

1.1 Purpose

The Federal Aviation Administration (FAA) designed this handbook to help launch and reentry vehicle operators conduct flight safety analyses. We surveyed common industry practices for flight safety analyses and have identified those most appropriate to launch vehicles. The approaches described in this handbook represent the results of this effort. Launch and reentry vehicle operators that follow these approaches should find their flight safety analyses meet FAA regulatory requirements. Other approaches that fulfill the regulatory objectives may also be acceptable to the FAA.

The FAA Office of Commercial Space Transportation (AST) is responsible for licensing and regulating commercial space transportation to ensure public health and safety and the safety of property. AST issues licenses for expendable launch vehicle (ELV), reusable launch vehicle (RLV), and reentry vehicle (RV) launch and reentry activities. Flight safety analyses play an important role in protecting public safety during these activities.

The licensing process for ELV, RLV, and RV launch and reentry activities comprises several steps. Important among these is a pre-application consultation and an application evaluation. We encourage applicants to consult with AST early during their vehicle development stage. Early consultation may reveal potential problems with a proposal and allow changes when they are less likely to result in significant delay or costs to the applicant.

Flight safety analyses are useful during all phases of the licensing process to:

- quantitatively demonstrate that acceptable risk limits will not be exceeded,
- support assessments of risks identified in the system safety process, and
- assist in specifying operating requirements.

Title 14 of the Code of Federal Regulations (14 CFR) sections 415.35 and 431.35 require an applicant to demonstrate that the risk level associated with debris from an applicant's proposed launch or reentry does not exceed acceptable limits. Title 14 CFR sections 417.107 and 431.35 set acceptable the risk levels to the collective members of the public exposed to vehicle or vehicle debris impact hazards associated with a proposed launch or reentry. An acceptable risk level is one that does not exceed an expected average number of 0.00003 casualties per mission (or E_C criterion of 30E-6) to members of the public from the applicant's proposed activity. An acceptable risk level to an individual does not exceed 0.000001 per mission (or individual risk criterion of 1E-6).

Note: When there is a conflict between the regulation guidance that this handbook provides and the regulations, the regulations govern.

In addition to demonstrating acceptable risk, a thorough flight safety analysis should also (1) provide a basis for well informed safety decisions by identifying the dominant sources of public risks and potential mitigations, and (2) help inform the FAA's Maximum Probable Loss (MPL) determination. Therefore, this handbook provides information to show how these analyses can serve these additional purposes.

1.2 Scope

This document provides guidance describing means to perform a quantitative analysis aimed at demonstrating that the risks to public safety posed by debris hazards associated with licensed launch and reentry activities for an ELV, RLV, or RV are acceptable. This document currently does not address risk from toxic release, far field blast overpressure, or debris impacts to ships and aircraft. Future versions of this handbook will address these subjects.

1.3 Authority

Title 49 USC Subtitle IX, chapter 701, Commercial Space Launch Activities, section 70105

Title 14 CFR part 417, subpart C, Flight Safety Analysis

Title 14 CFR part 431, subpart C, Safety Review and Approval for Launch and Reentry of a Reusable Launch Vehicle

Title 14 CFR part 435, subpart C, Safety Review and Approval for Reentry of a Reentry Vehicle

2.0 DEFINITIONS AND ACRONYMS

2.1 Definitions

The following definitions are established for the purposes of this handbook. Definitions of additional terms used in this handbook appear in § 401.5, § 417.3, § 420.5, and § 437.3. Where duplication exists between the terms defined in this handbook and those defined in those regulatory sections, the definitions provided herein should be used to implement the processes described in this handbook.

3-sigma — Three times the standard deviation of the value of a parameter. The 3-sigma value is typically referenced to the mean value. It is often used to express a confidence level (C) using the expression $C = \left(1 - e^{-\frac{1}{2}z^2}\right)^N$, where z is set to three to indicate a 3-sigma confidence and N is set to the number of degrees of freedom.

Abbreviated Injury Scale — An anatomically based, consensus derived, global severity grading system that classifies each injury in every body region according to its relative importance on a 6 point ordinal scale. Using AIS level 3 or greater is appropriate for describing a medical condition sufficiently to allow modeling of casualties for purposes of determining whether a launch satisfies the public risk criteria.

Accumulated risk — The combined collective risk to all individuals exposed to a particular hazard through all phases of a mission. For the flight of an orbital vehicle, risk should be accumulated from liftoff through orbital insertion. For an orbital RLV, accumulated risk should include reentry or descent flight, and landing. For the flight of a suborbital launch vehicle, risk should be accumulated from liftoff through the impact of all pieces of the launch vehicle, including the payload.

Accuracy	1. The degree of agreement between a measured value and the true value; usually expressed as +/- percent of full scale. 2. Closeness of a measured or computed value to its "true" value, where the true value is obtained with imperfect information. Due to the natural heterogeneity and stochasticity of many systems, this true value exists as a distribution rather than a discrete value. In these cases, the true value will be a function of spatial or temporal aggregation. 3. The degree of exactness of a model or simulation, with high accuracy implying low error. Accuracy equates to the quality of a result, and is distinguished from precision, which relates to the quality of the operation by which the result is obtained and can be repeated.
Aggregated risk	The accumulated risk due to all hazards associated with a flight. The aggregated risk includes, but is not limited to, the accumulated risk from all sources of risk, including debris impact, toxic release, and distant focusing of blast overpressure.
Aleatory uncertainty	The kind of uncertainty resulting from randomness or unpredictability due to inherent natural variability. Aleatory uncertainty is also known as variability, stochastic uncertainty, irreducible uncertainty, and objective uncertainty.
Bayesian analysis	A statistical procedure that endeavors to estimate parameters of an underlying distribution based on the observed distribution.
Catastrophe	Any event that produces a large number of casualties or has a severe impact on continued operations.
Censored Data Set	Used in reliability analysis to refer to a dataset in which not all tested items are operated to failure.
Clarity	An EPA principle of uncertainty characterization; the assessment is free from obscure language and is easy to understand. Brevity and plain English are employed; technical terms are avoided; simple tables, graphs, and equations are used. [EPA Science Policy Council - Risk Characterization Handbook]

Collective risk	The total risk to all individuals exposed to any hazard from an operation. Unless otherwise noted, collective risk is the expected value of casualties (E_C) predicted to result from all hazards associated with a mission/flight. Unless otherwise specified, the collective risk should include the aggregated and accumulated risk.
Conservative	A scientifically plausible method or choice that is more likely to result in overestimating risk or hazard given the existing uncertainties.
Consistency	An EPA principle of uncertainty characterization; conclusions of the risk assessment are characterized in harmony with other government actions.
Debris impact hazard	The potential for injury or death resulting from the impact of falling debris. (Separate from explosive or toxic debris hazard.)
Deterministic model	A model in which the results are determined through known relationships among the states and events, and in which a given input will always produce the same output; for example, a model depicting a known chemical reaction.
Epistemic uncertainty	The kind of uncertainty arising from imperfect knowledge. Epistemic uncertainty is also known as incertitude, ignorance, subjective uncertainty, reducible uncertainty, and state-of-knowledge uncertainty.
Expected casualties	An estimate of the average number of *casualties* expected if a large number of *launch vehicle flights* or experiments could be carried out under identical circumstances to personnel supporting an operation and to the *public* from a specific *hazard*; casualty expectation is equal to the sum of the products of the probability of each possible event and the *casualty* consequences of each possible *mission* event; casualty expectation is also referred to by the notation E_C or CE.
Fidelity	The accuracy of the representation when compared to the real world.
Hazard	Any real or potential condition that can cause injury, illness, or death of personnel, or damage to or loss of equipment or property.
Hazard area	A geographical or geometrical surface area that is susceptible to a hazard from a planned event or unplanned malfunction.

Hazard volume	A geographical or geometrical volume of airspace that is susceptible to a hazard from a planned event or unplanned malfunction.
Impact	The impingement of a fragment on a surface, a structure, a person, or a vehicle.
Individual risk	The risk that a single person will suffer a consequence. Unless otherwise noted, individual risk is expressed as the probability that an individual will become a casualty due to all hazards (P_C) from a mission at a specific location.
Monte Carlo simulation	1. A simulation in which random statistical sampling techniques are employed such that the result determines estimates for unknown values. 2. A method of calculating functions (often convolutions) of probability distributions by repeatedly sampling random values from those distributions and forming an empirical distribution function of the results.
Probabilistic modeling	A process that employs statistical principles and the laws of probability to quantify the variability and uncertainty in a quantity. The results of probabilistic models typically express the ratio of the outcomes that would produce a given event to the total number of possible outcomes.
Probability of casualty	The likelihood that a person will suffer a serious injury or worse, including a fatal injury, from a hazardous event.
Reasonableness	An EPA principle of uncertainty characterization; the assessment is based on sound judgment. The components of the risk characterization are well integrated into an overall conclusion of risk that is complete, informative, well balanced, and useful for decision making. The characterization is based on the best available scientific information. The policy judgments required to carry out the risk analyses use common sense given the statutory requirements and guidance from a higher authority. Appropriate plausible alternative estimates of risk under various candidate risk management alternatives are identified and explained.
Risk profile	A plot that shows the probability of an accident causing a given number of casualties or more (abscissa) versus the number of casualties (ordinate).

Sensitivity	The degree to which the model outputs are affected by changes in a selected input parameter.
Sensitivity analysis	The computation of the effect of changes in input values or assumptions (including boundaries and model function form) on the outputs. The study of how uncertainty in a model output can be systematically apportioned to different sources of uncertainty in the model input. By investigating the "relative sensitivity" of model parameters, one can become knowledgeable of the relative importance of parameters in the model.
Shard	A small piece of brittle substance, as of glass or metal.
Stochastic Model	A model in which the results are determined by using one or more random variables to represent uncertainty about a process or in which a given input will produce an output according to some statistical distribution: for example, a model that estimates the total dollars spent at each of the checkout stations in a supermarket, based on probable number of customers and probable purchase amount of each customer. Also *Probabilistic Model*. Contrasts with *Deterministic Model*.
Temporal	Relating to, concerned with, or limited by time.
Terminate	If an abort cannot be implemented to put the vehicle in a "safe" configuration and there are no other viable alternatives to maintaining public safety, the flight safety system or the contingency management system will be activated. This may include destroying the vehicle.
Transparency	An EPA principle of uncertainty characterization; explicitness in the risk assessment process. It ensures any reader understands all the steps, logic, key assumptions, limitations, and decisions in the risk assessment, and comprehends the supporting rationale that leads to the outcome.
Uncertainty	The absence of perfectly detailed knowledge. Uncertainty includes incertitude (the exact value is unknown) and variability (the value is changing). Uncertainty may also include other forms, such as vagueness, ambiguity, and fuzziness (in the sense of border-line cases).

Uncertainty analysis	1. A detailed examination of the systematic and random errors (i.e., epistemic and aleatory uncertainties) of a measurement or estimate; an analytical process to provide information regarding the uncertainty. 2. An investigation of the effects of lack of knowledge or potential errors on the model and when conducted in combination with a sensitivity analysis allows a model user to be more informed about the confidence that can be placed on model results.
Variability	1. The fluctuation or variation due to randomness or stochasticity. Variability is also associated with aleatory uncertainty, stochastic uncertainty, Type I or Type A uncertainty, irreducible uncertainty, and objective uncertainty. 2. Observed differences attributable to true heterogeneity or diversity. Variability is the result of natural random processes and is usually not reducible by further measurement or study (although it can be better characterized).
Weibull Distribution	A continuous probability distribution widely used as a lifetime distribution in reliability engineering. It is a versatile distribution that can take on the characteristics of other types of distributions based on the value of the shape parameter.
Worst-case	A semi-quantitative term referring to the maximum possible exposure, dose, or risk that can conceivably occur, whether or not this exposure, dose, or risk actually occurs in a specific population.

2.2 Acronyms

AC	Advisory Circular
AFETAC	Air Force Environmental Technical Applications Center
AFSPC	Air Force Space Command
AIAA	American Institute of Aeronautics and Astronautics
AIS	Abbreviated Injury Scale
AST	Office of Commercial Space Transportation (FAA)
BEI	Biodynamics Engineering, Inc.
BUSV	Breakup State Vector
CDF	Combined Distribution Function
CFR	Code of Federal Regulations
CSWG	Common Standards Working Group
DDESB	Department of Defense Explosives Safety Board
DOF	Degree of Freedom
ELV	Expendable Launch Vehicle
ER	Eastern Range
EPA	Environmental Protection Agency
ETA	Event Tree Analysis
FAA	Federal Aviation Administration
FMEA	Failure Modes Effects Analysis
FMECA	Failure Modes Effects and Criticality Analysis
FSS	Flight Safety System
FTS	Flight Termination System
GGUAS	Global Gridded Upper Atmosphere Statistics
GNC	Guidance, Navigation, and Control
GRAM	Global Reference Atmospheric Model
HACK	Hazard Area Computation Kernel
IIP	Instantaneous Impact Point
ILL	Impact Limit Line
IRIG	Inter-Range Instrumentation Group
IUS	Inertial Upper Stage
LLNL	Lawrence Livermore National Laboratory

MFT	Malfunction Turn
MLE	Maximum Likelihood Estimator
MPL	Maximum Probable Loss
NASA	National Aeronautics and Space Administration
NE	New vehicle launched by an Experienced developer
NN	New vehicle launched by a New developer
NOAA	National Oceanic and Atmospheric Administration
NRC	Nuclear Regulatory Commission
PERMS	Propellant Energetic Response to Mechanical Stimuli
PIRAT	Propellant Impact Risk Assessment Team
PRA	Probabilistic Risk Assessment
PYRO	NASA/USAF Liquid Propellant Blast Hazards Program (Project)
QRA	Quantitative Risk Analysis
RCC	Range Commanders Council
RLV	Reusable Launch Vehicle
RRA	Range Reference Atmosphere
RSG	Range Safety Group
RSS	Range Safety System, Root Sum Square
RTI	Research Triangle Institute
STS	Space Transportation System
TCCR	Transparency, Clarity, Consistency, & Reasonableness
TEC	Theoretical-Empirical Correlation
TNO	The Netherlands Organization of Applied Scientific Research
TNT	Trinitrotoluene
USAF	United States Air Force
VIIP	Vacuum Impact Prediction
VRM	Vehicle Response Mode
WR	Western Range
WSMR	White Sands Missile Range

3.0 BACKGROUND

3.1 A Discussion of Risk

The safety community defines risk as the product of the probability of occurrence of an event and the consequences of that event. If there is more than one possible outcome of the event, we determine the total risk associated with the event by adding all possible outcomes of the products of the probability of each outcome and its associated consequence. While the probability of an event always ranges between zero and one, the consequences of that event can take any value. Risk can be relatively high if the probability is high and can be high if the consequence is great even if the probability is low. Risk can be lowered by reducing the probability of an event occurring or by reducing the consequences of an event. For example, planning a mission that avoids flight operations over populated areas can decrease or eliminate consequences of human casualties and thereby reduce the risk.

Collective risk represents the total risk to all individuals exposed to any hazard from an operation. It provides a measure of the risk to society as a whole. The space launch industry often quantitatively expresses risk in terms of expected casualties (E_C). E_C is the expected average number of human casualties incurred per space mission. Since the FAA limits its consideration human casualties to just those incurred by members of the public, E_C for a mission measures the public safety risk of conducting the mission.

Collective risk is an accumulated risk. The products of the probabilities and consequences of all reasonable potential outcomes associated with a particular risk source are summed across all relevant mission phases. Risk sources include debris impact, toxic release, and distant focusing of blast overpressure. An accumulated risk value exists for each risk source. Individual risk is the risk that a single person will suffer a consequence of a mission. We generally express individual risk as the probability that an individual will become a casualty due to a risk source from a mission at a specific location.

We can consider both collective and individual risk on an annual basis and per mission basis. For example, collective risk on an annual basis is analogous to an estimate of the average number of people hit by lightning each year, while individual annual risk would be an individual's likelihood of being hit by lightning in any given year. Likewise, collective risk on a per mission basis is analogous to an estimate of the average number of people injured by an earthquake, while individual risk would be the likelihood of an individual in a given location being injured by the earthquake. In the space launch and reentry industry, we quantify collective and individual risks on a per mission basis.

Risk analysis should consider all reasonable mission scenarios that may result in a public casualty. This consideration should include the risks of catastrophic vehicle failures that may occur during otherwise nominal flight, during

malfunction flight, and during any abort maneuvers. The analyses do not consider every vehicle failure to be relevant to public risk. Generally, only failures that occur in flight are considered. An in-flight failure occurs when a launch or reentry vehicle does not complete any phase of its intended flight or when any anomalous condition exhibits the potential for the vehicle or its debris to impact the Earth. This precludes failures that occur before liftoff and after landing, as well as failures that occur after a vehicle has obtained orbital insertion.

3.2 Risk Management

The ideal way to minimize hazards in the region of a launch or reentry is to locate the activity in a remote area. Thus, hazards can be isolated and risks to the public can be minimized or even eliminated. However, complete containment of even a suborbital launch vehicle's hazards is usually difficult. Populated areas tend to encroach on even the most remote sites and areas at risk become too large to accommodate reasonable surveillance or access control measures. In these situations, a flight safety system becomes necessary to protect the public from the potential hazards associated with the launch or reentry activity. A flight safety system may be destructive or non-destructive. A traditional flight termination system, usually used on an expendable launch vehicle (ELV), is designed to terminate a vehicle's thrust and disperse its remaining propellants so as to render falling debris inert is an example of a destructive system. Non-destructive flight safety systems, usually used on an reusable launch vehicle (RLV), include abort systems designed to render the vehicle non-propulsive but yet still allow it to be recovered undamaged. In either case, residual risks exist.

A consequence analysis is a handy tool for bounding the risks associated with a hazardous activity. Using such an analysis, the vehicle is assumed to fail, often in the worst credible way, at each flight time. If the consequences associated with any such event are unacceptable, as is generally the case, the likelihood of such an event occurring can be considered, as well as the effects of measures taken to reduce its likelihood or consequences. In such cases, the quantitative risk analysis (QRA) must demonstrate that the residual risks do not exceed acceptable levels.

3.3 Overview of Launch and Reentry QRA Methods

3.3.1 Three-Prong Approach

Figure 3-1 depicts a three-prong approach used to ensure public safety for FAA RLV launches and reentries licensed activities, described in the preamble to Part 431.[1]

[1] 65 FR 56658, Sept 29, 2000

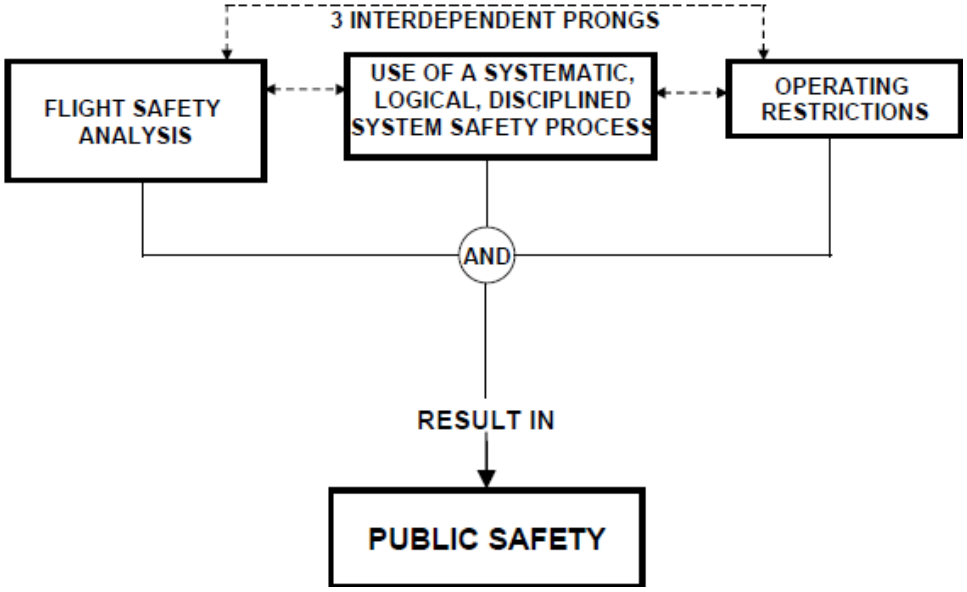

Figure 3-1. Three-Prong Approach to Public Safety for Commercial RLV Launches and reentries

The three prongs: a QRA, a formal system safety process, and operational restrictions, function as interdependent elements, much like the three legs of a stool. For maximum effectiveness, a QRA should be performed concurrently with the implementation of a formal system process and the development of operational restrictions. Thus, a preliminary QRA should be an integral part of the preliminary design review.

3.3.2 A Two-Tiered Approach for a QRA

The objective of a launch or reentry QRA is to demonstrate that the collective and individual risks from the flight are below acceptable levels, not necessarily to quantify the precise risk levels. You can use a tiered approach [1] to conduct this risk analyses.

This handbook describes a two tier approach: Tier 1, low order estimate of risk, and tier 2, high order estimate of risk.

Tier 1 - The Tier 1 approach employs relatively simple means and conservative assumptions to estimate the risks. For example, a Tier 1 approach to vulnerability modeling would count any person as a casualty if the person is predicted to receive an inert debris impact. If the analyst determines that the result of the Tier 1 analysis demonstrates adequate safety, no further analysis is required. In general, the thresholds and other Tier 1 methods presented here should be used:

1. to determine if a more sophisticated analysis is warranted,

2. as an alternative when higher-fidelity models are unavailable, or

3. as an alternative when the quality of the data available to support the analysis is so low that an additional margin of safety is prudent.

However, if the Tier 1 analysis indicates excessive risks, then a Tier 2 approach should be applied and risk mitigations should be implemented.

Tier 2 - The Tier 2 approach entails more accurate and sophisticated methods. For example, a Tier 2 analysis would replace simple hazard thresholds with validated vulnerability models. One should base each element of a Tier 2 risk analysis on the best available information and conservative assumptions made in each area where there is no conventional approach or there is un-quantified uncertainty. Investigate the sensitivity to highly uncertain input data, such as the debris generated by a particular vehicle failure, (e.g., run multiple debris lists to define the bounds to the real risk). The risk estimate is known to be generally sensitive to the presence of various shelter types, and no single approach to account for sheltering is always conservative. Therefore, use the best available information on sheltering types and vulnerability for a Tier 2 analysis.

There is a legitimate question about the appropriate level of fidelity for various model elements given the potential for relatively large uncertainties in some elements due to input data uncertainty or uncertainty associated with the modeling technique. There is a generally accepted principle in launch risk assessment that "assessments of models should focus on the accuracy of the risk estimation rather than the fidelity of a single element." [2] However, there are circumstances where the fidelity of certain sub-models should be refined beyond the fidelity achievable in other sub-models. For instance, quantify the risk based on a given set of input data as accurately as practicable. Then account for the input data uncertainty in the model or investigate with sensitivity analyses so that the final risk results reflect the input data uncertainty. For example, multiple combinations of debris lists and sets of feasible shelter distributions input to a model capable of discerning the influence of those on the consequences of an accident can be used to define the bounds to the real risk, and establish a mean risk estimate that accounts for those critical sources of input data uncertainty. Furthermore, a refined sub-model may be the best means to assess the potential consequences of an accident scenario, and thus necessary to facilitate an accurate estimate of the MPL. In addition, there may be a substantial level of irreducible uncertainty associated with the probability of failure for a new launch vehicle. However, one should still quantify the potential consequences of a failure using the best available information on sheltering types and vulnerability, etc.

4.0 GENERAL LAUNCH AND REENTRY RISK ANALYSIS PROCEDURE

The following subsections briefly describe steps in the general procedure typically used to perform a QRA for launch. Each of these steps is discussed in more detail in subsequent sections of this handbook.

4.1 Identify Hazards

Hazard identification consists of reviewing the vehicle's intended performance and potential malfunctions to assess:

1. credible sources of threats to life and property,

2. the sequences of events that result in these threats, and

3. the probability of each event sequence.

Table 4-1 identifies some potential threats (or failure modes) and their causes.

Table 4-1. Failure Modes and Their Causes

Failure Mode	Examples
structural failure	joint failure, buckling, fracture, material fatigue, loss of primary structure
loss of inertial reference by the guidance system;	
loss of control	nozzle hard-over, nozzle null, actuator jams, loss of primary and secondary flight controls, including electrical power, hydraulic systems, and the associated actuation wiring or cables
propulsion system failures	failure of engine control systems, case burn-through, premature thrust termination
flight safety system malfunctions	inadvertent flight termination system action, failure of the flight termination system

Once you identify the failure modes, system safety engineering methods (See AC 431.35-2A [3]), provide a way to determine which modes present a hazard to the public and the probability of their occurrence. These methods include failure modes, effects and critical analysis (FMECA); fault tree analyses; and event trees.

Additional information is available to help identify critical systems, hazards, and to develop fault trees [4] and event trees. [3][5] Sample RLV event trees and a description of how they may be used in a QRA are presented in Section 4.9.1.

4.2 Develop Failure Probabilities

Failure probabilities for a launch or reentry vehicle are frequently based on the results of the launch or reentry license applicant's failure modes and effects analysis (FMEA). However, some applicants tend to be optimistic about mission success, typically underestimating the possibility of human error and design flaws. Therefore, a more effective process is for the applicant's failure probability estimates to be consistent with the launch history of the vehicle or, if the vehicle is relatively new, to the failure history of vehicles developed and launched under similar circumstances. In addition to the failure probability analysis exposition provided in Chapter 5, guides to RLV and ELV reliability analyses and probabilistic risk assessment techniques are available. [6][7][8]

4.3 Develop Breakup State Vectors for Debris Generating Events

An accident may occur anywhere along the nominal, malfunction, or abort trajectory. A "break-up state vector" (BUSV) is often a convenient and flexible means to describe the time, position, and velocity of the state of the debris when control ceases.

Table 4-2. Breakup State Vectors

For computer guided rockets and unguided rockets	Determine the BUSV through numerical trajectory simulation of the vehicle and analysis of when break up or thrust termination would occur.
For a manually-piloted vehicle	Simulations may or may prove useful to estimate nominal and off-course trajectories [9]
If flight termination or abort criteria (flight rules) are in use	Compute the impact point or debris footprint projected onto the ground during the malfunction and compare with the abort criteria. Aborted or terminate trajectories that produce criteria violations to generate state vectors corresponding to the abort or termination criteria.
Vehicles may breakup or self destruct because of aerodynamic or inertial loads	Determine BUSVs for these events.
Vehicle guidance and	Determine the uncertainties in the BUSVs.

performance uncertainty, human performance (for piloted vehicles), winds or other environmental effects, and uncertainty in the range safety system delays	

4.4 Define Debris Characteristics

Evaluate the likelihood of an intact vehicle impact or vehicle breakup for each potentially hazardous event. For vehicle break-up, define the fragments in terms of their numbers, sizes, aerodynamic characteristics, and any imparted velocities (section 10.4.6) that they might receive from the breakup event. Divide the fragments into groups having similar characteristics, as described in A417.11(c)(10). These values are necessary for debris trajectory and impact consequence modeling. Use additional parameters for fragments that can change during fall, due to propellant burning or aero-thermal effects. If the hazard includes an explosion on impact, specify parameters for calculating the yield, including propellant type, weight, and dimensions. The yield from an explosive impact also depends on that nature of the impacted surface.

4.5 Propagate Debris to Impact

Use physics-based modeling to develop a statistical description of the debris trajectories. The debris fragments usually follow a ballistic path to impact (see Appendix of [10]). Develop impact distributions using Monte Carlo (random sampling) methods or by propagating state vector uncertainty (expressed as a covariance matrix) using linear relationships. The uncertainties in the ballistic trajectory result from the following:

- Fragment ballistic coefficient uncertainty (section 6.4, 10.4.4),
- Dispersion due to explosion imparted velocities (section 10.4.6),
- Lift effects (section 10.4.4), and
- Wind uncertainty (section 10.4.5)

4.6 Develop Impact Probability Distributions

The impact probability distributions developed based on impact location histograms or generated by summing the covariance matrices representing the impact uncertainties for each of the sources of uncertainty (the covariance matrices are typically expressed in an east (E) - north (N) coordinate system) are:

$$\Sigma_{Total} = \Sigma_{\beta} + \Sigma_{\Delta v} + \Sigma_{state\,vector} + \Sigma_{wind} + \Sigma_{lift/drag}$$

Transform to principal coordinates

$$\left[\sum \text{Total}\right]_{E,N} = \begin{bmatrix} \sigma_E^2 & \sigma_{EN} \\ \sigma_{EN} & \sigma_N^2 \end{bmatrix} \Rightarrow$$

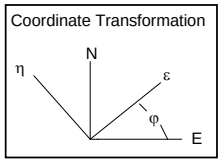

$$\Rightarrow \begin{bmatrix} \sigma_\xi^2 & O \\ O & \sigma_\eta^2 \end{bmatrix}$$

where $\varphi = \tan^{-1}\left(\dfrac{\sigma_E^2 - \sigma_N^2}{\sigma_{EN}}\right)$ *and* $\sigma_{EN} = \rho_{EN}\sigma_E\sigma_N$

Dispersion ellipses have semi-major and semi-minor axes ($\sigma\xi$,$\sigma\eta$) defined by the directions of the axes.

4.7 Compute Impact Probability

The total impact covariance matrix for a given fragment group is often defined by a bivariate normal impact distribution.[2] Obtain the impact probability (P_I) for a specified fragment and population center by integrating the bivariate normal density function over the region of the population center

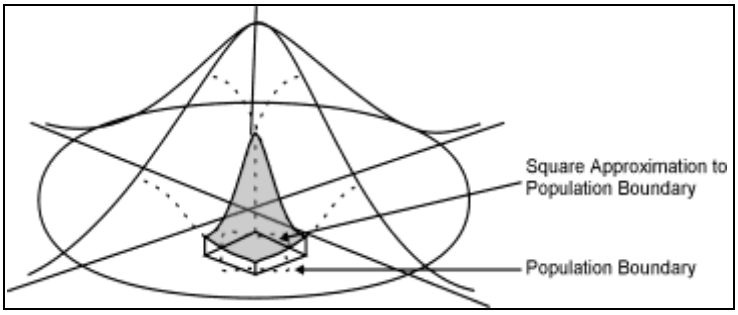

Figure 4-1. Bivariate Normal Density Function

To compute the probability of one-or-more fragment impacts, assume statistical independence resulting in the formula

$$P_I(\geq 1) = 1 - \prod_j \left(1 - P_j\right)$$

where P_I = impact probability of fragment j where j ranges from one to the total number of all of the fragments in all of the fragment groups.

To obtain the total impact probability for a mission, weight the $P_I(\geq 1)$ values for each failure time and failure mode by their corresponding probability of occurrence and aggregated these in a statistical sense.

[2] Based on the Central Limit Theorem. If the distribution is known to be significantly different than bivariate normal, an alternative risk analysis method can be used (such as a Monte Carlo technique).

4.8 Compute Casualty Expectation

The equation for casualty expectation for a debris group "*i*" for population center "*j*" for a given failure time and failure mode, is given by

$$E_{C_{ij}} = P_{I_{ij}} \left(\frac{N_{P_j}}{A_{P_j}} \right) \left(N_{F_i} A_{C_i} \right), \text{ where}$$

P_{Iij} is the probability of a fragment from debris group "*i*" impacting on population center "*j*,"
A_{Ci} is the effective casualty area for a fragment from debris group "*i*" (the area on the ground within which a person will become a casualty) for the given population center and shelter category (outside or in a specified type of sheltering),
N_{Fi} is the number of fragments in debris group "*i*,"
N_{Pj} is the number of people in population center "*j*" in the given shelter category, and
A_{Pj} is the area of the population center.

To obtain the total casualty expectation for a given failure time and failure mode, the E_C values are summed over all fragment classes, shelter categories, and population centers, i. e.:

$$E_{C-Total} = \sum_i \sum_j E_{Cij}$$

Weight the E_C-Total values by their corresponding probability of occurrence and summed over all failure times and failure modes to get the total (mission) casualty expectation due to debris impact hazards: the accumulated debris risk as formally defined. The mission risk, expressed in terms of the "expected average number of casualties (E_C)," in § 431.35 refers to the total casualty expectation for all hazards posed by the mission, which is the aggregated risk as formally defined (see page 56660 in reference [11]). In general aggregated risks, both collective and individual, should account for each of the three principle launch hazards, and may be computed as the sum of the accumulated risks from each hazard posed by the vehicle.

4.9 Cumulative Procedure to Compute Risks

1. Select a flight time (representing a failure time interval) and assume a failure occurs.

2. Consider a specific mode of failure and define the vehicle dispersions.

3. Select a fragment group resulting from vehicle breakup.

4. Develop the fragment group impact probability distribution.

5. Compute the impact probability and casualty expectation for each population center.

6. Weight the impact probabilities and casualty expectations by the probability of failure associated with the specific failure time and failure mode.

7. Repeat for all combinations of failure time/interval, failure mode, and fragment group.

8. Statistically combine to obtain the total risks (individual and collective).

The QRA determines the expected casualties from inert and explosive debris impacts, for all of the potentially affected populated areas. For inert debris, compute probabilities of casualty based on the impact velocity, area, and mass of the impacting debris, or by more simplified methods described below. For people in structures, calculate the ability of the debris to penetrate the roof (or in rare cases with large horizontal velocity to impact the walls) and the number of casualties considering the fragment characteristics as well as the roof and upper floor characteristics or by more simplified methods described below. If the debris explodes upon impact, such as for intact stages (liquid or solid propellant) or for large chunks of solid propellant, compute the resulting casualties for people in the open and for people located in damaged buildings based on the overpressure and impulse from the blast wave or by more simplified methods described below. Explosive consequence models should consider the effects of thrown fragments and flying glass [12], which is often the dominant source of casualties from an explosion, as well as failing walls and ceilings due to the blast wave.

The QRA computation process is cumulative. Risk computations are made for failures occurring during specified time intervals (usually a few seconds long) and for each of the failure response modes (also sometimes referred to as vehicle response modes) that can occur during each time interval. For each time and mode, the computations are made over all of the individual debris categories and for all of the affected population centers. Obtain the E_C for the entire flight (or flight phase) obtained by summing over all times and all failure response modes.

$$E_{Ctotal} = \sum_{Time} \sum_{Fail\ \mathrm{Re}sp\ Mode} \sum_{Deb\ Cat} \sum_{Pop\ Ctr} E_{C_{ijkl}}$$

Considering the number of failure times, the number of failure response modes, the number of debris groups and the number of population centers, QRA may entail a million computations of E_{Cij}.

Figure 4-2 summarizes the procedure graphically.

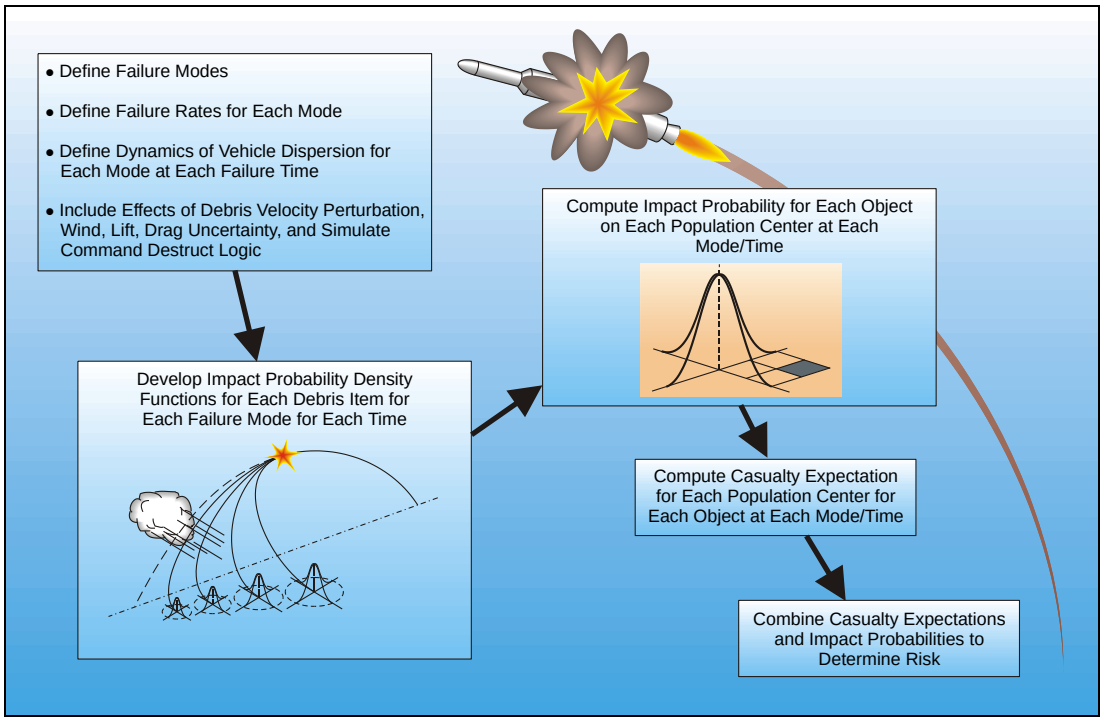

Figure 4-2. Overview of the General Cumulative Risk Analysis Procedure

4.9.1 Use of Event Trees

An event tree is a useful tool for estimating the debris impact risks for launch and reentry vehicle operations, and to account for the most critical events that may or may not occur following a potentially catastrophic failure of the vehicle. The use of event trees in a flight safety analysis can differ in important ways from their use in reliability analysis as described in [6]. For example, an event tree useful in a flight safety analysis should not eliminate branches that represent *non-recoverable failures*, such as failures that will result in debris impacts. This section describes the use of event tree in flight safety analyses.

An event tree starts with the potentially catastrophic initial failure modes (where *initial* refers to the initial failure of the vehicle as opposed to a failure that subsequently occurs, such as during an abort) and their associated probabilities of occurrence. For each potentially casualty-causing failure mode, the event tree traces the various sequences of events that may or may not occur. The event tree should consider all events that can have a significant effect on the end state of the vehicle, and thus on the resulting risk. A typical RLV event tree has two parts:

1. a top level event tree that starts with the potential casualty-causing failure modes and traces through to all end events that do not result in successful initiation of an abort mode, and

2. an abort mode event tree that traces through the significant events that may or may not occur during an abort.

Figure 4-3 shows a sample top-level event tree. Figure 4-4 shows a sample abort mode event tree. For the sequences in the top level tree (Figure 4-3) that end in *Vehicle Recovery Attempted*, the continuation of the sequence passes over to the abort mode tree. The event trees end in sixteen (16) total end events. The end events in the top level tree are those for which an abort could not be successfully initiated, and consist of events that are similar to those for ELVs. One exception to this is that two of the events involve activation of a propellant dump system to disperse the propellants prior to impact. (Note: The dump system may not disperse the propellants needed for engines for an abort landing. We assume for simplicity in this example that a highly reliable dump system is available to disperse enough of the propellants to preclude an explosion at impact.) One can compute the risks for all the top-level tree end events with a footprint-based debris risk analysis model.

The end events on the abort mode event tree (Figure 4-4) are those for which an abort was successfully initiated. The sequences then involve the critical events during the abort that determine if the abort results in a normal abort landing at the planned landing site, a landing at an unplanned location, a potential crash landing at either the planned landing site or another location, or an uncontrolled landing with or without breakup before impact. The risk for some of these end events is either zero or expected to be very small relative to those for other end events. One can compute the risk for other end events using the standard debris risk analysis model.

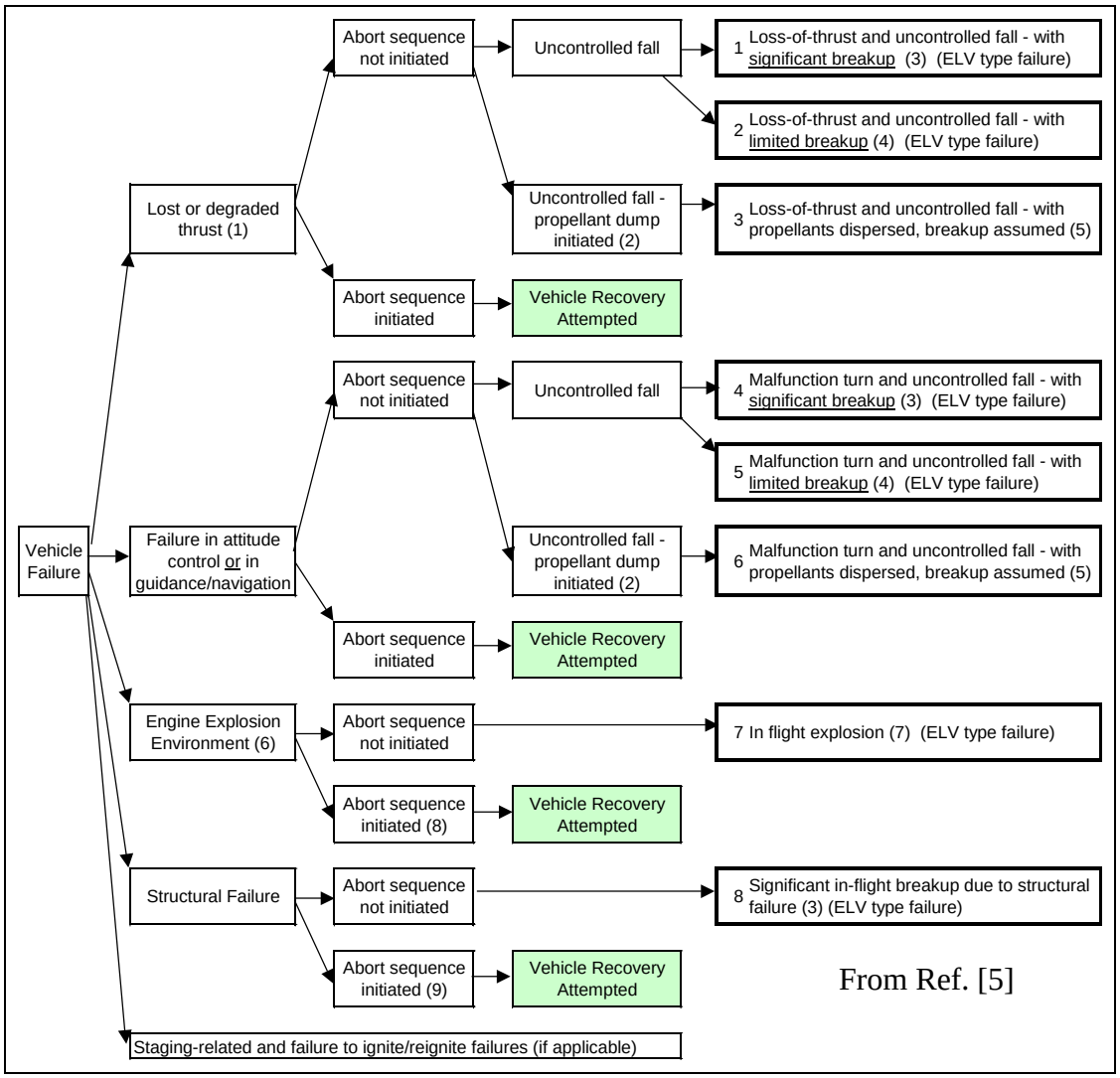

Figure 4-3. Sample Top Level Event Tree

(1) Assumes degraded thrust results in thrust shutdown and/or loss of control, and that vehicle falls uncontrolled unless the operator can initiate an abort mode.
(2) Assumes activation of a propellant dispersal system that dumps the propellant from both the rocket motor fuel and oxidizer tanks.
(3) Assumes breakup during reentry (from air loads, inertial loads and heating) results in significant vehicle breakup causing the propellant tanks to rupture or, at least, the fuel tank(s) to separate from the oxidizer tank(s) so as to prevent an explosion at impact.
(4) Assumes limited breakup (main body plus torn off aero surfaces, tiles, etc.) or no breakup such that impact occurs with propellants still on board. Assumes the amount of propellant remaining at impact to be the same as that at initial failure.
(5) Assumes breakup during reentry from air loads, inertial loads, and heating, possibly aided by activation of the propellant dump system, to result in limited (a main body plus torn off aero surfaces, tiles, etc.) or significant breakup and with all propellant dispersed.
(6) Assumes an explosion will result unless the operator takes mitigating actions, to include abort activation.
(7) Assumes that explosion results in violent vehicle breakup and propellant dispersal.
(8) Assumes that a health monitoring system detects an impending explosion, shuts down engine, and initiates abort; or that the explosion is contained allowing an abort.
(9) Assumes that the structural failure is not catastrophic and that the operator can initiate an abort.

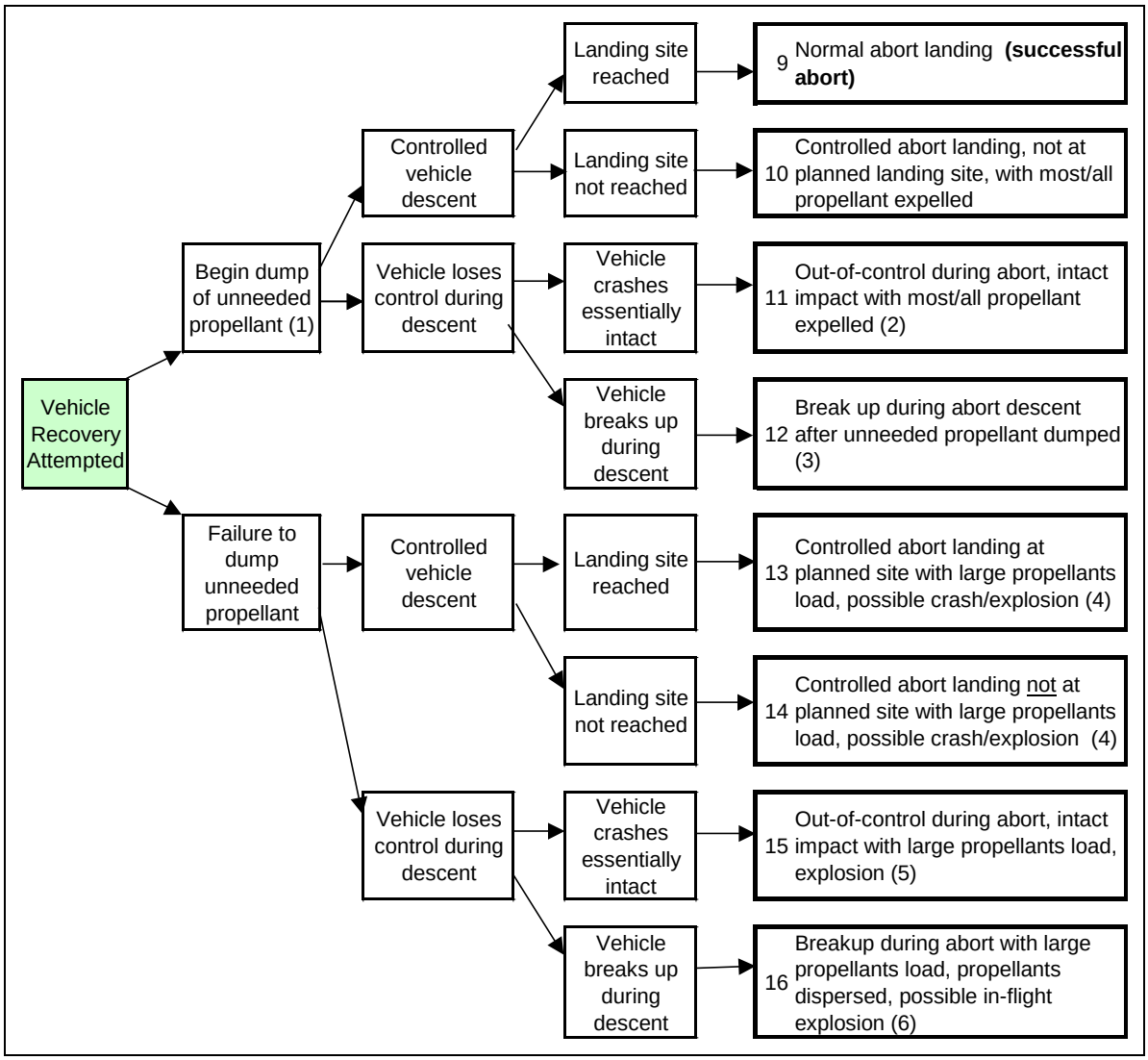

Figure 4-4. Sample Abort Mode Event Tree

(1) Unneeded propellant is the propellant not required for auxiliary systems that is available during the abort landing. The operator could initiate dumping anytime during the abort that allows sufficient time to expel all unneeded propellant before landing (or impact), and could occur after a loss of vehicle control.
(2) Assumes impact with little or no propellant and no explosion. Includes cases with limited vehicle breakup during descent.
(3) Assumes significant vehicle breakup occurring after dumping most or all of the unneeded propellants. No in-flight explosion.
(4) A crash landing, with a possible explosion, could result due to the failure to expel sufficient propellant prior to landing.
(5) Assumes impact with significant propellant and an explosion. Includes cases with limited vehicle breakup during descent that does not result in dispersal of propellants or separation of fuel and oxidizer tanks.
(6) Assumes significant vehicle breakup resulting in dispersal of the propellants or, at least, separation of the fuel and oxidizer tanks. An in-flight explosion from mixing propellants is possible.

Accurate estimates of the risk for some end events require data defining the abort mode trajectories and corresponding planned landing sites, as a function of the flight time that the primary failure occurs.

To compute the total risk from the event tree, first compute the probabilities of occurrence for the end events in the event trees.

1. Start with the probability for the initial potentially casualty-causing failure mode.

2. Multiply this by the successive conditional probabilities at each step in the sequence that leads to the end event.

   Example: Consider the sequence leading to the end event number 1, "Loss-of-thrust and uncontrolled fall – with significant breakup"
   Initial probability = the probability of lost or (significantly) degraded thrust multiply by the probability that an abort sequence is <u>not</u> successfully initiated, the probability that propellant dump is <u>not</u> initiated during fall, and the probability that the vehicle <u>does</u> break up significantly (causing dispersal of the propellants) during the fall to impact.

3. Compute the conditional risks (e.g., casualty expectation and individual probability of casualty) for each of the end events, assuming that the probability of the end event occurring at some time during the launch is one (1.0).

4. Calculate the total risk by multiplying the conditional risk for each end event by its probability of occurrence, and then summing the results over all of the end events. You may analyze uncertainty in the conditional probabilities at various event tree nodes using techniques published in [13].

Identify probabilities of occurrence used in an event tree from data describing the past performance of the vehicle, from analysis of historical data from similar vehicles launched under similar circumstances, from reliability analyses, or from a combination of these. We provide a full discussion of probability of failure in section 5.0.

The event tree figures include the assumptions and other information pertaining to each end event in the event tree. An important assumption concerns the two types of vehicle breakup that occurs after a failure.

<u>Significant breakup</u> - Significant breakup means that breakup occurs during reentry from aerodynamic loads, inertial loads, or heating and results in significant vehicle breakup that causes the propellant tanks to rupture or, at least, the fuel tank(s) to separate from the oxidizer tank(s) so as to prevent an explosion at impact. Tank debris may or may not have propellant remaining at impact

depending on the use of a propellant dump system or the degree of vehicle breakup. If one or more tanks impact with propellant, then we conservatively assume the amount of propellants remaining at impact to equal that at the time of the initial failure.

Limited breakup - Limited breakup means the assumptionthat there is no breakup or that the resulting debris consists of the main body with possible tearing off of aero surfaces, thermal protection system, etc. The impacting vehicle or the main body may or may not have propellants still on board, depending on the effectiveness of a propellant dump system. If there is no propellant dump system or the propellant dump system does not activate, then assume the amount of propellant remaining at impact equals that at the time of the initial failure, and the risk calculations include the effect of an explosion at impact.

4.9.2 Generic Failure/Vehicle Response Mode Descriptions

Of course, there are many potential causes of launch failures, or accident initiating events. However, there are relatively few types of responses to the failures in terms of predicted vehicle behavior. In order to assess the risk from all types of accident initiating conditions, a QRA typically uses three generic vehicle response modes, also sometimes referred to as failure response modes.

1. An on-trajectory failure. These include on-trajectory explosions, aerodynamic break-up, or command destruct events caused by failure of the propulsion system, structural failure, a premature FTS event, etc. Challenger disaster (STS-51L) is an example of an on-trajectory failure.

2. A malfunction turn failure. These may or may not include aerodynamic break-up or command destruct events caused by a failure of the propulsion, guidance, or control systems, etc. Section 10.4.8 describes modeling of malfunction turn responses. The 15P flight of SpaceShipOne, in which a flight control system anomaly caused trajectory excursion that resulted in the vehicle reentering south of its intended recovery point (http://www.scaled.com/projects/tierone/logs-WK-SS1.htm), is an example a malfunction turn that did not result in a break-up or an accident.

3. The random attitude failure or diabolic turn. The random attitude failure response mode is a modeling construct that is useful to bound the potential impacts due to guidance malfunctions. It is not necessarily a realistic scenario for a particular launch. At each time step along the trajectory, the trajectory simulation rotates the vehicle randomly as if the guidance system has lost all reference. Then the simulation flies the vehicle stably in the new direction until it reaches either a command destruct or structural failure condition. Depending on the time of failure, mission rules, and FSS reliability, a diabolic turn can produce an intact impact. There are no past failures that exactly qualify as a diabolic turn. However, some past accidents clearly indicate a potential for this response mode. The Titan IV-A20 failure on August 12, 1998 is an example where a guidance system failure (more precisely an

electrical system failure) resulted in immediate breakup without casualties, and the Long March accident on February 14, 1996 is an example without immediate breakup that resulted in a number of casualties.

4.9.3 Overview of the Footprint Method

This section explains basic characteristics of the debris impact pattern, often called a debris footprint. The footprint is a mathematical/probabilistic description of the scatter of debris resulting from a vehicle breakup at a particular time in flight. It is a basic building block of numerous risk analyses performed for many space vehicles. The initial conditions are described by position (x, y, z), velocity (V_x, V_y, V_z), and time of occurrence. The debris from the breakup is divided into categories based on ballistic coefficient (section 6.4) (β), velocity induced from the breakup event and the casualty area (section 6.0) associated with impact. The location of mean impact points of the fragment groups are dominated by their ballistic coefficients and the wind. Higher ballistic coefficient debris tends to impact far downrange, relatively uninfluenced by the wind. Low ballistic coefficient debris will slow down rapidly, falling more directly below the break-up point or being carried in the direction of the wind. This is illustrated in Figure 4-5. However, in a progressive breakup such as experienced by the Space Shuttle *Columbia*, low ballistic coefficient debris can be found toward the toe of the footprint also [14].

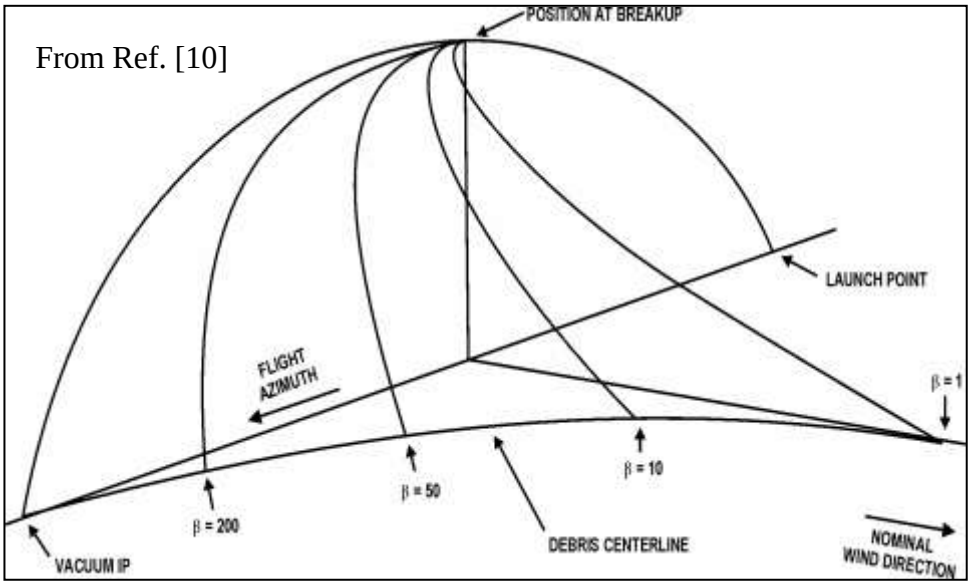

Figure 4-5. The influence of the ballistic coefficient, β and wind upon mean debris impact points.

Several launch vehicle failures under the same conditions (time in flight, failure mode, wind conditions, etc.) would not be expected to produce exactly the same impact locations and consequences due to the inherent variability in such factors as the debris generated or the size of the impact explosions. The four frames in

Figure 4-6 represent four different randomly selected debris impact distributions from a simulated Space Shuttle breakup based on the same failure time and the same set of debris impact probability distributions. Each of these four distributions, with the distinct fragment impact points overlaid on the same set of people or buildings, will produce different probabilities of exactly one, two, three, etc., casualties. Thus, the variability associated with inherently random events means that the number of casualties produced even for a specific scenario (i.e., failure mode, failure time, etc.) should be modeled as a probabilistic distribution.

This variability is accounted for by averaging. In fact, the very definition of expected casualties involves averages: the average number of casualties that can occur as a result of an event if the event were to be repeated thousands of times. For example, an E_C equal to 30E-6 corresponds to a launch that would result in 30 casualties on average if repeated one million times.

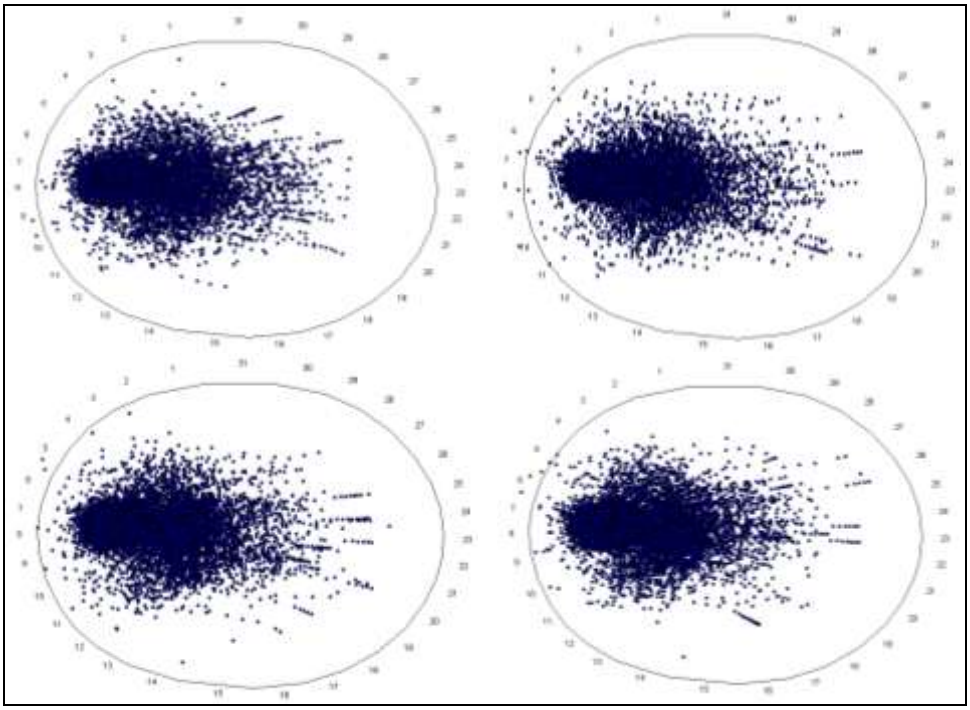

Figure 4-6. An Example of Variability or Randomness in Impact Locations (Aleatory Uncertainty)

The impact points for each piece of debris within the various groups/categories are uncertain due to the effects of five sources of dispersion: induced velocity, wind uncertainty, ballistic coefficient uncertainty, lift uncertainty, and state vector uncertainty. The state vector uncertainty can be due to both uncertainty in the nominal guidance and performance and any aberrant vehicle behavior before the breakup. These sources of impact point dispersion lead to the impact distributions for each of the debris categories as shown in Figure 4-7.

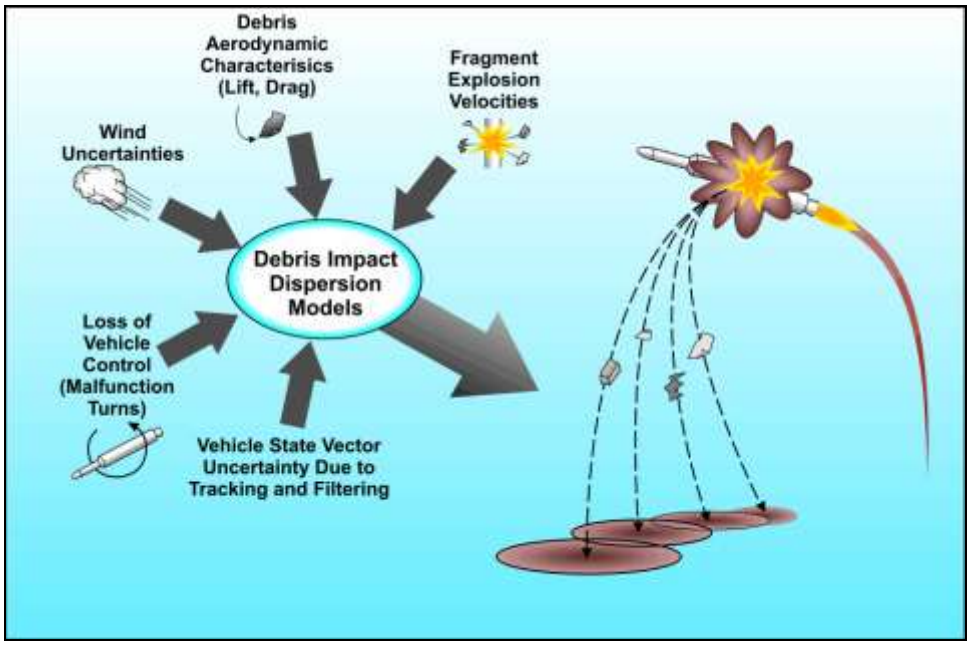

Figure 4-7. Contributions to debris impact dispersion models

The "disks" illustrating the impact dispersions in Figure 4-7 are often represented by bivariate normal (binormal) probability distributions.[3] Thus, each debris footprint is typically modeled as a series of bivariate normal distributions representing the impact uncertainties of each of the debris categories[4]. Each of these distributions is accompanied by the number of fragments in the group, the average weight of the fragments in the group, and a projected area of the average fragment when it impacts. If the fragment is explosive, it will include the explosive yield of the fragment upon impact. Guidelines for all the sub-models involved in these calculations are provided in the subsequent sections of this handbook.

The footprint approach facilitates numerical simulation of scenarios because a footprint can represent a single accident: a possible outcome due to a failure mode occurring at a failure time. The footprint based QRA is built from thousands of these scenarios where each scenario has a probability, has a failure time, and represents some vehicle behavior at that time. The primary challenge for a debris risk analysis is to be able to define a set of scenarios that describe all of the possible conditions sufficiently to produce a valid determination of risk.

[3] Based on the Central Limit Theorem. If the distribution is known to be significantly different than bivariate normal, an alternative risk analysis method can be used (such as a Monte Carlo technique).

[4] Caution should be exercised with the bivariate normal distribution assumption. Some impact distributions become skewed, particularly when one source of uncertainty is much larger than the others, and along the uprange-downrange axis if uncertainties in induced velocities or ballistic coefficient are very large.

4.9.4 Overview of the Corridor Method

Use the relatively simple corridor method illustrated in Figure 4-8 if the debris risks are due to: (1) flight phases where the IIP is moving steadily downrange, and (2) failure modes that do not involve distorted impact distributions, such as those caused by actions taken in response to abort criteria.

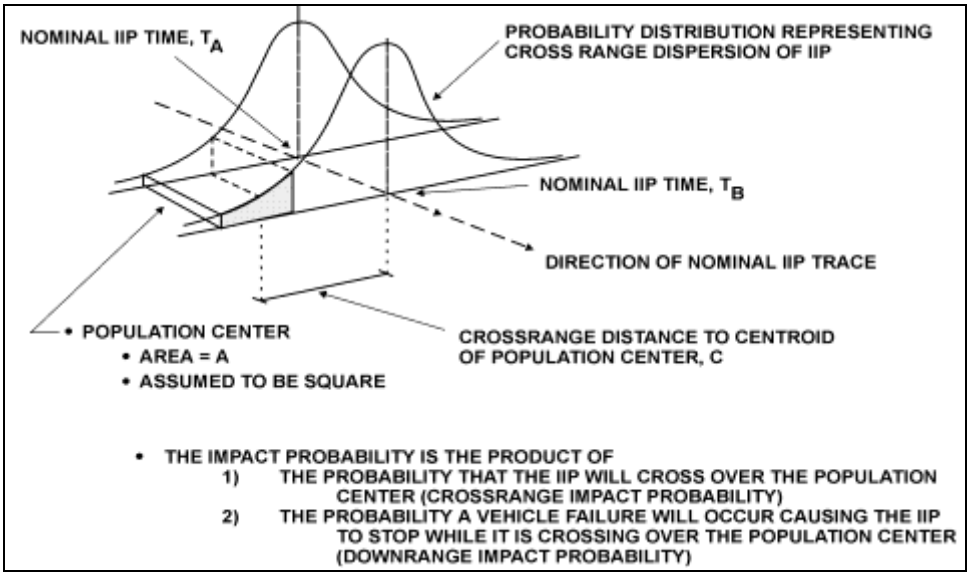

Figure 4-8. Diagram of the Elements of the Downrange Corridor Methodology

The equations associated with the corridor methodology are as follows:

Impact Probability on a population center: $P_I = P_I\,(downrange) \times P_I\,(crossrange)$

where

P_I (downrange) = (failure rate) $\times$ $(A_{pop})^{1/2}$/ (IIP rate)

P_I (crossrange) = $\int$ p(y)dy between the limits of $y_c - ½\ (A_{pop})^{1/2}$ and $y_c + ½\ (A_{pop})^{1/2}$

where *p(y)* is the probability density function for crossrange dispersion for the particular fragment category and A_{pop} is the area of the population center.

Casualty Expectation:

Casualty expectation from fragment group i on the population center is (the same equation that was presented in section 4.8)

$$E_{C_{ij}} = P_{I_{ij}} \left(\frac{N_{P_j}}{A_{P_j}} \right) \left(N_{F_i} A_{C_i} \right)$$

Total casualty expectation from all fragment groups on the population center

$$E_C = \sum E_{Ci}$$

Apply this method to all exposed population centers for all fragment groups and failure modes to obtain the total casualty expectation. The impact points used in a corridor analysis should be drag corrected for the appropriate fragment group.

A simpler version of the corridor method uses only the vacuum impact points and groups all of the effective casualty areas of all the fragments into a single effective casualty area, as described in the 14 CFR part 420 appendices B and C. This will produce approximate results for use in mission planning. They are not for use for final risk estimates because drag often has an important influence on the impact location and thus impact probability of debris.

Do not underestimate the cross-range dispersion effects of debris. The cross-range standard deviation should account for the variations in the guidance and performance of the vehicle (section 8.4.1), non-nominal trajectories (section 8.4.4), as well as other influences, such as velocity imparted to the debris from any explosion (section 10.4.6) or other energy release in the breakup. The cross-range standard deviation for normally distributed dispersions can be root sum squared to characterize the total cross-range dispersion, as described in section 8.4.2. Separate cross range dispersion estimates may be necessary to account for various failure modes (e.g., one for on-trajectory failures, and another for malfunction turns, etc.). Depending on the specific situation, an underestimate of the cross-range dispersion may produce an underestimate or an overestimate of the risks. Thus, you should perform some sensitivity analysis to account for the potential influence of cross-range uncertainty due to all foreseeable sources of debris dispersion perturbations such as winds, breakup induced velocities, etc. (see Section 6.0). If the corridor method results indicate marginal risk acceptability, perform a more robust debris footprint methodology to simulate the actions of the range safety abort system.

4.9.5 Overview of the Bivariate Normal Method for Jettisoned Debris

During typical launches, the operator jettisons certain elements of the rocket as the launch progresses (this is standard for ELVs). As each stage burns out and separates, it often follows a ballistic path to impact. In addition, the operator may jettison certain other panels, fairings, etc., as well. This scheduled (or planned) debris happens with every successful multi-stage ELV launch, and thus the mission should undergo careful planning so that these items of debris do not create an unacceptable risk. Even if the vehicle has a significant probability of failure, the analysis should use a probability of occurrence of 1.0 for the planned debris fragments produced by every normal planned event during flight. This is done to assure the public of adequate protection during any successful launch.

The procedure to compute the risk for jettisoned debris is:

1. Define the state vector (position and velocity) of the jettisoned debris at the time of separation from the vehicle.

2. Determine the aerodynamic characteristics of the jettisoned debris (drag coefficient, aerodynamic reference area, weight) and compute a drag corrected impact point[5]. Give consideration to whether the jettisoned debris tumbles or stabilizes at a particular attitude during descent.

3. Develop impact uncertainties of the stage based on the following:

   - The uncertainties in the vehicle state vector at the time of jettison (the vehicle may be flying fast, slow, high, low, right, or left relative to the nominal due to winds, guidance, and performance uncertainties),
   - Any perturbation velocities that may be applied during jettison, and
   - The effect of wind and wind uncertainties after jettison.

   This process should produce a standard deviation of impact uncertainty in the uprange and downrange direction and another standard deviation in the cross-range direction. A more sophisticated analysis may produce an impact covariance matrix of the impact dispersion that may indicate some rotation of the dispersions relative to the downrange and cross-range directions.

4. Use the standard deviations computed in Step 3 to define a bivariate normal distribution with its mean at the nominal impact point and with its two axes aligned respectively with the downrange direction and the cross-range direction (orthogonal).

5. If there is an island, offshore oil platform, or any other population center that is potentially at risk, compute the impact probability by integrating under the bivariate normal distribution in the two directions. Figure 4-9 and the following equation show the bivariate normal distribution, the impact area (A), at risk and an equation for computing the probability of impact.

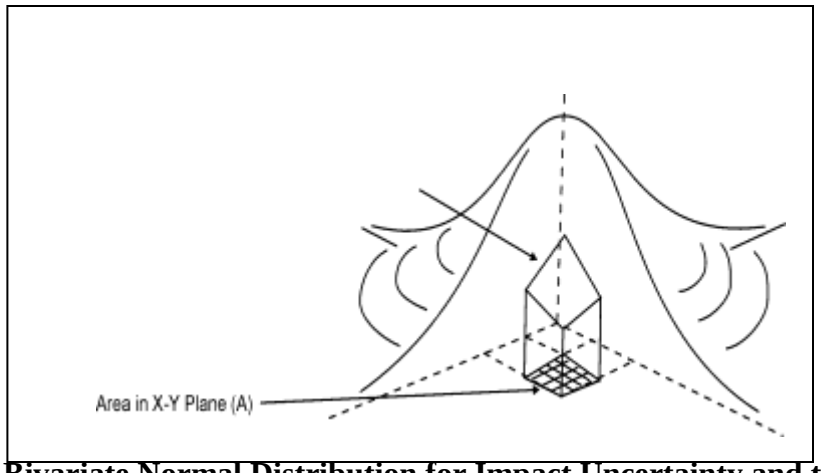

Figure 4-9. Bivariate Normal Distribution for Impact Uncertainty and the Area at Risk

[5] Accounting for the addition of a parachute requires special attention that is beyond the scope of this handbook.

The equation below defines the calculation of the impact probability of a single object in the area (A), where the impact distribution is a bivariate normal distribution with the major and minor axes aligned along the x and y directions, respectively. The center of the area (A), is at (x_A, y_A). Assume that x is in the downrange direction, and y is cross-range, positive to the left looking downrange. Assume the mean for this distribution to be at the nominal impact location for the stage (or fairing or fragment) thus $\mu_X = \mu_Y = 0$. For small values of P_I and few stage/fragments, the individual P_I is multiplied by the number of stages/fragments to get the total P_I.

The casualty expectation for one population center in the impact distribution is found by solving for the area under the curve:

$$P_I = \frac{1}{\sqrt{2\pi}\sigma_x} \int_{x_A-\sqrt{A}/2}^{x_A+\sqrt{A}/2} e^{-\frac{x^2}{2\sigma_x^2}}\, dx \times \frac{1}{\sqrt{2\pi}\sigma_y} \int_{x_A-\sqrt{A}/2}^{x_A+\sqrt{A}/2} e^{-\frac{y^2}{2\sigma_y^2}}\, dy$$

$$E_C = P_I \times \frac{1}{A} \times N \times \sum_i (A_{C_i} \times P_i)$$

where

P_I = Impact probability on the population center
A = Area of the population center
N = Number of jettisoned fragments with identical characteristics
A_{Ci} = Effective casualty area per fragment to the ith level of population sheltering
P_i = Population in the ith shelter category (assumed to be uniformly distributed over the population center area, A)

6. Repeat the above process for every population center potentially impacted and for every jettisoned stage, fairing, etc.

The integrated example in the appendix (section A) includes an example of computing risks from scheduled debris. Unless they are dropped together and have the same nominal ballistic characteristics, treat the risks from each piece separately. Do not group jettisoned components in the same bivariate distribution unless they have the same mean impact point and down-range and cross-range uncertainties. If they do not, compute a new distribution for each. One can treat two or more identical objects together. However, the impact probability (for relatively small P_i) is simply the product of the number of objects times the P_i for one. The same is true for casualty expectation, E_C.

5.0 PROBABILITY OF FAILURE

5.1 Purpose

The purpose of probability of failure analyses for a QRA is to characterize the likelihood of debris generating events that could constitute a hazard to the public.

5.2 Input Data Sources

Empirical evidence, such as flight experience and test data, is often the primary source of input data for a valid probability of failure analysis. The flight experience and test data from other vehicles developed and launched under similar circumstances are often valuable input data sources for relatively new vehicles, as described in the FAA's *Guide to Probability of Failure Analysis for New Expendable Launch Vehicles*. [7] If a vehicle has flown several times under similar conditions and without significant modifications, estimate the overall probability of failure directly from the actual flight history. [7] History shows that probability of failure estimates based on subsystem reliability, redundancy, and design simplicity often produce overly optimistic results that are not appropriate for public safety analyses.[6] [15] An acceptable probability of failure analysis, used as input for a public safety QRA, need not be based only on empirical evidence. However, the results should be consistent with relevant flight experience and applicable test data. In some cases, engineering judgment and expert opinion are viable data sources in the absence of applicable empirical data. This is particularly the case with RLVs, since empirical evidence on these vehicles is currently lacking.

5.3 Minimum Features

A probability of failure analysis should quantify the likelihood of all potentially casualty-causing events. Base a valid QRA on a probability of failure analysis that:

- Accounts for launch vehicle failure probability in a consistent manner for various flight phases, sources of hazard, flight experiences, etc.
- Uses accurate data, scientific principles, and a method that is statistically or probabilistically valid,
- Is consistent with the outcomes of all applicable tests and all previous flights of vehicles developed and launched under similar circumstances, [7]
- Accounts for changes to the vehicle configuration and other factors, and

[6] Empirical evidence, documented in [7], shows that the experience level of the vehicle developer (which is often manifested in design flaws and human error) is the dominant factor in the reliability of a new launch vehicle.

- Accounts for aleatory and epistemic uncertainty.

In this context, accurate data means completeness, exactness, and fidelity to the maximum extent possible. Scientific principles refer to knowledge, based on the scientific method, such as that established in the fields of physics, chemistry, and engineering. A probability of failure estimate that is statistically and probabilistically valid should at least be the result of a sound application of mathematics. A sound application of mathematics uses correct premises and makes only conclusions that are properly derived from the premises. A valid statistical analysis should account for the uncertainty in a statistical inference caused by sample size limits, degree of applicability of data to a particular system, and degree of homogeneity of the data.

5.4 Introduction to Probability of Failure Modeling

Probability is an abstract concept that satisfies certain mathematical rules. One can interpret probability as relative-frequency or as the degree-of-belief. The relative-frequency interpretation views the probability of a particular outcome as the frequency of that outcome divided by the total number of outcomes if you repeat an event many times. For example, the probability of heads in an equally-weighted coin toss is 0.50 because heads will result about 50 times out of 100 tosses. The degree-of-belief interpretation bypasses the need for numerous identical trials. The degree-of-belief interpretation is most useful for a launch QRA because launch conditions are so dynamic that numerous identical trials are unrealistic.

Probability of failure analyses are often classified as deductive or inductive. Deductive analyses are top-down, postulating system failure and analyzing behaviors contributing to the failure. Inductive analyses are bottom-up, analyzing the failure of individual components to determine the likelihood of system failure. However, each analytic approach contains inherent limitations, and the results of any analytical construct are by nature uncertain. Over time, NASA, the U.S. military, the nuclear industry, and the commercial airline industry have recognized that a single analytical approach to reliability estimates is usually insufficient. These industries use both top-down and bottom-up analysis approaches, including measures of uncertainty. Likewise, a QRA of a commercial space launch or reentry should look to multiple approaches to estimate the probabilities of failure input.

The following subsections describe three methods that use empirical data either on the subject vehicle or vehicles developed and launched under similar circumstances to produce a conservative failure probability estimate. The first is a "top-down" approach developed by the Common Standards Working Group (CSWG), the second is a relatively simple Bayesian method that uses a "weak prior" based on historical flight experience, and the third is a Bayesian method that combines manufacturer predictions with experiential data. We also discuss a bottom-up approach based on a probabilistic risk assessment (PRA). Allocation

treatment of the failure probability to flight times and vehicle response modes follows after these discussions.

All of the launch vehicle failure probability analysis methods that are accepted in current practice treat launches as Bernoulli trials. These are trials where the vehicle has a constant "true probability" of failure for each and every launch and where the outcome of each launch is statistically independent of all others. A toss of an evenly-weighted coin is a classic example of a Bernoulli trial. Of course, launches are not exactly Bernoulli trials because no two launches are precisely the same. For example, the vehicle may be modified or improved as needed during the sequence of launches, particularly if it has failed on previous launches. Also, there are natural variations due to environmental conditions during the vehicle manufacturing, processing, and launch.

In light of the approximate nature of the failure probability estimates based on the assumption of Bernoulli trials and the use of historical flight experience data sorted by the experience level of the launch vehicle developer, it is important to note that the results of analyses using these bases have proven far more accurate than those from subsystem-based reliability analyses.

The first launch of a fictitious ELV named Glob-6 provides an example. Before that launch, assume an analysis sponsored by the manufacturer and performed by an independent organization estimated the overall vehicle probability of failure for several launch vehicles based on subsystem failure rates. Presuppose that the design reliability analysis led to a failure probability estimate of less than 0.05 (5%) for the Glob-6, which was also purportedly on par with the Atlas V and Delta IV [15]. However, a statistical consideration of the historical data on the first two launches of a new vehicle developed by a new developer would have produced overall vehicle failure estimates near 0.75, and a much lower estimate for vehicles developed by experienced manufacturers, like the Atlas V and Delta IV. However, if the flight experience from the first few launches of these vehicles resulted in failures, the failure probability analysis methods described below would produce a far more accurate conclusion than those from subsystem-based reliability analyses.

Furthermore, the relatively high demonstrated reliability of the two extremely complex launch vehicles, the Space Shuttle and the Delta II with numerous solid rocket motors attached, indicates that launch vehicle complexity does not simply correlate with overall failure probability. The fact that subsystem-based reliability analysis methods have often underestimated the demonstrated failure probability of launch vehicles illustrates the importance of factors that can be difficult to quantify such as potential human errors, system interdependencies, environmental conditions, etc. Thus, the failure probabilities for new vehicles have typically been underestimated by subsystem-based reliability analysis methods. In addition, it is not unusual for even experienced manufacturers to underestimate the relative likelihood of occurrence of vehicle response modes that have the potential to cause significant deviations from the intended flight path

relative to demonstrated experience. Consequently, to ensure reasonability in light of actual experience, a flight safety analysis should check predicted failure probabilities, for the vehicle overall and for those assigned to various failure modes.

5.5 Historical Flight Experience for New Launch Vehicles

History confirms the intuitive notion that the chance of failure is significantly higher during the initial launches of a vehicle that is new. Empirical evidence shows that the probability of failure for the first and second launches of ELVs launched to orbit depends largely upon the developer's past experience. Specifically, the worldwide flight history of orbital ELVs from 1980 to 2008 reveals that vehicle developers who had previously never successfully launched a vehicle to orbit had 13 failures in 16 initial launch attempts. Over the same period, worldwide flight history for developers who had previously launched at least one vehicle to orbit successfully indicates 7 failures in 24 launch attempts.

Table 5-1 and Table 5-2 list data on the historical flight experience (i.e., history of successes and failures) for the first several launches of orbital ELVs developed by new and experienced developers over the period from 1980 to mid 2008. These tables use abbreviations as follows so that the information can be summarized on a single page:

- Category NN in Table 5-1 indicates a new vehicle launched by a new developer, whereas NE (Table 5-2) denotes a new vehicle launched by an experienced developer.
- Stage Config. refers to the vehicle configurations and uses *Simple stage* for a vertical stack without strap-on rocket motors. If the configuration is not *Simple*, then the table includes a brief explanation. Summary tables following the main tables show data on individual performance of stages.
- The launch numbers are in sequence, 1 to 10. Each box gives a summary of the flight. For instance, *123s* means a three stage flight that was a success. *1t* indicates a flight that was terminated during the first phase (usually equivalent to the first stage of flight). A small *d* after a phase number, e.g. 12d34, indicates degraded performance. In the case of 12d34, performance was degraded during phase 2 but the vehicle continued to fly through the 3rd and 4th phases (stages).
- The Propulsion column has just three options: liquid, hybrid, or solid propellant. In developing applicable statistics for a particular new vehicle, it may be appropriate to limit the statistics to historical vehicles that have the same propulsion categories. In fact, a vehicle can have different propellant types in different stages. We may in the future sort the historical data relevant to the vehicle accordingly. .

The time period associated with the launch histories presented in Table 5-1 and Table 5-2 presents a dataset representative of current orbital ELV designs.

Launch histories and failure narratives exist for certain vehicles back to the late 1950s [16]. We could have included them here. However, the advent of digital guidance computers and other technical advances of the 1960s and 1970s culminated in what is commonly seen as a transition to a modern era of launch vehicles in or around 1980. Data from earlier missions is, therefore, somewhat less applicable. Further, descriptive data for flights conducted before 1980 no longer exist for some of the vehicles in use at the time, adding uncertainty to their potential contribution to the historical failure tally.

The FAA has employed techniques to incorporate the pre-1980 data that does exist in an effort to expand the historical dataset presented in Table 5-1 and Table 5-2 to a more statistically significant set. These include using fading memory filters that weight the results of more recent flights more heavily than earlier flights, as described in Section 5.8 and Reference [17] providing these earlier flights less influence on the result.

Table 5-1. First Ten Flight History of New ELVs Launched by New Developers (1980 – September 2008)

Vehicle	Category	1st Launch	Propulsion	Stage Config.	Launch Number 1	2	3	4	5	6	7	8	9	10
SLV3 India	NN	8/10/1979	All Solid	Simple	12t	1234s	1234d	1234s	None					
Ariane 1	NN	12/24/1979	All Liquid	Simple	123s	1t	123s	123s	123t	123s	123s	123s	123s	123s
Percheron	NN	8/5/1981	Liquid	Simple/None	1t	None								
Dolphin	NN	8/3/1984	Hybrid	Simple/None	1t	None								
ASLV	NN	3/24/1987	All Solid	Stage 0 - Stage 1	12t	1t	1234d	1234s	None					
Shavit	NN	9/19/1988	All Solid	Simple	123s	123s	123s	12t	123s	123t	123s			
AMROC	NN	10/5/1989	Hybrid	Simple/None	1t	None								
Pegasus	NN	4/15/1990	All Solid	Simple	123s	12d34	123s	123s	1234t	123s	123s	123s	123s	123s
PSLV	NN	9/20/1993	Stg1/Strapons Solid, Stg 2 Liq	Staggered Strap-ons + Stage 1	123t	123s	123s	1234d	1234s	1234s	1234s	1234s	1234s	1234s
Conestoga 1620	NN	10/23/1995	All Solid	Staggered Stg 0 Strap-ons	1t	None								
VLS	NN	11/2/1997	All Solid	Stage 0 - Stage 1	1t	12t	Blew up on pad							
Taepodong 1	NN	8/31/1998	Liq 1,2, Solid 3	Simple	123t	1t								
Kaituozhe-1 (diff. Chinese org, therefore NN)	NN	9/15/2002	All Solid	Simple	12t	1234t								
Falcon 1	NN	3/24/2006	All Liquid	Simple	1t	12t	12t							
Safir	NN	8/16/2008	Liq 1,2, Solid 3	Simple	12t									
ATK X-1	NN	8/22/2008	All Solid	Simple	1t									

	Summary of Attempts, Successes (s), Terminations (t), Degradations (d) by Phase/Stage of Flight 1	2	3	4	5	6	7	8	9	10
Stage/Phase 1	16, 9s, 7t	10 7s 3t	7 7s	6 6s	4 4s	4 4s	4 4s	3 3s	3 3s	3 3s
Stage/Phase 2	9 5s 4t	7 4s 2t 1d	7 6s 1d	6 1T	4 4s	4 4s	4 4s	3 3s	3 3s	3 3s
Stage/Phase 3	5 3s 2t	5 5s	6 6s	5 5s	4 3s 1t	4 3s 1t	4 4s	3 3s	3 3s	3 3s
Stage/Phase 4		3 2s 1t	2 2d	3 2s 1d	2 1s 1t	1 1s	1 1s	1 1s	1 1s	1 1s

Table 5-2. First Ten Flight History of New ELVs Launched by Experienced Developers (1980 – September 2008)

Vehicle	Category	1st Launch	Propulsion	Stage Config.	Launch Number 1	2	3	4	5	6	7	8	9	10
Mu-3S	NE	2/17/1980	All Solid	Strap-ons + Stage 1	123s	123s	123s	123s	123s	123s	123s	123s	123s	123s
CZ-3	NE	1/19/1984	All Liquid	Simple	123t	123s	123s	123s	123s	123s	123s	123t	123s	123s
Zenit	NE	4/13/1985	All Liquid	Simple	12t	12t	123s	12t	123s	123s	123s	123s	123s	123s
Energiya	NE	5/15/1987	All Liquid	Staggered Strap-ons + Stage 1	12t	12s	None							
CZ-2E	NE	7/16/1990	Liq Core, and Liq Strap-ons	Strap-ons + Stage 1	12d	1234s	1d234	1234s	1t	1234s	1234s	None		
Rokot	NE	11/20/1990	All Liquid	Simple	123s	123s	123s	123s	123s	123s	123s	123s	123s	12t
Start	NE	3/25/1993	All Solid	Simple	1234s	1234t	1234s	1234s	1234s	1234s	1234s			
H-II	NE	2/3/1994	Liq Core, and Liq Strap-ons	Strap-ons + Stage 1	1234s	1234d	1234s	1234s	1234s	12d34	1d2			
CZ-3A	NE	2/8/1994	All Liquid	Simple	1234s	1234d	1234s	1234s	1234s	1234s	1234s	1234s	1234s	1234s
Taurus	NE	3/13/1994	All Solid	Simple	1234s	1234s	1234s	1234s	1234s	12d34	1234s			
Athena 1	NE	8/15/1995	All Solid	Simple	1d2t	123s	123s	123s	None					
CZ-3B	NE	2/14/1996	Liq Core, and Liq Strap-ons	Strap-ons + Stage 1	1t	123d4	1234s	1234s	1234s	1234s	1234s	1234s	1234s	
Ariane 5	NE	6/4/1996	Liq Core, Solid Strap-ons	Strap-ons + core	1t	1d23	123s	123s	123s	123s	123s	123s	123s	123d
M-V	NE	2/12/1997	All Solid	Simple	1234s	1234s	1d23	1234s	1234s	1234s	1234s			
Athena 2	NE	1/7/1998	All Solid	Simple	1234s	12t	1234s	None						
Shtil	NE	7/7/1998	All Liquid	Simple	123s	123s								
Dnepr	NE	4/21/1999	All Liquid	Simple	123s	123s	123s	123s	123s	123s	1t	123s	123s	123s
CZ-2F	NE	11/18/1999	Liq Core, and Liq Strap-ons	Strap-ons + Stage 1	123s	123s	123s	123s	123s	123s				
Minotaur	NE	1/27/2000	All Solid	Simple	1234s	1234s	1234s	1234s	1234s	1234s	1234s			
GLSV	NE	4/18/2001	Solid Core, Liq Strap-ons, Stg 2,3 Liq	Strap-ons + Stage 1	1234d	1234s	1234s	1t	1234s	1234s				
Volna	NE	7/20/2001	All Liquid	Simple	123t	123t	123t	1t						
Atlas 5	NE	8/21/2002	Liq Core, Solid Strap-ons	Strap-ons + Stage 1	123s	123s	123s	123s	123s	123s	1234s	123s	123s	12d3
Delta IV	NE	11/20/2002	Liq Core, Solid Strap-ons	Strap-ons + Stage 1	123s	123s	123s	123s	123s	123s				
Delta IV Heavy	NE	12/21/1004	Liq Core, Liq Strap-ons	Strap-ons + Stage 1	1d2	12s								

	Summary of Attempts, Successes (s), Terminations (t), Degradations (d) by Phase/Stage of Flight 1	2	3	4	5	6	7	8	9	10
Stage/Phase 1	24 20s 2t 2d	24 23s 1d	21 19s 2d	20 18s 2t	18 17s 1t	18 18s	15 13s 1t 1d	9 9s	9 9s	8 8s
Stage/Phase 2	22 18s 3t 1d	24 22s 2t	21 21s	18 17s 1t	17 17s	18 16s 2d	14 14s	9 9s	9 9s	8 6s 1d 1t
Stage/Phase 3	17 15s 2t	20 18s 1t 1d	21 20s 1t	17 17s	17 17s	18 18s	13 13s	9 8s 1t	9 9s	7 6s 1d
Stage/Phase 4	8 7s 1d	9 6s 1t 2d	9 9s	8 8s	8 8s	9 9s	8 8s	2 2s	2 2s	1 1s

5.5.1 Definition of a Failure

The results compiled in Table 5-1 and Table 5-2 all represent in-flight outcomes. Title 14 CFR § C417.9(b)(5)(ii) states that "a failure occurs when a vehicle does not complete any phase of normal flight or exhibits the potential for the stage or its debris to impact the Earth or reenter the atmosphere during the mission or any future mission of similar vehicle capability." In the context of a probability of failure analysis, an in-flight failure does not include a failure that may occur before liftoff or after orbital insertion.

As stated in [7], the FAA, in consultation with the CSWG, initially considered defining flight from the beginning of engine ignition to account for failures that resulted in liftoff or toppled the vehicle. However, there are times where a preplanned engine shutdown can occur that precludes liftoff but remains within the confines of planned or normal mission behavior. These types of occurrences would obviously not be considered in-flight failures. As a result, although instances where anomalies in the final moments of a countdown have resulted in destruction of a vehicle, liftoff better serves to define the beginning of flight.

In Table 5-1 and Table 5-2, off-nominal flight results are classified as either terminations or degraded performance. Termination refers to a termination of the flight by range safety or a vehicle catastrophic failure. Examine each launch with degraded performance closely to determine if a future launch with a similar degradation of performance could pose a hazard to the public. However, in the absence of clear evidence that such an event could not pose a threat to the public on a future launch, the probability of failure analysis should classify a degradation of performance as a failure.

5.5.2 Distinguishing Between New and Experienced Developers

Many factors influence the level of experience of a launch vehicle developer. [7] However, in the study that generated the data in Table 5-1 and Table 5-2, the term *experienced launch vehicle developer* corresponded to developers who had produced at least one previous launch of a vehicle that had achieved orbit successfully and demonstrated a probability of potentially hazardous failure less than or equal to 0.33 (33%). The empirical evidence presented above shows that new developers have demonstrated an initial probability of failure that is at least twice as high as that of experienced developers.

The NN category as defined above implicitly assumes that the total vehicle probability of failure is independent of any differences within the NN group, such as the number of stages used, the nationality of the developer, the type of propulsion, the size of the vehicle, the mission profile, etc. For example, the top-down approach, as described below, applied to the NN grouping would lead to the same estimated probability of failure for a NN launch vehicle that attains orbit using two stages or using four stages. The CSWG justified this approach with an analysis of the observed history of new launch vehicles (both US vehicles only and worldwide) where the developer's level of experience was the dominant factor related to the demonstrated probability of failure. This approach is reasonable in the absence of any analysis of the observed history of new launch vehicles demonstrating a statistically significant dependence of the probability of

failure on the number of stages for orbital vehicles or any other factors. In other words, this is logical if no other single source of uncertainty drives the probability of failure within the NN vehicle group.

In addition, examinations of the launches of NN vehicles have demonstrated a probability of failure distinctly higher for the first two launches than for subsequent launches. Studies of the data, such as the one conducted by Guikema and Pate-Cornell [18], have confirmed that "the mean failure rates appear to be higher in the first and second flights." Therefore, when assessing the probability of failure for the first two launches of an NN vehicle, consider only the first two launches of vehicles developed and launched under similar circumstances. This of course does not rule out the possibility of an adjustment to the failure probability estimate based on evidence from the first flight.

When sufficient data exists, additional characteristics, such as propellant type, stage configuration, and country of origin, may be used to extract a subset of the data presented in Table 5-2. The purpose is to identify the probability of failure associated with vehicles developed and launched under similar circumstances. You can then use the data in the probability of failure analysis of an NE vehicle. In the absence of more specific data that separates the experience of vehicles based on propellant type (for example only all liquid or all solid propellants), this data may be appropriate to inform estimates on the probability of failure for an NE category vehicle. If a proposed NE vehicle is, for example, all liquid propellant, historical data on solid propellant vehicles might not be relevant.

5.5.3 Staged-based Statistics

Upper stages that never fire because the vehicle was destroyed in the previous stage/phase gain no stage reliability information from that launch. If you use stage data that is conditional on the stage operating, you can develop the probability of failure for a stage either by using the entire data set to compute the overall probability of failure for the vehicle in a top-down manner, or by using a subset relevant to each stage to develop a stage-based bottom-up approximation.

Table 5-3 and Table 5-4 provide a summary and sample statistical analysis results for the data presented in Table 5-1 and Table 5-2 based on stage reliability. The empirically based statistical results in Table 5-3 and Table 5-4 provide a basis for a valid failure probability estimate for the first launch of vehicles developed by new and experienced developers if it can be demonstrated that the subject vehicle was developed and launched under similar circumstances.

Table 5-3. First Launch History for New ELVs from New Developers

Stage of flight	No. of vehicles	No. of flights terminated	No. of flights with degraded performance	Stage failure probability	90% confidence bounds	Vehicle failure probability	90% confidence bounds
1	14	6	0	0.43	0.22 to 0.65	0.43	0.22 to 0.65
2	8	3	0	0.38	0.15 to 0.75	0.38	0.15 to 0.75
3	5	2	0	0.40	0.11 to 0.75	0.40	0.11 to 0.75
4	0	0	0	-	-	-	-
Total vehicle	**14**	**11**	**0**	**0.79**	**0.58 to 0.92**	**0.79**	**0.58 to 0.92**

Table 5-4. First Launch History for New ELVs from Experienced Developers

Stage of flight	No. of vehicles	No. of flights terminated	No. of flights with degraded performance	Stage failure probability	90% confidence bounds	Vehicle failure probability	90% confidence bounds
1	24	2	2	0.08	0.02 to 0.22	0.17	0.08 to 0.32
2	22	3	0	0.14	0.05 to 0.29	0.14	0.05 to 0.29
3	18	2	1	0.11	0.03 to 0.28	0.17	0.06 to 0.35
4	8	0	1	0.00	0.02 to 0.30	0.13	0.08 to 0.68
Total vehicle	**24**	**7**	**4**	**0.29**	**0.17 to 0.45**	**0.46**	**0.26 to 0.63**

Notes on Table 5-3 and Table 5-4:

1. The vehicle failure probability is not the sum of the stage failure probabilities, but rather the ratio of the sum of terminations in all of the stages of flight to total launch attempts.
2. The confidence bounds are based on Bernoulli trials, i.e., random sampling of independent random variables all having the identical failure probability. This is not true of the diverse launch vehicles being sampled here. Therefore, consider the confidence bounds as indicative rather than precise.

Guidance system failures are not necessarily applicable to a single stage, but rather to the whole system. In the interests of simplicity, we ignored that fact and treated the guidance failures as stage failures in Table 5-3 and Table 5-4.

5.5.4 Distinguishing Between New and Derived Vehicles

Determining whether to treat a launch vehicle as new or derived can be complicated due to the evolutionary nature of launch vehicles and the use of vehicle stages with previous flight experience. Because integrating launch vehicle systems can be so important, even a vehicle built entirely of subsystems or even entire stages that have flown successfully in the past may be most appropriately treated as new. When determining whether to treat a launch vehicle as new or derived consider the degree of change in each stage to–

1. The structural elements of a vehicle, especially the first stage since this is when loads are generally the highest,

2. Propulsion, including strap-on rockets,

3. The vehicle guidance and control system, assuming that the absence of changes does not leave latent errors to cause new hazards,

4. The payload fairing,

5. The vehicle performance, in terms of payload equivalent weight to low earth orbit (LEO), to geosynchronous transfer orbit (GTO), or total impulse as appropriate for the vehicle,

6. The dynamic environment, in terms of loads, accelerations, vibrations, and velocity attained.

Vehicle or stage performance is perhaps the most easily quantifiable parameter. Performance data are usually readily available, and the desire for increased performance is the most common reason for significant vehicle modifications. A key consideration is how much weight to assign to performance changes. While most major modifications produce fairly large performance changes, there are exceptions. The Ariane 5 EC-A version of the Ariane 5 produced a 56% increase in vehicle performance, while the fairly complex modification of the Japanese H-2, the H-2A, resulted in only a 4% performance increase. This issue is complicated by the fact that a number of boosters, such as the Ariane 4 series, the Atlas V, and the Delta IV, have been designed from the start with stepped, incremental performance capabilities in mind. In those cases, adding strap-on rocket motors can produce impressive performance increase without the any real changes to the booster systems. However, such a large increase in performance can mean that at least some stages of the vehicle operate in a much more challenging flight environment, over and above the purely new aspects of the modifications. In developing the data presented above, any design modification(s) that corresponded to more than a 100% increase in performance led to designating a launch vehicle as new. The perceived need for a demonstration or test flight is another indicator that modifications are substantial enough to warrant new launch vehicle status, such as the difference between a Delta IV Medium and a Delta IV Heavy.

5.6 Methods to Estimate Vehicle Failure Probability

The following subsections present acceptable methods to estimate vehicle and vehicle stage failure probabilities. You can base allocating the failure probability to flight times and vehicle response modes on either the detailed reliability analyses or the historical experience of other vehicles as described in Section 5.6.

5.6.1 Top-Down Approach for a Whole Vehicle

The top-down approach uses the binomial distribution and the failure-success experience of the subject vehicle after two launches. It also uses the demonstrated flight experience of vehicles developed and launched under similar circumstances before the first two launches, as explained in detail in [7].

The top-down approach can develop success-failure predictions for the first two launches of a new launch vehicle based on the data, such as shown in Table 5-1 and Table 5-2. To ensure a reasonably conservative estimate that adequately provides for public safety, use the upper 60% confidence limit of the binomial distribution. Include the historical data on all previous flights of a vehicle developed and launched under similar circumstances as the reference value[7] to predict the total vehicle failure probability for NN and NE launch vehicles.

After the second launch, you may use Figure 5-1 with the subject vehicle's own experience to estimate the failure probability for the next launch. Use the mid-point of the 60% confidence limits to establish a reference (or default) value for the vehicle failure probability. A flight safety analysis should use this reference value for the launch vehicle failure probability, based on the outcomes of all previous flights of the subject vehicle, unless an adjustment is warranted (see paragraph 6.0 of [7]). For example, one can use the values in the row labeled Launch Number 3 of this table to estimate the failure probability for the third launch. This method uses confidence limits based on the binomial distribution. Because this method treats launch vehicles as Bernoulli trials, which is never exactly true, the confidence bounds in Figure 5-1 are only indicative of the true confidence bounds. Reference [7] states (with some minor modifications).

> *After two launch attempts, the analysis uses the reference value for the launch vehicle failure probability of Figure 5-1 based on the outcomes of all previous flights of the subject vehicle. The FAA may adjust the failure probability estimate to account for evidence obtained from the flight history of the vehicle, corrective actions taken in response to a failure of the vehicle, or other vehicle modifications that may affect reliability. The FAA may adjust the failure probability estimate to account for the demonstrated quality of the engineering approach to launch vehicle processing, and associated hazard mitigation. The analysis should use a final failure estimate within the confidence limits of Figure 5-1. Values listed on the far left of Figure 5-1 apply when no launch failures are experienced. Values on the far right apply when only launch failures are experienced. Values in between apply to flight histories that include both failures and successes.*
>
> *For a launch vehicle with at least 2 flights completed, the FAA will accept a Bayesian estimate based on a uniform prior distribution of one hypothetical failure in two hypothetical flights updated with the outcomes of all previous flights of the subject vehicle.*

[7] A reference value is the estimated launch vehicle failure probability for the first two flights unless adjustments away from the reference value are justified to account for particular circumstances as explained in [7].

Next Launch	<--------Success					Failure ------->					
					0.55	0.89	1.00				
3					**0.28**	**0.50**	**0.72**				
					0.00	0.11	0.45				
				0.42	0.71	0.93	1.00				
4				**0.21**	**0.39**	**0.61**	**0.79**				
				0.00	0.07	0.29	0.58				
			0.33	0.58	0.79	0.95	1.00				
5			**0.17**	**0.32**	**0.50**	**0.68**	**0.83**				
			0.00	0.05	0.21	0.42	0.67				
		0.28	0.49	0.67	0.83	0.96	1.00				
6		**0.14**	**0.27**	**0.42**	**0.58**	**0.73**	**0.86**				
		0.00	0.04	0.17	0.33	0.51	0.72				
	0.24	0.42	0.59	0.73	0.86	0.96	1.00				
7	**0.12**	**0.23**	**0.36**	**0.50**	**0.64**	**0.77**	**0.88**				
	0.00	0.04	0.14	0.27	0.41	0.58	0.76				
	0.21	0.37	0.52	0.65	0.77	0.88	0.97	1.00			
8	**0.10**	**0.20**	**0.32**	**0.44**	**0.56**	**0.68**	**0.80**	**0.90**			
	0.00	0.03	0.12	0.23	0.35	0.48	0.63	0.79			
	0.18	0.33	0.46	0.58	0.70	0.80	0.90	0.97	1.00		
9	**0.09**	**0.18**	**0.28**	**0.39**	**0.50**	**0.61**	**0.72**	**0.82**	**0.91**		
	0.00	0.03	0.10	0.20	0.30	0.42	0.54	0.67	0.82		
	0.16	0.30	0.42	0.53	0.63	0.73	0.82	0.91	0.98	1.00	
10	**0.08**	**0.16**	**0.26**	**0.35**	**0.45**	**0.55**	**0.65**	**0.74**	**0.84**	**0.92**	
	0.00	0.02	0.09	0.18	0.27	0.37	0.47	0.58	0.70	0.84	
	0.15	0.27	0.38	0.48	0.58	0.67	0.76	0.84	0.92	0.98	1.00
11	**0.07**	**0.15**	**0.23**	**0.32**	**0.41**	**0.50**	**0.59**	**0.68**	**0.77**	**0.85**	**0.93**
	0.00	0.02	0.08	0.16	0.24	0.33	0.42	0.52	0.62	0.73	0.85
	0	1	2	3	4	5	6	7	8	9	10

Failures on Previous *n* Launches

Figure 5-1. Reference Estimates and Confidence Limits for the Failure Probability

Notes supporting the figure:

1. Reference values are the center values in each vertical trio of numbers.
2. Upper and lower confidence limits are shown directly above and below each reference value.
3. Upper and lower confidence limits are based on 60% two-sided confidence limits of the binomial distribution. For the special cases of zero or N failures in N launch attempts, the upper and lower confidence limits are based on the 80% one-sided confidence limit, respectively.
4. For the special cases of zero or N failures in N launch attempts, the reference values are the midpoint between the 80% one-sided confidence limit of the binomial distribution and zero or one, respectively.

After considering numerous alternative approaches and a variety of important factors, the FAA chose to use 60% confidence limits of the binomial distribution to derive failure probability estimates for launch vehicles. Specifically, the FAA specifies the midpoint between the 60% two-sided confidence limits of the binomial distribution and the

outcomes of all previous launches, as a reference value. The CSWG confirmed that the ranges have used the midpoint between various confidence limits of the binomial distribution in numerous past launch vehicle failure probability estimates. The FAA is aware that operators have used many other methods to estimate the failure probability of launch vehicles. However, the FAA found that the midpoint between various confidence limits of the binomial distribution is a common method used in numerous past launch vehicle failure probability estimates.

The FAA considered using 50% confidence limits of the binomial distribution. However, that creates the potential for non-conservative estimates in the case of zero failures. For example, after only five flights without a failure the midpoint between the 50% confidence bounds is 0.07. However, if the true failure probability is 0.1 for each flight, then there is a 59% chance that no failure will occur within the first five flights. Thus, in this case, the 50% confidence bounds would lead to a probability of failure estimate of 0.07, which is less than 0.10, even though zero failures in five flights is an expected outcome when the true failure probability is 0.10. This example shows that using the midpoint between the 50% confidence bounds is likely to produce a higher failure probability estimate in cases where no failures occur within the first few flights. Thus, the FAA decided against proposing the midpoint between the 50% confidence bounds because of the high priority placed on protection of the public.

The case of zero failures renders unusable a method that based launch vehicle failure probability on the classical Maximum Likelihood Estimator (MLE) values [11]. The MLE value for k failures in N launches is given by:

$$MLE = \frac{k}{N}.$$

Therefore, if a launch vehicle flight history included zero failures, then the MLE value is zero. This result would imply that there was no risk in overflight of major cities as long as a vehicle has not experienced a failure. However, assuming a launch vehicle history made up of Bernoulli trials, a vehicle with a true failure probability of 0.1 has a 59% chance to demonstrate a flight history of zero failures after five flights. Even though the MLE might be more accurate (except in cases with all failures or all successes), the mid-point of the 60% confidence bounds of the binomial distribution provides a conservative estimate for cases where that conservatism is justified to ensure adequate protection of the public: if there are relatively few failures and many successes. Thus, the FAA rejected an MLE method for new launch vehicle failure probability estimates based on the potential for inadequate protection of the public.

The FAA considered using failure probability estimates based on the 50% confidence level upper bound itself. Using the 50% confidence level upper bound itself as an estimate of failure probability would avoid the potential non-conservatism in the case of all successes. However, using the 50% confidence level upper bound of the binomial distribution leads to potential logical inconsistencies. For example, after ten launches and one failure the 50% confidence level upper bound of the binomial distribution would be lower than after nine launches and no failures. Furthermore, using 50% confidence level

upper bound with mixed flight results may produce excessively conservative estimates. For example, after only one failure in the first five flights the 50% confidence level upper bound is 0.39.

The top down method has several strengths and weaknesses. Strengths include:

1. it is easy to understand,
2. implementation is very straight forward,
3. it does not require the effort associated with a traditional reliability or PRA analysis, and
4. it uses only the flight experience of the whole vehicle, and so does not require differentiation between the experiences of different vehicle stages.

In some cases, it can be difficult to discern the relevance of a particular failure to various vehicle stages or to major subsystems for RLV's, such as a guidance failure where the same guidance system is used for multiple stages. Weaknesses of top down methods include

1. uncertainty associated with allocating failure probability to flight times and failure response modes using historical data for vehicles developed and launched under similar circumstance,
2. statistical uncertainty,
3. uncertainty in the applicability of past events to the subject vehicle, and
4. perhaps more importantly, this method does not consistently evaluate a vehicle made up of stages with widely different launch histories.

EXAMPLE: Top-Down Probability of Failure

The following example demonstrates how a flight safety analysis may determine a top-down vehicle total probability of failure estimate from historical launch data. This example uses a hypothetical two-stage, all solid propellant launch vehicle called the *Astrocraft 1* that is being prepared by a U.S. company for its first flight. The *Astrocraft 1* is a new launch vehicle developed by a new vehicle manufacturer.

Based on the discussion above, use the data for the first two launches of the vehicles described in Table 5-1 to identify existing vehicles most similar to the *Astrocraft 1* in the way in which they were launched and developed. Of the 16 vehicles listed in Table 5-1, 13 failed on their first flight and 7 on the second flight (of those flown more than once), producing a total of 20 failures in 26 launches.

Based on this data, use the FAA's Guide to Probability of Failure Analysis for New Expendable Launch Vehicles to identify a reference value and 60% upper and lower confidence bounds for the total vehicle failure probability estimate. Table A of the guide provides estimates up to only the 11th flight. Compute the reference value and 60% confidence bounds for a 27th flight using the following equations.

Upper Bound	Lower Bound
$v_1 = (2 \times N_F) + 2 = 42$	$v_1 = 2 + (2 \times N_T) - (2 \times N_F) = 14$
$v_2 = (2 \times N_T) - (2 \times N_F) = 12$	$v_2 = (2 \times N_F) = 40$
$\alpha = \frac{(1-C)}{2} = \frac{(1-0.6)}{2} = 0.2$	$\alpha = \frac{(1-C)}{2} = \frac{(1-0.6)}{2} = 0.2$
$F = FINV(\alpha, v_1, v_2) = 1.574$	$F = FINV(\alpha, v_1, v_2) = 1.396$
$P_{up} = \frac{(N_F + 1)F}{(N_T - N_F + (N_F + 1)F)} = 0.846$	$P_{low} = \frac{N_F}{(N_F + (N_T - N_F + 1)F)} = 0.672$

In these equations, v_1 and v_2 represent the number of degrees of freedom in the F-distribution denoted as *F*, *C* represents the confidence bounds applied, α represents the probability of obtaining a value beyond these bounds, and *FINV* represents the inverse of the *F* distribution (computed in Microsoft EXCEL© using the built-in FINV function). The midpoint between the upper and lower bounds represents the reference value.

$$P_{mid} = P_{low} + \frac{P_{up} + P_{low}}{2} = 0.759$$

Based on the guidance in *Guide to Probability of Failure Analysis for New Expendable Launch Vehicles*, the 60% upper confidence bound determined in the manner above should be used as the total probability of failure estimate for a launch vehicle that has not yet completed two flights.

$$P_F = \mathbf{0.846}$$

5.6.2 Top-Down Approach for a Vehicle Stage

Some vehicles are not all new. For example, a vehicle might have a first stage that has flown previously and failed such that the upper stage had no flight experience. As discussed in Sections 5.4 and 5.5, determining what constitutes a new vehicle can be complicated due to the evolutionary nature of launch vehicles, the use of vehicle stages with previous flight experience, system interdependencies, and the critical importance of system integration to the success of a launch vehicle.

For a vehicle made up of stages with widely different launch histories, it may be reasonable to apply the top down approach to each vehicle stage. By treating the vehicle by stage, the empirical evidence on the failure probability of stages with different demonstrated flight histories can be accounted for readily. For example, obtain a failure probability estimate for an upper stage with no flight experience, developed by an experienced manufacturer, from world-wide experience with vehicles developed and launched under similar circumstances. Samples appear in

Table 5-4. Use Figure 5-1 to evaluate a failure probability estimate for a more mature first stage, with more than two flights, based on direct flight experience .

Use a probability tree to develop the overall vehicle failure probability estimates for input to a QRA. Figure 5-2 is a sample probability tree that demonstrates this method for a vehicle with three stages. Assume for simplicity to illustrate the effect of conditional failure probability estimates on the probability of failure for the whole vehicle that empirical evidence indicates that each stage has a failure probability of 0.1 *given* that the previous stage is successful. Note that the total probability of failure for such a three stage vehicle is about 0.27, which is less than the sum of the failure probabilities for the three stages (i.e. 0.3). For vehicles with higher stage failure probabilities this effect becomes more significant.

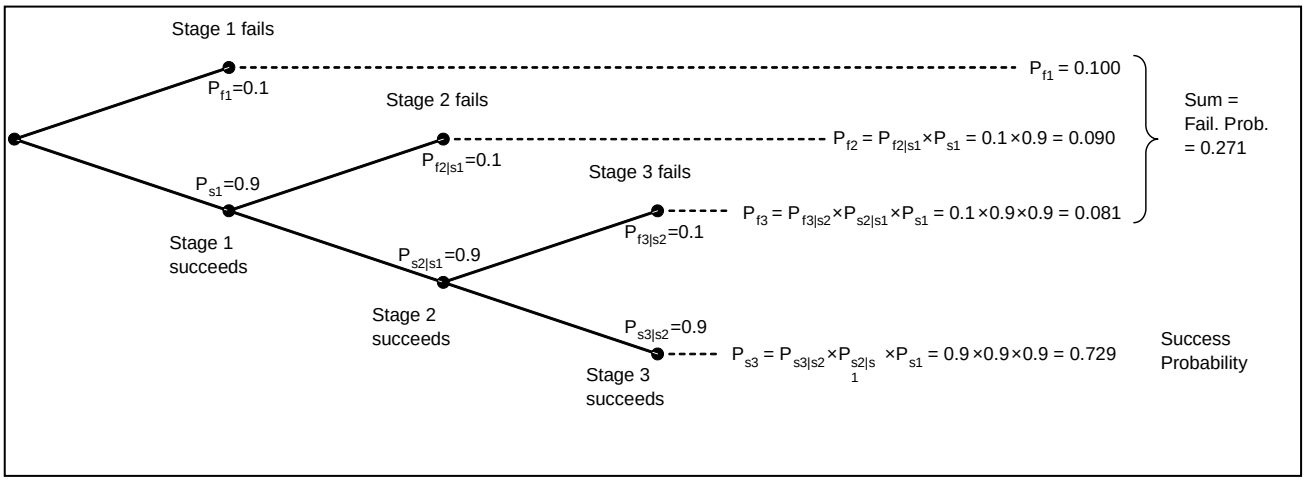

Figure 5-2. Sample Launch Failure Probability Tree

5.6.3 A Bayesian Method

You can apply this method at the whole vehicle level or at the vehicle stage level in order to allow stages to accumulate their own failure-success history. Like the top-down approach, it does not require the effort associated with a traditional reliability or PRA analysis. It uses statistics rooted in the launch history of vehicles developed and launched under similar circumstances. However, it may start with a more refined Bayesian prior prediction for each stage as explained below.

The basic definitions used in the model are as follows.[8]

R is defined as the number of actual failures in n attempts of the subject vehicle

$\frac{r}{n}$ is the point estimate (mean) of the failure probability based on the available data on the subject vehicle only

The problem is that r and n may be very small numbers – perhaps zero when the subject vehicle is new. Thus, in order to get started, provide surrogate data based on relevant similar conditions or even based on opinion – or both. Let n' be the number of surrogate events and r' be the number of surrogate failures, typically taken from the historical experience of vehicles developed and launched under similar circumstances. The ratio of $\frac{r'}{n'}$ is an estimate of the failure probability based solely on this surrogate data. This is the Bayesian prior estimate. (The uncertainty distribution associated with this may be represented with a beta distribution – also referred to as the conjugate prior.)

The next step is to combine the subject vehicle data with the surrogate data to establish a better estimate of reality, referred to as the Bayesian posterior estimate. This is accomplished simply by adding the surrogate (prior) data to the actual subject vehicle data to get the posterior data, which denoted by double prime notation such that the n'' and r'' are the posterior estimates. Therefore: $n'' = n' + n$ and $r'' = r' + r$. The posterior estimate of the failure probability, $\frac{r''}{n''}$, is the point estimate (mean) of the failure probability for the vehicle based on all the available data. The posterior uncertainty distribution may be represented with a beta distribution, as described below.

For new vehicles, historical data can be used as the prior, and actual experience can be added to get posterior estimates of the ratio of failures to the number of launches. As the number of launches increases, the n and the r increase according to the success of the vehicle. However, the prior values, r' and n', remain constant and if they are large numbers, e.g., $r' = 10$ and $n' = 100$ (i.e., $\frac{r'}{n'} = 0.1$), the posterior values, r'' and n'' hardly change because the prior experience totally dominates the actual experience. This particular case is known as a strong prior and it will influence the posterior estimates long

[8] See a reference such as *Statistics: Probability, Inference and Decision* by Robert L. Winker and William L. Hays, published by Holt, Rinehart and Winston, New York, 1975, for further explanation.

after the apparent true failure probability is known. Thus, it is desirable to have the influence of the prior diminish rapidly as you obtain real launch experience.

As an example to illustrate this aspect of a Bayesian method, accomplish this decrement by maintaining the ratio, e.g., $\frac{r'}{n'} = 0.1$, but artificially reducing n' to 1 (or a similar small value), and proportionally reducing r' (in this case to 0.1 to maintain $\frac{r'}{n'} = 0.1$). This starts the prediction when there is no actual launch experience for the vehicle and the influence of the weaker prior diminishes more rapidly with ensuing launches so that the real experience dominates in the long run. The most appropriate choice for the strength of the prior estimate, reflected by the value n' used, is debatable and related to determining the relevance of the available historical data to a particular new vehicle or new stage.

To illustrate this method, consider a new three-stage vehicle developed by a new developer. Each stage, "i," will have a prior failure probability, p_i'. If the data presented in Table 5-3 is representative of vehicle developed and launched under similar circumstances, then $p_1' = 0.43$, $p_2' = 0.38$ and $p_3' = 0.40$. Figure 5-3 demonstrates the computation of estimated total vehicle failure probability using the prior estimates of the stage failure probabilities. Note that

$$P_{F(Total\ Vehicle)} = 1 - P_{S_1'} \times P_{S_2'|S_1'} \times P_{S_3'|(S_2' \cap S_1')}$$

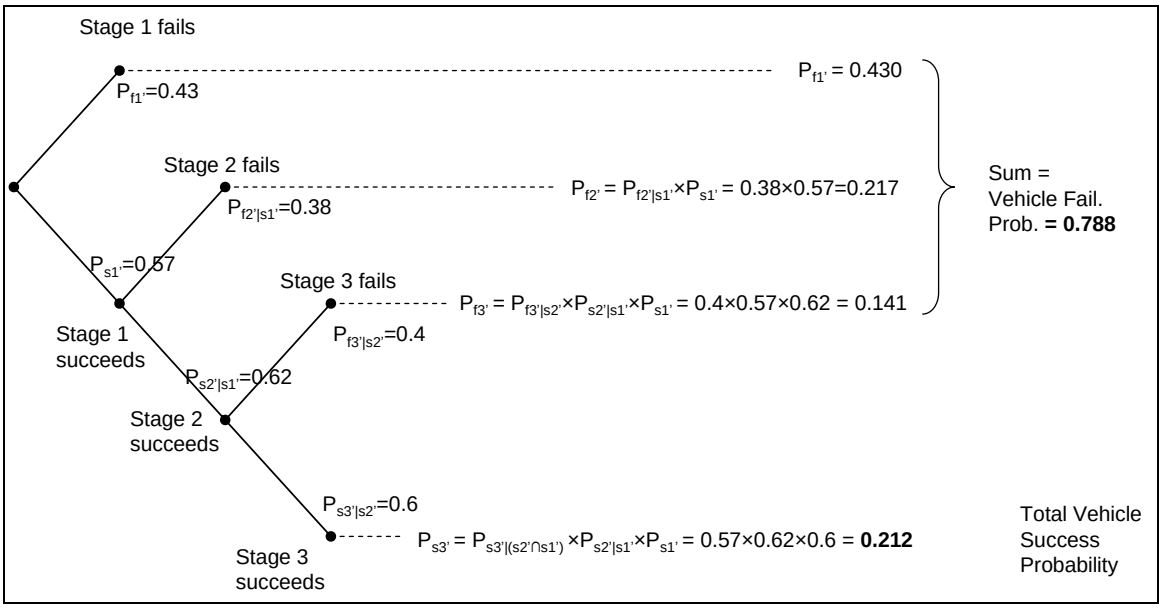

Figure 5-3. Probability Tree Demonstrating the Computation of Total Vehicle Failure Probability Based on "Prior" Failure Probability Estimates for Each Stage

Since $p_i' = \frac{r_i'}{n_i'}$, any combination of r_i' and n_i' that produces p_i' is theoretically feasible. However, to begin with an appropriate value based on historical experience with similar vehicles, and yet have the influence of the prior be weak as the flight history advances, n' should be small and r' should be derived from the product, $r' = n' \times p'$. Often $n' = 1$ is a satisfactorily small value.

We present sample calculations at the end of this subsection to demonstrate the complete implementation of this method. Specifically, an example demonstrates how this method will support an analysis where the failure probability of the stages of the vehicle are each assigned their own prior $\frac{r'}{n'}$ and then are evaluated through the flight history of the total vehicle. Thus, this method can explicitly account for the fact that the second stage of an entirely new vehicle that fails during first stage flight still has no flight experience per se. Thus, when advancing through the flight history of a vehicle, the number of attempts for a stage is generally the total number of launches to that point minus the number of failures of lower stages.

As long as the prior has non-zero values for r' and n', this method will produce a non-zero estimate of the probability of failure, regardless of whether there is any failure in the launch sequence. However, an entirely new launch vehicle launched several times without failure is an important special case. In such a case, this method can produce non-conservative estimates of the failure probability if you base the prior on $n' = 1$. In such a case, use a Bayesian estimate based on a uniform prior distribution of one hypothetical failure in two hypothetical flights updated with the outcomes of all previous flights of the subject vehicle.

The beta distribution provides an approximation to the binomial confidence distribution and is very easy to implement in order to estimate what is referred to as a *beta distribution confidence range*. The formula for the beta distribution is

$$f(x;\alpha,\beta) = \frac{x^{\alpha-1}(1-x)^{\beta-1}}{\int_0^1 u^{\alpha-1}(1-u)^{\beta-1}\,du} \quad \text{where } 0 \le x \le 1 \text{ and } \alpha \text{ and } \beta \text{ are parameters} > 1$$

When used as a Bayesian conjugate distribution, $\alpha = r$ and $\beta = n - r$. The x in the equation can represent the vehicle (or stage) failure probability.

Another feature that is important with this Bayesian method is the treatment of stages that have different histories joined in the same vehicle. The term hybrid vehicle describes this situation. You may join a new stage with a stage that has an extensive previous flight history. For example, consider a new vehicle that has a new first stage joined with a second stage that has flown successfully 9 times in its first 10 launches before being joined with the new first stage. Assume that this is a new developer that has acquired the stage. Assume the first stage has a prior failure probability of 0.41 and the second stage

will have a prior failure probability of 1/10 = 0.1 based on real flight experience. Ignore, for now, the fact that a new developer could adversely affect the reliability of a mature stage. In this case, there are no failures in five flights. Figure 5-4 shows the results of the weak Bayesian method applied by stage for this example. The first launch shows a high probability of failure because of the first stage, but as the first stage succeeds, its failure probability drops and consequently the whole vehicle's failure probability drops. The second stage failure probability does not drop as much because it has its own flight history from the prior, which has one failure.

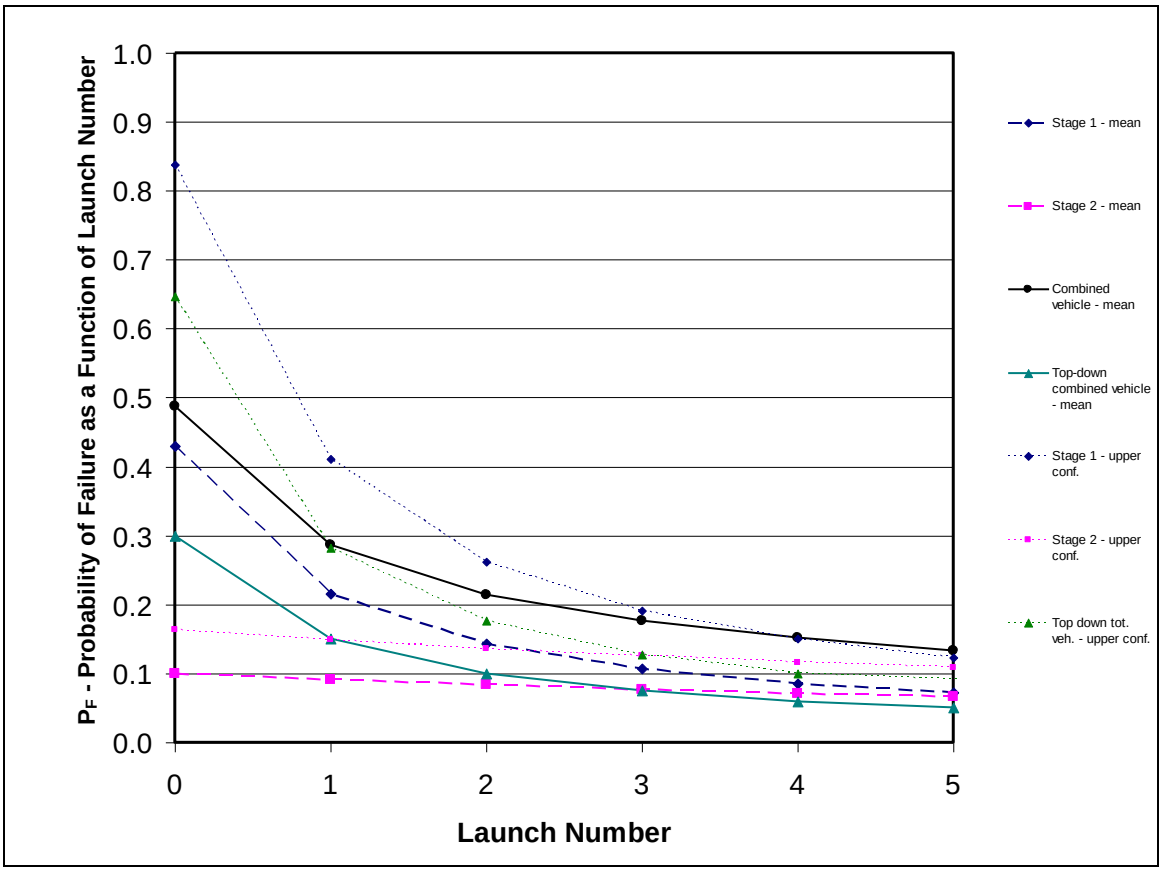

Figure 5-4. Launch Failure Predictions for a Vehicle Composed of Both a New and a Mature Stage

The Bayesian method with a weak prior has several positive and negative aspects. On the positive side,

1. it is easy to understand,
2. it is fairly straight forward to implement,
3. it does not require a traditional reliability or PRA analysis,
4. it produces estimates consistent with historical flight experience, and
5. it includes an uncertainty model that may be useful in MPL analyses.

Drawbacks include

1. the differentiation between the experiences of different vehicle stages is, of course, necessary to take advantage of the ability to account for different flight histories for various vehicle stages. These can be difficult in some cases, such as where a guidance failure occurred and the same guidance system was used for multiple stages.
2. the uncertainty associated with allocating failure probability to failure response modes using historical data for vehicles developed and launched under similar circumstance,
3. statistical uncertainty as well as uncertainty in the applicability of past events to the subject vehicle, and
3. most importantly, the most appropriate strength of the prior estimate is debatable.

Other approaches to the prior estimate have been used, including the uniform prior and Jeffreys prior. The uniform prior uses one failure in two attempts as mentioned in the FAA *Guide to Probability of Failure Analysis for New Expendable Launch Vehicles*. The Jeffreys prior uses a half a failure in one attempt, which a weak and non-informative prior estimate designed to provide maximum responsiveness to the data used for the update.

EXAMPLE Probability of Failure Allocation Using the Bayesian Method

This example considers a new, three stage launch vehicle called the *Astrocraft 6*, developed by a new manufacturer (NN) with the following flight history: a failure during Stage 1 in the first launch, a failure during Stage 2 in the second launch, no failure in the 3rd launch, and a Stage 3 failure in the 4th launch, and no failure in the 5th launch. Table 5-5 summarizes this data. Hypothetical historical data of the flight histories of launch vehicles developed and launched under similar circumstances is also available.

Table 5-5. Flight History of NN ELV

		Launch Number				
Vehicle	**Category**	**1**	**2**	**3**	**4**	**5**
Astrocraft 6	NN	1t	12t	123s	123t	123s

After the 5th launch, Stage 1 has had 5 attempts plus a prior estimate of 0.43 failures for one launch based on hypothetical flight history based on vehicles developed and launched under similar circumstances. The predicted (posterior) failure probability estimate for Stage 1 after 5 launches is:

$$p'' = \frac{r''}{n''} = \frac{r' + r}{n' + n} = \frac{0.43 + 1}{1 + 5} = 0.238.$$

Stage 2 has no performance in the first launch, but has a failure in the 2nd and no failures in the 3rd, 4th, and 5th. Based on this subject vehicle flight experience and a prior estimate of 0.38 failures for one launch, the predicted failure probability (a posterior) for Stage 2 after the 5th launch is

$$p'' = \frac{r''}{n''} = \frac{r' + r}{n' + n} = \frac{0.38 + 1}{1 + 4} = 0.276.$$

Stage 3 has no performance in the 1st and 2nd launches because a previous stage failed first. Stage 3 has a failure in the 3rd launch and no failures in the 4th and 5th. Based on this subject vehicle flight experience and a prior estimate of 0.4 failures for one launch, the predicted failure probability (a posterior) for Stage 3 after the 5th launch is

$$p'' = \frac{r''}{n''} = \frac{r' + r}{n' + n} = \frac{0.4 + 1}{1 + 3} = 0.35.$$

The total predicted vehicle failure probability after the 5th launch based on the failure probabilities of the three stages is computed by the formula

$$p_T = 1 - (1 - p_1)(1 - p_2)(1 - p_3) = 1 - \prod_{i=1}^{3} (1 - p_i) \text{ which in this case is}$$

$$p_T = 1 - (1 - 0.238)(1 - 0.276)(1 - 0.350) = 0.642.$$

If you consider only the total success/failure ratio for the vehicle as a whole (top down), the predicted failure probability after the 5th launch is

$$p'' = \frac{r''}{n''} = \frac{r' + r}{n' + n} = \frac{0.79 + 3}{1 + 5} = 0.632.$$

Figure 5-5 illustrates the progression of failure predictions from before launch no. 1 to after launch no. 5

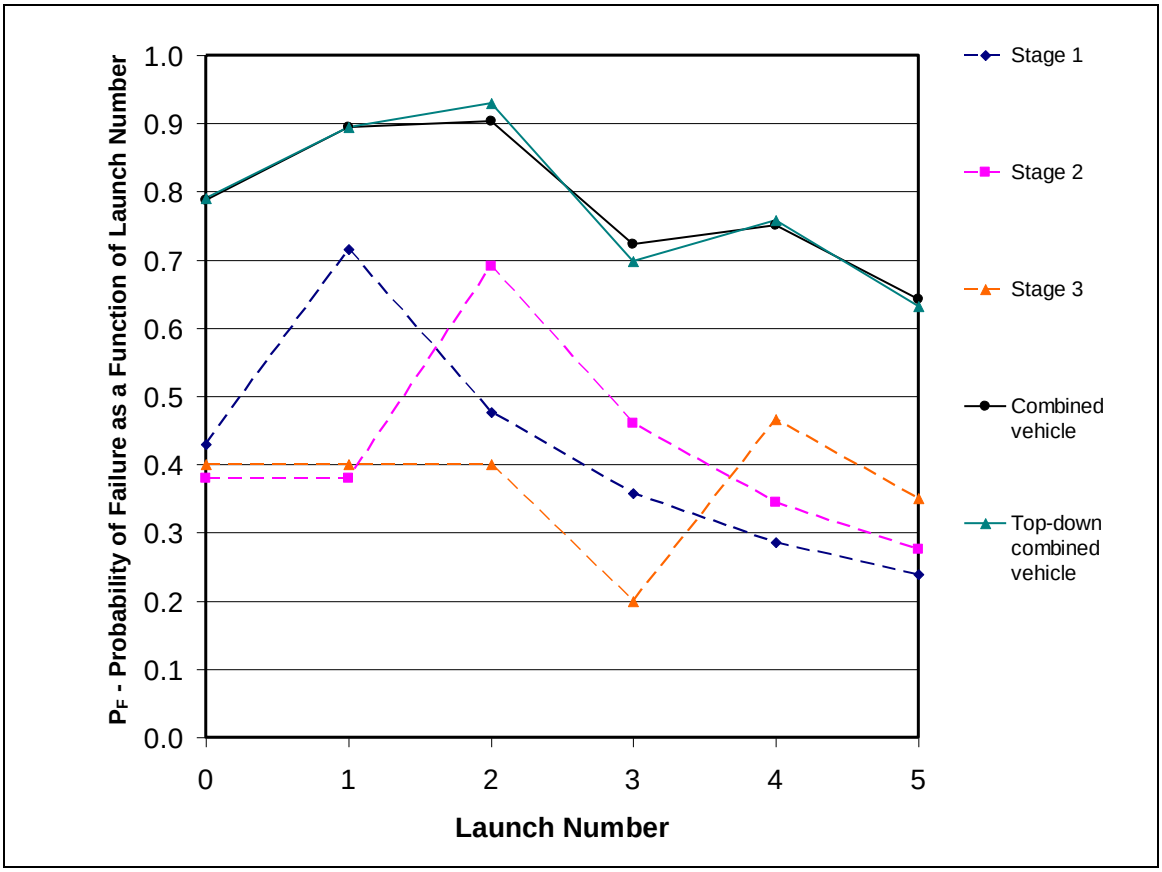

Figure 5-5. Progression of Failure Predictions for a NN Vehicle Using the Bayesian Model

With small values of *n* and *r*, it is clear that there is considerable uncertainty in the estimates of the failure probabilities. Using the beta distribution as a model, you can compute the confidence range using the Microsoft EXCEL© function BETAINV (*probability* ,*alpha*, *beta*, *A*, *B*). *Probability* is associated with the bound of the confidence range (e.g., *probability* = 0.80 is the upper bound of a 60% confidence range), *alpha* = *r*, *beta* = *n* - *r*, *A*=0 and *B*=1.[9] Figure 5-6 illustrates the same problem as in Figure 5-5 except that now the upper bounds (0.80) have been added.

[9] A and B establish the range of the distribution. For this case, A=0 and B=1, representing the range of a probability estimate, 0 to 1.

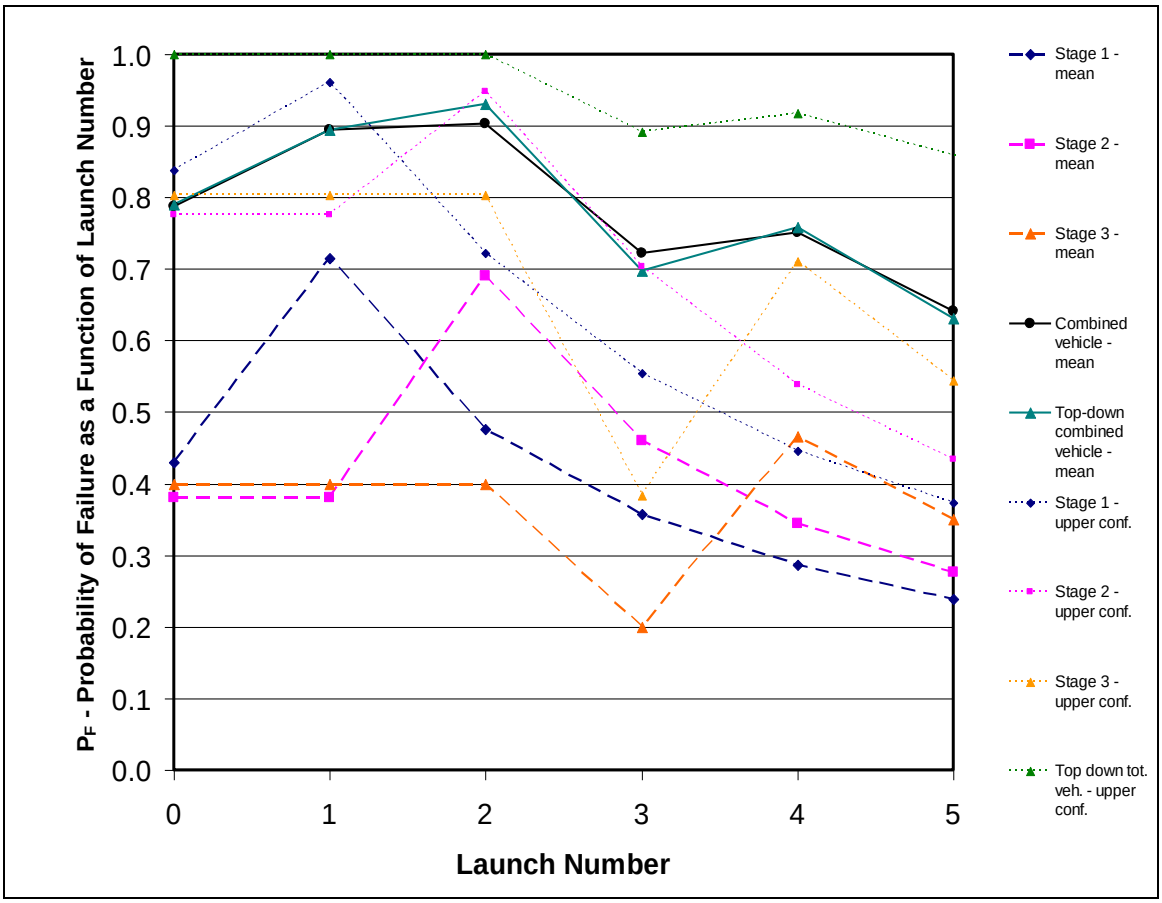

Figure 5-6. Progression of Failure Predictions with Uncertainty for an NN Vehicle Using the Bayesian Model

5.6.4 "Bottom Up" Reliability and PRA Approach

Ideally, careful reliability analysis of the system should allow you to make predictions of the failure probability of the vehicle, and to allocate the failure probability to the appropriate flight times and vehicle response modes used in flight safety analysis. This process is fairly well documented in several FAA and NASA documents: FAA *Guide to Reusable Launch and Reentry Vehicle Reliability Analysis* [6]; FAA *Guide to Probability of Failure Analysis for New Expendable Launch Vehicles* [7]; NASA *Fault Tree Handbook with Aerospace Applications* [4] and NASA *Probabilistic Risk Assessment Procedures Guide* [8].

These bottom-up methods start with the failure probabilities of basic components. They then work upward through subsystems and system until you can define probabilities at the system level and allocate these probabilities to the different failure behaviors of the vehicle that can lead to the vehicle response modes. These other documents describe the procedure. This section begins with a summary of key elements of reliability analysis and then provides a description how it can be used in a flight safety analysis.

The FAA *Guide to Reusable Launch and Reentry Vehicle Reliability Analysis* [6] describes various methods used in reliability analyses. These methods often combine top-down and bottom-up approaches to produce estimates of the relative probability of vehicle failure modes that may be useful in a flight safety analysis. The PRA and Monte Carlo simulation are often the most useful elements of a reliability analysis for the purposes of a flight safety analysis. The FAA *Guide to Reusable Launch and Reentry Vehicle Reliability Analysis* [6] includes an example to demonstrate how you can use a PRA and Monte Carlo simulation to estimate the probability of a failure mode, such as the inability to shut down an engine at the proper time, including the mean value and confidence levels. The FAA guide describes both of these in some detail and includes appendices with examples of approaches used to support an expected casualty analysis. Perhaps most importantly, the FAA Guide shows how different analysis approaches can work together to produce a valid analysis assessment of system reliability.

The PRA process contains key elements from NASA, the nuclear industry, commercial aircraft, and military aerospace approaches to analyzing risk and reliability for complex systems. A PRA examines the sequence of events (scenarios) that can lead to failure, develops failure models to analyze those scenarios, and then analyzes the effects of uncertainty of the models and input parameters on the failure probability estimates. Figure 5-7 shows the steps in the PRA approach as defined in reference [6].

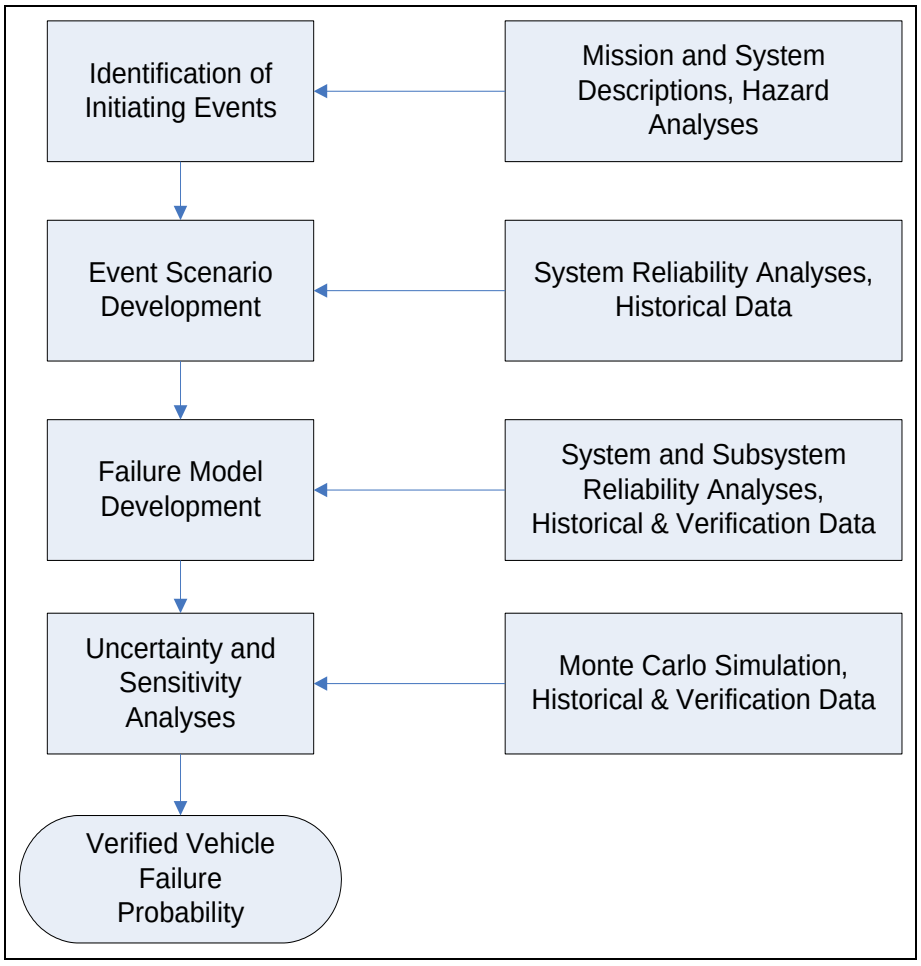

Figure 5-7. Probabilistic Risk Assessment

1. Identify specific system and mission parameters, such as vehicle configuration, phases of flight, and methods of operation.

2. Identify initiating events. Initiating events are the triggering events in sequences of events (scenarios) that ultimately lead to either successful or unsuccessful states, such as mission success with no impact on public safety or abort to landing site. An initiating event can be normal operation, such as launch, or an anomalous event, such as valve sticks. You can use Preliminary Hazard Analyses, Preliminary Hazard Lists, and FMECA in identifying the initiating events. Initiating events can also arise from nominal and non-nominal system functions, such as engine shutdown or failure of software to close valve when commanded.

3. Develop scenarios that can lead to the defined end states once you identify the initiating events. Acceptable methods for developing event scenarios include ETA and event sequence diagrams (ESD). The event scenarios start with the initiating event and progress through what are known as pivotal events until an end state is reached. Pivotal events are those successes and failures that can ultimately lead to the success of a mission or a mishap. In other words, a pivotal event is the first in a

sequence of events that lead to the mishap or success scenario. An example of a pivotal event might be failure of thrust termination system.

4. Develop failure models for pivotal events from these event scenarios. A failure model describes how a pivotal event occurs. The FTA is the top-down system reliability analysis normally used to develop system failure models of pivotal events in the ETA or ESD. You can use bottom-up techniques, such as FMECA and reliability block diagram (RBD), to assist in developing the failure models. Collect and analyze the data for use in quantifying the failure models. This data includes probabilities for component failures, structural failures, human errors, process failures, and common causes.

5. Apply uncertainty bounds to input data to account for the uncertainty in the input parameter data. Quantify this uncertainty for the entire system. Use uncertainty analyses, such as Monte Carlo simulation, for analyzing this input parameter uncertainty. You can also analyze model uncertainty using sensitivity analyses.

Obtain the fundamental failure probabilities that are used in reliability analyses either from test information, launch data, or from studies relating failure probability to environmental levels or duration of operation. Unfortunately, these analyses often fail to identify completely the types of human error, either in design or execution, which are often the reason for actual failures of the vehicle. Furthermore, reliability analyses often ignore the potential for software faults and make simplifying assumptions that are not entirely true for a launch vehicle, such as that component failures are independent and occur at a constant rate. Thus, the only place where the entire scope of human error and other complex causes of failures (such as system interdependencies and environmental dynamics) are evident is in the empirical data gathered from launch experience. Thus after the extensive, but often worthwhile, analysis to produce an estimate of the reliability (or conversely the failure probability), the product generally underestimates the failure probability. Even so, the reliability and PRA methods are very important, regardless of the often optimistic result because they help the developer to identify potential failure-prone elements of the system and also to allocate reliability budgets to systems and subsystems. Also, a valid reliability analysis can be an excellent basis for estimating the relative probabilities between failure response modes. However, a valid reliability analysis is generally produced only when the developer/agency has invested a major effort into the development of a detailed reliability model of the vehicle. Examples include the PRA conducted for the Space Shuttle [19]. Even when a valid reliability analysis is available, a flight safety analysis should compare the relative probabilities of the different response modes with those empirically developed from historical launch data to ensure the appropriateness of the application of the final results in analyses intended to demonstrate public safety. You can make adjustments to the results of a reliability analysis to match the demonstrated flight experience of the subject vehicle, or more commonly the experience of vehicles developed and launched under similar circumstances, either by simple scaling or by a Bayesian statistical analysis.

5.7 Probability of Failure Allocation

5.7.1 Allocation to Flight Time

A probability of failure analysis for launch should allocate the chance of failure to flight times between lift-off and orbital insertion to be useful in computing expected casualties. Initial steps involved in such an allocation may be to (1) identify the phases of flight appropriate for a vehicle, and (2) identify the vehicle response modes for each phase of flight that may pose a debris risk. For the purposes of a probability of failure analysis, a flight phase is a period of flight defined by particular system characteristics. For example, flight phases could correspond to the burn times of various vehicle stages and staging period when changes in the vehicle configuration occur.

You may divide a generic launch vehicle flight may be divided into four phases as illustrated in Figure 5-8 and listed in Table 5-6. These four generic flight phases will not be appropriate for all launch vehicles. They provide an illustration to facilitate discussion of acceptable failure probability allocation methods.

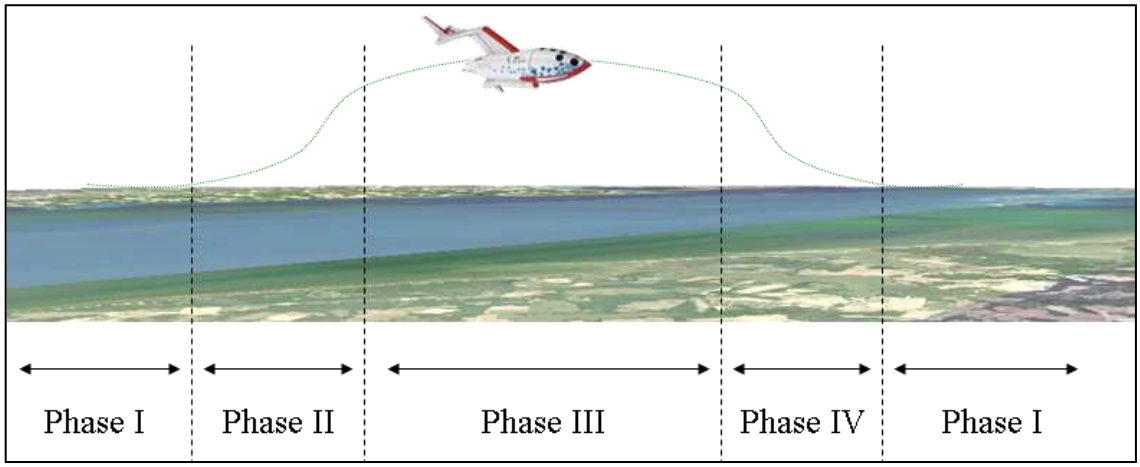

Figure 5-8. Illustration of Four Generic Flight Phases

Table 5-6. Description of Four Generic Flight Phases

Phase	Definition
I	Start-up or shut-down (i.e., ignition, the initiation of flight, vehicle configuration changes and safing after flight)
II	Ascent (i.e., period of ascending flight through a dynamic flight environment)
III	Steady state (i.e., after ascent and before descent)
IV	Descent/reentry (i.e., period of descending flight through a dynamic flight environment)

During thrusting phases of flight, we often model failures as occurring at a constant conditional rate. This means constant with respect to time given that a failure has not already occurred. This is described in some detail below. There are also failures that may occur only at very specific times. These often include planned events such vehicle configuration changes (i.e., staging or any vehicle shape changes such as the jettison of a fairing, etc.). Figure 5-9 is a slightly more elaborate probability tree than that shown in Figure 5-3. It adds a fail/succeed branch for a discrete event: a failure during staging between stages 1 and 2. The branches representing failures during continuous burn could also be further divided into the different failure response modes, such as malfunction turn, loss of thrust, explosion on-course, etc. The event tree described in Figure 5-10, used for Titan IV launch risk analyses, shows some of the detail that can exist in the branches.

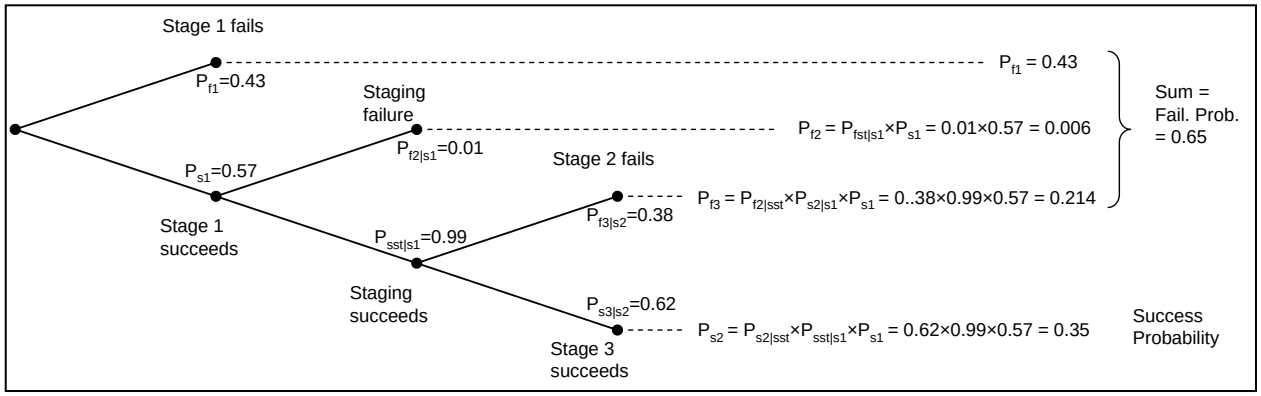

Figure 5-9. Probability Tree with Staging Events

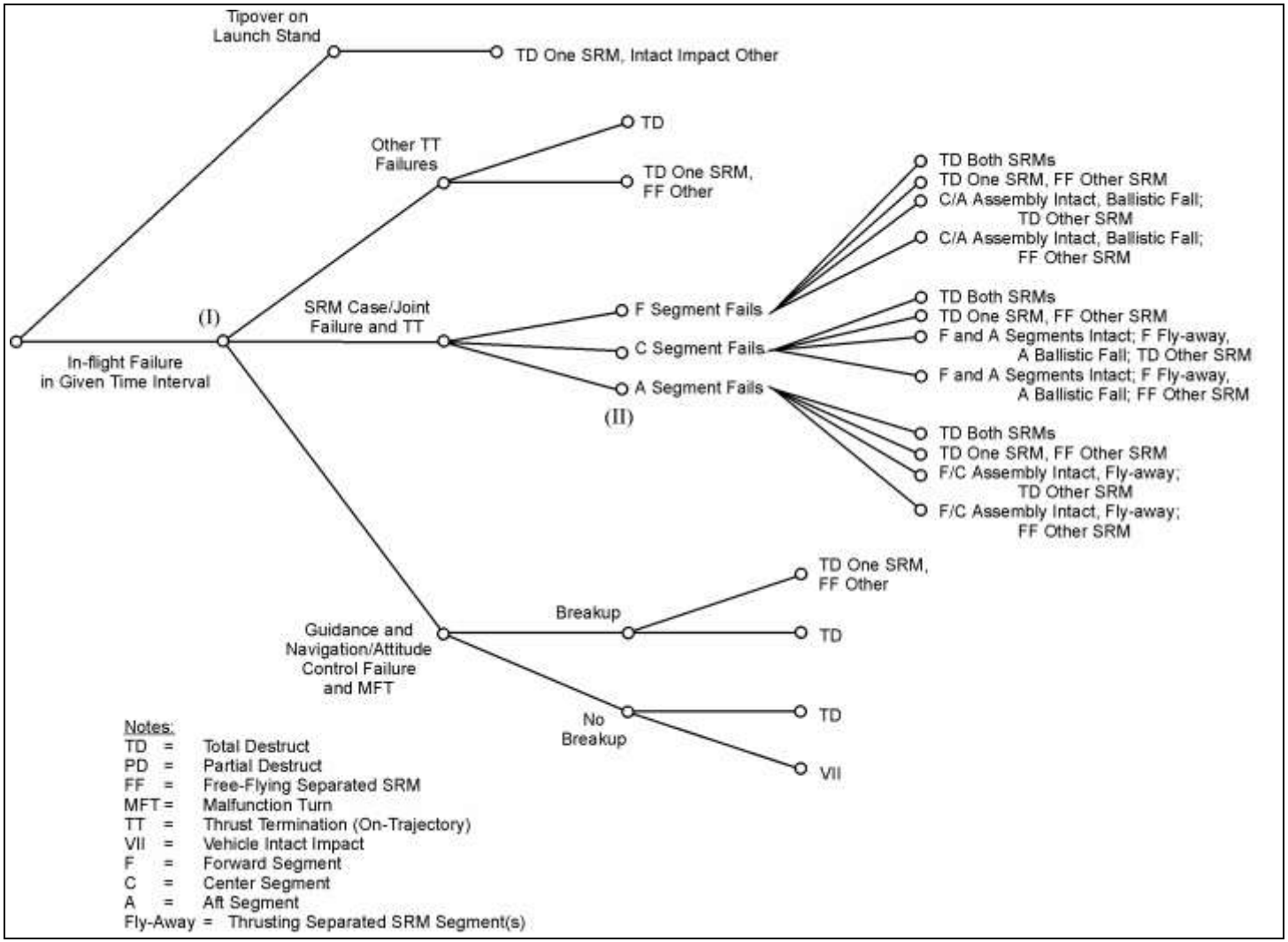

Figure 5-10. Event Tree for an ELV with Three Segment Solid Strap-On Rockets (Titan IV)

During steady state rocket motor burn times, a common assumption is a constant failure rate, i.e., a constant failure probability per burn time. Supporting data on actual flight experience or engine test can help to determine whether the constant rate is appropriate. If there is no evidence of any flight-time peculiar failures, and any observed failures appear purely random, then a flight safety analysis can assume a constant conditional failure rate given that the vehicle has survived up to that point in time.

Let *C* be a constant failure rate given that the vehicle has survived to the current time, *t*. Then the overall failure rate versus time is

$$\varphi(t) = C\left(1 - \int_0^t \varphi(x)dx\right)$$

where $\left(1 - \int_0^t \varphi(x)dx\right)$ is the probability of a stage with a failure rate vs. time of φ(t) having *not* failed at "*t*." [20] Solving for $\varphi(t)$, we obtain $\varphi(t) = C\,e^{-Ct}$ and, for a failure probability of P_f for the entire flight of the stage (*T* seconds), $C = \frac{-\ln(1-P_F)}{T}$.

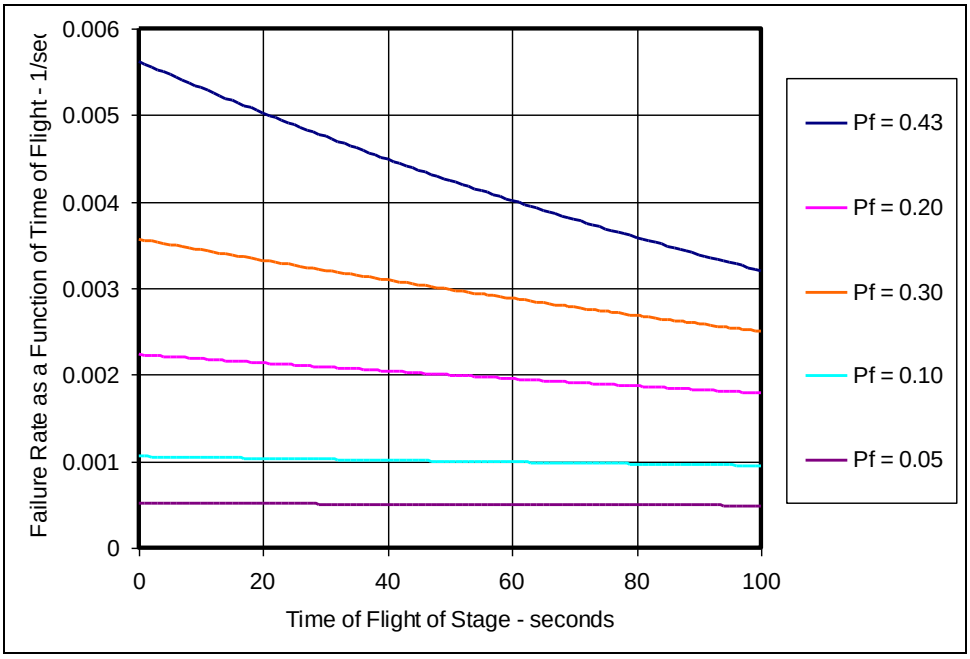

Figure 5-11. Failure Rates vs. Time for Stages with 100 Second Burn Times Having Various Failure Probabilities

Figure 5-11 illustrates the effect of the constant failure rate given that the stage has not yet failed. The effect is very pronounced for stages with high failure probabilities and can be ignored for stages with low failure probabilities. For those stages with high failure probabilities, the effect essentially front-loads the failure. For first stages, this often means that the portion of flight most typically risky to the public (i.e., in the vicinity of

the launch site or shortly after initiation of a new stage) has an even higher effective failure probability.

EXAMPLE: Probability of Failure Allocation By Flight Time

The following example demonstrates how a flight safety analysis may allocate a vehicle failure probability estimate across failure modes and flight times. This example uses a hypothetical multi-stage launch vehicle called the *Astrocraft 6*. The second stage of this vehicle burns for 345 seconds and has a probability of failure of 0.5. You will also find hypothetical historical data with which to determine the allocations.

The failure rate for a system as a function of time, $\lambda(t)$, is equal to the probability that the system will fail during a particular time interval, conditional on it reaching that interval, divided by the length of the interval. You can relate this to its reliability, $R(t)$, as follows:

$$\lambda(t) = -\frac{1}{R(t)}\frac{d}{dt}R(t) \qquad (1)$$

Since $R(t)$ is defined as the probability that a system will operate without failure for an identified length of time, *t*, the probability that a system will fail at a time less than or equal to t is represented as $F(t)$.

A Tier 1 Approach: Uniform Failure Rate

If the failure rate remains constant for all points in time along a trajectory, the probability that the vehicle will fail at or before *t* is related to the uniform failure rate $F(t)$ as follows:

$$F(t) = 1 - e^{-\lambda t} \qquad (2)$$

Industry generally accepts using the uniform failure rate as a reasonable first-order approximation of the failure rate as a function of time when higher fidelity failure data regarding a particular vehicle, stage, or phase of flight is not available. Therefore, if there are no indications that the risk posed to the public would not be underestimated by doing so, a uniform failure rate across a stage is an appropriate assumption for a Tier 1 analysis.

To apply this assumption, first determine the failure probability for the stage using any of the methods described in the preceding section. In this Tier 1 example, assume that the *Astrocraft 6* probability of failure for the second stage is equal to 0.146, and apply this probability over the planned 345 seconds of thrusting flight. Solve for the failure rate using the equation

$$F(t) = 1 - e^{-\lambda t} \qquad (2)$$

$$0.5 = 1 - e^{-\lambda 345} \qquad (3)$$

Solving for the failure rate:

$$\lambda = -\frac{1}{345}\ln(1-0.5) = 2.0x10^{-3} \qquad (4)$$

Thus, the failure rate for the second stage of the *Astrocraft 6* assuming a uniform failure rate and the probability of failure for the stage identified in this Tier 1 method is **$2.0x10^{-3}$**.

A Tier 2 Approach: Variable Failure Rate

If the failure rate varies as a function of time, the vehicle reliability involves an integration:

$$R(t) = 1 - F(t) = \exp\left[-\int_0^t \lambda(t')dt'\right] \qquad (5)$$

If there are multiple independent failure modes, then the system failure rate is equal to the sum of these independent modes:

$$\lambda(t) = \sum_i \lambda_i(t) \qquad (6)$$

Depending on the level of data available, you may employ a failure rate curve to account for infancy, random, and duration failure types (defined below). This Tier 2 method typically uses these three types as defined below. For each failure type, a more advanced method may use a separate Weibull distribution to define the failure rate for each independent failure mode:

$$\lambda(t) = \frac{m}{\theta}\left(\frac{t}{\theta}\right)^{m-1} \qquad (7)$$

As employed in the equation above, the Weibull distribution is dependent on a shape parameter (m) and a scale parameter (θ). The total failure rate for a system if all contributing modes are independent is the sum of all of the independent failure modes. Combining the failure rates and integrating would result in the following, we identify where each type of failure mode by the subscript *a*, *b*, and *c*, respectively:

$$\int_0^t \lambda(t')dt' = \left(\frac{t}{\theta_a}\right)^{m_a} + \left(\frac{t}{\theta_b}\right)^{m_b} + \left(\frac{t}{\theta_c}\right)^{m_c} \qquad (8)$$

By substituting equations into equation (8), we can relate the parameters for each Weibull distribution directly to the probability of failure of the system as a function of time. However, at this point in the analysis, both the probability of failure as a function of time and the Weibull parameters are unknown. At the same time, you will want to find these unknowns associated with a small and censored dataset (i.e., one in which not all tested items are operated to failure) in a manner that retains consistency with:

1. the top-down probability of failure for the entire vehicle,

2. the allocation of this probability of failure across each stage,

3. the percentage of this probability of stage failure that is associated with each failure type, and

4. the time into flight associated with each failure of a given type.

Launch vehicle reliability assessment is unlike traditional reliability testing in that there is no failure data obtained from a successful stage. This results in what is effectively a censored dataset. Traditional reliability analysis can directly use the results of the observed failures to gain an understanding of the lot. Using observed flight history in a traditional manner for a heavily censored dataset composed of observed flight history would result in total probability of failure estimates that are not representative of the top-down probability of failure estimates even though the relative decrease in failure rate as a function of time would be accurate. Therefore, the Tier 2 method uses a multi-step process when computing the failure rate curve for each stage of a launch vehicle:

1. Group failures within the observed dataset based on type,

2. Normalize the failure time as a function of stage time,

3. Perform a Weibull fit of the observed failures for infancy and duration failures based on the normalized failure times,

4. Scale the curves to the top-down probabilities,

5. Apply isolated events of interest, and

6. Combine the type curves and scale them to the stage of interest.

Each step is described in detail below.

Step 1: Group Failures by Type:

The Tier 2 method defines three types of failures:

1. Infancy failure is a failure in which normal flight of a stage does not commence,

2. Random failures are those that could occur at any point in flight, and

3. Sunset failures (also called duration failures) are those that would not occur until after a period of normal flight for a stage has caused the failure to occur.

Unless a failure is clearly an infancy or sunset failure type, consider it a random failure type. Table 5-7 shows how to group the failure modes into failure types.

Table 5-7. Failure Modes Grouped as Infancy, Random, or Duration Failure Types.

Infancy
Liquid Engine Failure to Ignite
SRM Failure to Ignite
Random
Control Failure
Inadvertent Ordnance Activation
Guidance and Control Failure
Liquid Engine Explosion
Liquid Engine Loss of Thrust
SRM Case Rupture
Structural Failure
Sunset
Payload or Fairing Separation Failure
SRM Burn Through
Stage Separation Failure

For this analysis, consider the past history of entire vehicles to be relevant to the examined stage. This may not always be the case: if an analysis can demonstrate that the experience of a particular vehicle is not relevant, you could amend the dataset to exclude any associated failure. Under the identified assumption that all vehicles are relevant, using the groupings identified in Table 5-7, approximately 6.9% of failures are infancy failures and 8.5% are duration failures based on the hypothetical historical data provided. The number of duration failures is significantly affected by the fact that separation failures are allocated to the end of the previous stage as opposed to the beginning of the next. This is consistent with the fact that a malfunction of the bolts that completely prevents liftoff would not count against the flight history of the vehicle, as flight begins with liftoff. However, this percentage of duration failures is dominated by separation events. Only 2.3% of all failures identified in the table are attributed to burn throughs.

Step 2: Normalize the Failure Times

Once you group the observed failures in a manner that clearly identifies infancy and duration failures, normalize the time of failure for each relative to the total time of stage operation. This is done to apply the results to a stage of any operational length so long as

the systems employed by that stage are suitably similar to those used within the dataset used to construct the failure rate curve.

Because the vehicle dataset used to find the percentages in Step 1 results in data points for which specific flight or operational data is unavailable, Step 2 of this example only identifies those failures for which vehicle data is suitably reliable. Given this restriction, Table 5-8 and Table 5-9 present the normalized failure times for the infancy and duration failures identified as part of Step 1 for the entire worldwide flight history in.

Table 5-8. Time of Infancy Failure as a Percentage of Liquid Stage Operation Time

N	Vehicle and Launch	Time into Stage (sec)	Total time of Stage (sec)	Normalized Stage Time
1	Chang Zeng 3, China 14	1	800	0.0013
2	Ariane 3, Eutelsat 103	1	731	0.0014
3	Ariane 2, Intelsat 5A	1	731	0.0014
4	Atlas 1, AC-70	1	402	0.0025
5	Atlas 1, AC-71	1	402	0.0025
6	Kosmos 11K65M, Cosmos 2321	2	375	0.0053

Table 5-9. Time of Duration Failure as a Percentage of Liquid Stage Operation Time

N	Vehicle and Launch	Time into Stage (sec)	Total time of Stage (sec)	Normalized Stage Time
1	Titan 4A 403A, K-11	1	120	0.8417
2	Delta 3914, Orbital Test Satellite	55	55	1.0000
3	Delta 2, 7925, Mugunghwa 1	64	64	1.0000
4	Pegasus, F-2 HAPS	72	72	1.0000
5	Pegasus XL, F-9 STEP-3	76	76	1.0000
6	Taurus 2110, Orbview	83	83	1.0000
7	Proton 8K82M, JCSAT-11	108	108	1.0000
8	H-2A 2024, Radar-2	110	110	1.0000
9	Thor LV-2F, DMSP	220	220	1.0000
10	PSLV D1, IRS-1E	263	263	1.0000
11	Athena 2, Ikonos-1	267	267	1.0000
12	Tsiklon 3, Tselina-D	280	280	1.0000
13	Soyuz 11A511, Manned Mission	292	292	1.0000
14	Tsikon 3 S/N 801, Sich-1	405	405	1.0000
15	Kosmos 11K65M, Mozhayets-5	505	505	1.0000
16	Pegasus XL, F-14 SAC-B/HETE	660	660	1.0000
17	Titan 4B IUS 4B-27, K-32	23314	23314	1.0000

Using the data from these tables, find the Weibull distribution parameters with this censored dataset as follows.

Step 3: Fit to the Infancy and Duration Data

Find the Weibull parameters representing the identified data by performing a least-squares fit of the data. By developing the *x*, *y* parameters as a function of the time and probability of failure for the censored set, the *x*, *y* pairs to be plotted for such a fit are presented in Table 5-10 for the infancy data, where *N* equals 6 launches, and Table 5-11 for the duration data, where *N* equals 17.

Table 5-10. Data points used in the least squares technique for fitting the Weibull distribution to the infancy failure data.

Infancy failures				
i	**t**	**F(t)=i/(N+1)**	**x = ln(t)**	**y = ln(ln(1/(1-F(t))))**
1	0.0013	0.142857	-6.64539	-1.86982
2	0.0014	0.285714	-6.57128	-1.08924
3	0.0014	0.428571	-6.57128	-0.5805
4	0.0025	0.571429	-5.99146	-0.1657
5	0.0025	0.714286	-5.99146	0.225351
6	0.0053	0.857143	-5.24005	0.66573

Table 5-11. Data points used in the least squares technique for fitting the Weibull distribution to the duration failure data.

Duration failures				
i	**t**	**F(t)=i/(N+1)**	**x = ln(t)**	**y = ln(ln(1/(1-F(t))))**
1	0.8717	0.055556	-0.13731	-2.86193
2	1	0.111111	0	-2.13891
3	1	0.166667	0	-1.70198
4	1	0.222222	0	-1.38105
5	1	0.277778	0	-1.12263
6	1	0.333333	0	-0.90272
7	1	0.388889	0	-0.70831
8	1	0.444444	0	-0.53139
9	1	0.5	0	-0.36651
10	1	0.555556	0	-0.20957
11	1	0.611111	0	-0.05714
12	1	0.666667	0	0.094048
13	1	0.722222	0	0.247589
14	1	0.777778	0	0.40818
15	1	0.833333	0	0.583198
16	1	0.888889	0	0.787195
17	1	0.944444	0	1.061385

Find a least squares approximation through the x, y pairs identified in Table 5-10 and Table 5-11 using the Microsoft EXCEL© function TREND. Figure 5-12 plots the distribution.

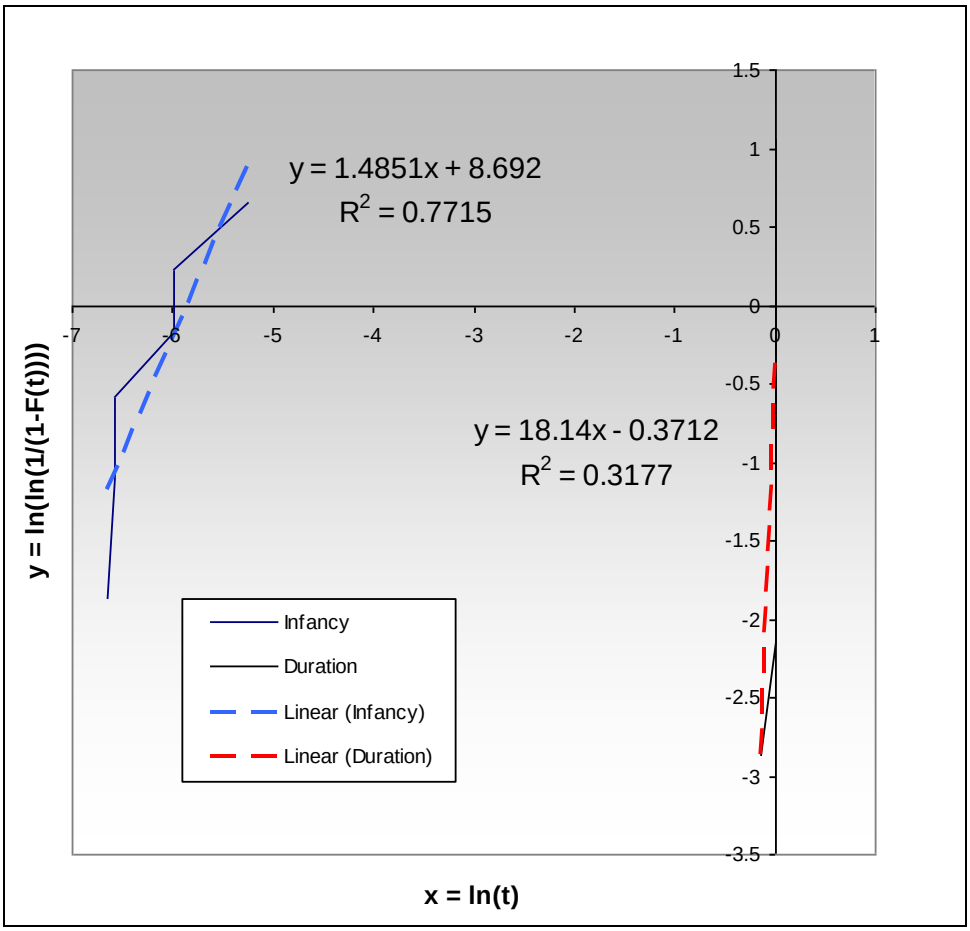

Figure 5-12. Weibull Distribution fitting for the Infancy failures identified in Table 5-10 and the Duration failures identified in Table 5-11.

The result of a least squares approximation is a line ($y = ax+b$). The shape parameter (m) for the Weibull distribution is the slope (a) of the least squares approximation. The scale parameter (θ) is equal to $\exp[-b/a]$ where b is the intercept of the least squares approximation. Table 5-12 identifies the shape and scale parameters for the infancy and duration type failures based on the least squares approximations in Figure 5-12.

Table 5-12. Shape and scale parameters for the normalized Weibull functions defining infancy and duration failure rates using just the censored dataset identified above.

Type of Failure	Shape Parameter (m)	Scale Parameter (θ)
Infancy Failures	1.4851	0.0029
Duration Failures	18.140	1.0206

Step 4: Scale the Curves to the Top-Down Probabilities

As identified above, it is important to note that the results found in Step 3 define the infancy and duration curves given only the censored data identified in Step 2. You cannot apply these results directly since the probability of failure at the end of each stage given this censored dataset would be 1.0 for each curve. This is because successful flights are not accounted for, resulting in a dataset where every examined vehicle has failed.

Thus, to use these curves, scale the shape and scale parameters defining the infancy and duration failure rate curves to produce results consistent with the top down probability of failure for each stage. We apply this analysis to the *Astrocraft 6* second stage, which has a probability of failure of 0.5 in this example. In addition, the hypothetical historical data from Step 1 showed that the infancy failures account for 6.9% of all failures in a stage and duration failures account for 8.5%. Therefore, we compute the probability of an infancy failure in second stage of the *Astrocraft 6* as the product of the stage failure rate (0.5) and the percentage of that probability associated with infancy failures (0.069), giving 0.0345. Likewise, the probability of a duration failure occurring in second stage is 0.0425.

By using a single multiplier for the shape and scale parameters for the infancy failure rate curve and another independent multiplier for the scale parameter of the duration failure rate curve, the normalized infancy and duration failure rate curves that fit these top-down probability of failure estimates is that presented in Table 5-13.

Table 5-13. Shape and scale parameters for the normalized Weibull functions defining infancy, random, and duration failure rates based on the top-down probability of failure estimate for Stage 2 of the *Astrocraft 6*.

Type of Failure	Shape Parameter (m)	Scale Parameter (θ)
Infancy Failures	0.0064	1.243e-5
Random Failures	1.0000	??
Duration Failures	18.140	1.194e00

In Table 5-13, the scale parameter defining random failures is not identified while its shape parameter is equal to 1.0000. This is because we modeled random failures as a uniform failure rate and the scale parameter defining the failure rate for random failures is found given the infancy and duration curves. This is done by substituting equation (8) into equation (5) and solving for the random scale parameter when setting the probability of failure at the completion of the stage (i.e., $F(1)$ in equation (5)) equal to the 0.5 for the *Astrocraft 6* second stage.

By doing this, the normalized failure rate curves for all failure types are presented as in Table 5-14 and plotted as a function of normalized time as in Figure 5-13.

Table 5-14. Shape and scale parameters for the normalized Weibull functions defining infancy, random, and duration failure rates based on the top-down probability of failure estimate for Stage 2 of the *Astrocraft 6*.

Type of Failure	Shape Parameter (m)	Scale Parameter (θ)
Infancy Failures	0.0064	1.239e-5
Random Failures	1.0000	1.633e0
Duration Failures	18.140	1.194e0

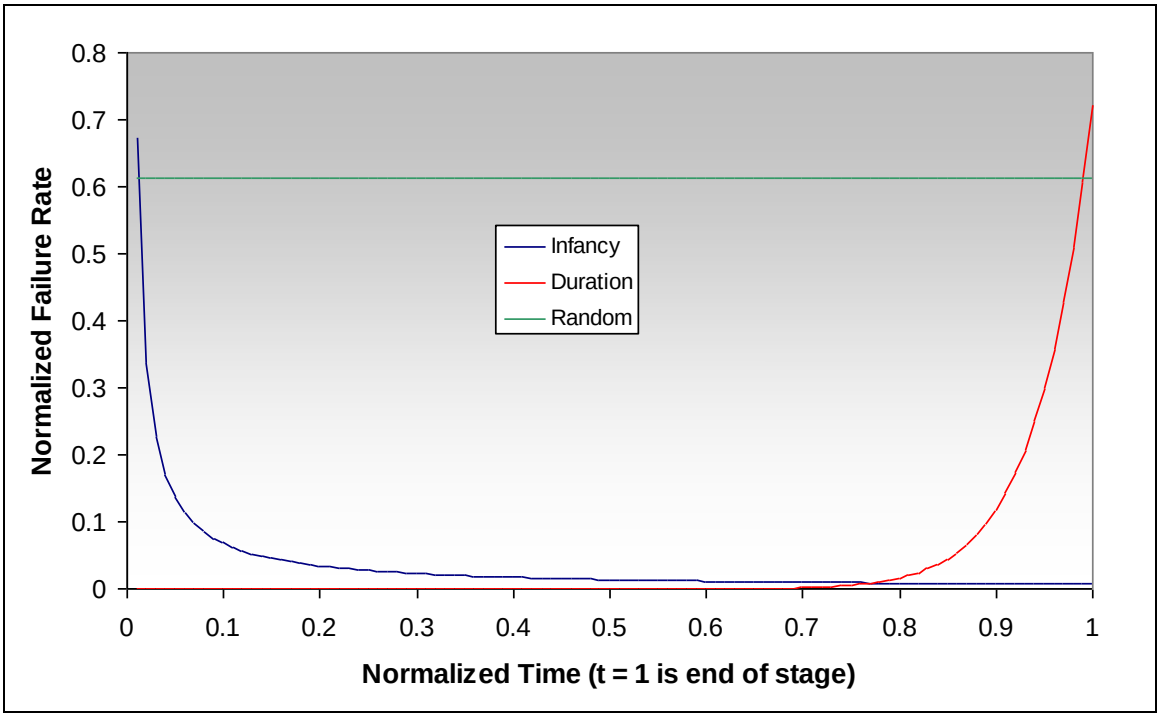

Figure 5-13. Normalized infancy, duration, and random failure rate curves.

Step 5: Apply Isolated Events of Interest

You can address isolated events, such as staging during a coast phase, in a manner analogous to the infancy and duration failure curves. After selecting a suitable function (e.g., Dirac Delta Function), you can add these to the curves identified in Figure 5-13.

Step 6: Combine and Apply to the Stage of Interest

The total failure rate at any time is equal to the sum of all independent failure rates. Therefore, the sum of the failure rates identified in Step 4 is the normalized failure rate for the examined stage. Apply this normalized failure rate curve to the stage of interest by scaling it over the total time of the stage.

In the case of the second stage of the *Astrocraft 6*, the time over which the probability of failure is applied is 345 seconds. However, it is not sufficient to just scale the normalized

curve over this time. When you apply the normalized time applied over the 345 seconds of the second stage, adjust the failure rate per normalized time to account for the reference time for that stage. By making these adjustments, the failure rate curve for the *Astrocraft 6* second stage is as presented in Figure 5-14.

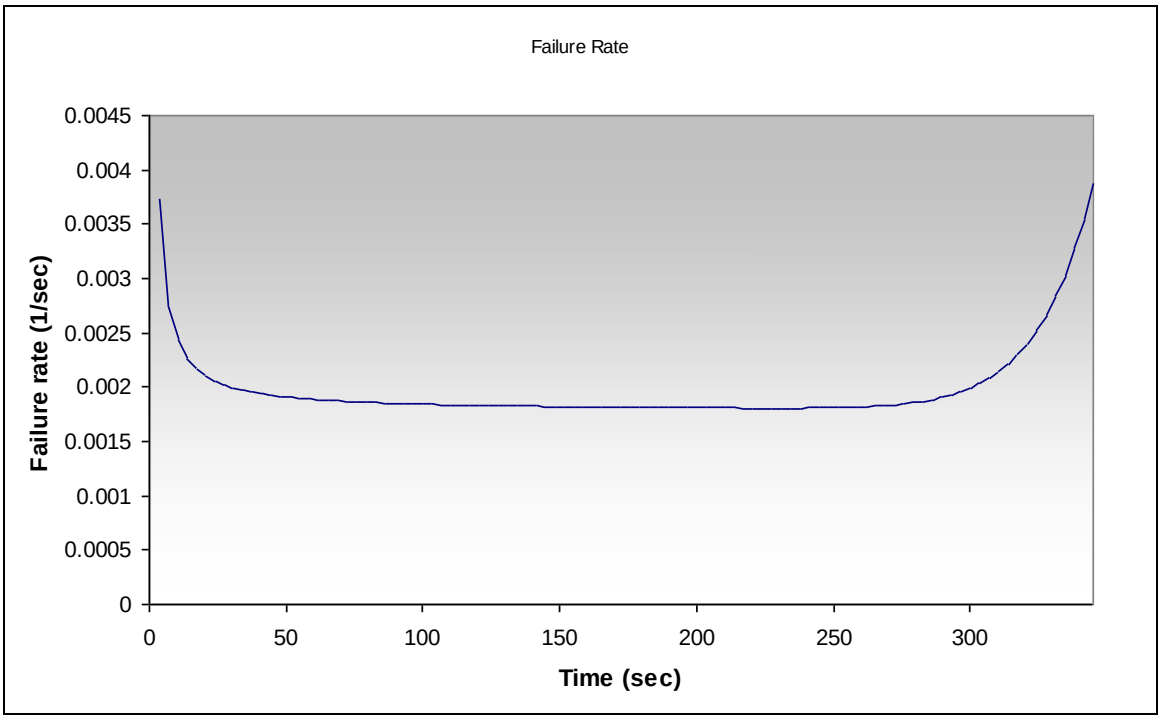

Figure 5-14. Failure rate curve for the *Astrocraft 6* second stage example data.

Using the failure rate curve in Figure 5-14, find the probability of failure for a particular section of flight for use in a flight safety analysis.

EXAMPLE: Assessment of Uncertainty In Bayesian Prediction

One of the features of this method is that you base the uncertainty on a beta distribution, which is quite easy to compute. In addition, the distribution associated with the weak prior is very wide, reflecting the uncertainty in the real probability of failure. For example, consider the uncertainty distribution for the first stage failure probability for a new vehicle from a new developer, r'/n' = 0.43 (with r' assumed to be 0.43 and n' assumed to be 1.0). Figure 5-15 and Figure 5-16 show the density function and the cumulative distribution function.

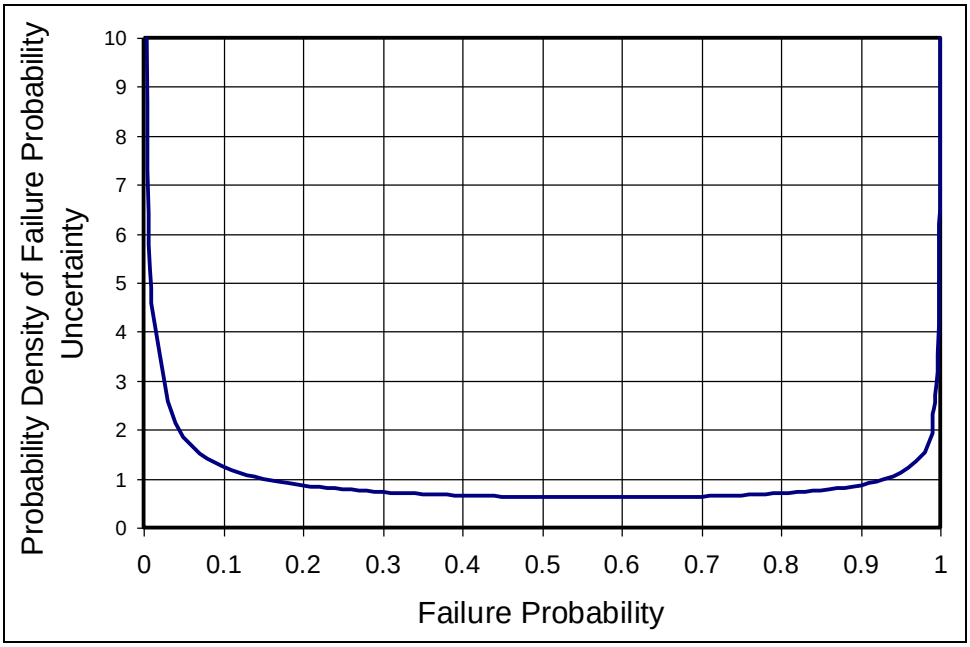

Figure 5-15. Probability Density Function of Failure Probability for the First Stage (NN and *r'*=0.43, *n'*=1.0)

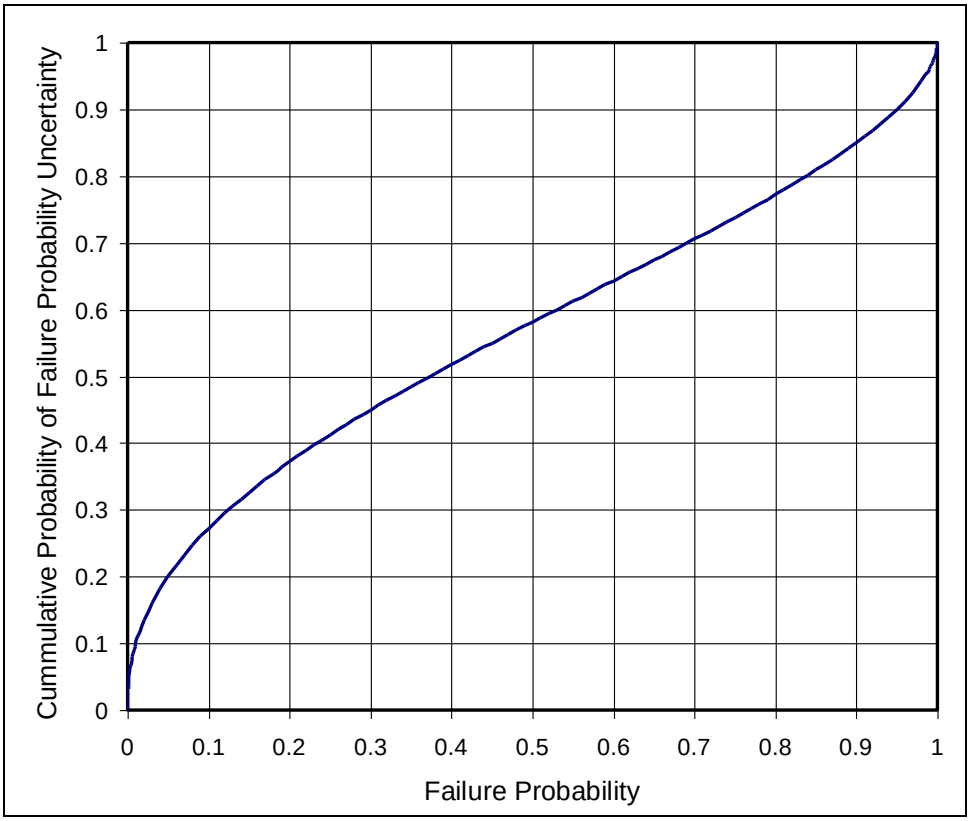

Figure 5-16. Cumulative Distribution Function of Failure Probability for the First Stage (NN and *r'*=0.43, *n'*=1.0)

Notice how wide the density function is - giving very wide uncertainty bounds, e.g. 20% to 80% is 0.05 to 0.838. As the vehicle has more launches this distribution narrows.

Consider the case where a new vehicle has had 10 straight successful first stage burns. The posterior estimate of failure probability is now P_F" = (0.43+0)/(1+10) = 0.039 and the density function is as shown in Figure 5-17.

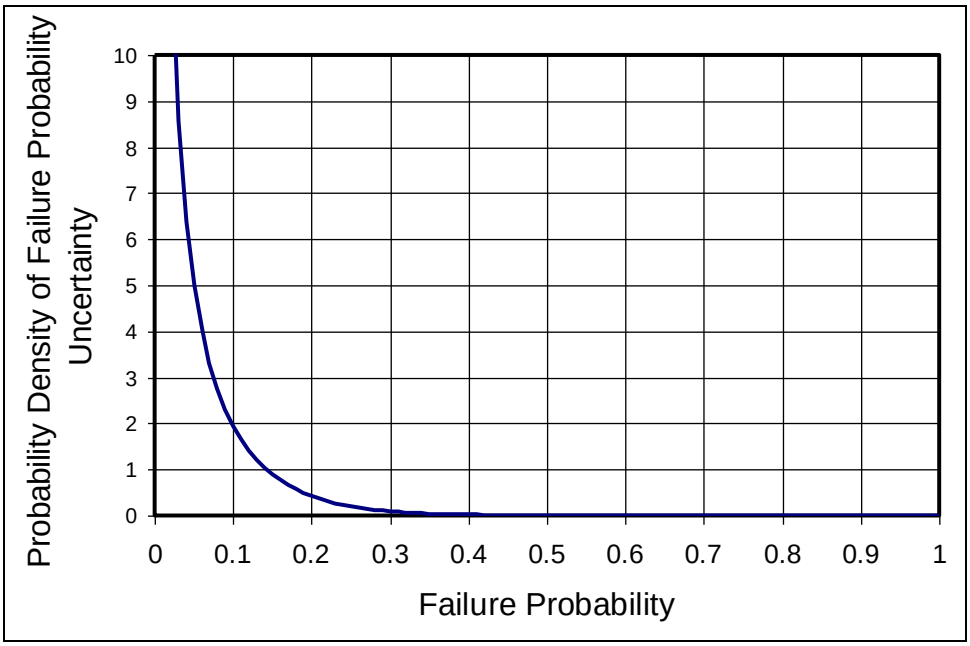

Figure 5-17. Probability Density Function of Failure Probability for the Same First Stage after 10 Successful Launches (r"=0.43, n"=11)

After the sequence of 10 successful Stage I flights, the 20% to 80% Bayesian uncertainty bound are reduced to 0.002 to 0.066. These are smaller than those for the corresponding conditions in Figure 5-18. They would be larger if the prior had been stronger, i.e. $n' > 1$.

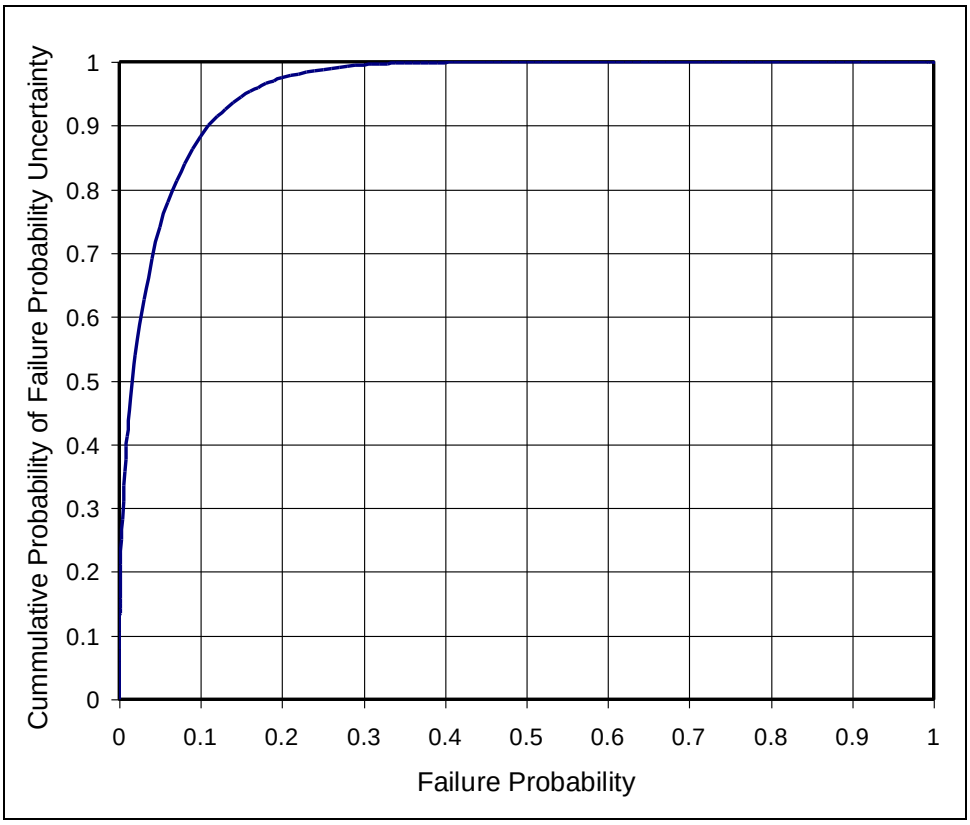

Figure 5-18. Cumulative Distribution Function of Failure Probability for the Same First Stage after 10 Successful Launches (r"=0.43, n"=11)

5.7.2 Allocation to Vehicle Response Modes

Section 4.9.2 introduced vehicle response modes and identified some generic vehicle response modes used in past flight safety analyses.

The vehicle response modes used in a valid flight safety analysis are necessarily correlated with the tools applied to account for the feasible trajectories (e.g., corresponding to normal and malfunction conditions) and vehicle break-up modes (e.g., following termination of flight, termination of thrust, break-up due to aerodynamic loads, etc.). Of course, a flight safety analysis should also account for planned debris releases during normal flight (and malfunctions). These releases could be considered vehicle response modes as well (although not technically a failure response mode). A generic vehicle response mode classification system that may be useful for flight safety analysis distinguishes feasible combinations of two outcomes: if a significant trajectory excursion occurred for the vehicle or parts of the vehicle and if fragmentation occurred immediately as shown in Table 5-15. Not all failure modes may be feasible in all phases of flight.

Table 5-15. Generic Vehicle Response Modes

Mode	Definition	Example
OT1	On-trajectory failure with immediate fragmentation	Engine explosion
OT2	On-trajectory failure without immediate fragmentation	Total loss of thrust
MFT1	Malfunction turn with immediate fragmentation	Rapid tumble turn resulting in immediate break-up
MFT2	Malfunction turn without immediate fragmentation	Sustained turn resulting in significant departure from nominal trajectory
RA	Random attitude	Vehicle reorients to a random attitude and continues to fly along that path until thrust termination

As an example of how vehicle break-up modes could influence selecting appropriate vehicle response modes for a flight safety analysis, consider a malfunction turn failure with immediate fragmentation. This may be appropriately classified as an on-trajectory (OT) failure with immediate fragmentation, unless the turn induces significant re-orientation and the induced velocities are not uniform in direction. As an example of how the trajectory dispersion model used could influence selecting appropriate vehicle response modes for a flight safety analysis, consider a malfunction turn failure without immediate fragmentation that nevertheless breaks-up before the vehicle reaches outside the bounds of normal flight defined by 3-sigma nominal trajectories. This may be best be classified as a MFT-2 if the dispersion computation keeps the normal guidance and performance dispersion separate from the dispersion due to a malfunction turn, even a short lived malfunction turn. Process failures that do not result in immediate

fragmentation with a tool that accounts for violation of criteria for break-up or destruct, including intact impacts.

A flight safety analysis may need to distinguish malfunction turn failures that involve a loss of attitude reference from those that do not involve disorientation, such as a simple thrust offset. For example, a flight safety analysis may define three types of turns:

1. Those that initiate a thrust offset while OT,

2. Those that involve a loss of attitude reference without re-stabilization, or

3. Those that involve in a loss of attitude reference with re-stabilization

Model those that initiate a thrust offset while on-trajectory with traditional turn curve data, or valid trajectory analysis software. Model loss of attitude reference with or without re- stabilization with valid trajectory analysis software.

Once you define appropriate vehicle response modes for a given launch and set of analysis tools, there are two options: (1) refer to the manufacturer's FMEA and reliability analyses to help discern the relative frequency of the different failure response modes and then map those into vehicle response modes, or (2) use empirical data on past launches of the vehicle or similar vehicle to estimate these relative probability of the vehicle response modes.

5.7.2.1 Allocation of Failure Response Modes Based on Historical World-Wide Failure Data

The top-down and Bayesian approaches described above may use historical data to allocate failures among the various failure response modes in a manner consistent with the evidence from vehicles developed and launched under similar circumstances. Table 5-16 and Table 5-17 provide counts of failures in different categories for liquid only propellant vehicle stages. In some cases, it may be appropriate to combine historical evidence on failures associated with vehicles that use both liquid and solid propellants. Translation from the relative probability of the failure modes demonstrated by the past flight history into vehicle response modes used in a QRA clearly depends on the choice of vehicle response modes. An example of this is provided in Table 5-18 and Table 5-19 below.

Four general vehicle response modes used to determine launch risks from debris include the following.

1. On-pad fire and explosion (although not associated with flight, still relevant to launch risks, explosive hazard areas, and the MPL)

2. On trajectory, including an explosion and loss of vehicle thrust,

3. Malfunction turn, including tumble turns, gradual turns, and diabolical turns, and

4. Stage failures, including failure to start a rocket motor.

Find additional discussion of generic vehicle response modes in Section 4.9.2.

We often model malfunction turns as turns with a fixed thrust vector offset about an axis perpendicular to the velocity vector or body axis and oriented randomly. An example in Section 8.4.4 illustrates that this may be possible using a three degree of freedom trajectory model in some cases. Other malfunction turns are usually simulated and provided in the form of a collection of many malfunctioning trajectories based on a 6-DOF trajectory model. Thrust vector offsets generally produce a tumble of the vehicle about a lateral axis, commonly referred to as a tumble turn. Unless data are available to facilitate a better estimate, calculate the thrust vector offset failure for ELVs to occur 15% of the time - given a vehicle failure - based on historical data [21].

Guidance failures fall into two categories: steering vector failure and other. The steering vector failure includes those conditions where the guidance system can get confused or reoriented and direct the vehicle off into a new direction. We consider these failures to be rare but they have the highest potential risk to the public. We typically model these failures as random-attitude failures where the vehicle reorients and proceeds stably in a new direction. Research is continuing into past failures to determine the realism of these failures and subsequent vehicle behavior. Unless data are available to facilitate a better estimate, calculate the steering vector failure as 1% of the vehicle failures.

We almost always associate structural failures with failures of the payload fairing. Premature ordnance activation has only occurred in the pre-flight phase, often with devastating results. Consider these in developing an MPL determination.

Table 5-16 and Table 5-17 provide data on potentially hazardous failures of orbital class ELVs that used liquid propellants for launches between 1980 and mid- 2008 worldwide, some of which were launched on a planned suborbital trajectory. This data demonstrates that structural failures have not occurred on upper stages, where aerodynamic loads are relatively light, but are fairly common during the first stage of flight. This evidence indicates the potential importance of accounting for the relative probability of vehicle response modes differently during different phases of flight.

Table 5-16. Failure Mode Frequency of Liquid Fueled First Stages from the World-Wide Launch Failure Database

Failure Mode	Stage I Failures	Fraction
Control failure - malfunction turn	9	0.220
Guidance - steering vector failure	3	0.073
Guidance - other		
Liquid engine explodes	8	0.195
Liquid eng loss of thrust	14	0.341
PLF separation failure	0	0.000
Stage separation failure	1	0.024
Structural failure	6	0.146
Totals	41	1

Table 5-17. Failure Mode Frequency of Liquid Fueled Upper Stages from the World-Wide Launch Failure Database

Failure Mode	Stage 2 Failures	Stage 3 Failures	Stage 4 Failures	All Upper Stages	
				Failures	Fraction
Control failure - malfunction turn	3	1	0	4	0.105
Guidance - steering vector failure	5	1	0	6	0.158
Guidance - other					
Liquid engine explodes	5	0	0	5	0.132
Liquid eng. failure to ignite	4	0	0	4	0.105
Liquid eng loss of thrust	9	4	0	13	0.342
PLF separation failure	1	0	0	1	0.026
Stage separation failure	3	2	0	5	0.132
Structural failure	0	0	0	0	0.000
Totals	30	8	0	38	1

Table 5-18 and Table 5-19 are examples of how historical data on the failure modes listed in Table 5-16 and Table 5-17 could be mapped into the four general vehicle response modes used in the past to determine launch risks from debris.

Table 5-18. Example Mapping of First Stage Failure Modes into Four General Vehicle Response Modes

Failure Mode	Stage I Failures	Fraction	OT	MFT	Staging
Control failure - malfunction turn	9	0.220		9	
Guidance - steering vector failure	3	0.073		3	
Guidance - other					
Liquid engine explodes	8	0.195	7	1	
Liquid eng loss of thrust	14	0.341	12	2	
PLF separation failure	0	0.000			
Stage separation failure	1	0.024			1
Structural failure	6	0.146	6		
Totals	41	1	61%	37%	2%

Table 5-19. Example Mapping of Upper Stage Failure Modes into Four General Vehicle Response Modes

Failure Mode	OT	MFT	Staging	All Upper Stages	
				Failures	Fraction
Control failure - malfunction turn		4		4	0.105
Guidance - steering vector failure		6		6	0.158
Guidance - other					
Liquid engine explodes	4	1		5	0.132
Liquid eng. failure to ignite	2	2		4	0.105
Liquid eng loss of thrust	11	2		13	0.342
PLF separation failure			1	1	0.026
Stage separation failure			5	5	0.132
Structural failure	0	0	0	0	0.000
Totals	45%	39%	16%	1	1

A more sophisticated set of vehicle response modes might include the following.

1. On-Pad Conflagration (not applicable for flight expected casualty analysis)
2. Ballistic Trajectory, associated with total loss of thrust

3. Decaying Trajectory, associated with partial loss of thrust sufficient that orbit cannot be reached

4. Wrong Orbit

5. Malfunction Turn, which is subdivided into those that results in immediate fragmentation or those without immediate fragmentation (including those where part of the vehicle survives with residual thrust)

6. Spacecraft Damaged[10]

7. Liquid Engine Explodes

8. Vehicle Break-up

A future effort could review historical data to discern reasonable allocations to this more sophisticated set of vehicle response modes, as well as identifying the percentages of failures that resulted in the feasible combinations of (1) a significant trajectory excursion for the vehicle or parts of the vehicle and (2) immediate fragmentation.

5.7.2.2 Allocation of Failure Response Modes Based on Reliability Analyses

Use the fault trees typically prepared by a launch operator during vehicle development to estimate the relative probability of various vehicle response modes. Then use the relative probability of various response modes to determine a feasible allocation of failure probability. However, two significant factors that influence the relative probability of various failure/vehicle response modes are generally not well covered in fault tree analyses: (1) human error in all stages from design through building to final vehicle checkout prior to a launch, and (2) failures associated with the integration of all hardware and software into the final vehicle design. For these reasons, we generally prefer the response mode probability allocation approach, based on historical flight experience as described in the previous subsection.

5.8 Weighting Flight History

The FAA may adjust the failure probability estimate to account for evidence obtained from the flight history of the vehicle, corrective actions taken in response to a failure of the vehicle, vehicle configuration changes, or other factors that affect vehicle reliability as described in [7]. Note, however, in all cases the launch risk analysis should use a final failure probability estimate that falls within the confidence limits given in Figure 5-1. Implicit in the FAA's approach to failure probability adjustments is the recognition that more recent launch experience of a vehicle may be more relevant and useful for an accurate probability of failure estimate than what may have happened with the vehicle years before. This is particularly true for a mature vehicle with design modifications

[10] While spacecraft damage is typically thought of as a mission success factor and not a public safety factor, there are spacecraft damage scenarios that may be of interest to range safety, such as fairing separation failures and environmental miscalculations.

made in response to a failure that occurred during one of the first few launches. Also, a launch vehicle or launch vehicle subsystem may demonstrate a high degree of reliability when operated within a limited and well-defined parameter range, but demonstrate less reliability when operated outside that parameter range. The observed correlation between ambient temperature and incidence of O-ring blow-by observed for the Space Transportation System (STS) solid rocket boosters before STS 51-L provides such an example. In such cases, it may be appropriate to adjust the weight or relevance of a past launch to account for the nature of launch outcomes under distinct environmental conditions or earlier experience either of the subject vehicle, or earlier versions of the subject vehicle in the case of a derived vehicle.

Hence, you may consider a method that weights earlier experience differently than the most recent experience. With the Bayesian model it is possible to list in a column every flight of a stage and every failure and success associated with the flight of the stage. If you list the information consecutively in pairs, you can discount the added *r* value and *n* value of each pair by an exponential based on the flight number. You can then accumulate the factored values of *n* and *r* and the Bayesian model will have been based on data that emphasizes the more current information and discounts older information. No aging factors are provided here, but something quite similar has been implemented in the past [17].

In addition, a recent effort has produced a method that does not assume Bernoulli trials. This bivariate approach attempts to quantify a learning rate and estimate how the growth in knowledge of the developer of a vehicle is likely to affect the future reliability of the vehicle [22]. The methods applied in past flight safety analyses have assumed that there is no significant learning curve, other than that of more recent vehicle data may more relevance than older data.

6.0 CASUALTY AREA

6.1 Purpose

When a launch takes place, there is a risk of a launch vehicle failure and the resulting debris impacts. There is also the risk of serious injury to people not associated with the launch. The purpose of a casualty area analysis for a launch QRA is to estimate the area surrounding each potential debris impact where injuries (or worse) could occur for all debris impacts.

6.2 Minimum Features

The effective casualty area for inert debris, or more simply the casualty area (A_C), is the region associated with a fragment's impact location where we assume a person would become a casualty. For unsheltered people, Figure 6-1 identifies some of the events that can cause a casualty from either direct or indirect effects. Indirect effects include debris dispersion or formation from splatter, bounce, or crater ejecta. We also refer to these as secondary effects.

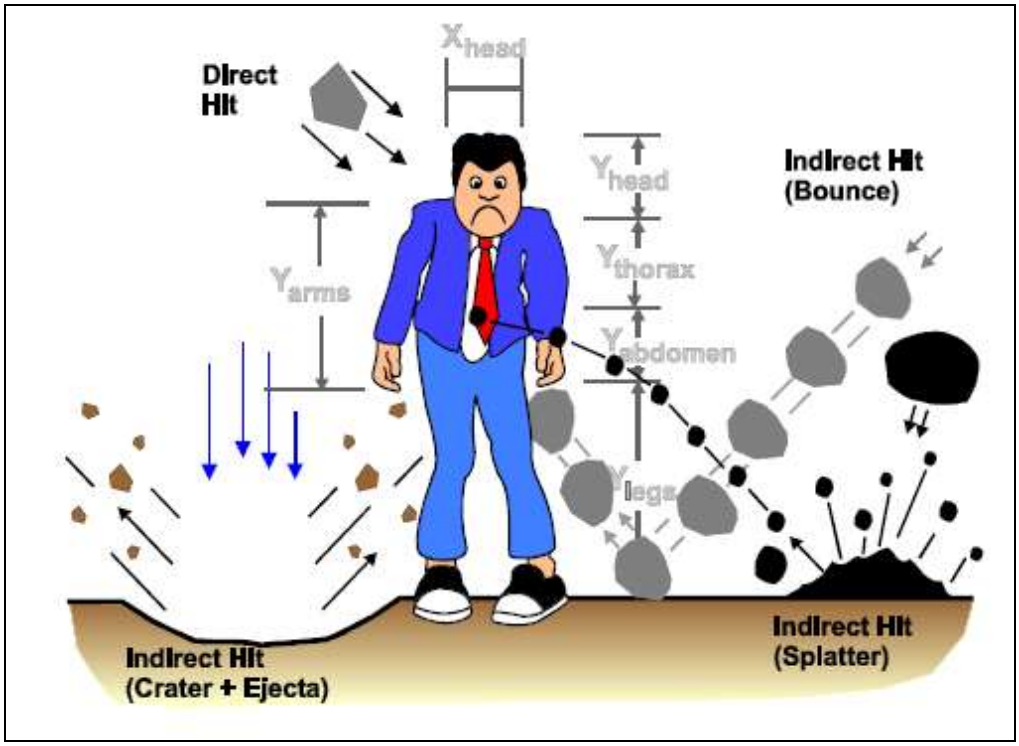

Figure 6-1. Casualty Producing Events from Inert Debris Impacts in the Open

The casualty expectation formulation in Section 4.8 has three basic parts:

$$E_{C_{ij}} = P_{I_{ij}} \left(\frac{N_{P_j}}{A_{P_j}} \right) \left(N_{F_i} A_{C_i} \right)$$

1. P_{Iij}, the probability of impact of a piece of debris on a population center;

2. $\frac{N_{Pj}}{A_{Pj}}$, the population density in the population center; and

3. $N_{Fi} \times A_{Ci}$, the total "effective casualty area" of the N_{Fi} fragments in fragment category "i." A_{Ci} is the casualty area of a single fragment. The definition of an "effective casualty area" is a region associated with the impact location of a fragment within which a person will become a casualty as discussed below.

There are four basic cases that need casualty area estimates:

1. Impact of inert debris on people in the open,

2. Impact of inert debris on roofs of shelters that may penetrate the roof or collapse the structure and injure the occupant(s)

3. Impact of explosive debris in the vicinity of people in the open within a distance that could injure the exposed people

4. Impact of explosive debris in the vicinity of structures that could lead to injuries of occupants of the structure.

In each case, an effective casualty area is computed that can be used with the impact probability and population density to determine casualty expectation for that fragment group – population center combination. Thus, four basic models are required to cover the range of possibilities. These models have additional sub-models that cover all of the elements of determining the probability of being a casualty in each case.

There are additional cases that are not covered in this discussion. The first is aircraft in flight that can be hit by debris and lead to catastrophic consequences; and another is ships and their occupants. The ship problem is on the ocean surface (two dimensional) and can be modeled using method similar to those for population centers on-shore. The aircraft problem is four dimensional (x, y, z, t) and is deferred to a future revision of this publication.

6.3 Modeling Discussion

The effective casualty area is a modeling construct used to simplify expected casualty computations involving explosive impacts where the true probability of casualty is a function of the range from the explosion. The expected casualties due to an impact can be computed by assuming everyone within the effective casualty area of an impact

sustains an injury of at least a certain level of severity (e.g. AIS 3), whereas everyone outside that area is not injured or has injuries at a level less than the specified level of severity. Example calculations for effective casualty areas due to inert and explosive debris impacts are presented in this section. The examples and discussion in the following subsection cover all of the four basic casualty model topics. Wherever possible, current casualty models and data are given to provide a practical means for analysis of a wide variety of commercial launches.

Casualty area models, and those for other elements of a flight safety analysis, should attempt to minimize the uncertainty that arises from simplistic modeling practice. If simple models are used, every effort should be taken to ensure the results are conservative and prevent underestimation of risk, because all of the problem aspects have not been thoroughly examined and accounted for. References [23] and [24] discuss casualty area computation used to manage risk from space object reentry, including the potential for demise of the debris due to aero-thermal heating. The NASA and the European Space Agency have produced software, available for free, with methods that may be acceptable for reentry demise evaluation depending on their proper application and implementation. [24]

6.4 Ballistic Coefficient

The ballistic coefficient is an important debris parameter that indicates the relative importance of inertial and aerodynamic forces on a body in free fall. The ballistic coefficient, often referred to as beta, is defined as

$$\beta = \frac{W}{C_D A_{ref}}$$

where W is the weight, C_D is the drag coefficient and A_{ref} is a reference area associated with the drag coefficient. Since drag coefficients are typically derived experimentally, the A_{ref} can be set by the experimentalist, but A_{ref} is often equal to the area projected on to the direction of the flow. The drag coefficient is a non-dimensional value defined as $C_D = \frac{2F_D}{\rho A_{ref} V^2}$ where F_D is the total (friction and form) drag force, ρ is the density of the fluid the object moves through (air in the case of launch vehicle debris), and V is the velocity of the object relative to the fluid. A drag coefficient represents the ratio of the total drag force exerted on an object to the force due to dynamic pressure acting on the reference area. Drag coefficients typically exhibit significant dependence on the object's shape, Mach number ($M = \frac{V}{c}$), and Reynolds number ($\mathrm{Re}=\frac{\rho V L}{\mu}$) where c is the speed of sound in air, L is a characteristic length for the object (for example, the diameter of a sphere), and μ is the absolute viscosity of the fluid. The Reynolds number is a dimensionless parameter that characterizes the ratio of inertial force and viscous drag force. The drag coefficients of cylindrical and spherical objects decrease by a factor of three when the Reynolds number exceeds a critical value (which depends on surface

roughness) near $3x10^5$ for a smooth surfaced cylinder. This precipitous drop in drag coefficient for rounded bodies is attributed to delayed flow separation, which reduces the size of the low pressure wake region, due to increased momentum in a fully turbulent boundary layer. Delayed separation is impossible for a sharp edged object; hence the drag coefficient for a flat plate does not display a dramatic decrease with the Reynolds number. Instead, the drag coefficient for a flat plate (directly facing the flow direction) maintains a constant value for Reynolds numbers above 10^3. The dominant influence of flow separation on drag coefficients suggests that idealizing non-rounded debris as boxes with equivalent dimensions can provide a reasonable approximation. The impact location and physical characteristics of debris recovered from launch vehicle accidents has been used to confirm that the tumbling box idealization for non-bluff shaped debris items produced ballistic coefficient estimates consistent with the available data. [26]

As a given fragment falls through the atmosphere, the Reynolds number, and potentially the drag coefficient, generally changes due to density gradients and velocity changes. The absolute viscosity of air is virtually independent of altitude. Therefore, drag coefficient and debris velocity are generally coupled: to estimate the drag coefficient requires a Reynolds number (which depends on velocity), yet the drag coefficient is needed to estimate velocity. Analysis of debris velocities, Reynolds number, and Mach number has produced the following conclusions. [26]

- Fragments with ballistic coefficients less than 100 psf generally fall at speeds near (within ten percent) their local terminal velocity for initial altitudes less than 70,000 ft.
- Debris falling at supersonic velocities is unlikely, with the exception of large ballistic coefficient fragments (on the order of 100 psf or greater) with high initial altitudes (above 50,000 ft).
- Debris with ballistic coefficients of 50 psf or less fall at Mach numbers less than 0.5 for altitudes below about 30,000 ft.
- Atmospheric density gradients (and subsequent terminal velocity changes) produce a Reynolds number at terminal velocity that increases by almost an order of magnitude as a fragment with a constant ballistic coefficient falls from 100,000 ft.
- The minimum feasible Reynolds number for launch vehicle fragments that can threaten people on the ground is approximately 600 at 100,000 ft and over 5000 at 3,000 ft.
- A precipitous decrease in drag coefficient due to delayed flow separation is unlikely for debris, except perhaps intact cylindrical or spherical objects. Typical spherical objects, such as fuel tanks, are so large that the Reynolds number exceeds the critical value throughout the ballistic trajectory. However, delayed separation is not possible for axial flow over a cylinder (i.e., in an end-on orientation where the free stream velocity of the flow is parallel to the length of the cylinder), where the separation point is attached to the corner. Also, since the drop in drag coefficient is observed for smooth objects only, where separation is not triggered by or attached to a protrusion, it is logical to make no adjustment to the drag coefficient for cylinders and rough spherical objects in supercritical flow.

Thus, it is valid to compute a drag coefficient independent of altitude for typical launch vehicle debris, except for large ballistic coefficient fragments falling from altitudes above 100 kft. The earth's atmosphere contains three aerodynamic regimes: free molecular flow (at high altitudes), continuum flow (at low altitudes), and an intermediate regime. A robust risk assessment will account for drag force changes in these three regimes. The free molecular flow regime occurs at very high altitudes where air no longer behaves as a fluid. Applying a constant ballistic coefficient derived for continuum flow to regions where free molecular conditions exist tends to underestimate the drag force. Therefore, accounting for drag force changes between the continuum and free molecular flow regimes typically reduces the size of the impact dispersion areas estimated. A C_D versus Mach table is used to account for the drag force dependence on the flow regime. The use of a C_D versus Mach table may be deemed unnecessary in some cases due to the low risk estimates produced with the standard assumptions of (1) a drag coefficient independent of altitude in the continuum flow region, and (2) a drag coefficient that varies to account for free molecular drag effects during free fall at extremely high altitudes.

Hoerner shows the experimentally determined drag coefficient for a tumbling cube as a function of Mach number [27]. The lower curve in this data indicates that the drag coefficient for a randomly tumbling cube at low Mach numbers is near 0.8 [23] (based on a reference area of $1.5L^2$ that "roughly represents an average projected frontal area of the cubes when rotating" [27]). The upper curve in this data shows the drag coefficient as a function of Mach number for a cube tested in a cornerwise position (i.e., the corner of the cube was pointed in the flow direction) based on a reference area of L^2 [23]. After accounting for the different reference areas, the drag coefficient results for a randomly tumbling cube are compatible to the cube fixed in a cornerwise position. An empirically determined average drag coefficient for subsonic randomly tumbling cubes equal to 0.75 should be applied to all debris idealized as a rectangular box. This value for the average drag coefficient of subsonic randomly tumbling cubes uses a reference area approximately equal to the average projected area of a randomly tumbling cube ($1.5L^2$). Applying drag coefficient values for tumbling cubes to tumbling parallelepipeds appears reasonable given the insensitivity to aspect ratio: the drag coefficient of a non-tumbling cube is within ten percent of that for a non-tumbling parallelepiped with an aspect ratio of ten [28].

In order to apply the experimentally determined drag coefficient for a tumbling cube to debris items idealized as randomly tumbling rectangular cubes, an expression was derived for the average projected area of a rectangular box with dimensions L_1, L_2, L_3 (from longest to shortest). An approximation for the average projected area of a uniformly random rotating rectangular box was found by integrating the projected area over attitude (α) and yaw (δ) as follows:

$$A = \frac{4}{\pi^2} \int_0^{\pi/2} \int_0^{\pi/2} \left(L_1 L_2 \cos\alpha \cos\delta + L_1 L_3 \cos\alpha \sin\delta + L_2 L_3 \cos^2\delta \sin\alpha + L_2 L_3 \sin^2\delta \sin\alpha \right) d\alpha d\delta$$

The integrand is an approximate expression for the projected area of a rectangular box as a function of pitch and yaw angles. It was derived with the box oriented such that the projected area equals the largest face of the box when the pitch and yaw angles are zero. The integrand produces a close match (1.707) to Hoerner's value of $1.7L^2$ for the maximum projected area of a cube (i.e., a cube in the cornerwise position). After integration, the average projected area of a rectangular box with dimensions L_1, L_2, L_3 is approximately

$$A = \frac{4}{\pi^2}\left(L_1L_2 + L_1L_3 + \frac{\pi}{2}L_2L_3\right).$$

This formula for the average projected area of a randomly rotating rectangular box yields $1.45L^2$ as the average projected area of a randomly tumbling cube, which agrees well with Hoerner's roughly $1.5L^2$. This expression for the average projected area of a tumbling rectangular box also applies to a tumbling plate where the minimum dimension (L_3) is the thickness. If the thickness is approximately zero, this expression reduces to the average projected area calculated directly for a randomly tumbling flat plate of negligible thickness. Thus, this formula for the projected area of a tumbling rectangular box has been validated by three separate pieces of information.

The following formulas for drag coefficient and reference area may be used.

6.4.1 Spherical Objects

The mean subsonic C_D for a sphere diameter (D) depends on the flow state and surface type.

$C_D = 0.14$ for supercritical flow ($Re > 1\text{x}10^6$) with a smooth surface[11].

$C_D = 0.47$ for sub-critical flow ($Re < 1\text{x}10^6$) or with rough surface

Use a reference area (A) calculated as $A = \frac{\pi D^2}{4}$

Use piecewise linear fits to the data in Table 6-1 without extrapolation for the dependence of drag coefficient on Mach number for sub-critical flows. (The same data can be used for supercritical flow if multiplied by the ratio of subsonic drag coefficients for sub and super critical flow, i.e., 0.14/0.47.)

Table 6-1. Influence of Mach on Drag Coefficient for Spheres

MACH	0.3	0.5	0.6	0.8	0.9	1.0	1.4	2	4	10
C_D	0.47	0.5	0.52	0.64	0.73	0.82	1.05	1.0	0.93	0.92

[11] For example, no protrusion for the flow separation point would attach to what?. Many launch vehicle tanks have fittings or otherwise rough surfaces that effectively prevent delayed flow separation and increase drag.

Table 6-1 shows the relationship between Mach number and the drag coefficient for a sphere based for k=1.4. The drag coefficient in the hypersonic regime ($M \geq 5$) changes as on [27], with the precise value at Mach ten based on the continuum flow limit given in [29]the flow transitions from a continuum to free molecular flow. In the free molecular regime, the drag coefficient depends on the wall temperature and the accommodation coefficient for the surface, which are more difficult to compute. With the reasonably conservative assumptions that the wall temperature equals the stagnation temperature and the accommodation coefficient is one, the drag coefficient on a flat plate facing a free molecular flow equals 2.95. [29] Based on [29] the drag coefficient for a sphere in free molecular flow can be approximated as a function of the Reynolds number (Re_2) based on the density and viscosity behind the shock (not free stream).

$$C_D = 0.92 + 1.7\exp(-0.1\mathrm{Re}_2)$$

6.4.2 Cylindrical Objects

The mean subsonic C_D is a function of length (L) and diameter (D),

$$\textit{for} \quad \textit{all} \quad \frac{L}{D} \qquad\qquad C_D = 0.65\frac{L}{D} + 0.46$$

Use a reference area (A) calculated as $A = \dfrac{\pi D^2}{4}$

Use the piecewise linear fits to the data in Table 6-2 without extrapolation for the dependence drag coefficient on Mach number. The data should be scaled by the ratio of subsonic drag coefficients for the length-to-diameter ratio (L/D) of interest, e.g., for L/D = 4, the data for a cylinder in an axial flow should be multiplied by 3.06/0.825.

Table 6-2. Influence of Mach on Drag Coefficient for Randomly Tumbling Cylinder

MACH	0.3	0.5	0.8	0.9	1.0	1.4	2	4	5	10
C_D at L/D=4	3.06	3.15	3.45	3.56	4.30	5.79	6.27	5.82	5.97	6.04

6.4.3 Plate Shaped Objects and All Other Shapes idealized as Rectangular Boxes

$C_D = 0.75$

$$A = \frac{4}{\pi^2}\left(L_1L_2 + L_1L_3 + \frac{\pi}{2}L_2L_3\right)$$

where $L_1 > L_2 > L_3$

Use the piecewise linear fits to the data in Table 6-3 without extrapolation for the dependence drag coefficient on Mach number.

Table 6-3. Influence of Mach on Drag Coefficient for Randomly Tumbling Flat Plate

MACH	0.3	0.8	1.0	1.4	2	3	4	6	10
C_D	0.75	0.78	0.92	1.05	1.06	1.09	1.09	1.12	1.17

6.4.4 Thin Plate Shaped Objects with High Aspect Ratios

For plate-shaped debris (i.e., $L_2 >= 5L_3$) and L_2/ L_1 greater than 0.2, use $C_D = 0.75$

$$A = \frac{4}{\pi^2}\left(L_1L_2 + L_1L_3 + \frac{\pi}{2}L_2L_3 \right)$$

For $L_2/ L_1 \leq 0.05$, use

$C_D = 1.27\text{-}6.35(L_2/ L_1)$

For $0.05 < L_2/ L_1 \leq 0.1$, use

$C_D = 1.08\text{-}2.54(L_2/ L_1)$

For $0.1 < L_2/ L_1 <= 0.2$, use

$C_D = 0.903\text{-}0.76(L_2/ L_1)$.

Use the piecewise linear fits to the data in Table 6-4 for the dependence drag coefficient on Mach number. The data should be scaled by the ratio of subsonic drag coefficients for the aspect ratio of interest. (e.g., for $L_2/L_1 = 0.05$, the rectangular box values should be multiplied by 0.953/0.75)

Table 6-4. Influence of Mach on Drag Coefficient for Randomly Tumbling Thin Flat Plate

MACH	0.3	0.8	1.0	1.4	2	3	4	6	10
C_D at L_2/L_1=0.05	0.95	0.99	1.17	1.33	1.35	1.38	1.38	1.42	1.49

6.5 Inert Debris Effects

6.5.1 Inert Debris Effects on People in the Open

Several factors should be considered in computing casualty areas for inert debris. These include the vulnerability of the person, the size of the fragment, the size of a person, the velocity vector at impact, and whether the fragment remains intact or disintegrates (splatters) after impact. If it stays intact, it may ricochet or slide upon impact, depending on the velocity vector (magnitude and angle), the effective coefficient of restitution, and the effective coefficient of friction between the fragment and the surface impacted. Included in ricochet are the effects of tumble as well as rebound or bounce.

Using AIS level 3 as the threshold for human casualty, any time a person is struck by a debris fragment with a kinetic energy greater than 11 ft-lbs, the strike is considered a casualty producing impact. For example, if a person stands directly under a piece of debris falling vertically with a kinetic energy above 11 ft-lb, we assume that the person

will be a casualty upon impact due to direct debris impact effects. If the debris fragment strikes the ground and it rebounds up either intact or in pieces such that the rebounding debris has a kinetic energy greater than 11 ft-lbs when it strikes a person, such a strike would be a casualty producing impact due to secondary effects.

In practice, if the velocity and mass of the fragment exceed criteria presented in Figure 6-2, the person becomes a casualty. Criteria in Figure 6-2 apply to the "average general public." We believe the criteria are conservative because the basis of injury in this figure is a person being struck vertically on the head and not all impacts are to the head. Note that the impact velocity should account for the contribution due to feasible winds. The example computations presented below demonstrate acceptable methods for computing casualty areas associated with inert debris impacts to people in the open, both with and without winds. Significant winds are a typical cause of non-vertical impacts for launch vehicle debris.

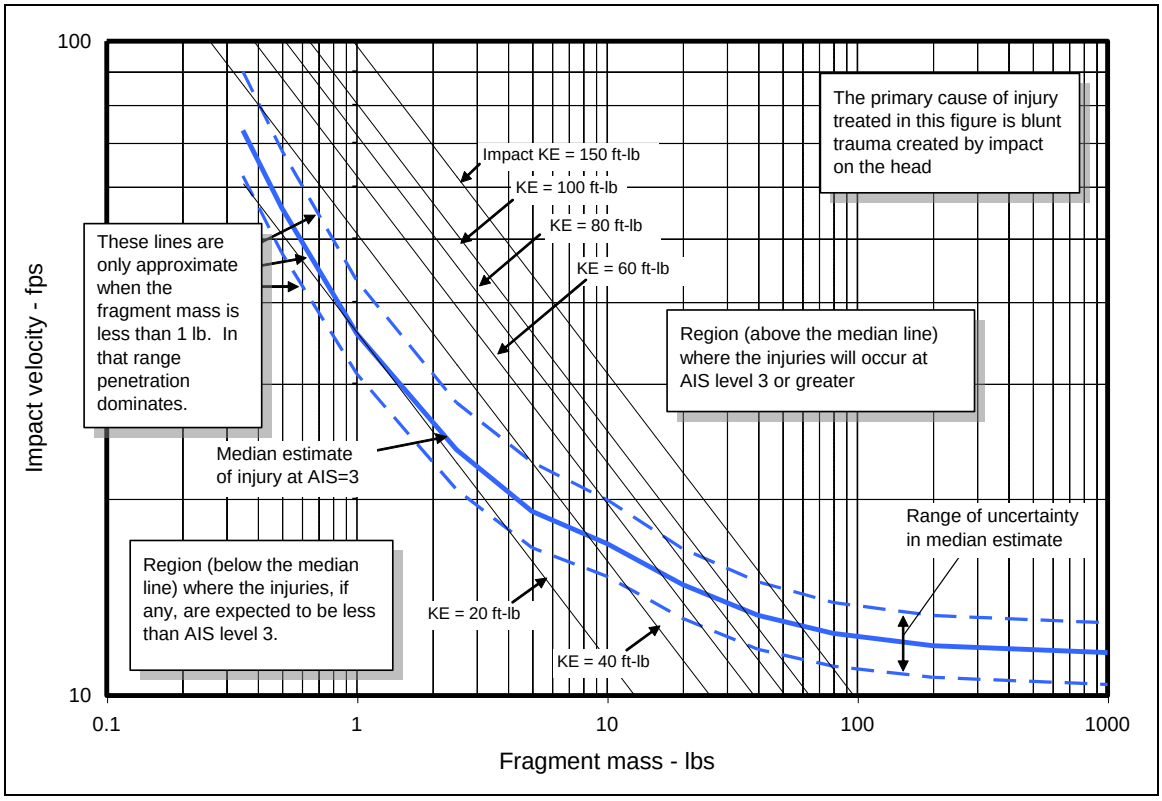

Figure 6-2 Median between Casualty (AIS ≥ 3) and Non-Casualty as a Function of Fragment Weight and Impact Velocity

For direct impact from debris falling vertically, the casualty area should take into account both the projected area of the debris fragment (A_F) and the projected area of the human body from above. We typically represent a standing person by a 6 ft tall cylinder with a 1 ft radius. When these two projections overlap such that the debris projection overlaps the center of the projected area of a person (i.e., we assume the center of the circle is the head/center of the human torso), the person becomes a casualty. The left side of Figure

6-3 identifies a piece of vertically falling debris and locations where a person would become a casualty if struck by the falling debris. The resulting projections, their overlap, and the ensuing basic casualty area defined by the radius r_D are presented on the right hand side of Figure 6-3.

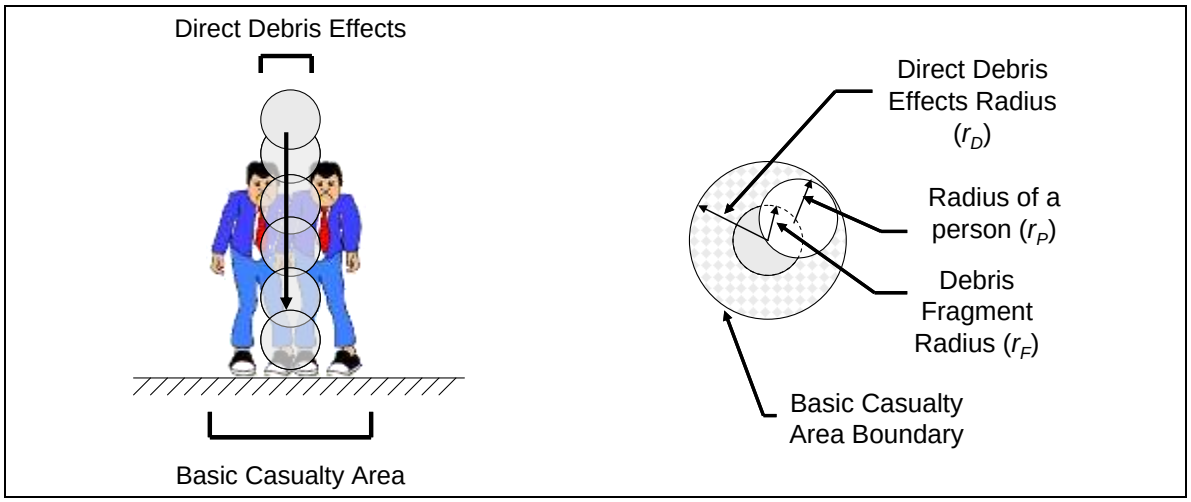

Figure 6-3. Illustration of the Basic Casualty Area resulting from direct debris effect

As indicated in Figure 6-3, there are secondary impact effects that could cause a casualty due to post impact events. For example, if the debris piece stays intact, it may ricochet or slide upon impact, depending on several parameters including the magnitude and angle of the velocity vector, the effective coefficient of restitution, and the effective coefficient of friction between the fragment and the surface impacted. Included in ricochet are the effects of tumble as well as rebound or bounce. Since a person who is struck by a casualty producing secondary impact effect should also be considered a casualty, the casualty area should also include the full extent of these secondary impact effects. Casualty area models that are designed to account for secondary effects often involve uncertainty regarding shapes, coefficients of restitution, friction coefficients, and the vulnerability of people to the fragment after bounce, skid, roll, etc. This process can be complex and subject to substantial uncertainty.

The total extent of these secondary impact effects can be modeled with the secondary impact effects factor (F_A). The projected area of the debris fragment is multiplied by this secondary impact effects factor to find the total area within which a person could be considered a casualty if the area reaches the center of the person's projected area. The reach of these secondary impact effects and the location of a person that could result in a casualty are presented in the left hand side of Figure 6-4. The right hand side shows the components of the resulting casualty area that accounts for all secondary impact effects.

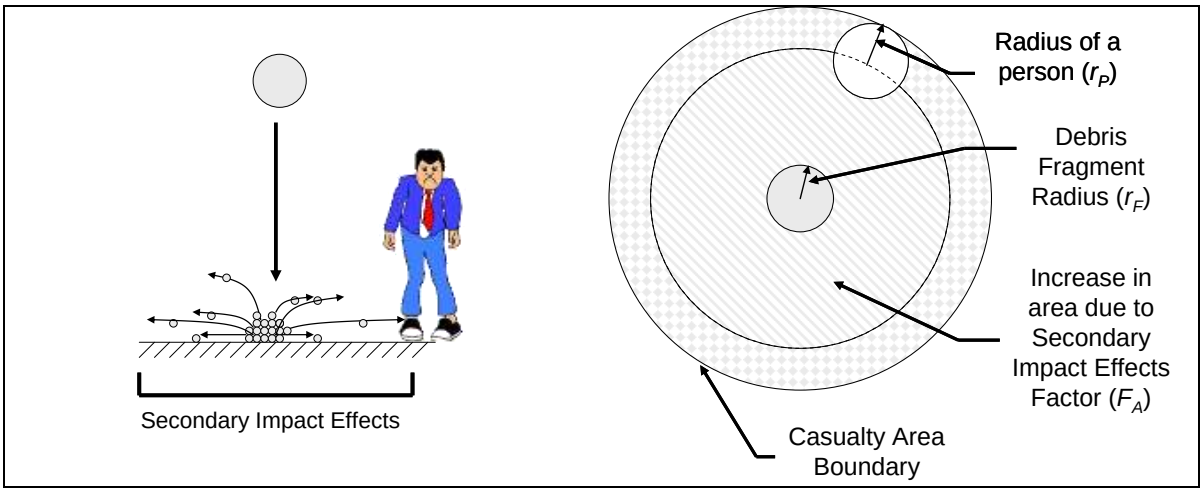

Figure 6-4. Illustration of secondary debris effects for vertically falling debris

The casualty area identified in Figure 6-4 is calculated as a function of the effective debris fragment radius accounting for secondary impact effects (r_{F_A}) and the radius of a person, r_P, as in equation (9).

$$A_c = \pi\left(r_P + r_{F_A}\right)^2 \qquad (9)$$

Where r_{F_A} is defined as $$r_{F_A} = \sqrt{\frac{F_A A_F}{\pi}} \qquad (10)$$

With these radii defined, the casualty area accounting for all secondary impact effects is found using equation (11).

$$A_c = \pi\left(r_P + r_F\sqrt{F_A}\right)^2 \qquad (11)$$

F_A is defined as the ratio of the area containing secondary debris impact effects and the projected area of the fragment (A_F). Modeling and experimentation has shown that F_A depends on several factors, including debris fragment characteristics, the magnitude and angle of the impacting fragment velocity vector, and the hardness of the impacted surface. Applicable research to date is not exhaustive but includes the work of [30] and [31]. Converting the results of these studies into a form consistent with equation (11) produces the secondary impact effects factor statistics for conventional launch vehicles presented in Table 6-5. Table 6-5 lists the average and 95% high F_A for various surface types and a combination representative of typical flight safety applications. It is important to remember that the values listed in Table 6-5 were derived based on limited investigations of conventional launch vehicles. It is conservative for conventional launch vehicle operations to employ the assumption that the vertical component of velocity vector is equal to the local terminal velocity of the fragment and the horizontal component of velocity is equal to the surface wind, as is done herein. For flight profiles where these velocity vector assumptions are not conservative, (flight profiles with significant horizontal velocities), the validity of the secondary impact effects factors presented herein should be investigated before application.

Table 6-5. Average and 95% high F_A values for hard surfaces, soft surfaces, and the 20/80 combined distribution identified in [31].

	Hard Surface	Soft Surface	20/80 Combined
Median	10.16	3.31	4.36
95% High	175.0	25.0	57.5

It is important to note that the factor F_A as used here is not equivalent to that employed in the study of [30]. While [30] modifies the basic casualty area, found as a function of the debris radius and the radius of a person, the F_A employed herein modifies the projected area of the debris fragment alone to account for the secondary effects which emerge once the debris fragment impacts the surface of the Earth. Further, the conversion assumes that the presented casualty areas are circular, which is a significant approximation when the ratio of the distance traveled during a bounce, for example, to the debris fragment radius is large. For a situation where the ratio is equal to 6 for a debris fragment of radius equal to 1 ft, the circular assumption produces a difference of just less than 14%, since the computation for debris of this size or smaller is dominated by the radius of a person. However, given the uncertainties associated with the dataset and further research that indicates potential variation of up to 30% in the predicted casualty areas, we do not anticipate that this level of error will significantly affect the validity of the approximations presented in [31]. Thus, this effect may be neglected.

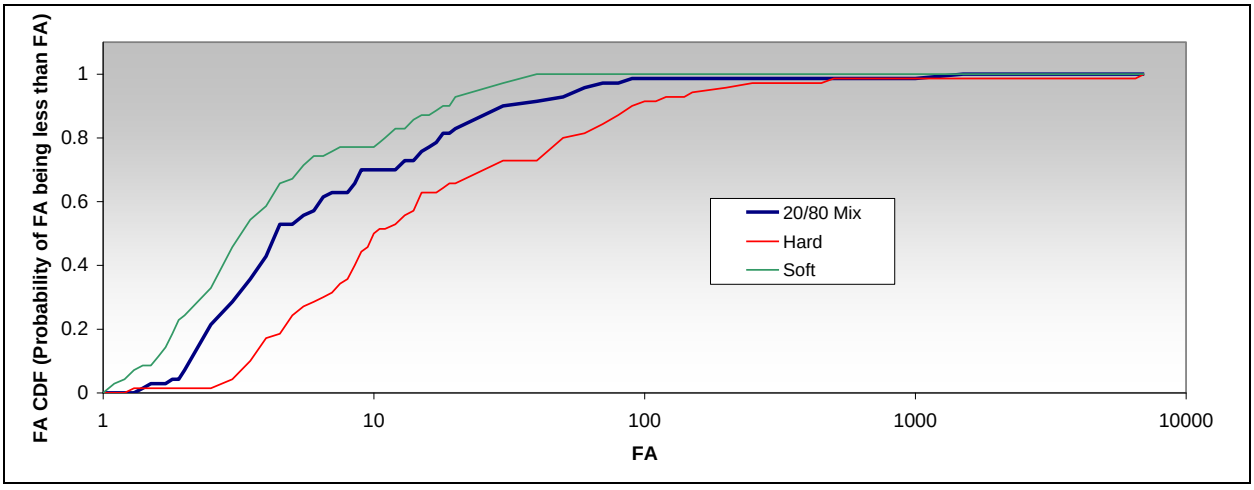

Figure 6-5. Cumulative distribution of F_A developed using the data presented in Appendices A and B of [30] for Hard and Soft impact surfaces and the 20/80 CDF based on the surface distribution identified in [31]

The 20/80 combined distribution function (CDF) identified in Table 6-5 and Figure 6-5 refers to a typical distribution of surfaces for flight safety analysis applications: where 20% of the impacted surfaces are modeled as a hard surface (such as pavement or cement), and the other 80% are modeled as a soft surface (such as soil) [31].

Equations (9) and (11) are appropriate for debris fragments falling in a near vertical manner. However, Figure 6-6 illustrates how debris approaching at an angle, α, elongates the basic casualty area: instead of a person only being at risk when directly under the debris fragment, the non-zero approach angle means that anyone whose midline is located within the swept volume of the debris fragment (i.e., the volume through which the debris fragment passes) once it breaks the 6 ft altitude would become a casualty.

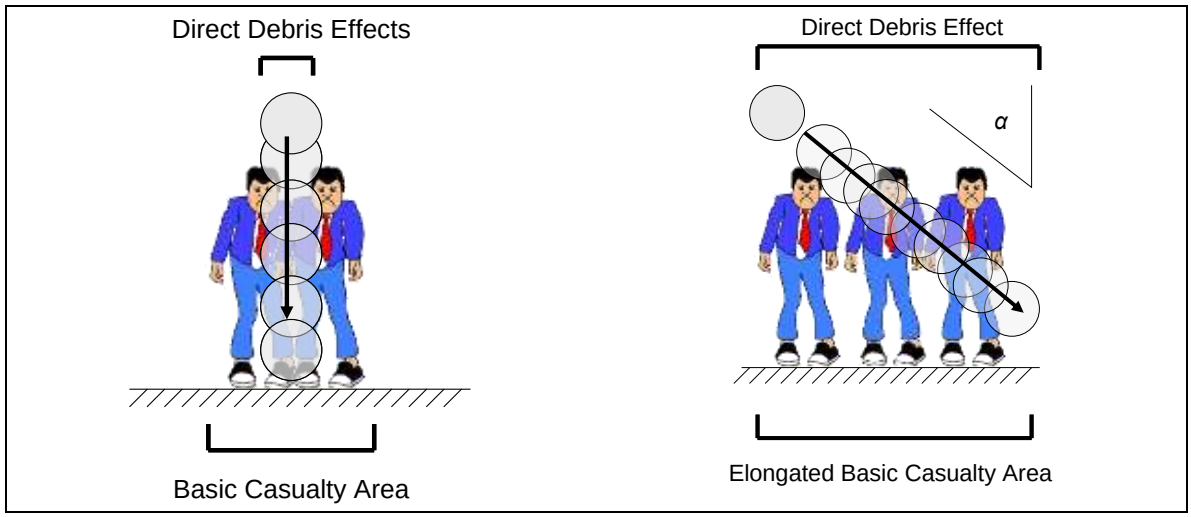

Figure 6-6. Illustration demonstrating the basic casualty area and its elongation due to a non-zero approach angle, α

While the left side of Figure 6-6 is the basis of the basic casualty are for debris fragments falling vertically, the right side identifies how this basic casualty area is elongated if the debris approaches at an angle, α, to the vertical. When the debris is approaching at α, as defined in Figure 6-6, the basic casualty area $A_\alpha(\alpha)$ is defined by equation (12).

$$A_\alpha(\alpha) = \pi r_D^{\,2} + 2 r_D h \tan\alpha \qquad (12)$$

Where:

$$r_D = r_F + r_P \qquad (13)$$

This elongated basic casualty area, like that defined by equation (12), only accounts for direct debris effects. As with vertically falling debris, a debris fragment impacting in a near vertical manner causes secondary impact effects that expand the casualty area around the impact location as a function of F_A. Within the constraints of conventional launch vehicle operations, the factors presented above are less conservative but still suitable for non-vertical impacts.

Combining the elongated basic casualty area with the casualty area accounting for secondary impact effects results in the non-circular area identified in Figure 6-8.

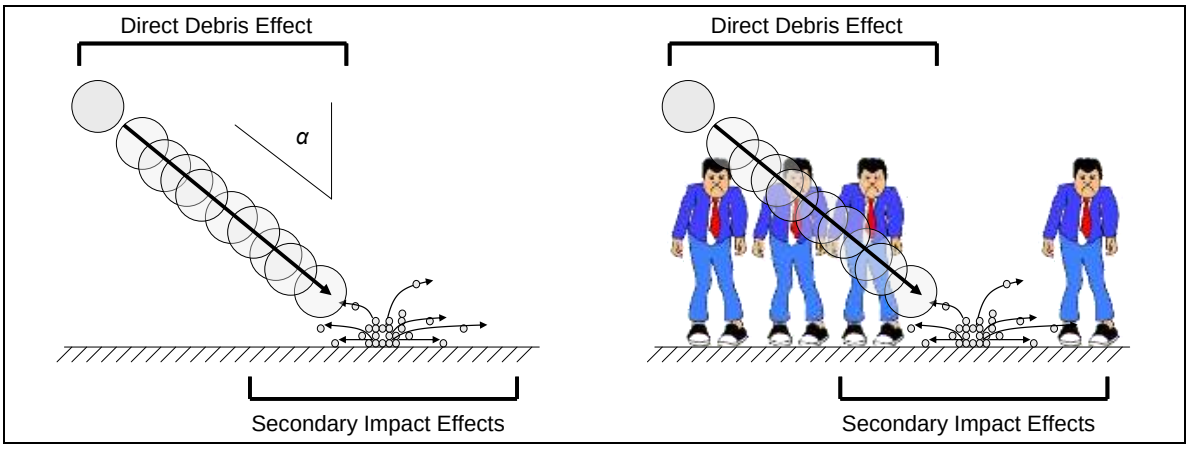

Figure 6-7. Direct and secondary debris effects for debris approaching at an angle, *α*, from vertical (left) and locations along the debris trajectory where a person could be affected (right)

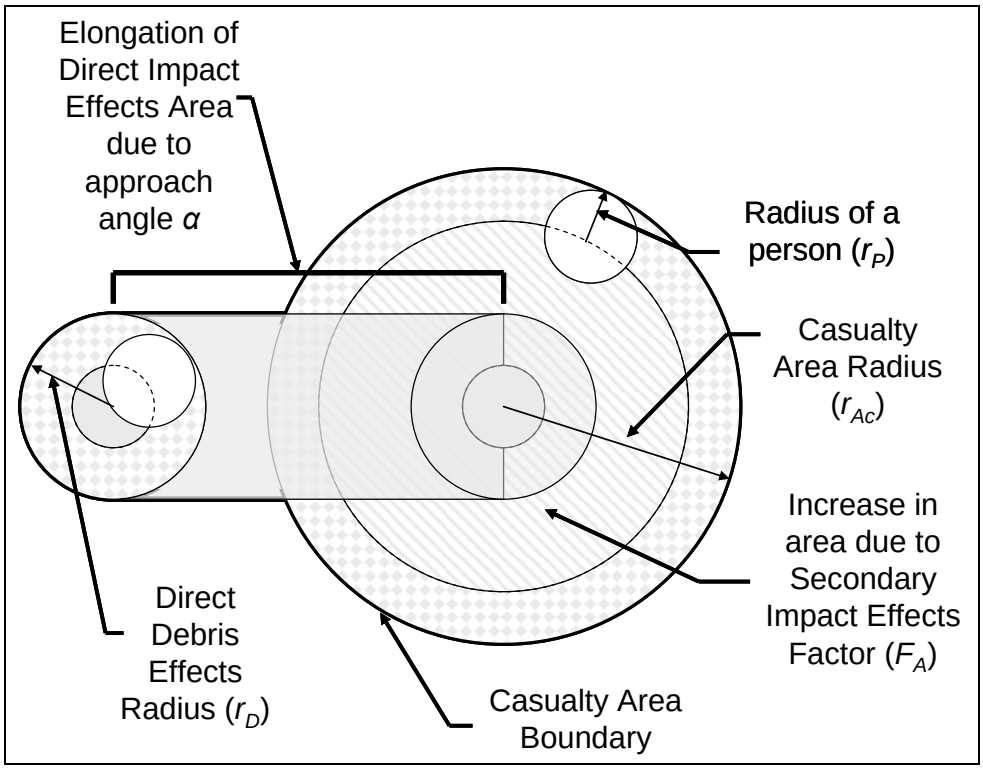

Figure 6-8. Components of the total casualty area for a debris fragment approaching the surface of the Earth in a non-vertical manner

While the elongation identified in Figure 6-8 results in a significant protrusion of the casualty area accounting for secondary impact effects, this is not always the case. This is important to note because any region of the elongated basic casualty area that overlaps the casualty area resulting from secondary impact effects should not be counted twice. Figure 6-9 identifies both an elongation that results in a significant protrusion on the left and an elongation where no protrusion is present on the right.

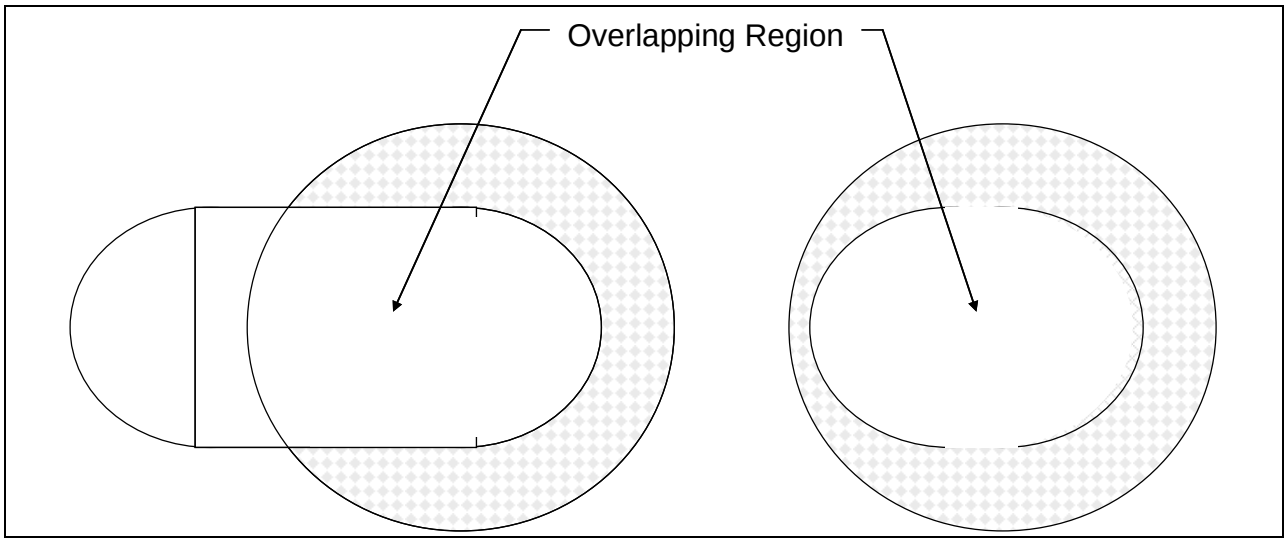

Figure 6-9. Regions where the projected direct debris impact effects overlap the secondary debris effects for large angles (left) and small angles (right)

If these overlapping regions are not subtracted when combining the casualty areas from both direct and secondary effects, the resulting casualty area will be overly conservative casualty area predictions. Therefore, for cases where the overlap does not produce a casualty area that exceeds the area given by equation (11) (i.e., the right hand side of Figure 6-9), no modifications are required to the casualty area of a vertically falling debris fragment. As previously noted, this lack of modification is valid because the average values of F_A given in Table 6-5 already account for secondary effects caused by non-normal impacts from conventional launch vehicles.[12]

For cases where the overlap does produce a casualty area that exceeds the area given by equation (11) (i.e., the left hand side of Figure 6-9), the overlapping region should be subtracted from $A_\alpha(\alpha)$. The remainder is identified as net expansion of the basic casualty area due to non-vertical impacts, A_c', shown as the shaded area in Figure 6-10.[13]

[12] When the impact angle from vertical is outside the range of those examined by [30], the suitability of the average F_A should be examined. A factor greater than the average may need to be considered if such a condition exists.

[13] Figure 6-10 assumes that the debris has a horizontal component of velocity in the negative-x direction and impacts at the origin.

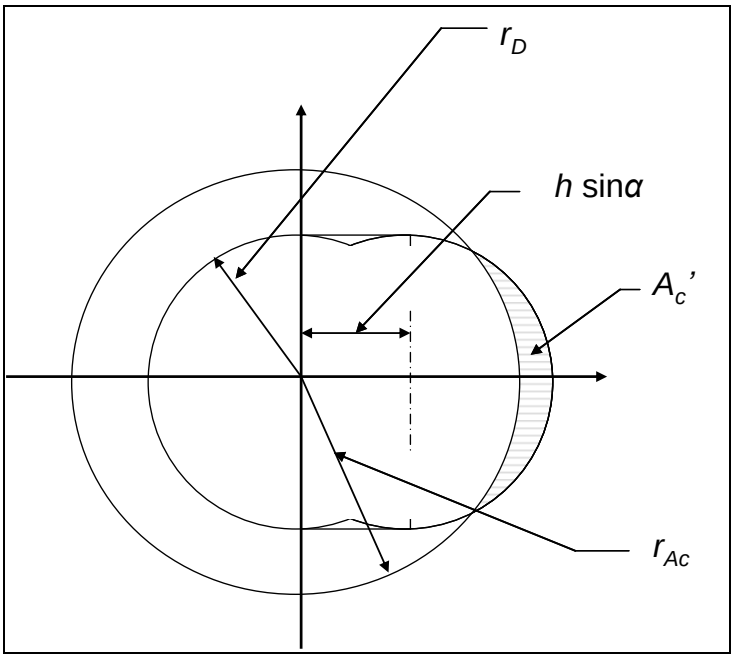

Figure 6-10. Relationship between the casualty area contributions from direct debris fragment impacts and secondary debris effects in terms of the positive-x

The total casualty area is found as in equation (14). This equation adds the direct effects of a non-vertical debris fragment impact less the overlapping region.

$$A_c = \pi\left(r_P + r_F\sqrt{F_A}\right)^2 + A_c' \qquad (14)$$

There are two conditions of interest when accounting for net expansion of the basic casualty area due to non-vertical impacts (A_c'):

(1) overlap that does not extend to the full radius of the basic casualty area and

(2) overlap that extends to the full radius of the basic casualty area.

These conditions are identified in the left and right-hand-sides of Figure 6-11, respectively.

The shaded area depicting A_c' in Figure 6-11 can be computed by the integration identified in equation (15).

$$A_c' = 2\int_0^{y_2}\left[\left(h\sin\alpha + \sqrt{r_D^2 - y^2}\right) - \left(\sqrt{r_{A_c}^2 - y^2}\right)\right]dy \qquad (15)$$

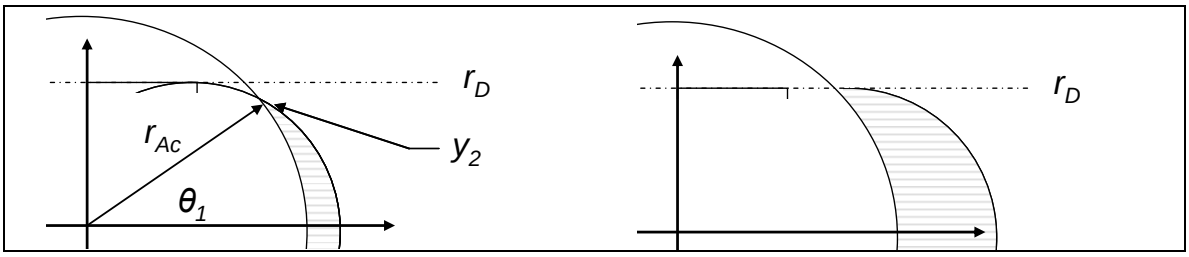

Figure 6-11. Scenarios where the integration limit is less than r_D (left) and where it is equal to r_D (right)

Where r_{Ac} is the radius associated with the casualty area for vertical impacts, including secondary effects, as shown in Figure 6-11. Therefore,

$$A_c' = 2y_2 h\sin\alpha + \left(r_D\sqrt{r_D^2 - y_2^2} + r_D^2 \sin^{-1}\left(\frac{y_2}{r_D}\right)\right) - \left(r_{A_c}\sqrt{r_{A_c}^2 - y_2^2} + r_{A_c}^2 \sin^{-1}\left(\frac{y_2}{r_{A_c}}\right)\right) \qquad (16)$$

When $y_2 = r_D$, this equation simplifies as follows:

$$A_c' = 2r_D h\sin\alpha + \left(\frac{\pi}{2} r_D^2\right) - \left(r_{A_c}\sqrt{r_{A_c}^2 - r_D^2} + r_{A_c}^2 \sin^{-1}\left(\frac{r_D}{r_{A_c}}\right)\right) \qquad (17)$$

If $\left(r_{A_c} - r_D\right) < h\sin\alpha < \sqrt{r_{A_c}^2 - r_D^2}$, then y_2 is less than r_D as shown in the left hand side of Figure 6-11. When y_2 is less than r_D, y_2 is defined as follows:

$$y_2 = r_{A_c}\sin\theta_1 \qquad (18)$$

Where θ_1 is as shown in Figure 6-11. In accordance with the Law of Cosines:

$$\cos\theta_1 = \frac{r_{A_c}^2 + \left(h\sin\alpha\right)^2 - r_D^2}{2r_{A_c} h\sin\alpha} \qquad (19)$$

Which results in the following:

$$y_2 = \frac{\sqrt{\left(2r_{A_c} h\sin\alpha\right)^2 - \left(r_{A_c}^2 + \left(h\sin\alpha\right)^2 - r_D^2\right)^2}}{2h\sin\alpha} \qquad (20)$$

Therefore, when y_2 is less than r_D as in the left hand side of Figure 6-11, substitution of equation 11 into equation 17 allows for computing A_c'.

EXAMPLE: Inert Debris Effects on People in the Open (Vertical Impacts)

To avoid the complications associated with human vulnerability models, a tier 1 analysis may assume that any piece of inert debris that impacts with energy greater than 11 ft-lbs produces a casualty due to blunt trauma per 14 CFR §417.107(c). Therefore, the area affected by debris with energy above this threshold is considered the effective casualty area (A_C). The casualty area for inert debris falling straight down towards the surface of the Earth encompasses the debris fragment projected area (A_F), the plan view of a person in the open (A_P), and a scaling factor. As an example, Table 6-6 contains information characterizing an abbreviated generic debris fragment list.

Table 6-6. Example Debris List for a Conventional Launch Vehicle.

Fragment Piece/Group and Description	Number of Fragments	Weight per Fragment (lb)	Ballistic Coefficient (psf)	Projected Area (ft2)
Upper Feedpipe	1	220.64	44.2	8.15
Middle Feedpipe	1	1007.66	46.4	40.87
Feedline with Valves	3	32.63	35.8	1.60
Payload	1	17746.0	74.9	315.00
Oxidizer Tank	8	41.64	7.7	7.21
Skirt	8	14.36	12.5	1.37
Interstage Panel	62	0.67	4.2	0.22
Interstage Panel	73	0.26	3.1	0.11
Interstage Panel	73	0.26	3.0	0.12
Interstage Panel	73	0.26	3.0	0.12
Interstage Panel	72	0.26	3.1	0.11
Support Structure	1	7209.21	93.2	103.09
Engine Assembly	9	219.15	56.0	5.22
Insulation	10	22.36	4.7	6.36
Tank Valves	2	23.40	83.1	0.38
Pressurized Gas Tanks	8	72.23	157.8	3.27
Propellant Tanks	2	23.45	47.6	3.52
Pressurized Gas Bottles	4	73.20	127.9	4.09

Given this table, the kinetic energy of each piece at impact should be calculated. Kinetic energy (E_k) is a function of mass (m) and velocity magnitude (v) and is calculated as in equation (21).

$$E_k = \frac{1}{2} m v^2 \tag{21}$$

From Table 6-6, the mass of each debris fragment can be found by using the fragment weight, *W*, (i.e., mass equals weight divided by acceleration due to gravity). Finding the velocity of an object at any point in time as it travels through the atmosphere is found by examining the forces acting upon that object throughout its flight. The forces acting on an object falling in a ballistic manner at a velocity relative to the local wind (v_{rel}) are identified in the free-body-diagram presented in Figure 6-12.

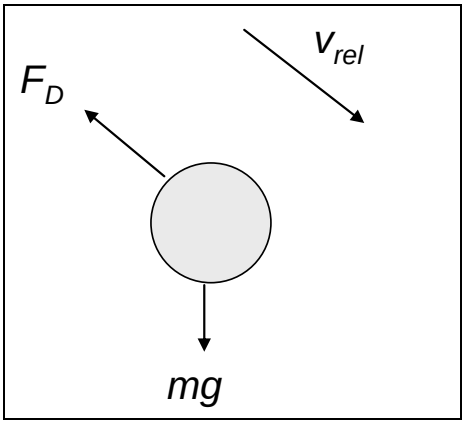

Figure 6-12. Free body diagram for an object traveling at a velocity relative to the local wind equal to v_{rel}

While the force of gravity (i.e., *mg*) is constant for altitudes of interest, the force of drag (F_D) directly opposes v_{rel} with a magnitude as identified in equation (22).

$$F_D = \frac{1}{2} \rho c_D A v_{rel}^2 \tag{22}$$

In equation (22), ρ is the local air density, *A* is the effective projected area, and c_D is the coefficient of drag, which depends on the shape and surface characteristics of the falling object. While c_D is often presented in terms of Mach, it may be necessary to examine the Reynolds number to ensure the approximation based on Mach is sufficient.

Understanding the forces acting on an object falling in a ballistic manner is important for understanding the concept and limitations of terminal velocity. While its name may imply an absolute value that cannot be exceeded, terminal velocity (v_t) is the velocity of an object when there is no net vertical acceleration on an object traveling in a ballistic manner. This occurs when the force of drag (F_D) in the y-direction is equal to the force of gravity (*mg*), as identified by the free body diagram of Figure 6-13.

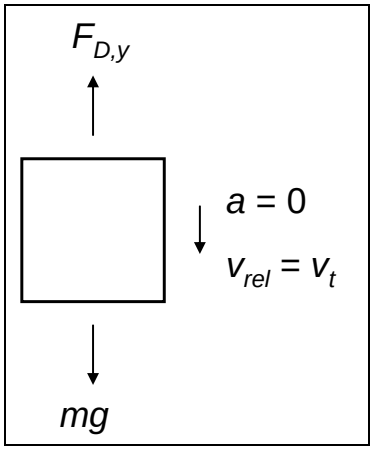

Figure 6-13. Free body diagram associated with a debris fragment at terminal velocity.

The equation of motion for this condition can be developed from this free-body-diagram and then solved for the velocity under this condition as follows.

$$0 = mg - F_D \tag{23}$$

$$mg = \frac{1}{2}\rho c_D A v_t^2 \tag{24}$$

$$v_t^2 = \frac{2mg}{\rho c_D A} \tag{25}$$

$$v_t = \sqrt{\frac{2\beta}{\rho}} \tag{26}$$

For standard atmospheric conditions at sea level, equation (26) is often approximated by:

$$v_t = 30\sqrt{\beta} \tag{27}$$

For an object falling in a vertical manner, the value of terminal velocity is then used to find the kinetic energy in ft-lbs of the fragment at impact using equation (28) with W in pounds and the velocity magnitude in feet per second.

$$E_k = \frac{1}{2}\left(\frac{W}{32.2}\right)v_t^2 \tag{28}$$

Equations (26) and (28) are used to develop the values in Table 6-7.

Table 6-7. Terminal velocity and kinetic energy values for the identified fragments

Fragment Piece/Group and Description	Number of Fragments	Weight per Fragment (lb)	Ballistic Coefficient (psf)	Terminal Velocity (fps)	Kinetic Energy (ft-lbs)
Upper Feedpipe	1	220.64	44.2	199.45	1.37E+05
Middle Feedpipe	1	1007.66	46.4	204.35	6.57E+05
Feedline with Valves	3	32.63	35.8	179.50	1.64E+04
Payload	1	17746	74.9	259.63	1.87E+07
Oxidizer Tank	8	41.64	7.7	83.25	4.51E+03
Skirt	8	14.36	12.5	106.07	2.52E+03
Interstage Panel	62	0.67	4.2	61.48	39.57
Interstage Panel	73	0.26	3.1	52.82	11.33
Interstage Panel	73	0.26	3	51.96	10.97
Interstage Panel	73	0.26	3	51.96	10.97
Interstage Panel	72	0.26	3.1	52.82	11.33
Support Structure	1	7209.21	93.2	289.62	9.45E+06
Engine Assembly	9	219.15	56	224.50	1.73E+05
Insulation	10	22.36	4.7	65.04	1.48E+03
Tank Valves	2	23.4	83.1	273.48	2.73E+04
Pressurized Gas Tanks	8	72.23	157.8	376.86	1.60E+05
Propellant Tanks	2	23.45	47.6	206.98	1.57E+04
Pressurized Gas Bottles	4	73.2	127.9	339.28	1.32E+05

Examination of Table 6-7 reveals that the kinetic energy of the highlighted debris fragments is less than 11 ft-lbs. If these debris fragments were falling straight down, these pieces would not be included in further analysis of the expected ground casualties (but may still be important to account for in the determination of appropriate aircraft hazard areas). This is the reason that, through examination of Table 6-8, it is evident that these pieces are no longer considered when computing the total casualty area.

Once the casualty area of each piece that has a kinetic energy above the 11 ft-lbs threshold is computed, the casualty area in each case is multiplied by the number of debris fragments which share the same characteristics to find the total casualty area for each debris group as listed in the final column of Table 6-8.

Table 6-8. Casualty area computations for each debris fragment identified in Table 6-7 as having a kinetic energy above the 11 ft-lbs threshold.

Fragment Piece/Group and Description	Number of Fragments	Projected Area (ft2)	Basic Ac per Fragment (ft2)	Ac per Fragment with Secondary Effects (ft2)	Ac(Secondary) / Ac(Basic)	Total Casualty Area (ft2)
Upper Feedpipe	1	8.15	21.41	59.81	2.79	59.81
Middle Feedpipe	1	40.87	66.67	228.66	3.43	228.66
Feedline with Valves	3	1.6	9.23	19.48	2.11	58.44
Payload	1	315	381.06	1507.91	3.96	1507.91
Oxidizer Tank	8	7.21	19.87	54.45	2.74	435.62
Skirt	8	1.37	8.66	17.78	2.05	142.23
Interstage Panel	62	0.22	5.02	7.57	1.51	469.50
Interstage Panel	73	0.11	4.43	6.08	1.37	443.56
Interstage Panel	72	0.11	4.43	6.08	1.37	437.48
Support Structure	1	103.09	142.22	527.77	3.71	527.77
Engine Assembly	9	5.22	16.46	42.81	2.60	385.31
Insulation	10	6.36	18.44	49.54	2.69	495.38
Tank Valves	2	0.38	5.71	9.36	1.64	18.72
Pressurized Gas Tanks	8	3.27	12.82	30.78	2.40	246.27
Propellant Tanks	2	3.52	13.31	32.38	2.43	64.75
Pressurized Gas Bottles	4	4.09	14.40	35.94	2.50	143.77
TOTAL	**265**	**500.57**	**744.15**	**2636.40**		**5665.20**

From the final line of Table 6-8, the total casualty area is about 5665 ft^2

EXAMPLE: Inert Debris Effects on People in the Open (Non-vertical Impacts)

Whether due to factors such as trajectory, imparted velocity (section 10.4.6), or wind (section 10.4.5), it is rare that a debris fragment falls in a purely vertical manner towards the surface of the Earth. This means:

(1) that each non-vertically impacting debris fragment produces an increase in casualty area represented by A_c', as identified graphically in Figure 6-10, and

(2) the velocity of an object relative to its impact location (v) is rarely equal to v_{rel}.

From Figure 6-14, the two components of the debris fragment velocity vector relative to the surface of the Earth are identified. For debris that is being accelerated by the wind in the x-direction, it is not likely that the debris fragment will reach a velocity equal to the wind. To assume the velocity of a debris fragment traveling in a ballistic manner is equal to the velocity of the wind would be over-estimating the velocity of the fragment relative to the surface of the Earth for cases where the initial horizontal velocity is consistent with traditional launch vehicle analyses. Further, as the force of drag is directly related to the atmospheric conditions local to the debris fragment, it is not uncommon for the magnitude of the velocity in the vertical direction to exceed that of the local terminal velocity.

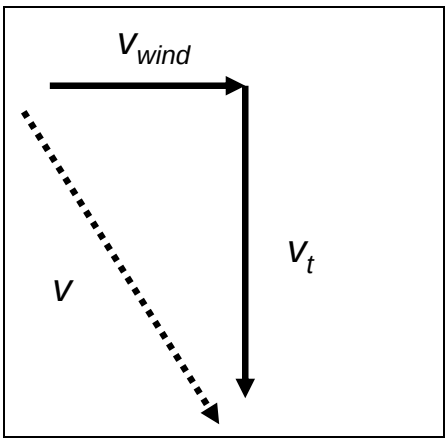

Figure 6-14. Wind and terminal velocity components of a debris fragment velocity vector relative to the surface of the Earth

For simplicity, however, it is often assumed that debris is falling in the vertical direction at a velocity equal to the local terminal velocity at sea level and traveling horizontally with a velocity vector equal to the local wind. As this overestimates the horizontal velocity and underestimates the vertical velocity towards impact, the approach angle is conservative. As an example of how this impact angle would affect the computed casualty area, we examine the debris list from Table 6-7 in the presence of a 10 knot wind. In this example, we assume that the debris is traveling downwards at terminal velocity while traveling horizontally at the wind speed. Under this assumption, the angle

relative to vertical is computed and presented in Table 6-9, along with the new kinetic energy value for each piece.

Table 6-9. Angle from vertical and kinetic energy at impact in the presence of a 10 knot wind.

Fragment Piece/Group and Description	Number of Fragments	Terminal Velocity (fps)	Vertical Kinetic Energy (ft-lbs)	Angle from Vertical with 10 knot Wind (deg)	Kinetic Energy with Wind Contribution (ft-lbs)
Upper Feedpipe	1	199.45	1.37E+05	4.84	1.38E+05
Middle Feedpipe	1	204.35	6.57E+05	4.72	6.62E+05
Feedline with Valves	3	179.50	1.64E+04	5.37	1.66E+04
Payload	1	259.63	1.87E+07	3.72	1.88E+07
Oxidizer Tank	8	83.25	4.51E+03	11.46	4.69E+03
Skirt	8	106.07	2.52E+03	9.04	2.59E+03
Interstage Panel	62	61.48	39.57	15.35	42.55
Interstage Panel	73	52.82	11.33	17.72	12.49
Interstage Panel	73	51.96	10.97	17.99	12.13
Interstage Panel	73	51.96	10.97	17.99	12.13
Interstage Panel	72	52.82	11.33	17.72	12.49
Support Structure	1	289.62	9.45E+06	3.34	9.48E+06
Engine Assembly	9	224.50	1.73E+05	4.30	1.74E+05
Insulation	10	65.04	1.48E+03	14.55	1.58E+03
Tank Valves	2	273.48	2.73E+04	3.53	2.74E+04
Pressurized Gas Tanks	8	376.86	1.60E+05	2.56	1.61E+05
Propellant Tanks	2	206.98	1.57E+04	4.66	1.58E+04
Pressurized Gas Bottles	4	339.28	1.32E+05	2.85	1.32E+05

It is important to note that the highlighted debris fragment groups, while below the 11 ft-lbs energy threshold when falling straight down as presented in Table 6-7, are now above the threshold and should now be considered when computing casualty area.[14]

Table 6-10 presents the radii defined by Figure 6-10 and the resulting expansion of the direct impact area due to the impact angle. Based on these radii, the 5th column indicates whether or not the condition associated with equation (18) is met. For cases where the condition is not met because of too little expansion, A_c' in the final column is zero. When the expansion is such that y_2 is equal to r_D, equation (16) is applied to calculate the non-zero value identified in the final column.

[14] The fact that such a small increase in velocity can bring these debris fragment groups above the 11 ft-lbs threshold should serve as a warning to ensure that any simplification used (i.e., the horizontal debris fragment velocity is equal to the wind velocity and the vertical component of velocity is equal to terminal velocity at sea level) is suitable for the mission profile being examined.

Table 6-10. Radii, expansion, and Ac' from direct impact effects

Fragment Piece/Group and Description	rD	rA	Expansion of Direct Impact Area (ft2)	Does y2 exist and is less than rD?	Is Ac' non-zero?	Ac' (ft2)
Upper Feedpipe	2.61	4.36	0.51	NO	NO	0.000
Middle Feedpipe	4.61	8.53	0.50	NO	NO	0.000
Feedline with Valves	1.71	2.49	0.56	NO	NO	0.000
Payload	11.01	21.91	0.39	NO	NO	0.000
Oxidizer Tank	2.51	4.16	1.22	NO	NO	0.000
Skirt	1.66	2.38	0.95	YES	YES	0.443
Interstage Panel	1.26	1.55	1.65	NO	YES	3.245
Interstage Panel	1.19	1.39	1.92	NO	YES	3.927
Interstage Panel	1.20	1.41	1.95	NO	YES	4.004
Interstage Panel	1.20	1.41	1.95	NO	YES	4.004
Interstage Panel	1.19	1.39	1.92	NO	YES	3.927
Support Structure	6.73	12.96	0.35	NO	NO	0.000
Engine Assembly	2.29	3.69	0.45	NO	NO	0.000
Insulation	2.42	3.97	1.56	YES	YES	0.004
Tank Valves	1.35	1.73	0.37	NO	NO	0.000
Pressurized Gas Tanks	2.02	3.13	0.27	NO	NO	0.000
Propellant Tanks	2.06	3.21	0.49	NO	NO	0.000
Pressurized Gas Bottles	2.14	3.38	0.30	NO	NO	0.000

From here, the casualty area for each fragment is found with equation (14). The summation of the casualty area on the surface of the earth encompassing all secondary effects plus A_c' is presented in Table 6-11.

Table 6-11. Casualty areas from Secondary Effects for debris fragments approaching in a non-vertical manner due to a 10 knot wind

Fragment Piece/Group and Description	Number of Fragments	Projected Area (ft2)	Casualty Area per Fragment with Wind (ft2)	Ac(Wind)/ Ac(Basic)	Total Casualty Area with Wind (ft2)
Upper Feedpipe	1	8.15	59.81	2.79	59.81
Middle Feedpipe	1	40.87	228.66	3.43	228.66
Feedline with Valves	3	1.6	19.48	2.11	58.44
Payload	1	315	1507.91	3.96	1507.91
Oxidizer Tank	8	7.21	54.45	2.74	435.62
Skirt	8	1.37	18.22	2.10	145.77
Interstage Panel	62	0.22	10.82	2.15	670.67
Interstage Panel	73	0.11	10.00	2.26	730.25
Interstage Panel	73	0.12	10.23	2.28	747.03
Interstage Panel	73	0.12	10.23	2.28	747.03
Interstage Panel	72	0.11	10.00	2.26	720.25
Support Structure	1	103.09	527.77	3.71	527.77
Engine Assembly	9	5.22	42.81	2.60	385.31
Insulation	10	6.36	49.54	2.69	495.42
Tank Valves	2	0.38	9.36	1.64	18.72
Pressurized Gas Tanks	8	3.27	30.78	2.40	246.27
Propellant Tanks	2	3.52	32.38	2.43	64.75
Pressurized Gas Bottles	4	4.09	35.94	2.50	143.77
TOTAL	**411**	**500.81**	**2668.41**		**7933.45**

The total casualty area for each debris group is identified in the final column. The total casualty area for the debris list as a result of the 11 ft-lbs threshold and the 10 knot wind is now nearly **7933 ft^2**.

With a relatively moderate increase in wind speed, the result is greater than a 40% increase in casualty area. It is important to note that this example sees such a significant increase not as a direct result of the additional casualty area from direct impacts due to debris approaching in a non-vertical manner, but from the increase in the number of pieces to account for due to the 11 ft-lbs energy threshold.

If the kinetic energy of the two interstage panel debris fragment groups identified in

Table 6-11 had not increased past the 11 ft-lbs threshold as a result of the 10 knot wind, the increase in casualty area due to direct impacts from non-vertical debris would only have been a few percent.

6.5.2 Inert Debris Effects on People in Structures

Occupants of structures are not necessarily protected from the debris. Fragments can penetrate roofs and hazard the occupants. Penetrability is based on the impact velocity, the fragment area and the fragment weight, as well as the capability of the roof to resist the impact. Once the fragment does penetrate, it can also produce secondary fragments that will also hazard the occupants. This section provides effective casualty areas considering conditions where roof penetration is possible. It is divided into two parts: definition of the fragments into ballistic coefficient categories, and then classification of the roofs that may be impacted by the fragments.

The roof penetration capability of a fragment will vary with the impact location. For example, impacts midway between joists or beams, directly on joists, or somewhere between, will have different penetration capability. The processes modeled for roof/floor penetration and the production of secondary debris are illustrated in Figure 6-15. The effective casualty area from roof penetration is also a function of the impact velocity and the size of the fragment. Although the figure shows multiple floors, the material provided in this section conservatively assumes that all vulnerable people are on the top floor sheltered only by the roof.

Figure 6-15 shows the layout of a typical wood roof and different impact configurations. The red (large) and blue (small) circles indicate two different sizes of the impacting debris.

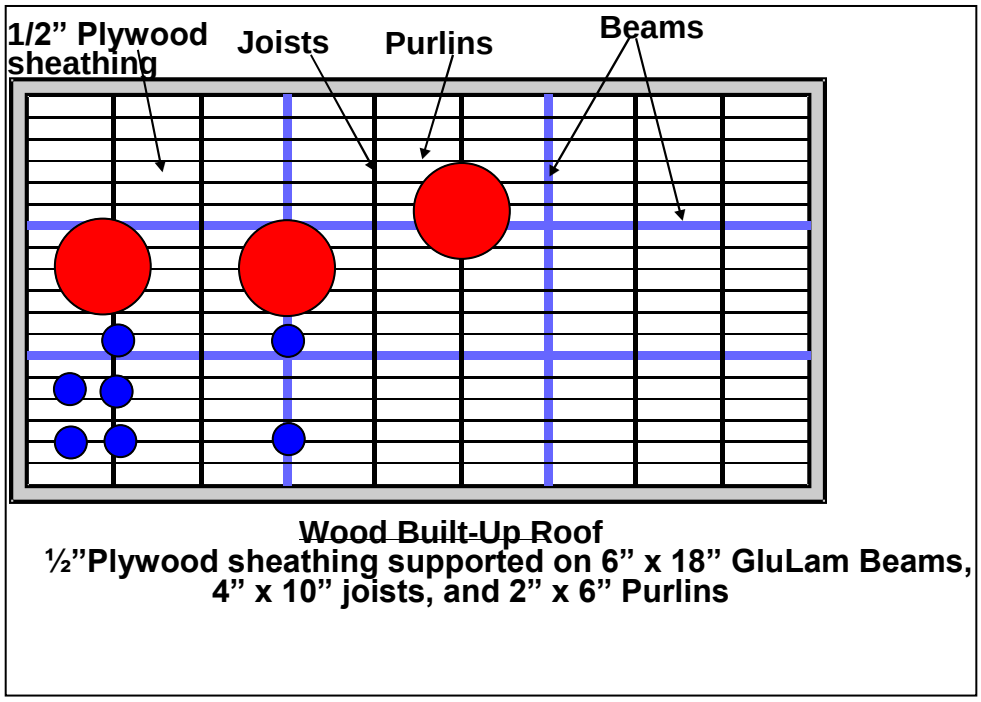

Figure 6-15 Roof Construction and Some Debris Impact Locations

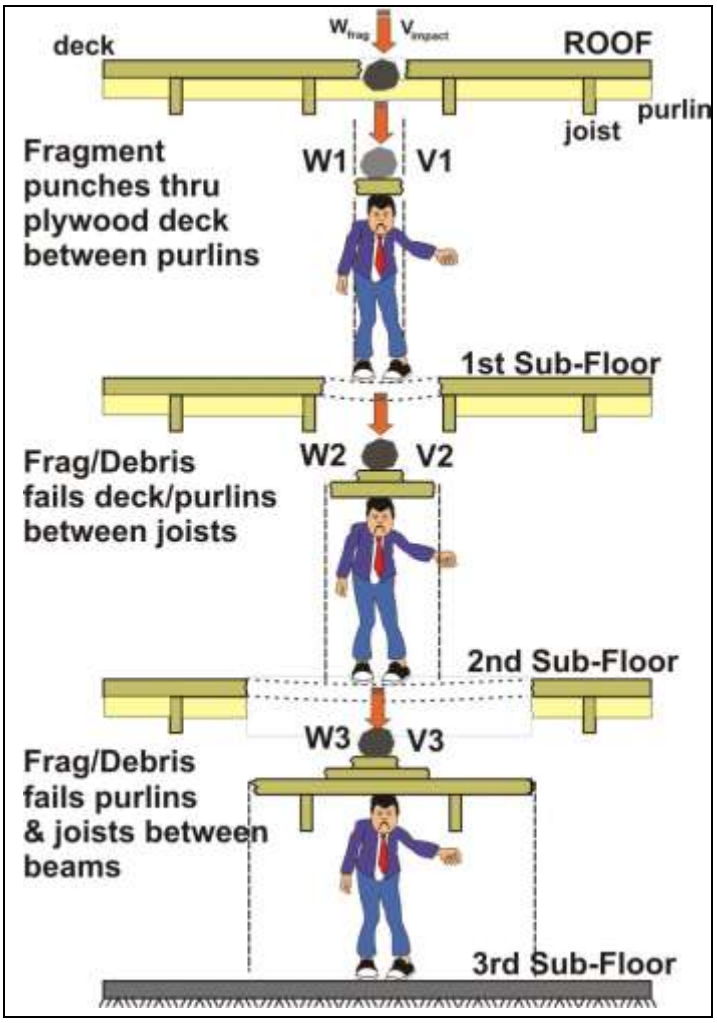

Figure 6-16. Illustration of Modeling Roof/Floor Penetration

The method used to develop the results in this section assumes a uniform probability distribution for the impact points on a roof. Simulations modeling thousands of impact conditions were performed to provide the curves of effective casualty area as a function debris class, debris weight, and roof type.

Table 6-12 shows six fragment categories defined by ballistic coefficient ranges and describes typical debris that may be in those ballistic coefficient ranges. Note that some fragment descriptions are listed in more than one ballistic coefficient category. This can happen because configurations of some common fragment categories vary and consequently alter weight and aerodynamic characteristics.

Table 6-12 Ballistic Coefficient Classes for Debris Roof Penetration Analysis

Balllistic Coefficient Class	β range	Representative β Used in the Penetration Analysis	Typical Vehicle Fragments in this Class
1	1.8 to 3 psf	2.3 psf	Skin, doors, interstage structure, skirt, lighter bulkhead parts, straps, fairing sections
2	3 to 10 psf	6.4 psf	Ducts, heavier bulkhead parts, antennas, medium mass interstage parts, some fairing parts, struts, nozzle extension
3	10 to 17.5 psf	13.8 psf	Heavier antennas, interstage structure, telemetry box, small actuators, electronics packages, ACS jets, more massive fairing parts
4	17.5 to 30 psf	21.3 psf	Small engines, batteries, receivers, helium tanks, nitrogen tanks, propellant lines
5	30 to 55 psf	44 psf	Batteries, actuators, large helium tanks
6	55 to 100 psf	69.9 psf	Main engines, heat exchangers, gas generators

Next, consider the roof types that might be impacted by debris. The list in Table 6-13 categorizes roofs into four general classes, A to D. The A Class is for lighter roofs on more temporary structures. The categories progress to the least vulnerable D Class - roofs on robust commercial structures. This simplified model does not address debris impacts on blockhouse-type structures. Those structures, being much closer to the launch, often warrant individual analyses.

Table 6-13. Representative Roof Classes for Debris Penetration Analyses

Structure Roof Class	Building Description	Typical Roof Construction	Representative Roof for Penetration Analysis
A	Mobile home and trailers Temporary office trailers	22 gage corrugated steel roof, 24 gage corrugated aluminum roof or 1/2 inch plywood roof	24 gage corrugated aluminum
B	Single family dwellings Duplex and fourplex residential dwellings Small condominiums and townhouses Small apartment buildings	Wood roof	5/8 inch plywood
C	Small retail commercial buildings (gas stations, stores, restaurants, strip malls) Small office and medical office buildings	Composite roof (rigid insulation on steel purlins), corrugated steel roof (pre-engineered metal building-type roof, or light weight concrete on corrugated steel decking roof	Composite roof (2 inch rigid gypsum insulation of steel purlines)
D	Manufacturing plants Warehouses Public buildings (large shopping malls, large office buildings, large apartment buildings, hotels, etc.)	Lightweight concrete on corrugated steel decking roof, or reinforced concrete slab roof	3½ inch lightweight concrete on 22 gage corrugated steel decking

The third column in the table presents typical roof constructions for structures in the four categories. The fourth column contains the primary roof characteristics used in analyzing

penetration for the four classes of structures. The corresponding underlying rafters, beams, framing, etc., were all modeled in the analyses of these roofs.

We analyzed the four roof classifications for penetration by the six ballistic coefficient classes for the debris. We assumed the debris fragments would impact the roofs at terminal velocity and had weights ranging from 0.1 lb. to 10,000 lb. Figure 6-17 through Figure 6-20 show the resulting effective casualty areas for people in structures impacted by inert debris. Each figure provides the casualty area for a given roof-type as a function of fragment weight in each of the beta classes.

The effective casualty areas in the figures are based on many impact points over a roof for each fragment weight and roof type. In some cases, penetration will not occur every time because the fragment is stopped by the joist supporting the surface. The average effective casualty area considers those cases where there is no penetration and, consequently, the effective casualty area due to roof penetration can be less than the basic casualty area.

The next four figures require a period after the word ‘direction.’

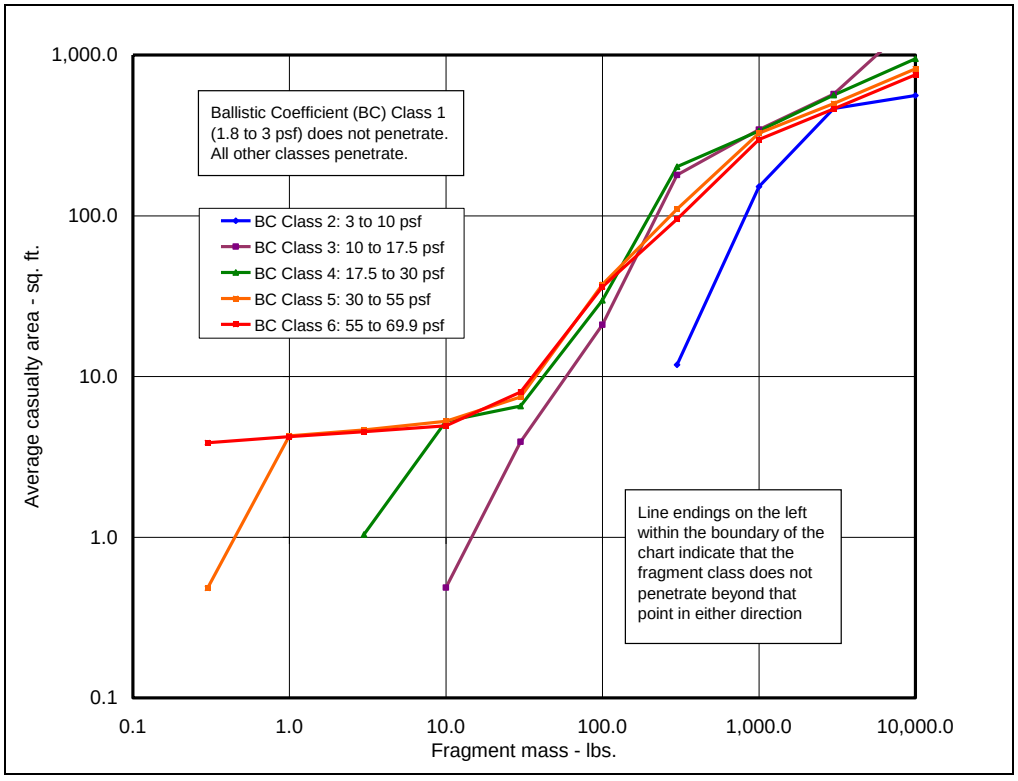

Figure 6-17. Effective Casualty Areas Due to Debris Hitting a Light Metal Roof (Class A)

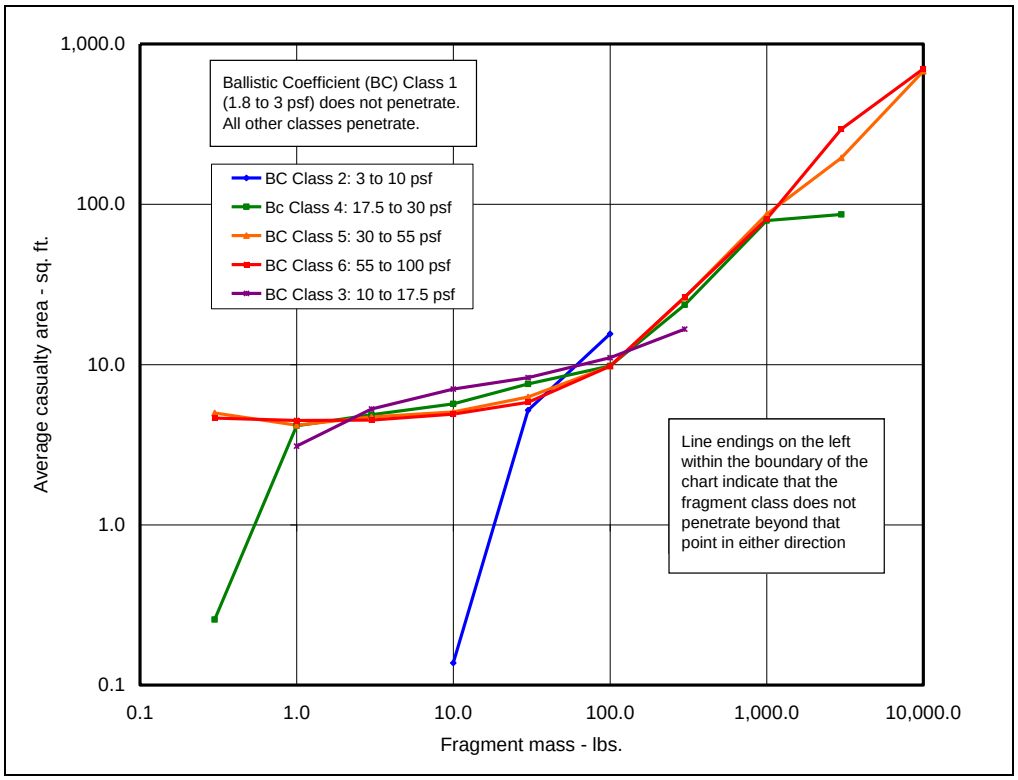

Figure 6-18 Effective Casualty Areas Due to Debris Hitting a Composite Roof (Class C)

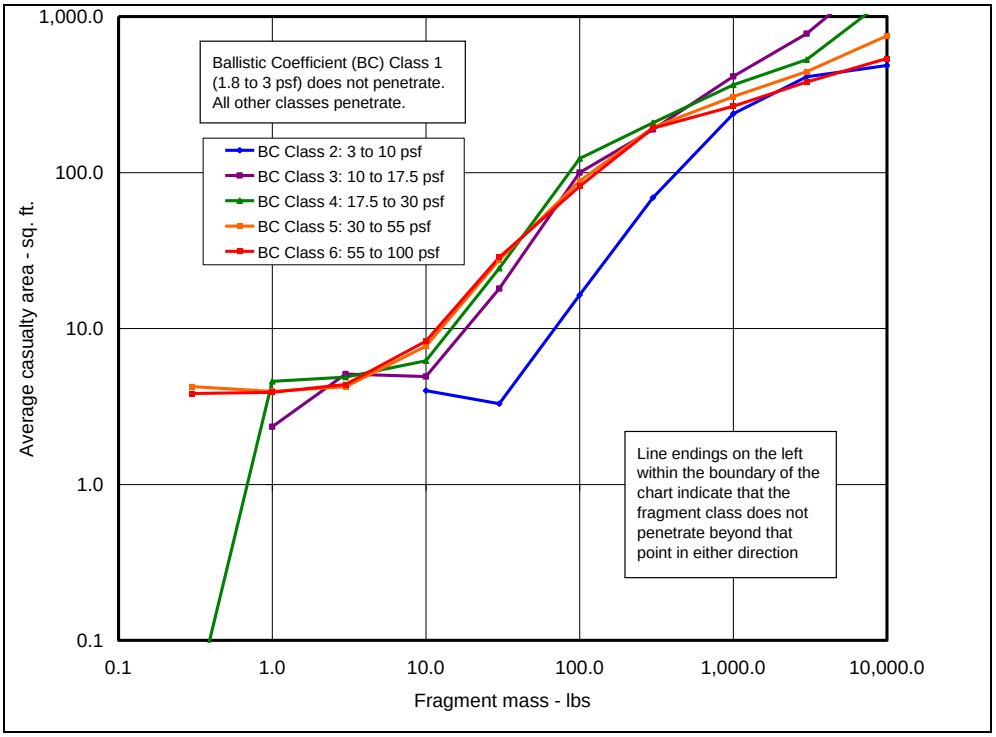

Figure 6-19 Effective Casualty Areas Due to Debris Hitting a Wood Roof (Class B)

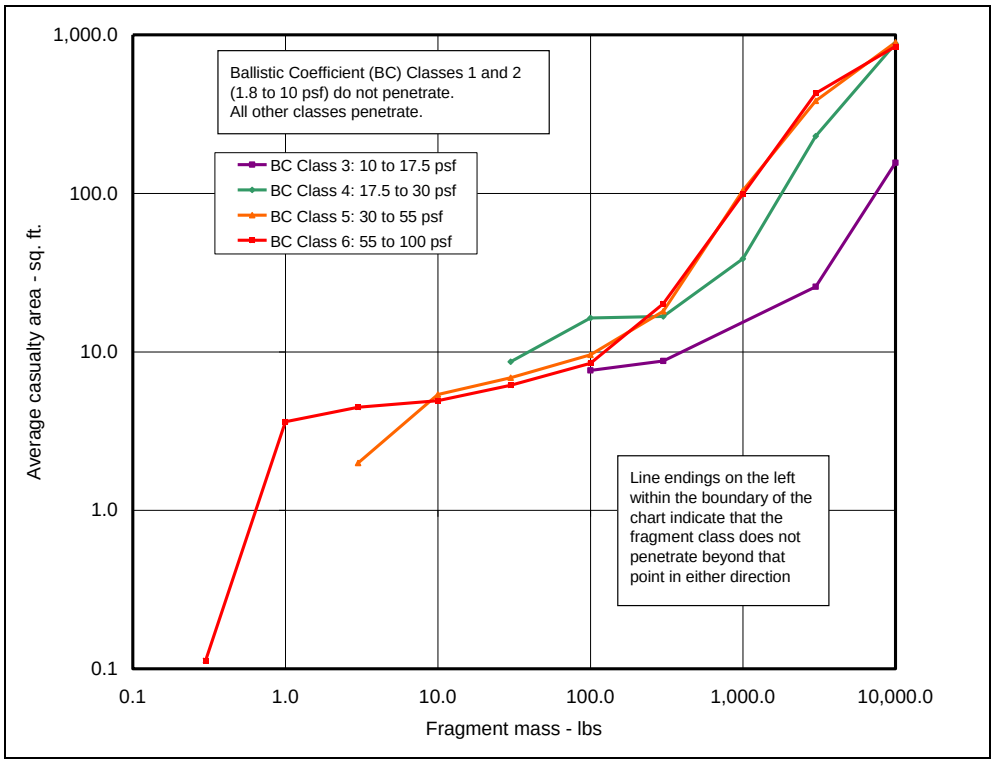

Figure 6-20 Effective Casualty Areas Due to Debris Hitting a Concrete Reinforced with Steel Roof (Class D)

The effective casualty area computations were made with a fast running model based on the output of the Hazard Area Computational Kernel (HACK) program [6][13][14].

6.6 Explosive Debris Effects on People in the Open and in Shelters

6.6.1 Yield from Explosions of Impacting Propellant or Stages

Liquid and solid propellant stages as well as chunks of solid propellant can impact and produce explosions of wide ranging intensities. Figure 6-21 illustrates the explosive environment resulting from an impact. The explosion produces a shock wave, which is characterized by overpressure and time duration. The integrated overpressure over time is the impulse and its value is very important. The figure shows overpressure, Δp, decreasing with range. Peak overpressure is a function of yield (Y) and distance (r) from the source. It scales by $r/Y^{0.33}$ [32]. Increasing yield not only increases the peak overpressure, but it also increases the impulse. Since impulse is dependant upon both overpressure and duration, impulse is very dependant upon the yield. The combination of peak overpressure and impulse (P, I) is the most important set of independent variables upon which injury and damage models can be based. This is why many vulnerability models for explosive debris impacts are presented using Pressure-Impulse (P-I) diagrams.

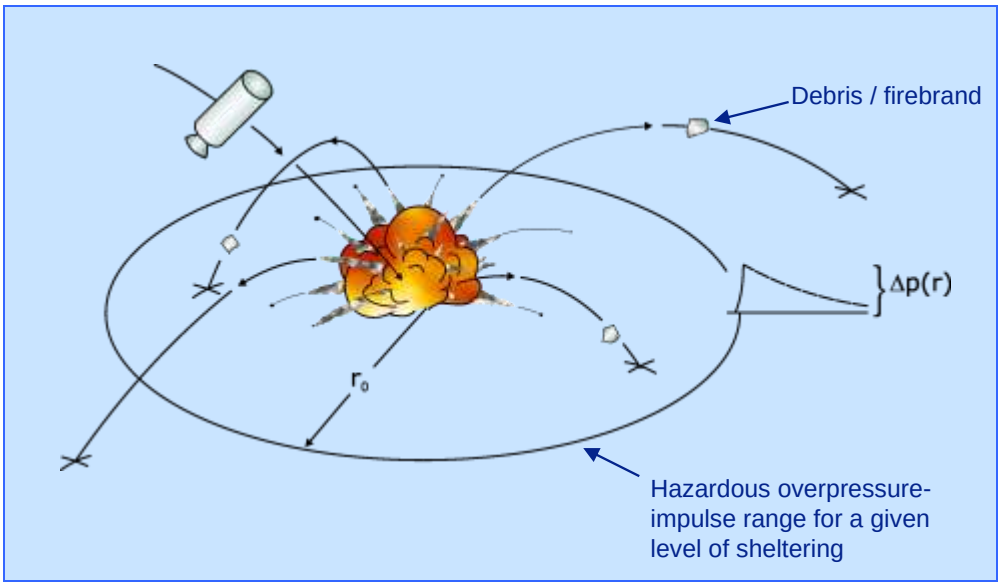

Figure 6-21. Illustration Showing the Products of an Explosive Impact

The other effects of the explosion are debris and heat. Explosions of solid propellant upon impact produce partial detonations with the remainder of the energy going into ejecting firebrands of burning propellant. The fire risk from these firebrands can be significant. The Titan 34D9 accident on SLC-4E at Vandenberg Air Force Base (18 April 1986) produced a spectacular display of firebrands as did a number of Minuteman failures in previous years. The risk to people from the firebrands is usually mitigated by judicious placement of Impact Limit Lines by Range Safety personnel. However, vacated structures and vehicles are still at risk. This was demonstrated in the Delta II failure at LC-17A at Cape Canaveral Air Force Station (17 January 1997). There, the damage due to fire resulting from firebrands may have exceeded all other sources (overpressure and debris impact). Previous studies suggested that for determining casualties, firebrands can be ignored. However, more recent investigations indicate that firebrands may be important in some cases at least. If damage is an issue, do not ignore the firebrands. Further investigation is needed to resolve how a flight safety analysis should account for firebrands. In addition, the potential for casualties due to inert fragments propelled by an explosion has been under investigation recently [33]. The conventional wisdom is that the fragment hazards could be significant for smaller yields, especially for people in the open, but that overpressure effects will dominate for large yields. Further study is necessary to clarify fragment and firebrand related issues. The heat from the explosion is generally of no consequence in creating injuries because of the placement of people.

6.6.1.1 Yields from Explosive Impacts of Solid Propellant Motors, Segments and Fragments

There is only one test where a stage, on a sled, was fired into a wall to determine the yield from an end-on impact of a solid propellant stage. This was a test of a Titan III solid rocket motor in the early 1960s [34]. All other impact information is from accidents where it was very difficult to reconstruct the impact conditions and to estimate the yield.

Consequently, the impact yields have been highly speculative. Numerous explosives tests have been performed, but the initiation of the propellants has come from donors (i.e., small charges of high explosive detonated adjacent to a metal plate in contact with the solid propellant) and not impact. Salzmann [35] organized historical data from both donor tests and estimated yields from the limited accident data to provide a yield as a function of impact velocity, impact mass, and for various impact surfaces. The USAF, concerned about explosive risks from the Titan IV solid rocket motors, determined that a higher fidelity model was required. They formed a team of contractors (The Aerospace Corporation, Research Triangle Institute (RTI), ACTA and SRS) working with Lawrence Livermore National Laboratory (LLNL) and the Air Force Research Laboratory (formerly Phillips Laboratory) at Edwards Air Force Base, known as the Propellant Impact Risk Assessment Team (PIRAT). They knew that they could not perform actual impact tests, but they sponsored LLNL to develop a theoretical model called PERMS to predict the results of donor tests. Figure 6-22 shows a donor test with 13,745 lbs rocket propellant and 1735 lbs C4 explosive at Edwards AFB, 16 January 1999.

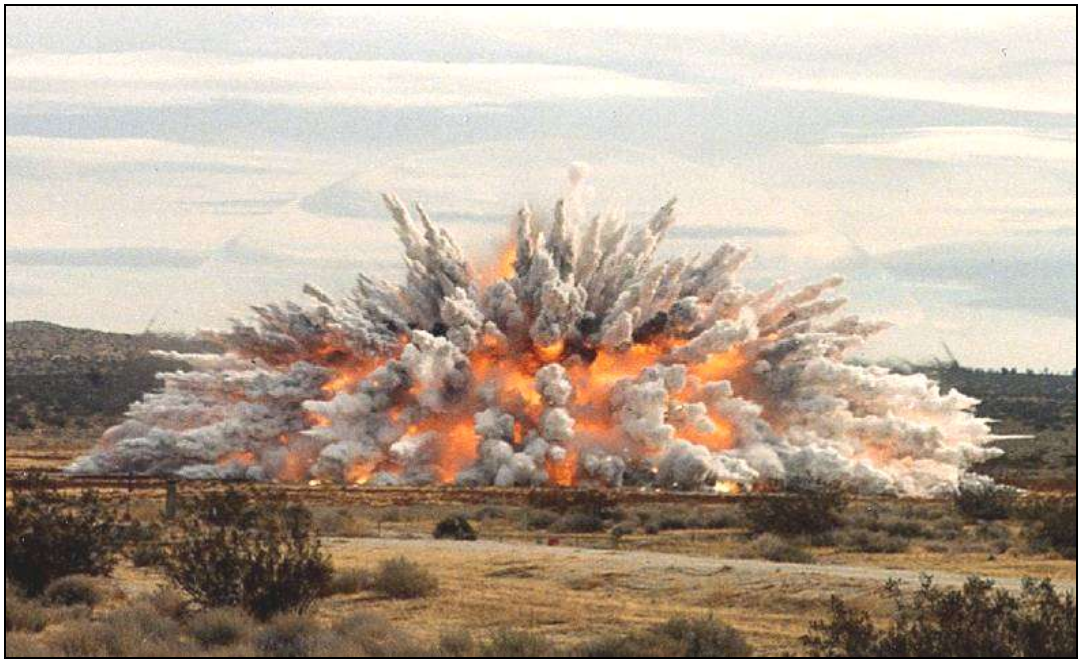

Figure 6-22 Donor Test with 13,745 lbs Rocket Propellant and 1735 lbs C4 Explosive at Edwards AFB, 16 January 1999

Comparison of the test results with PERMS results was used in a validation process of the PERMS model. The calibrated PERMS model was used to make predictions of explosions upon impact rather than with donors. These results were used to make predictions of yield for various impact conditions.

The LLNL PERMS output was interpreted in [36] to develop curves for the various impact conditions. This model has different yield curves for side-on impacts, front-end impacts, and propellant chunk impacts. The results are shown in Figure 6-23 through Figure 6-25.

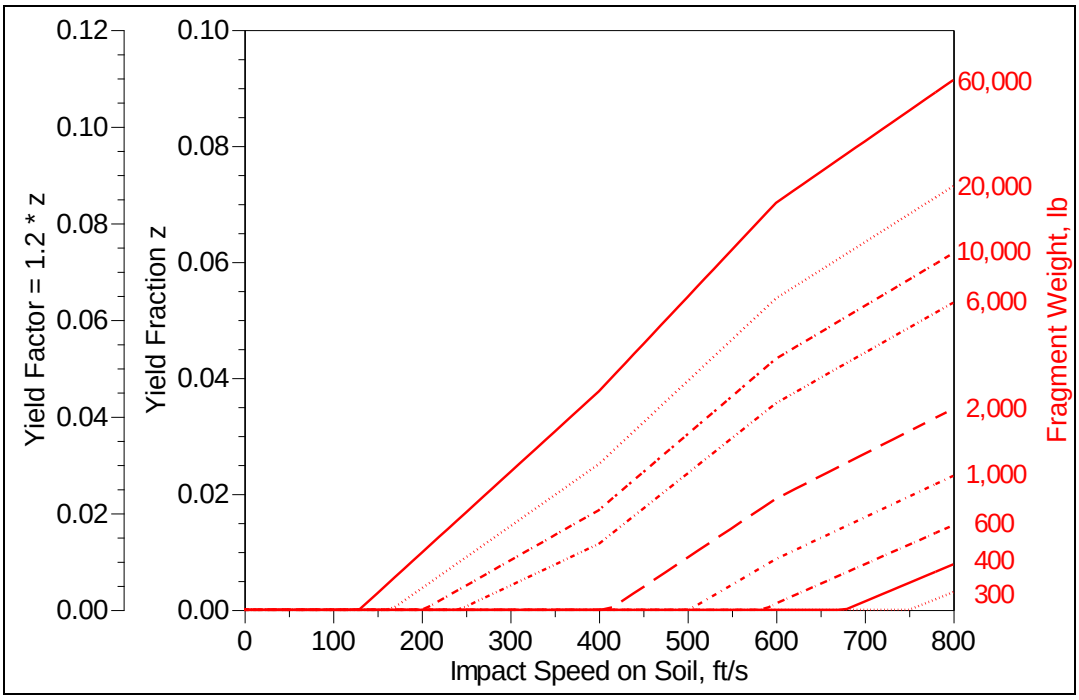

Figure 6-23. PIRAT Yield Factors for Impacts of Solid Rocket Motor Propellant Chunks on Soil

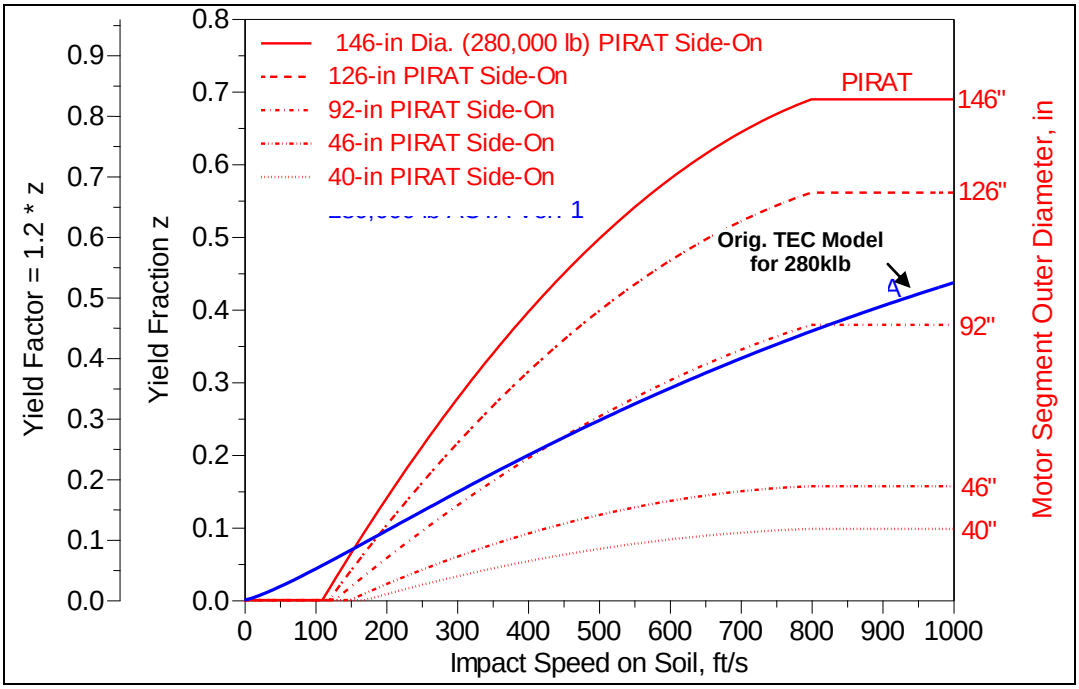

Figure 6-24. PIRAT Yield Factors for Side-On Impacts of Solid Rocket Motors on Soil with ACTA Correlation (FY99 version) for STS Segment Superposed

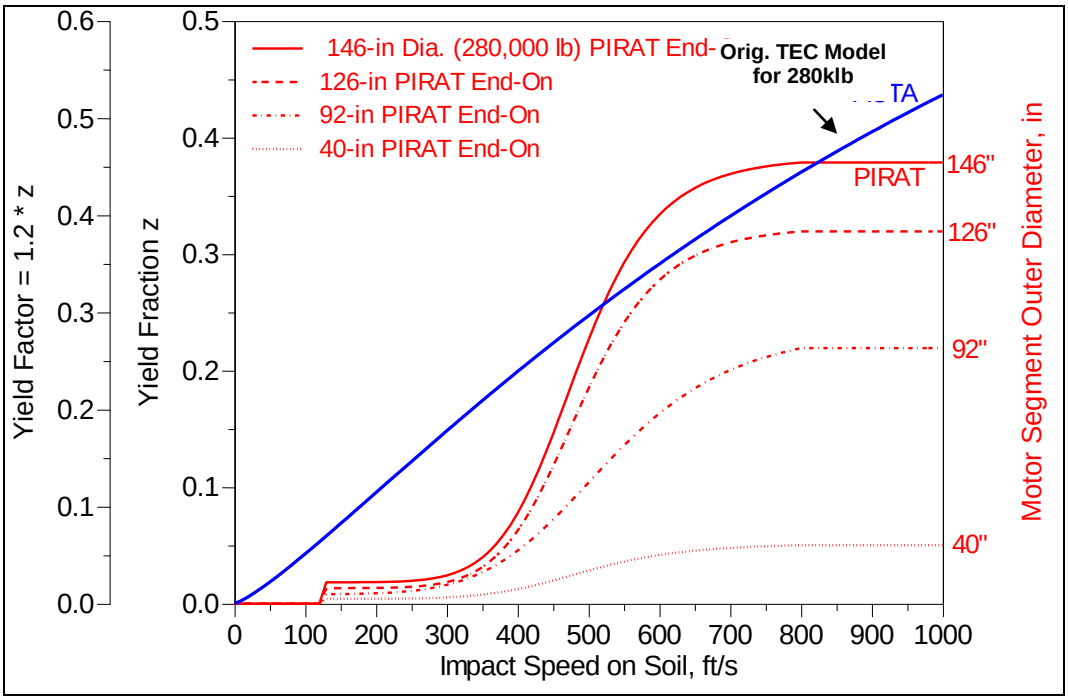

Figure 6-25. PIRAT Yield Factors for End-On Impacts of Solid Rocket Motors on Soft Soil with ACTA Correlation (FY99 version) for STS Segment Superposed

Another model was developed near the end of the PIRAT PERMS work. This model, referred to as the "ACTA Correlation" or the Theoretical–Empirical Correlation (TEC) was developed by Wilde and Anderson [37]. The TEC is a non-linear regression model that combines the historical accident and donor test data developed by Salzmann with the PERMS results. In formulating the TEC model, the sources were weighted, with relatively high weights assigned to the PERMS results. The TEC model not only produces point estimates, but also provides the necessary uncertainties useful for other range safety work, namely yield-histograms for analysis of risks from distant focusing overpressure. The TEC model provides yield sensitivity to different impact conditions but has no impact orientation sensitivity or sensitivity to stage size or whether the propellant is contained or uncontained. Its results are similar to the PIRAT impact yield end-on model, although the TEC model has no abrupt cut-off in yield with reducing impact velocity. The PIRAT model is considered by both USAF ranges to be more useful if impact orientation information is available.

The TEC formulation is as follows:

$$\text{Fraction of TNT} = 1.28\left(1+\frac{192,000}{W^{0.156}}\left(\frac{S}{V}\right)^{1.55}\right)^{-1}$$

where W = total propellant weight (lb), V = impact velocity (f/s)

S = surface hardness factor (S = 2.92 for water, S = 1.81 for soft soil, S = 1.41for concrete, S = 1 for steel)

Figure 6-26 presents output of the TEC model for impacts on soft soil.

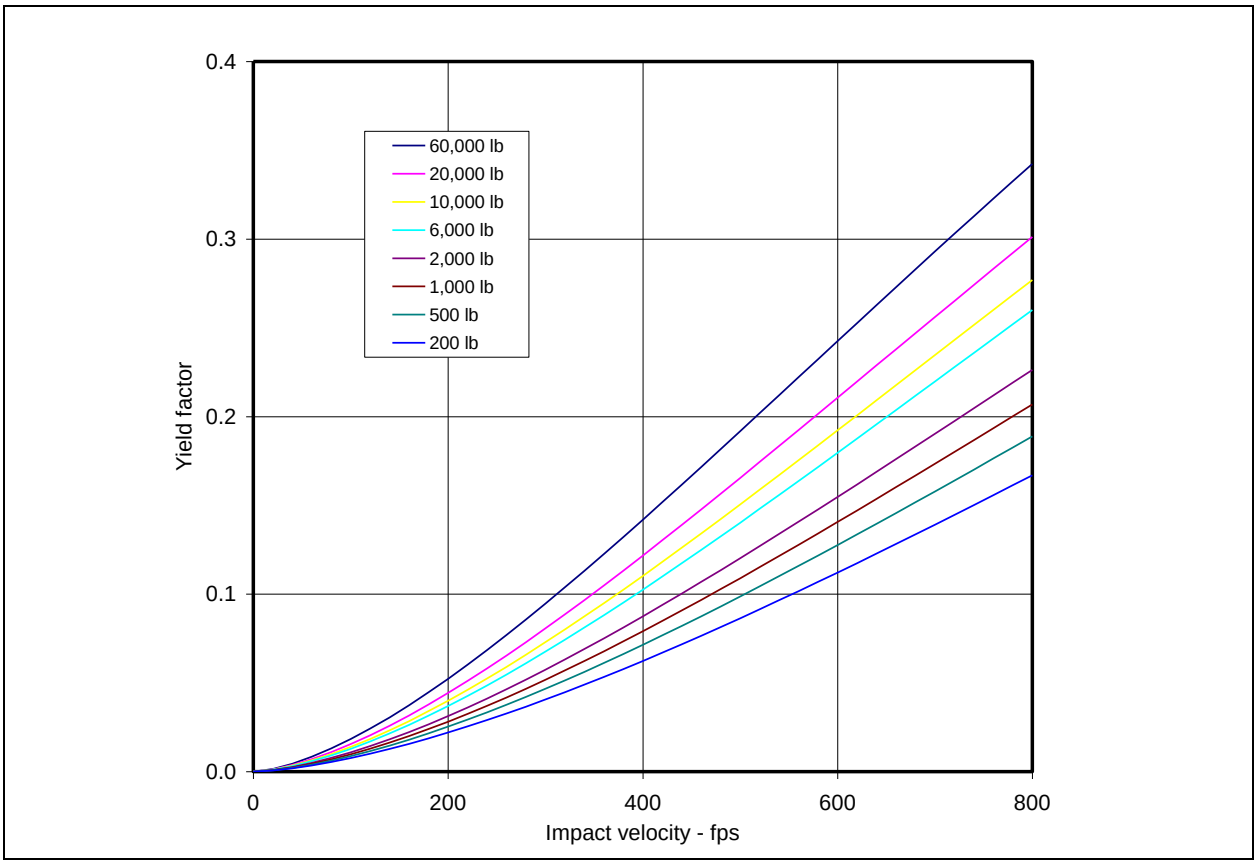

Figure 6-26. Yield Factor Using the Theoretical-Empirical Model for Impacts on Soft Soil

6.6.1.2 Yield Models for Impacting Stages with Liquid Propellant – Project PYRO

Current yield impact models for stages with liquid propellants are primarily based on the Project PYRO tests performed in 1967 [38][39]. The models resulting from these tests are shown in Figure 6-27.

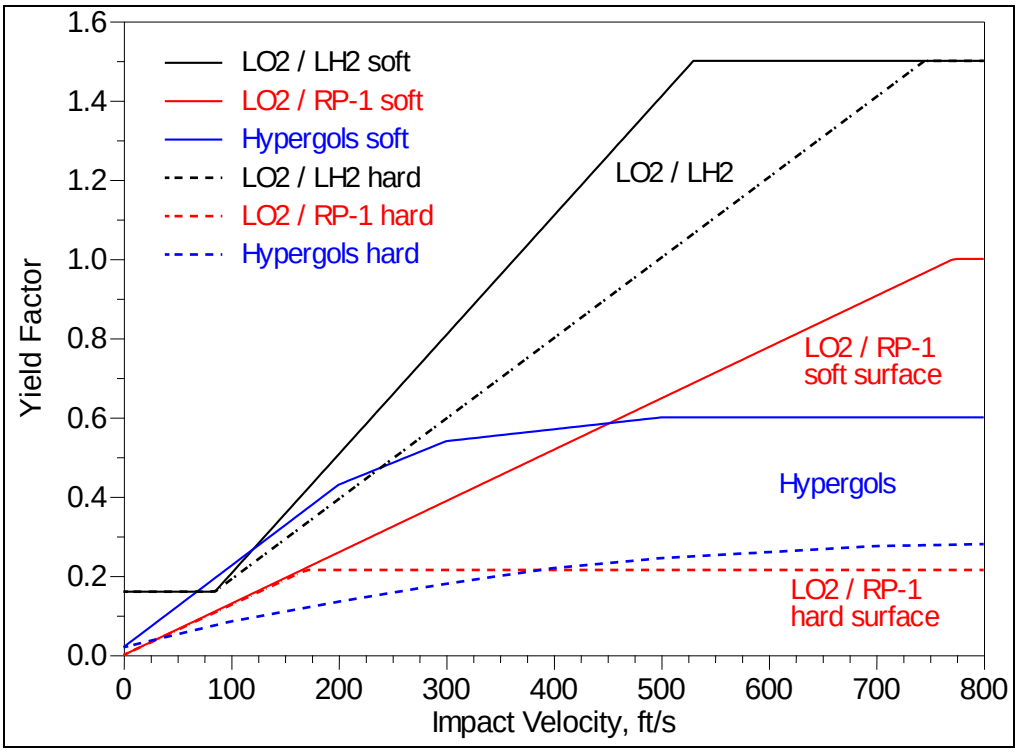

Figure 6-27. Project PYRO Yield Factors for Impacts of Contained Liquid Propellants

Hard surfaces, as defined in these tests, are made of reinforced concrete or similar materials. A soft surface is considered to be any surface other than a hard surface; a soft surface has the potential for a crater to develop and provide a means for increased propellant mixing to occur.

These curves have been challenged in recent years; they are based on very few data points at the high velocities. Moreover, Liquid Propellant Correlation tests at White Sands Missile Range (WSMR) have indicated that the maximum values should perhaps be lower. [36] However, the White Sands tests were not high velocity impact tests, and thus there is no consensus at this time as to what the maximum values should be. The principle investigators from both the project PYRO and WSMR agreed that, while the revised upper limits based on the WSMR tests are applicable for many impact scenarios, the possibility may exist that those limits could be exceeded. [40] This may occur, for example, if a high speed normal impact occurs with a tank containing LH_2 leading another tank containing LO_2, which is much denser than LH_2. Therefore, in the absence of any specific information to indicate otherwise, impact yield for stages with liquid propellants should be based on the Project PYRO tests, such as the curves shown in Figure 6-27.

Impacts of liquid propellant stages into water are assumed to produce the same yield as impacts onto soft soil. The basis for this is that the conditions for soft soil impact were produced in Project PYRO by having the explosion initiated from impact after entering a hole that provided containment. The water impact was assumed to produce the same type of containment conditions.

6.6.2 Effective Casualty Areas Due to Overpressure from Explosive Impacts

The effect of sheltering can produce substantially different casualty area estimates. In many instances, assuming that all people are in the open is not the most conservative assumption to employ. For this reason, compute values for both people in the open and people in structures.

6.6.2.1 People in the Open

For estimating the probability of casualties from a blast wave, consider the following effects:

1. Soft tissue effects - damage to lungs, gastrointestinal tract, larynx, and eardrum (rupture for serious injury and temporary hearing loss for minor injury)

2. Whole Body Translation - general body impact only

Lovelace data for each of the soft tissue damages were used to define the combined pressure and impulse (P-I) associated with the 1% (threshold) and 50% probability of serious injury. [41] These levels were then used to define probit functions[15] for each effect. The potential for serious injury due to whole body translation induced by a blast wave is a function of both the peak overpressure and positive impulse. Pressure-Impulse (P-I) diagrams for serious injury due to whole body translation were constructed using two different methods:

1. The Netherlands Organization of Applied Scientific Research (TNO) fatality probit function [42] for whole body translation was scaled based on the ratio between the impact velocity for fatality and serious injury at the 50% probability level. The fatality-to-serious injury ratio was based on comparing the impact velocity at the 50% probability level based on a skull fracture model for large masses.

2. TNO fatality probabilities for a given pressure and impulse were directly translated to serious injury probabilities by using the ratio between casualty and fatality probability based on the Biodynamics Engineering Inc. (BEI) skull fracture model for large masses.

P-I diagrams for soft tissue and whole body translation effects and for slight injury, serious injury and fatality have been developed based on the methods described above. These P-I diagrams were then used to determine the effective casualty area (for AIS 3 and above injuries) as a function of yield.

[15] A probit is the inverse of the standard cumulative normal distribution.

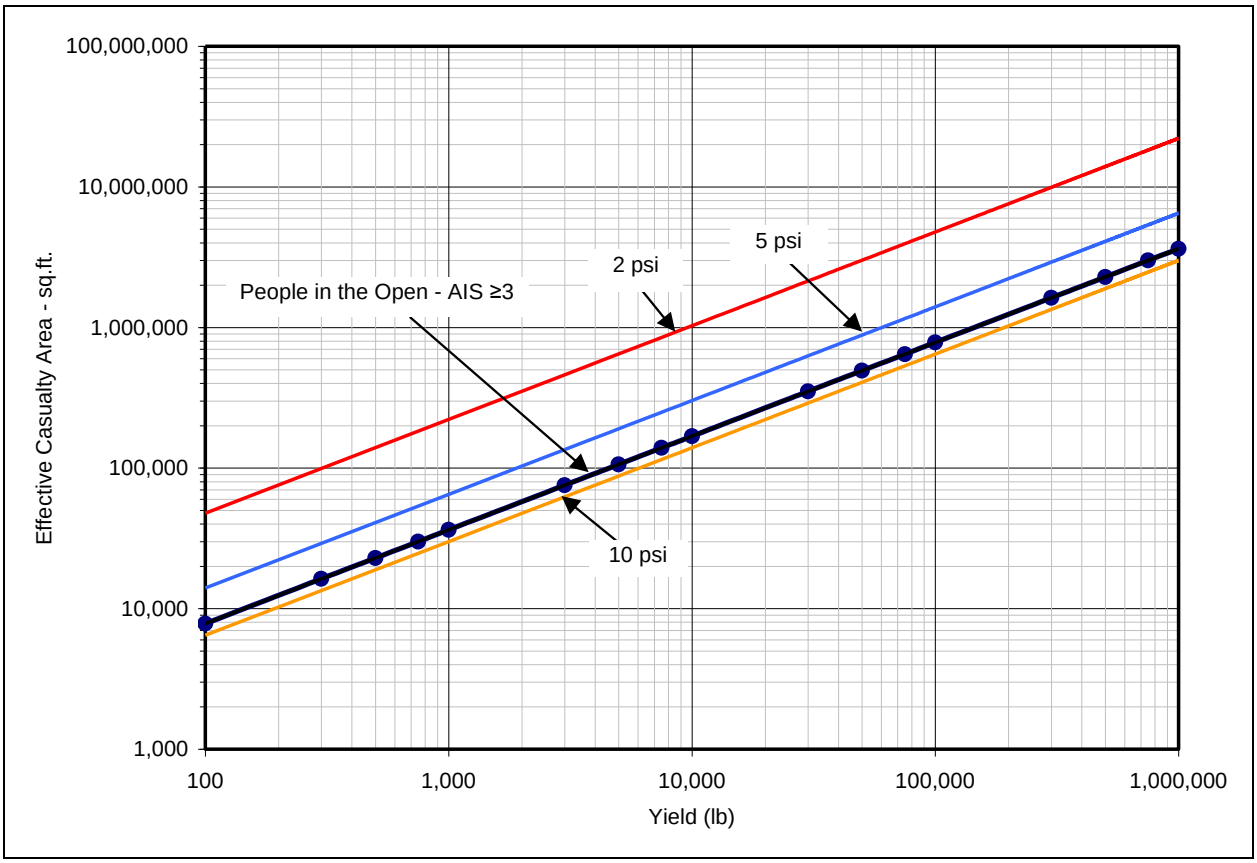

Figure 6-28. Effective Casualty Area for People in the Open as a function of Impact Yield

Figure 6-28 shows the effective casualty area along with areas associated with different overpressures that may be used to compute expected casualties due to the potential effects of a blast wave on people in the open. For solid propellant impacts, the potential for casualties due to firebrands should also be accounted for. The simplest method available to account for casualties due to firebrands is to define an effective casualty area based on the region where the peak incident overpressure is at least one psi. This approach is consistent with § 417.207(b), and produces results that are consistent with the analysis in [43].

EXAMPLE: Explosive Overpressure Effects on People in the Open

This example demonstrates using the effective casualty area concept and the Tier 1 approach: where any person within the area subject to at least 1 psi of peak overpressure would be considered a casualty. This example also illustrates some fundamental methods used in explosive casualty area computations.

The first step is to compute the net equivalent weight of TNT of the explosion (represented as *NEW*). There are several methods available to compute the *NEW*, depending on the type of propellant involved as several other factors. For example, the Theoretical–Empirical Correlation (TEC) may be used for typical solid propellant impacts as follows:

$$\text{Fraction of TNT} = 1.28\left(1+\frac{192,000}{W^{0.156}}\left(\frac{S}{V}\right)^{1.55}\right)^{-1}$$

where W = total propellant weight (lb), V = impact velocity (f/s)

S = surface hardness factor (S = 2.92 for water, S = 1.81 for soft soil, S = 1.41for concrete, S = 1 for steel)

For example, a 10,000 lb solid propellant impacting a concrete surface at 600 fps, the fraction of TNT equals 0.264 based on the TEC. The *NEW* is the total weight of the propellant at impact multiplied by the Fraction of TNT, which in this example is 2640 lb.

The next step is to compute the radius (R_1) from an explosion where the peak incident overpressure falls to one psi according to the following equation:

$$R_1 = K(NEW)^{1/3}$$

where the K-factor is 45 for the 1 psi distance [32]. (Different K-factor values can be used to find the radius for other peak incident overpressure levels, for example a K-factor of 20 corresponds to 3 psi.) For an *NEW* of 2640 lb, R_1 equals 622 ft. Therefore, in this example, the effective casualty area equals **1.215E+06 ft^2** (i.e., a circle with a radius of 622 feet).

This Tier 1 approach demonstrates an easy method to compute a casualty area *due to blast wave effects only* for explosive impact effects without any complex computations for any *NEW* less than 25,000 lb. It is important to note that fragments potentially propelled by an explosion typically hazard an area larger than the area subject to at least one psi peak overpressures for *NEW* below 30,000 lb [33].

6.6.2.2 People in Structures

Structures are usually thought of as providing protection to people from debris and blast waves. However, a blast wave can produce considerable harm to people inside the structure, either due to flying glass shards or elements (panels, etc.) of the structure itself. Therefore, the effective casualty area due to blast wave effects only (i.e., not including

firebrands or other fragments propelled away from an explosion) for people in some structure types is much larger than for people in the open.

Figure 6-29 shows the general approach adopted for systematically estimating effective casualty areas due to blast wave effects for people in structures. The steps shown in Figure 6-29 capture the basic phenomena that define the effects of air blast loading on a structure and its occupants. First, define the blast loading on the structure and check the window glazing for breakage. If breakage occurs, track the flying shards and use their impact on a building occupant to estimate their contribution to the probability of casualty given an explosive event occurs [P(c|e)]. After glass breakage occurs, revise the loads acting on the structure to account for potential pressure increases inside the structure (called venting) and check the external cladding for failure. If wall or roof segments fail, track the cladding debris and use its impact on building occupants to estimate their contribution to the probability of casualty. If the building is susceptible to collapse, revise the blast loads again to reflect the potential for additional venting and check the structure for collapse. If the building construction is susceptible to collapse, use the impact of large building components striking occupants to estimate their contribution to the probability of casualty. Then combine the contributions due to glass breakage, debris throw and collapse. Depending on the level of blast loading and the type of construction, the overall casualty probability may be dominated by glazing breakage alone, or from combinations of glass breakage, cladding failure, or collapse.

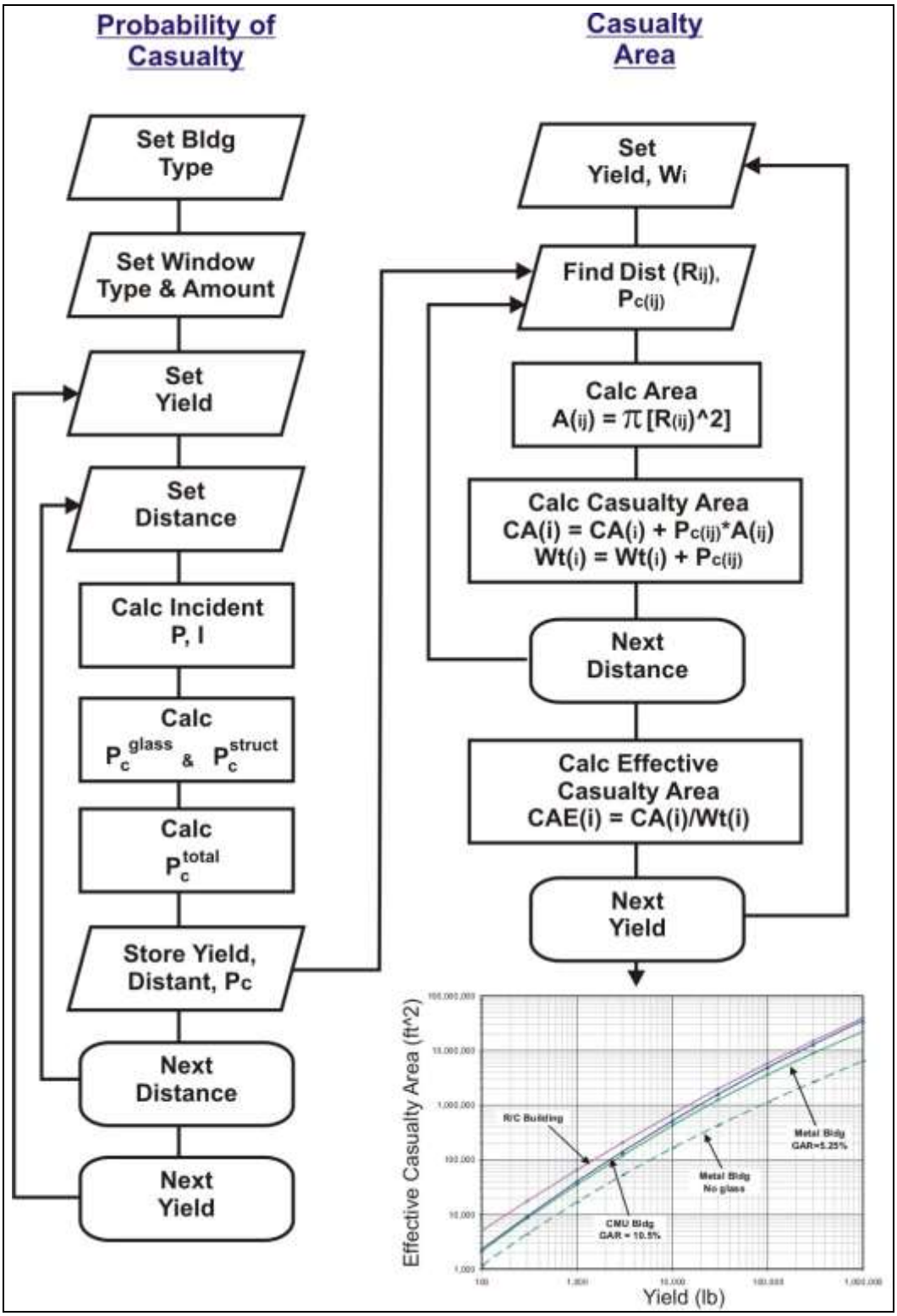

Figure 6-29. Steps for Determination of Casualty Area Due to Blast Wave Effects for People in Structures Given an Explosive Event

Table 6-14 shows four generic classes of buildings available to estimate effective casualty areas due to blast wave effects only. These four generic classes of building conservatively represent the construction types and glazing characteristics typical for buildings.

Table 6-14. Representative Building Classes for Blast Casualty Area Analyses

Structure Roof Class	Building Use Description	Typical Construction	Conservative Glass / Floor Area Ratio
A	Mobile home and trailers, temporary office trailers, school rooms	Wood studs with plywood used for walls and roof	20%
B	Single residential units of all types, single family dwellings, duplex, apartments, town homes, condos	Un-reinforced masonry walls with wood stud roof	30%
C	Commercial buildings less than 15,000 sft of all kinds, including retail, offices, restaurants, gas stations, strip malls	Metal stud and metal panel walls, steel moment resisting frame, metal panel roof	35%
D	Commercial buildings more than 15,000 sft of all kinds, including retail, offices, warehouses, manufacturing, malls	Lightly reinforced concrete tilt-up walls with wood or metal decking over steel joists.	10%

Figure 6-30 shows effective casualty areas as a function of explosive yield for four generic classes of buildings due to overpressure effects only. The 1-psi curve in Figure 6-30 offers a convenient and clearly conservative upper bound to the effective casualty area for people in structures due to blast wave effects from explosions below 20,000 lb TNT equivalent, again assuming the structure is adequate to protect against firebrands or other fragments propelled by the explosion.

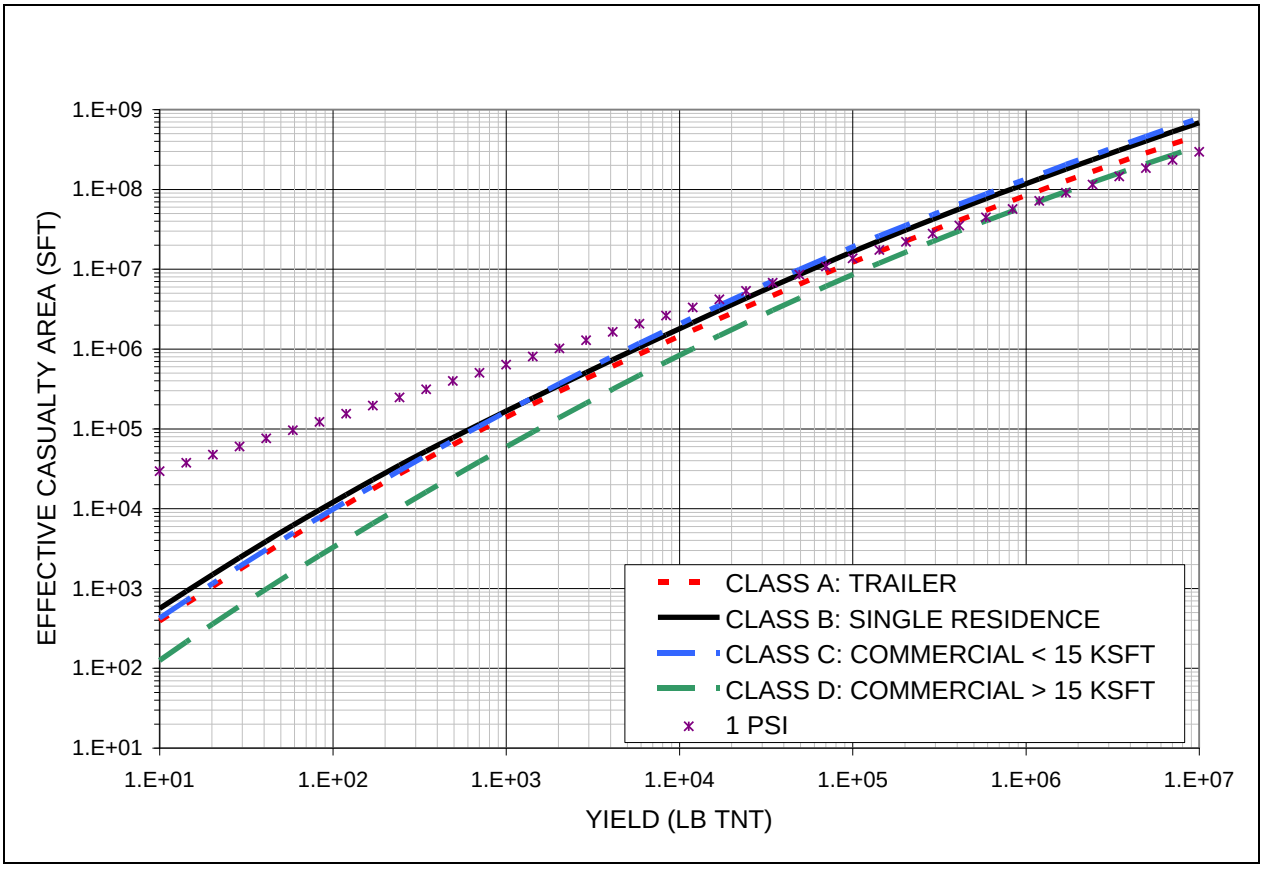

Figure 6-30. Effective Casualty Area for People in Structures as a function of Impact Yield

EXAMPLE: Explosive Overpressure Effects on People in Structures

This example demonstrates using the effective casualty area concept and the effective casualty data for four generic shelter types (i.e., structure classes) provided in this handbook.

The effective casualty area due to blast wave effects depends on the sheltering category. Thus, find the effective casualty area for an impacting fragment of explosive debris in the vicinity of sheltered people by first determining the most representative generic structure class based on the descriptions provided in Table 6-14. Once you identify the sheltering class, determine the effective casualty area due to overpressure effects as a function of TNT-equivalent yield (i.e., *NEW*) using figures such as Figure 6-30. On this chart, find the effective casualty area due to blast wave effects from an explosive debris impact, and compare it to the effective casualty area corresponding to the 1 psi threshold.

Table 6-15 identifies the effective casualty area for impacting debris with explosive TNT equivalence ranging from 100 lbs to 100,000 lbs. The radius corresponding to the effective casualty area is also presented for comparison to the 1 psi overpressure radius. It is evident from Figure 6-30 that the 1 psi overpressure radius is not directly equivalent to the effective casualty area presented herein. It is evident from Figure 6-30 and Table 6-15 that the area subject to at least 1 psi peak overpressure radius is an overly

conservative estimate of the effective casualty area *due to blast wave effects* (i.e., without accounting for potential casualties due to propelled fragments) for relatively small explosions, but non-conservative for *NEW* greater than 25,000 lb.

It is important to note that fragments potentially propelled by an explosion typically hazard an area smaller than the area hazarded by blast wave effects on sheltered people for *NEW* above 30,000 lb [29]. Therefore, the effective casualty areas due to overpressure effects computed for *NEW* above 30,000 lb may be considered adequate to account for fragments propelled by an explosion in some cases.

Table 6-15. Influence of Yield (*NEW*) on Effective casualty area for a generic residential structure compared against the 1 psi overpressure radius

Yield (lbs TNT)	1 psi Overpressure Radius (ft)	Effective Casualty Area (sft)	Effective Casualty Area Radius (ft)
100	208	10,936	59
1,000	450	156,228	223
10,000	969	1,651,230	725
100,000	2,089	16,031,802	2,259

6.6.3 Effective Casualty Areas Due to Fragment Throw from Explosive Impacts

As opposed to overpressure, where the shattering of glass windows can produce larger casualty areas for people inside structures than for people in the open, sheltering almost always provides some level of protection from fragment throw. For that reason, and because the effects of fragment throw on structures is largely still a work in progress, we consider only casualty areas due to fragment throw for people in the open in this version of the document.

6.6.3.1 People in the Open

The Department of Defense Explosive Safety Board (DDESB) provides a straightforward method for computing a hazardous fragment distance (HFD) in its Explosive Safety Standard 6055.9 [44]. An HFD computed using this method is based on a threshold impact energy of 58 ft-lb (79 Joules). The 58 ft-lb threshold represents the distance measured from the explosion at which a person in the open would have a 0.01 probability of becoming a fatality from thrown fragments given an explosive event. The FAA's launch safety regulations (§417.107) use 11 ft-lbs (15 Joules) as the minimum value for fragment impact energy capable of causing a casualty to people in the open. Analyses described in [45] and [46] indicate that the difference between HFDs based on 11 ft-lb and 58 ft-lb fragments is small, and therefore HFDs computed using a 58 ft-lb threshold value for impact energy represents an acceptable level of safety. Equations C9.T2-1 and C9.T2-2 of DoD 6055-9 can be used to compute HFDs for most launch vehicle explosive impacts.

In lieu of using the explosives standards to compute hazardous fragment distances, the FAA has developed higher fidelity procedures based on quantitative analyses. A considerable amount of data is required to conduct these analyses. This data is summarized below:

- Design drawings (with dimensions) that show various views of the vehicle (including cross-sections) showing major assemblies.
- Parts list that provides major component weights and locations.
- Drawings showing the location of liquid fuel and oxidizer along with equipment used to mix them and/or location of solid propellant stages and attached solid rocket motors. Also a description of the propellant systems including the type and amount of propellant.
- Estimates of the basic inert material fractions of the overall vehicle. For example, Aluminum – 60 percent, Steel – 30 percent, Composites – 7 percent, Rubber – 3 percent.
- Ullage pressures in the fuel and oxidizer tanks, either as functions of time or single values if they are approximately constant, and pressures of any other high pressure components (e.g., hydraulic, pneumatic, or cold gas systems).

From this data, you can develop event trees describing potential explosive scenarios, explosive potential, overpressure distance, hazardous fragment lists, and hazardous fragment density distances. This process is described in detail in [45].

7.0 DEBRIS LISTS

7.1 Purpose

The purpose of a debris list for a launch QRA is to characterize the physical, aerodynamic, and harmful characteristics of all debris potentially generated, including planned jettisoned debris. For example, a debris list typically defines the numbers of pieces, weights, sizes, aerodynamic characteristics, and breakup-imparted velocities (section 10.4.6) for the debris produced under all conditions that may pose a risk. Depending on the approach taken, the debris list or another element of the QRA will characterize the debris at the time of the failure and impact, including secondary effects.

7.2 Input Data Sources

There are a few empirical data sets from debris recovered after historical events. For example, the disintegration of *Columbia* at hypersonic speeds [12] over Texas, a Delta II destroyed early in flight from Cape Canaveral, [47] and some Minuteman missiles destroyed early in flight from Vandenberg AFB. [26] These empirical data sources have been valuable, particularly in refining debris models for those vehicles and validating debris dispersions models [48]. However, the present empirical data are insufficient as a basis for the developing debris lists for other vehicles.

The following are typical sources of data that may be available to assist in the development of debris lists.

- Descriptions of the vehicle and payload, including scaled diagrams that show the general arrangement and dimensions of components including alternate and optional components; data on the materials used in construction, inert weights and propellant types and weights for every stage and component; the nature and purpose of a typical flight.
- Data on the engine or motor including case material (outer case, lining, insulation, thickness, density), descriptions of nozzles and steering mechanisms, descriptions of propellant types and ingredients, propellant density, propellant weights versus time.
  - Solid Motor: motor core radius (to outer edge of propellant), grain design, internal pressure, and web thickness versus time.
  - Liquid Engine: pumping and pressurization systems and associated stored energy, materials, and pressurization.
- Descriptions of destruct systems (command, automatic, separation): descriptions of all components and activation mechanisms, exact locations of all charges (beginning point, length, gap, ending point), descriptions of circumstances for any delays in activation of charges, discussion of whether and under what circumstances destruct might ignite a non-thrusting motor.
- Trajectory data for a typical mission: nominal and dispersed trajectories, comprehensive malfunction trajectories or malfunction turn data, event times (ignitions, steering programs, burnouts, jettisons). Use trajectory data to obtain

vehicle velocity and altitude from which to calculate aerodynamic and inertial loads for use in estimating vehicle breakup. Use event times to indicate vehicle configuration at each breakup time.

- Mission rules that define the allowable conditions for launch and for activation of the flight safety system.
- Descriptions of planned debris-causing events: jettisoned components, aerodynamic and inertial breakup of jettisoned components.
- Breakup debris lists for similar vehicle: the manufacturer's expected debris resulting from destruct action and subsequent aerodynamic loads at various event times including numbers of fragments, weights and dimensions of pieces, construction materials, drag characteristics (reference area, ballistic coefficient or drag coefficient versus Mach number as described in Section 6.4), and breakup imparted velocities (Section 10.4.6). In some cases, manufacturers also provide expected debris from breakup resulting from aerodynamic and inertial loads on a malfunctioning vehicle. For failures occurring during downrange over-flight of populated areas, destruct action is assumed not to take place, so most breakups may occur from aerodynamic and inertial loads.
- Knowledge of the vehicle's material properties, anticipated operating envelope, design limitations, and structural weak points (attachment points and points of transition between component geometries), analytical techniques such as finite element analyses, and test results including the static and dynamic failure strengths of load-bearing components.

7.3 Minimum Features

A debris model (i.e., a set of debris lists) must, per 417.211(a) define the debris characteristics for all foreseeable debris generating events during flight. For a suborbital launch, the debris model should provide the debris characteristics from the planned ignition time until impact of the last component. A debris model should provide debris characteristics for as many time periods as necessary to produce smooth and continuous contours used to define hazard areas. A debris model should provide debris characteristics for each breakup time during flight corresponding to a critical event when the fragment catalog is significantly changed by the event. Critical events include staging, payload fairing jettison, and other normal hardware jettison activities. At each modeled breakup time, the individual fragment weights should approximately add up to the sum total weight of inert material in the vehicle and the weight of contained liquid propellants and solid propellants that are not consumed in the initial breakup or conflagration.

An adequate set of debris lists accounts for all launch vehicle debris fragments (which may in fact be intact vehicle components), individually or in groupings of fragments called classes. The characteristics of each debris fragment represented by a class should be similar enough to the characteristics of all the other debris fragments represented by that class that all the debris fragments of the class can be described by a single average set of characteristics.

A debris model must:

- Describe the physical, aerodynamic, and harmful characteristics of each debris fragment either individually or as a member of a class (14 CFR 417.211(c));
- Consist of lists of individual debris or debris classes for each cause of breakup and any planned jettison of debris, launch vehicle components, or payload (14 CFR 417.211(c));
- Identify the initial preflight weight of solid and liquid propellant for each launch vehicle component that contains solid or liquid propellant (14 CFR A417.11(c)(3));
- Identify the nominal and plus and minus three-sigma solid and liquid propellant consumption rate, and pre-malfunction consumption rate for each component that contains solid or liquid propellant (14 CFR A417.11(c)(3)).

Adequate debris lists account for the following.

- All debris due to any malfunction in flight where forces on the launch vehicle may exceed the launch vehicle's structural integrity limits (14 CFR A417.11(b)(2)).
- The characteristics of an intact launch vehicle and payload following any malfunction where breakup is not foreseen, such as a thrust termination or thrust degradation event (14 CFR A417.11(b)(2)).
- Launch vehicle breakup caused by the activation of any flight termination system. This includes the debris produced when flight termination system activation destroys an intact malfunctioning vehicle, when a breakup is assisted by the action of any inadvertent separation destruct system, and when debris is produced by the activation of any flight termination system after inadvertent breakup of the launch vehicle (14 CFR A417.11(b)(1)).
- The immediate post-breakup or jettison environment of the launch vehicle debris, and any change in debris characteristics over time from launch vehicle breakup or jettison until debris impact (14 CFR A417.11(b)(3)).
- The impact overpressure, fragmentation, and secondary debris effects of any confined or unconfined solid propellant chunks and fueled components containing either liquid or solid propellants that could survive to impact, as a function of vehicle malfunction time (14 CFR A417.11(b)(4)).
- The effects of impact of the intact vehicle as a function of failure time. The intact impact debris analysis must identify the trinitrotoluene (TNT) yield of impact explosions, and the numbers of fragments projected from all such explosions, including non-launch vehicle ejecta and the blast overpressure radius. The analysis must use a model for TNT yield of impact explosion that accounts for the propellant weight at impact, the impact speed, the orientation of the propellant, and the impacted surface material (14 CFR A417.11(b)(5)).
- For each thrusting or non-thrusting stage having residual thrust capability following a launch vehicle malfunction, a debris model should provide either the total residual impulse imparted or the full-residual thrust as a function of breakup time (14 CFR A417.11(d)(17)). For any stage not capable of thrust after a launch vehicle

malfunction, a debris model should provide the conditions under which the stage is no longer capable of thrust. For each stage that can be ignited as a result of a launch vehicle malfunction on a lower stage, a debris model should identify the effects and duration of the potential thrust, and the maximum deviation of the instantaneous impact point, which can be brought about by the thrust. A debris model should provide information to facilitate computation of the explosion effects of all remaining fuels, pressurized tanks, and remaining stages, particularly with respect to ignition or detonation of upper stages if the flight termination system is activated during the burning period of a lower stage.

- The possibility of the flight safety/destruct system failure. System failure may be due to loss of command communications, loss of battery power, failures or ruptures of vehicle systems resulting in loss of control or power connectivity, or inaction or delayed action of the flight safety crew. The latter should account for the mission rules established before launch. If the destruct system fails, there is a possibility of an intact impact accompanied by an explosive yield or the possibility of breakup from aerodynamic or inertial loads; associated debris models for these scenarios may be required.

Adequate debris lists include the following.

- Identification of all inert fragments (those that are not volatile and that do not burn or explode under normal and malfunction conditions) and all propellant fragments (14 CFR A417.11(c)(2)). This description should include the characteristics of each fragment, including its origin on the launch vehicle, representative dimensions, shape, and weight at the time of breakup and at the time of impact. Drawings of representative fragments are often useful.
- A description of each propellant fragment as a function of time, from the time of breakup through ballistic free-fall to impact (14 CFR A417.11(c)(2)). For any fragment identified as an un-contained or contained propellant fragment, whether explosive or non-explosive, the debris model should identify whether or not it burns during free fall, and provide the consumption rate during free fall. The debris model should identify (1) solid propellant that is exposed directly to the atmosphere and that burns but does not explode upon impact as "un-contained non-explosive solid propellant," (2) solid or liquid propellant that is enclosed in a container, such as a motor case or pressure vessel, and that burns but does not explode upon impact as "contained non-explosive propellant,", (3) solid or liquid propellant that is enclosed in a container, such as a motor case or pressure vessel, and that explodes upon impact as "contained explosive propellant fragment," and (4) solid propellant that is exposed directly to the atmosphere and that explodes upon impact as "un-contained explosive solid propellant fragment."
- An estimate of the maximum velocity imparted to each fragment due to potential explosion or pressure rupture (14 CFR A417.11(c)(6)). When accounting for imparted velocity, a debris model should use a Maxwellian distribution (see 10.4.6) with the specified maximum value equal to the 97^{th} percentile; or identify the distribution, and must state whether or not the specified maximum value is a fixed value with no uncertainty.

- An estimate of the axial, transverse, and mean tumbling areas of each fragment (14 CFR A417.11(c)(7)). If the fragment may stabilize under normal or malfunction conditions, the debris model must also provide the projected area normal to the drag force.
- An estimate of the ballistic coefficient corresponding to the axial, transverse, and tumble orientation for each fragment (14 CFR A417.11(c)(8)). Section 6.4 discusses ballistic coefficient modeling.
- An estimate of the total number of each type of fragment (14 CFR A417.11(c)(9)).

A debris model may categorize each fragment into classes where the characteristics of the mean fragment in each class conservatively represent every fragment in the class. The model should define fragment classes for fragments whose characteristics are similar enough to be described and treated by a single average set of characteristics. A debris class should categorize debris by each of the following characteristics (§ A417.11), and may include any other useful characteristics:

- The type of fragment as defined above. All fragments within a class should be the same type, such as inert or explosive.
- Debris class name, the range of values for each parameter used to categorize fragments within a fragment class, and the number of fragments in any fragment class. The mean and plus and minus three-sigma weight of each fragment or fragment class. The mean and plus and minus three-sigma axial, transverse, and tumbling areas for each fragment or fragment class.
- Debris subsonic ballistic coefficient (β_{sub}). The difference between the smallest $\log_{10}(\beta_{sub})$ value and the largest $\log_{10}(\beta_{sub})$ value in a class should not exceed 0.5, except for fragments with β_{sub} less than or equal to three. Fragments with β_{sub} less than or equal to three may be grouped within a class for the purpose of computing ground risks. If the risk to aircraft is being computed, low ballistic coefficient debris should generally be segregated into finer debris classes.
- The mean ballistic coefficient (β) and plus and minus three-sigma values of the β for each fragment class. A debris model should provide graphs of the coefficient of drag (C_D) as a function of Mach number for the nominal and three-sigma β variations for each fragment shape. A debris model should label each graph with the shape represented by the curve and reference area used to develop the curve. A debris model should provide a C_D vs. Mach curve for any tumble orientations for any fragment that will not stabilize during free-fall conditions. For any fragment that may stabilize during free-fall, a debris model should provide C_D vs. Mach curves for the stability angle of attack. If the angle of attack where the fragment stabilizes produces a net lift, a debris model should provide both the coefficient of lift (C_L) vs. Mach number and the C_D vs. Mach number curves. A debris model should provide the equations for each C_D vs. Mach curve, or data points adequate for a piecewise linear description.
- Breakup-imparted velocity (ΔV). A debris model should categorize fragments as a function of the range of ΔV for the fragments within a class and the class's median subsonic ballistic coefficient. For each class, the debris model should keep the ratio

of the maximum breakup-imparted velocity (ΔV_{max}) to minimum breakup-imparted velocity (ΔV_{min}) within the following bound:

$$\frac{\Delta V_{max}}{\Delta V_{min}} \approx \frac{5}{2 + \log_{10}(\beta'_{sub})}$$

Where: β'_{sub} is the median subsonic ballistic coefficient for the fragments in a class.

7.4 Modeling Discussion

Debris list can be difficult to develop, especially if you consider the many secondary breakups after the initial rupture of the tanks or failure at structural weak points. As previously mentioned, there is minimal data from past accidents that will help. Vehicle debris from launch accidents and Range Safety destruct are not generally gathered and categorized such that one could use the data to develop future debris lists. The most comprehensive debris gathered was from the breakup of the Space Shuttle *Columbia* and it had no command destruct charges but instead was exposed to the extreme reentry heating and loads environment that is likely to be more severe than the environments that launch vehicles are exposed to during the ascent phase. This section summarizes the results of past practice in the development of debris lists.

7.4.1 Basic Casualty Area Trends

Debris lists from fourteen different ELVs were examined to see how the "basic casualty area" and the number of fragments varied with vehicle dry weight. This "basic casualty area" is a simple approach that implies that people are all in the open (with no benefit from sheltering) and debris that falls vertically. It understates the actual casualty area because it ignores other effects such as impact at an angle, energy release in high velocity impact, effects of bounce and roll, and effects of break up and splatter. The "basic casualty area" for a single fragment is defined as the area of a fragment with an effective radius of a person (approximately one foot) added around the fragment to simulate a person at any position around the fragment. The formula is

$$A_{C_{basic}} = \left(\sqrt{A_F} + \sqrt{A_P}\right)^2$$

The total basic casualty area should not include fragments that have insufficient impact velocity and weight to create a casualty (i.e., those that impact with a kinetic energy below 11 ft-lb).

Figure 7-1 shows the total basic casualty areas for several vehicles as a function of total dry weight. Figure 7-2 shows the range of numbers of fragments as a function of total dry weight. These figures also show that hypersonic breakup during reentry appears to produce more fragments than breakups occurring at much slower speeds and at lower altitudes. The debris recovered from the *Columbia* averaged less than one pound of dry weight, which neglects the numerous smaller fragments that were not recovered. A debris list built from the parts list of the vehicle would vastly underestimate the debris generated by *Columbia's* demise because of the influence of aerodynamic heating.

With such a range of possibilities based upon past debris lists, it would be acceptable to perform a risk analysis with more than one debris list to determine the effect of debris list uncertainty on the final risk estimates.

It is important to note that this comparison has used basic casualty area, which is related to risk to people in the open. Not all people at risk are in the open and the fewer but more massive pieces of debris associated with the EELV model can be more of a threat to people in structures than the debris from the ELV model. Hence, one cannot automatically say that the difference in casualty areas in Figure 7-1 will directly transfer over the final E_C. There is also the influence of impacting explosive debris on the risk that is not considered in the inert debris list.

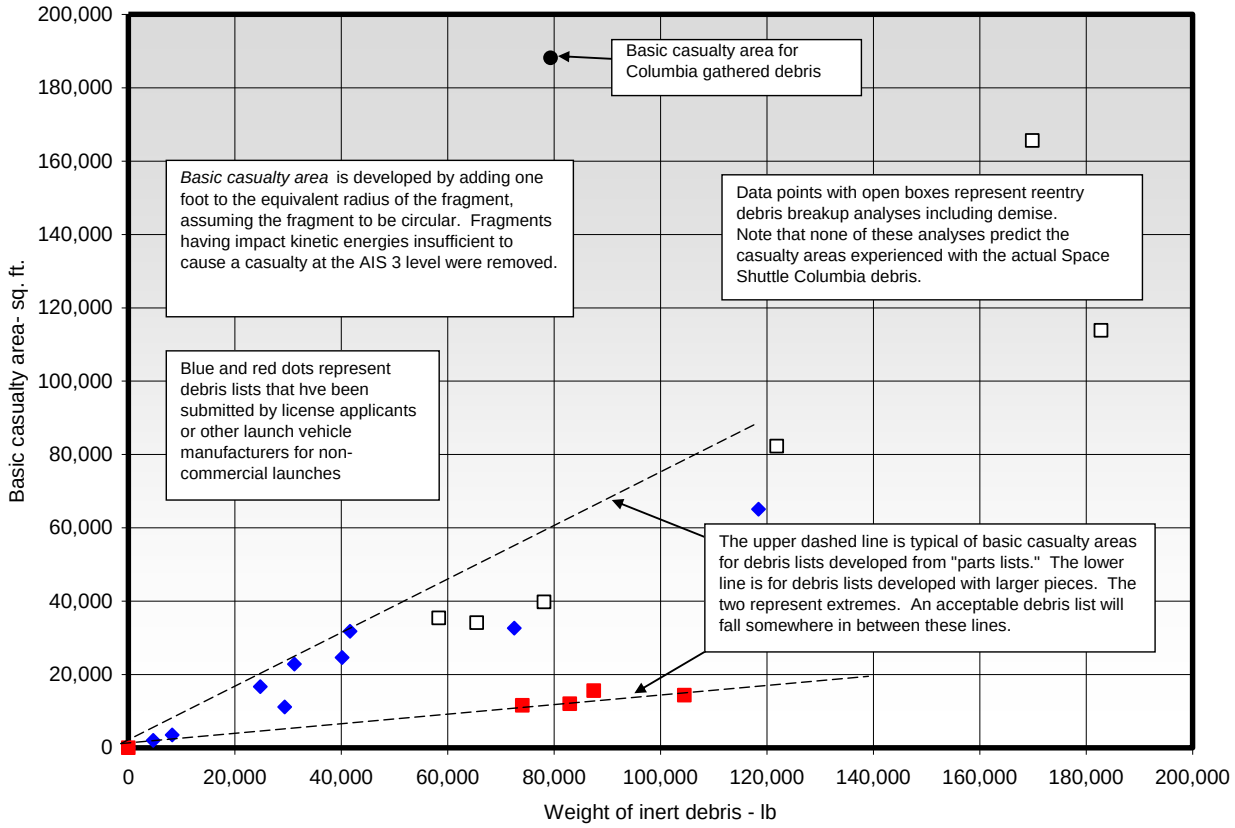

Figure 7-1. Total basic casualty areas as a function of dry weight for various vehicles

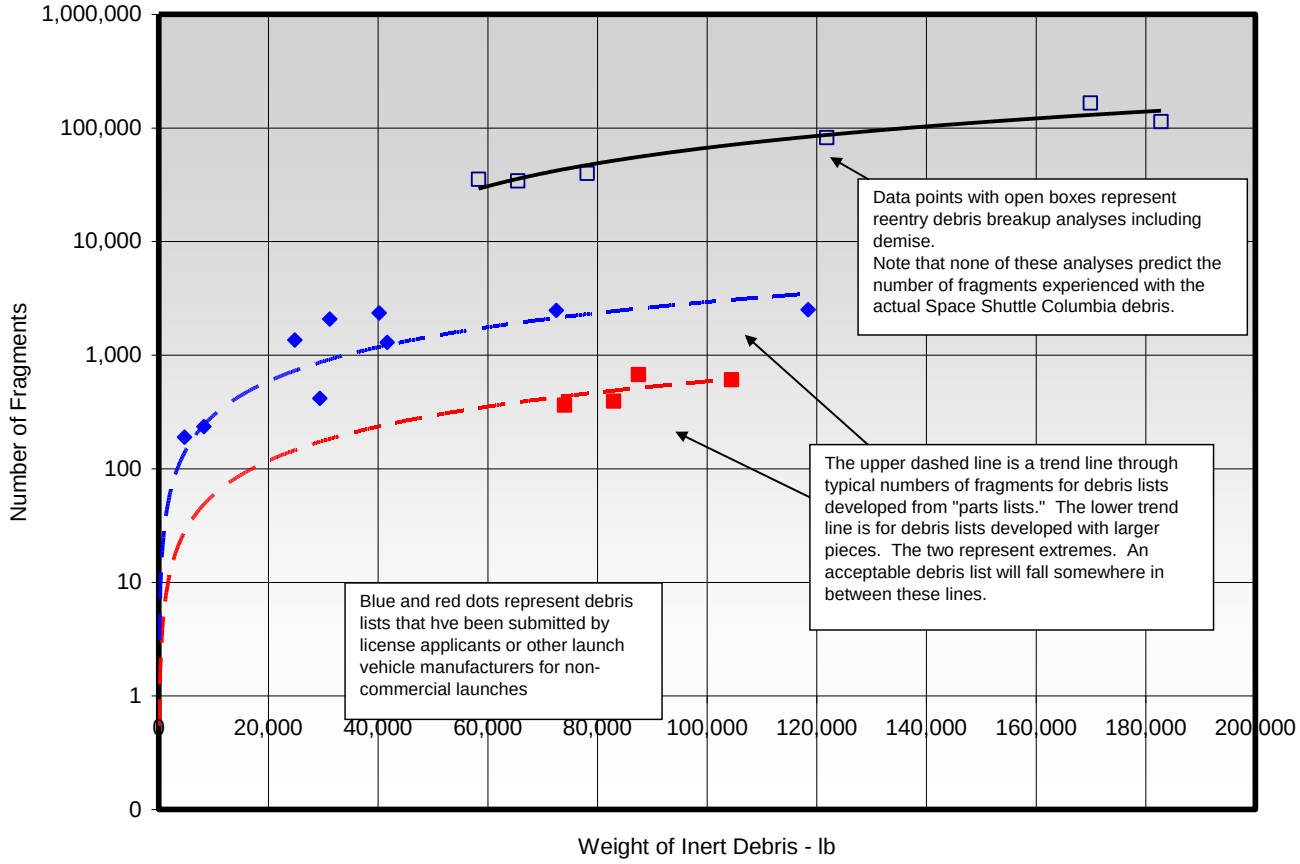

Figure 7-2. Total number of fragments as a function of dry weight for various vehicles

8.0 VEHICLE TRAJECTORY MODELING

An adequate vehicle trajectory model is an essential element of a successful risk analysis. Therefore, this section provides guidance only on those elements of vehicle trajectory modeling uniquely necessary for a sufficient QRA. Additional discussion relevant to modeling vehicle trajectory dispersions appears in Section 10.4.

8.1 Purpose

The purpose of the vehicle trajectory modeling performed for risk analyses is to characterize all the potential state vectors for debris generating events. A state vector specifies the position and velocity of the vehicle; in the typical Cartesian coordinates a state vector is given by $(x, y, z, \dot{x}, \dot{y}, \dot{z})$.

8.2 Input Data Sources

In order to design the vehicle trajectory for a successful mission, the operator naturally develops a trajectory simulation based on the laws of physics. A six-degree of freedom (6-DOF) trajectory simulation requires a great deal of detailed input data, such as aerodynamic constants, mass properties, and thrust profiles. An acceptable QRA based on state vector data generated with a vehicle trajectory simulation should satisfy at a minimum the general risk model requirements described in the supplement to RCC 321-07. If a vehicle has flown many times, you might estimate the nominal trajectory dispersion from the actual flight data. However, empirical characterization of nominal trajectory dispersion is rarely practical because flight profiles generally change from mission to mission.

8.3 Minimum Features

Operators should use a 6-DOF trajectory simulation to facilitate mission success and to provide at least the final input data for the QRA as required by §417.207(b). However, there are cases where a three degree of freedom (3-DOF) trajectory simulation may be sufficient for use in a preliminary flight safety analysis as illustrated in the Appendix.

There are many potential causes of launch failure (i.e. initiating events); however, there are relatively few responses to failures in terms of the vehicle behavior. The objective of a QRA is not to compute the precise risk presented by the flight, but rather to demonstrate that the risks from the flight are below acceptable levels. Therefore, while it is important to ensure that you compute the consequences of various failures conservatively (and as accurately as possible), it is unnecessary to determine all the initiating events that can produce an accident. Rather, it is sufficient to define and model vehicle failure response modes that encompass the entire range of foreseeable behavior. In order to assess the risk from all types of accident initiating conditions foreseeable for launches, a QRA should account for the appropriate vehicle response modes.

An adequate characterization of all the potential state vectors for debris generating events should explicitly account for or clearly encompass the following:

- Potential three-sigma trajectory dispersions due to foreseeable variations and uncertainty associated with vehicle performance, pilot actions, environmental parameters, and any other factors capable of influencing predicted behavior under nominal conditions. Environmental conditions should specifically include all wind effects, including profiles of winds that are no less severe than the worst wind conditions under which flight might be attempted, and should account for uncertainty in the wind conditions. A Monte Carlo analysis is often necessary to account for the potential non-linear interactions of various parameter perturbations. This is particularly important for cases where rotational momentum is substantial, such as spin stabilized sub-orbital rockets. [49]
- Trajectory dispersions due to foreseeable malfunctions that can cause the vehicle to depart from the nominal trajectory. Specifically, a vehicle trajectory model should account for potential state vectors that can result from thrust offsets, loss of control, loss of stability, loss of guidance, and other thrust anomalies.
- Nominal and non-nominal state vectors for all credible abort (contingency and emergency) and failure modes (including flight safety system failures) that may pose a public risk.
- State vectors associated with violation of flight termination criteria, breakup due to aerodynamic forces, breakup due to inertial loads, aero-thermal loads, and explosive breakup.
- Uncertainty due to variability in pilot actions, vehicle guidance and performance parameters, and environmental conditions under non-nominal conditions.

Since the QRA is used to inform the FAA's MPL determination for licenses, an adequate characterization of all the potential state vectors for debris generating events should facilitate resolution of the greatest dollar amount of loss for bodily injury or property damage that is *reasonably expected* to result from licensed or permitted activities. Thus, an adequate characterization of all the potential state vectors for debris generating events should account for any scenario where the chance of public casualties or losses to Government property and Government personnel approaches the respective thresholds.

8.4 Modeling Discussion

8.4.1 Vehicle Guidance and Performance Uncertainty

Uncertainties in the vehicle's guidance and performance produce uncertainty in the state vector of a vehicle at the time of breakup. A vehicle's trajectory is typically affected by environmental factors (such as the wind conditions), vehicle performance (such as the thrust magnitude), as well as the accuracy of the guidance program or pilot actions. The resulting state vector uncertainty leads to uncertainty (dispersions) in the locations of the vehicle breakup debris during free fall and at impact. The purpose of the vehicle guidance and performance debris dispersion model is to define these dispersions. A typical means to characterize the nominally dispersed trajectories is to provide

1. A 3-sigma low performing (low thrust) vehicle (often referred to as a cold trajectory),

2. A 3-sigma high performing vehicle (often referred to as a hot trajectory),

3. A 3-sigma deviation to the left of the nominal trajectory plane (left trajectory),

4. A 3-sigma deviation to the right of the nominal trajectory plane (right trajectory),

5. A 3-sigma high altitude (lofted) trajectory, and

6. A 3-sigma low altitude (depressed) trajectory.

These trajectories are generally referred to as 3-sigma trajectories to reflect the fact that they are intended to represent dispersions from the nominal trajectory that are near maximum (i.e., will be rarely exceeded). Three-sigma trajectories are generated for various conditions to cover the range of state vector variation.

8.4.2 Modeling Using Composite Trajectories

To generate a single composite 3-sigma trajectory in terms of instantaneous impact range, the following procedure is suggested from AFSPCMAN 91-710 [50].

Step 1: Identify individual parameters such as thrust, weight, specific impulse, and atmospheric density that significantly affect the performance of the vehicle instantaneous impact point (IIP). Estimate 3-sigma dispersions (three times the statistical standard deviation of the values) for these parameters.

Step 2: Run a series of trajectory computations or simulations where three-sigma values of significant perturbing parameters are introduced one at a time. At a suitable number of time points, tabulate the IIP deviations from nominal that have been caused by perturbing each parameter.

Step 3: At each time point and direction, calculate the square root of the sum of the squares (RSS) for all deviations to determine the three-sigma IIP deviations.

Step 4: By further trajectory computations or simulations, generate a thrusting flight trajectory (a three-sigma, no-wind trajectory) that matches as closely as possible the 3-sigma deviations calculated in Step 3. This may be done by perturbing only a few key parameters at varying magnitudes throughout the run.

Step 5: Compute the 3-sigma trajectory using worst-case winds together with the parameter magnitudes used to calculate the 3-sigma no-wind trajectory. The wind dispersed trajectories indicate vehicle performance deviations due to the effects of severe winds. This data should be applied until the vehicle attains an altitude where there is essentially no wind effect. It is usually sufficient to use 100,000 ft as this altitude limit. Do not limit computations to wind drift but include all wind effects.

8.4.3 Modeling Using Covariance Matrices

Operators may also characterize nominally dispersed trajectories by a covariance matrix that defines the state vector uncertainty statistics for each time in flight. A covariance matrix consists of the variances (standard deviations squared) in the state vector position and velocity components along the diagonal and the correlations between the standard deviations for the off-diagonal terms. The example below includes sample calculations to demonstrate generating a covariance matrix to characterize nominal trajectory dispersions.

You can use at least two approaches to propagate the nominal state vector covariance data to define dispersions. One approach is to propagate the state vector uncertainties, for given failure times, using partial derivatives relating impact (or altitude) displacements to perturbations in the initial state vector components. The partial derivative values will, of course, vary with the fragment drag characteristics (ballistic coefficient or drag coefficient versus Mach number). Another approach is to use the covariance matrix to generate random perturbed initial state vectors for a given failure time and to propagate these, for a given fragment (or fragment group), to impact using an impact predictor. You can use the resulting random impact points (referred to as a scatter plot) to define the statistics of the impact dispersions. Figure 8-1 shows a sample scatter plot where the random impact points from a randomly perturbed initial state vector display for two fragment ballistic coefficient values. Associated coordinates (latitude-longitude, x-y, or other coordinate system) define each impact point.

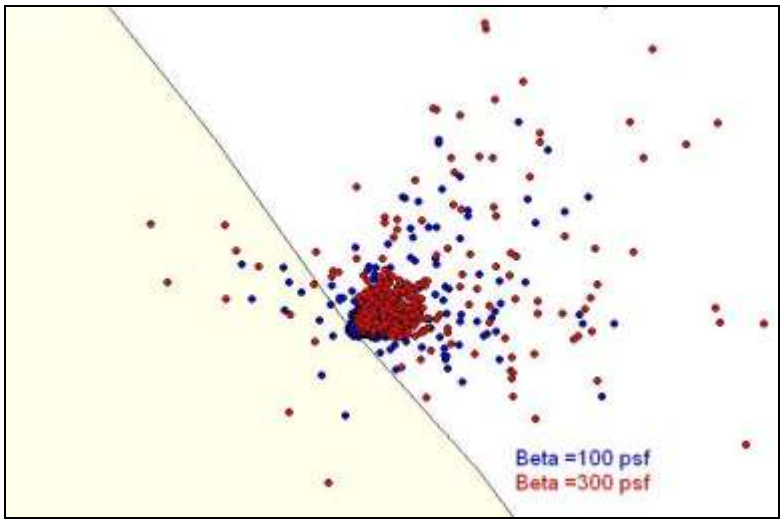

Figure 8-1. Sample Impact Point Scatter Plot

Modeling debris dispersions due to guidance and performance is more difficult when the dispersion data are in the form of 3-sigma trajectories. One approach is to use the state vectors at a given flight time from each of the 3-sigma trajectories to compute the corresponding impact points for a given fragment/fragment group. You can then use these points to define the 3-sigma limits for the impact dispersions. For example, the most extreme impact points in the up-range, downrange, cross-range left, and cross-range

right directions define a contour fit of the points and interpret this contour as a 3-sigma dispersion contour.

EXAMPLE: Covariance Matrix Computation

Covariance is a measure of the tendency for two variables to vary together, which is directly related to the correlation between random variables. Covariance matrices have many applications in flight safety analysis, such as modeling winds, impact dispersions, and trajectories. This example demonstrates constructing a covariance matrix for trajectory modeling.

Covariance is mathematically expressed as the correlation between two random variables (i.e. $\rho(X,Y)$) multiplied by their standard deviations (i.e., σ_X and σ_Y). This is presented as follows:

$$\mathrm{Cov}(X,Y) = \sigma_X \sigma_Y \rho(X,Y)$$

In terms of the expectation (or mean value) of each variable (i.e. $E(X) = \mu_X$), the covariance can be defined as follows:

$$\mathrm{Cov}(X,Y) = E[(X - \mu_X)(Y - \mu_Y)]$$

Or equivalently as:

$$\mathrm{Cov}(X,Y) = E(XY) - E(X)E(Y)$$

Modeling the trajectory of a launch vehicle requires an understanding of many complex interdependencies. The output variables from a trajectory analysis (e.g., position and velocity) under normal conditions are rarely independent. You can model each of these interrelated input and output variables as random variable defined by probability density functions. When performing any type of Monte Carlo analysis, where each observed quantity is represented by a random variable, a covariance matrix allows the model to characterize the underlying interdependencies between each variable.

You can use the Monte Carlo technique to reveal the potential non-linear interactions between various parameters: use probability distributions to account for uncertainties in each of the critical input parameters (such as thrust, thrust offset, thrust angle, etc) and compute a set of feasible trajectories based on sampled values for each input parameter. For example, compute a set of normal trajectories using a Monte Carlo analysis based on input parameter distributions that represent guidance and performance uncertainty for a properly performing vehicle and representative wind conditions allowable for a launch. We represent the output trajectories as a series of state vectors. For example, the vectors in Table 8-1 were computed for a sounding rocket at burnout.

Table 8-1. Sample State Vectors for Normal Sounding Rocket at Burnout

Fail Time	Long	Latgd	Alt	Vn	Ve	Vd	Yawgd	Pitchgd	Rollgd
(sec)	(deg)	(deg)	(ft)	(ft/sec)	(ft/sec)	(ft/sec)	(deg)	(deg)	(deg)
52.25	-75.3	37.6	203090.7	-3473.9	2454.7	-8918.3	144.7	64.5	-53.8
52.25	-75.2	37.7	204473.3	-2587.7	3421.5	-9000.7	126.9	64.5	135.5
52.25	-75.2	37.6	182715.0	-4289.1	3752.7	-7906.6	138.8	54.2	37.3
52.25	-75.2	37.7	196651.3	-2230.4	4206.3	-8598.6	117.7	61.0	138.8
52.25	-75.3	37.8	208695.5	-1216.3	2582.1	-9198.7	115.0	72.8	-14.4
52.25	-75.5	37.6	208750.0	-3294.9	448.8	-9221.4	172.1	70.2	-88.5
52.25	-75.3	37.8	209495.8	-1326.8	2911.0	-9253.9	114.2	71.0	-174.2
52.25	-75.3	37.7	207214.6	-1841.1	2737.2	-9124.9	123.7	70.1	-104.2
52.25	-75.3	37.7	206668.1	-2599.2	3160.8	-9111.9	129.3	65.8	30.1
52.25	-75.4	37.7	208156.5	-2950.9	1046.5	-9163.6	160.4	71.2	-16.2
52.25	-75.4	37.7	208636.2	-2963.0	1190.6	-9188.1	158.0	70.9	98.2
52.25	-75.3	37.7	205385.4	-2919.0	2731.1	-9019.8	136.7	66.1	167.6
52.25	-75.4	37.7	218421.7	-2407.2	1095.6	-9709.8	155.3	74.8	-53.9
52.25	-75.4	37.7	214183.5	-2772.3	1072.8	-9472.8	158.8	72.6	137.3
52.25	-75.1	37.7	185923.9	-2381.5	5452.6	-8065.6	113.4	53.6	152.9
52.25	-75.3	37.8	216045.9	-1364.4	2340.5	-9549.7	119.9	74.2	19.9
52.25	-75.5	37.6	211739.4	-3560.4	213.8	-9356.6	176.5	69.1	-125.1
52.25	-75.5	37.7	209968.9	-3095.4	104.0	-9273.3	177.9	71.6	118.4
52.25	-75.3	37.7	210074.6	-2300.2	2433.2	-9285.2	133.2	70.2	-115.9
52.25	-75.2	37.6	200086.2	-3504.6	3589.1	-8776.2	134.3	60.3	-145.9
52.25	-75.3	37.7	201807.5	-2830.9	2861.2	-8860.8	134.6	65.6	44.7
52.25	-75.3	37.7	203157.5	-2973.4	3021.3	-8951.3	134.4	64.7	-116.5
52.25	-75.3	37.7	215492.2	-1719.6	2649.4	-9554.5	122.7	71.7	88.7
52.25	-75.3	37.6	197566.4	-3940.8	2866.2	-8645.9	143.9	60.6	85.1
52.25	-75.3	37.7	198496.6	-3141.3	2032.2	-8679.0	147.1	66.7	8.9
52.25	-75.2	37.6	191153.0	-3556.4	3937.7	-8328.2	132.1	57.5	-48.2
52.25	-75.3	37.7	210030.0	-3129.2	1944.4	-9267.1	148.1	68.4	-148.5
52.25	-75.4	37.6	209130.3	-3285.1	1034.6	-9191.6	162.5	69.5	140.9
52.25	-75.2	37.7	196392.1	-2887.8	3566.3	-8597.3	128.9	62.0	123.2
52.25	-75.3	37.7	208084.3	-2137.0	2800.4	-9190.7	127.1	69.0	71.9

It is important that all units are consistent when constructing a covariance matrix. Therefore, the vectors above are converted into vectors defined by the Earth Centered Fixed (ECF) coordinate system, also known as Earth Centered Earth Fixed (ECEF). Instead of geodetic latitude (ϕ), longitude (λ), and altitude (h), the ECF system defines a position using the following parameters:

$$\mathrm{e} = \left(\frac{a}{\sqrt{1 - e^2 \sin^2 \phi}} + h \right) \cos \phi \cos \lambda$$

$$\mathrm{f} = \left(\frac{a}{\sqrt{1 - e^2 \sin^2 \phi}} + h \right) \cos \phi \sin \lambda$$

$$\mathrm{g} = \left(\frac{a\left(1 - e^2\right)}{\sqrt{1 - e^2 \sin^2 \phi}} + h \right) \sin \phi$$

Assuming the Earth can be represented by the World Geodetic System model of 1984 (WGS-84), the semi-major axis (a) is defined as 6378137 m in length and the reciprocal of flattening (1/f) is approximately 298.2572, which results in the first eccentricity squared (e^2) being approximately 6.6944×10^{-3}. Using these equations, the state vectors from Table 8-1 are expressed in the ECF coordinate system as shown in the table below.

Table 8-2. Sample ECF State Vectors for Normal Sounding Rocket at Burnout

Fail Time	E	F	G	dE	dF	dG	Yawgd	Pitchgd	Rollgd
(sec)	(ft)	(ft)	(ft)	(ft/sec)	(ft/sec)	(ft/sec)	(deg)	(deg)	(deg)
52.25	4248867	-16204822	12832588	4703.7	-8260.9	2695.0	144.7	64.5	-53.8
52.25	4265779	-16189824	12848074	5526.5	-7545.8	3454.7	126.9	64.5	135.5
52.25	4274556	-16192506	12806178	5895.3	-7629.6	1424.2	138.8	54.2	37.3
52.25	4279427	-16175146	12849138	6155.2	-6819.5	3494.5	117.7	61.0	138.8
52.25	4245193	-16180448	12873462	4532.0	-7099.0	4672.0	115.0	72.8	-14.4
52.25	4208456	-16217766	12838840	2773.9	-8902.6	3023.4	172.1	70.2	-88.5
52.25	4252238	-16180720	12872120	4881.4	-7121.7	4617.6	114.2	71.0	-174.2
52.25	4249902	-16186312	12862173	4766.4	-7374.9	4127.7	123.7	70.1	-104.2
52.25	4260920	-16192830	12849503	5296.1	-7705.8	3513.6	129.3	65.8	30.1
52.25	4219568	-16209842	12844184	3294.3	-8501.2	3263.5	160.4	71.2	-16.2
52.25	4222578	-16209683	12844186	3442.0	-8490.3	3268.8	158.0	70.9	98.2
52.25	4253052	-16198310	12843131	4907.7	-7937.4	3201.3	136.7	66.1	167.6
52.25	4220623	-16210643	12859629	3366.9	-8583.5	4032.7	155.3	74.8	-53.9
52.25	4220679	-16212020	12850953	3354.0	-8625.1	3595.6	158.8	72.6	137.3
52.25	4303606	-16161993	12840019	7285.9	-6171.2	3047.8	113.4	53.6	152.9
52.25	4242096	-16189247	12875491	4389.6	-7518.5	4768.7	119.9	74.2	19.9
52.25	4205100	-16224400	12836500	2611.5	-9223.7	2893.3	176.5	69.1	-125.1
52.25	4200934	-16218114	12842846	2415.8	-8911.5	3214.8	177.9	71.6	118.4
52.25	4246004	-16195744	12856330	4573.4	-7849.9	3858.7	133.2	70.2	-115.9
52.25	4271896	-16196863	12830055	5788.6	-7874.2	2583.5	134.3	60.3	-145.9
52.25	4255005	-16193777	12842312	4989.3	-7729.4	3174.6	134.6	65.6	44.7
52.25	4258876	-16195630	12840925	5186.1	-7841.6	3115.9	134.4	64.7	-116.5
52.25	4249265	-16191595	12869305	4747.8	-7654.0	4487.7	122.7	71.7	88.7
52.25	4257961	-16204222	12821295	5124.0	-8221.9	2154.5	143.9	60.6	85.1
52.25	4238534	-16199520	12835109	4191.0	-7989.6	2815.0	147.1	66.7	8.9
52.25	4277520	-16188734	12823756	6046.7	-7470.2	2268.5	132.1	57.5	-48.2
52.25	4238854	-16208596	12842504	4221.1	-8455.5	3184.1	148.1	68.4	-148.5
52.25	4220651	-16214815	12839188	3340.0	-8724.3	3013.0	162.5	69.5	140.9
52.25	4268621	-16186504	12838072	5633.7	-7377.2	2968.0	128.9	62.0	123.2
52.25	4252184	-16190285	12857877	4887.5	-7585.1	3931.4	127.1	69.0	71.9

These data points can be represented with the following variables and data sets:

$$e = \begin{bmatrix} 4248867 \\ 4265779 \\ \vdots \\ 4252184 \end{bmatrix} \quad f = \begin{bmatrix} -16204822 \\ -16189824 \\ \vdots \\ -16190285 \end{bmatrix} \quad g = \begin{bmatrix} 12832588 \\ 12848074 \\ \vdots \\ 12857877 \end{bmatrix} \quad \dot{e} = \begin{bmatrix} 4703.7 \\ 5526.5 \\ \vdots \\ 4887.5 \end{bmatrix} \quad \dot{f} = \begin{bmatrix} -8260.9 \\ -7545.8 \\ \vdots \\ -7585.1 \end{bmatrix} \quad \dot{g} = \begin{bmatrix} 2695.0 \\ 3454.7 \\ \vdots \\ 3931.4 \end{bmatrix}$$

Using these variables, the covariance matrix for the identified state vectors is defined as follows:

$$\Sigma = \begin{bmatrix} \mathrm{Cov}(e,e) & \mathrm{Cov}(e,f) & \cdots & \mathrm{Cov}(e,\dot{g}) \\ \mathrm{Cov}(f,e) & \mathrm{Cov}(f,f) & \cdots & \mathrm{Cov}(f,\dot{g}) \\ \vdots & \vdots & \ddots & \vdots \\ \mathrm{Cov}(\dot{g},e) & \mathrm{Cov}(\dot{g},f) & \cdots & \mathrm{Cov}(\dot{g},\dot{g}) \end{bmatrix}$$

Using the previously identified equations for covariance, $\mathrm{Cov}(e,\dot{g})$ given the 20 identified state vectors defining normal vehicle state vectors from Table 8-2 can be found as follows:

$$\mathrm{Cov}(\dot{e},\dot{g}) = \frac{1}{20}\left[\begin{array}{l} (4703.7 \times 2695.0 + 5526.5 \times 3454.7 + \cdots + 4887.5 \times 3931.4) - \ldots \\ ([4703.7 + 5526.5 + \cdots + 4887.5][2695.0 + 3454.7 + \cdots + 3931.4]) \end{array}\right]$$

By performing each of the covariances as done above, the covariance matrix for the identified state vectors at burnout is as follows in Table 8-3:

Table 8-3. Covariance Matrix for Sample State Vectors

	e	F	g	de	df	Dg
e	5.6583E+08	2.8157E+08	-6.9329E+07	2.6923E+07	1.3752E+07	-3.4600E+06
f	2.8157E+08	1.9023E+08	5.5147E+07	1.3441E+07	9.2244E+06	2.6074E+06
g	-6.9329E+07	5.5147E+07	2.3983E+08	-3.1314E+06	2.4752E+06	1.1615E+07
de	2.6923E+07	1.3441E+07	-3.1314E+06	1.2812E+06	6.5620E+05	-1.5650E+05
df	1.3752E+07	9.2244E+06	2.4752E+06	6.5620E+05	4.4761E+05	1.1673E+05
dg	-3.4600E+06	2.6074E+06	1.1615E+07	-1.5650E+05	1.1673E+05	5.6263E+05

It is important to note that this covariance matrix is only applicable for the identified state vectors. While this example is for only one time step, it is not uncommon for every analytical step along a trajectory to have a unique covariance matrix associated the state vector at a point in time.

8.4.4 Vehicle Malfunction Turns

The breakup state vector for an off course vehicle is highly uncertain because of the variations in the failure mode that caused the malfunction turn and the uncertainties in the response of the vehicle to the failure condition. Of course, uncertainty in these breakup

state vectors produces uncertainty (dispersions) in the locations of the vehicle debris during free fall and at impact. The purpose of the malfunction turn debris dispersion model is to define these dispersions.

There are many failure modes that can cause a malfunction turn and an adequate QRA should address each credible mode.

Examples of malfunction turn failure modes typically addressed with turn curves, as described in Section 10.4.8, include the following.

- A motor nozzle hardware failure causing loss of full control of the thrust direction resulting in an unplanned offset of the thrust vector. This could result, for example, from a failure of one or more nozzle actuators leading to a nozzle stuck in place, drifting to null, going hard-over, or randomly moving; or from a failure in a thrust injection system used to control the thrust vector direction.
- A failure in the vehicle control system (hardware or software) leading to an erroneous command to the thrust vector control system.
- A failure of a nozzle, such as a nozzle burn through, leading to a loss of a portion of a nozzle and a thrust offset.
- The complete loss of a nozzle assembly resulting in a complete loss of thrust control and/or a drop in the thrust.
- The loss or reduction of thrust for one of the motors on a vehicle with multiple operating motors (core vehicle or strap-on motor).
- An inadvertent separation of one or more strap-on motors.
- A case burn-through for a solid rocket motor, or a leak at a case joint, resulting in a side thrust at the location of the burn through and a reduction in the main thrust.

Develop malfunction turn data can be developed using an appropriate trajectory simulation. This approach requires a significant amount of data for the launch vehicle such as thrust, mass properties and aerodynamic coefficients, including coefficients at large angles of attack. Unless the failure is a simple one to model, such as a vehicle with a single thrusting motor with the nozzle locked in an offset position, the malfunction turn behavior should account for the potential response of the control system.

Velocity turn curves represent one form of malfunction turn data. These curves give the turning capability of a vehicle expressed in terms of the time history of the vehicle velocity vector magnitude and velocity vector turn angle, for turns initiating at various flight times. The turn angle is the angle between the vehicle velocity vector at the start of a turn and that at a given time into the turn. Figure 8-2 and Figure 8-3 show example curves for malfunction turns at six different turn angles occurring at one state vector time.

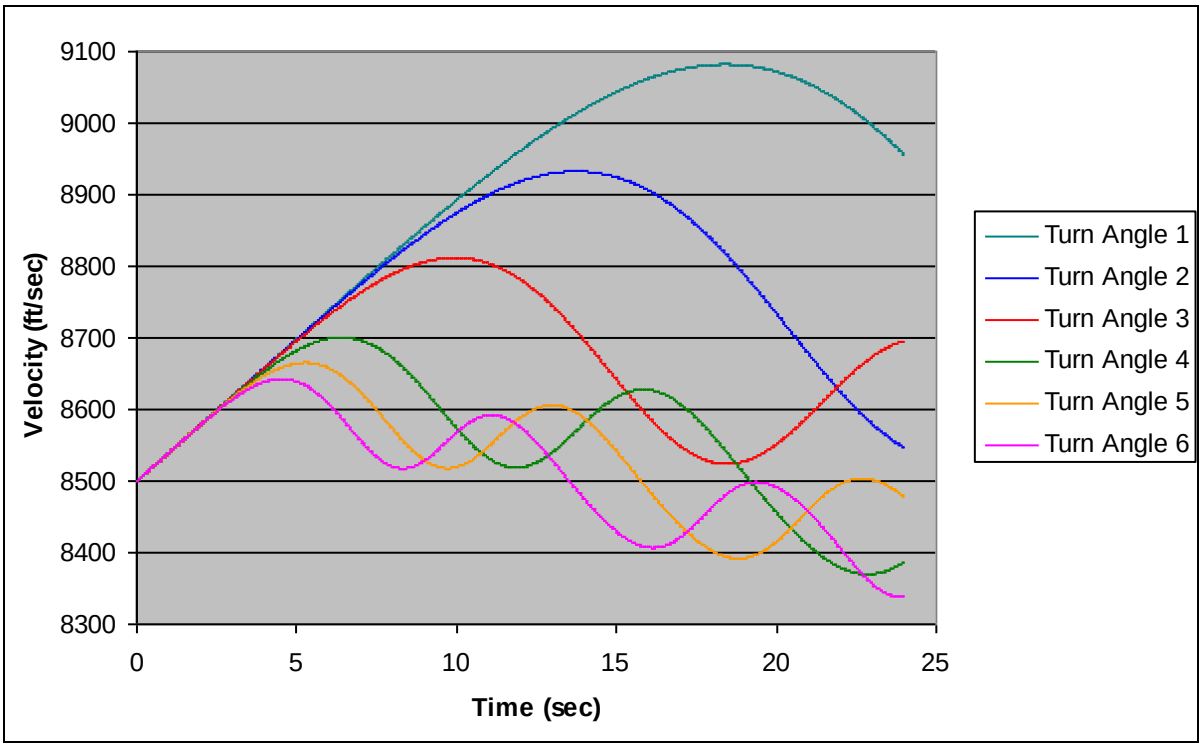

Figure 8-2. Example Velocity Turn Curve

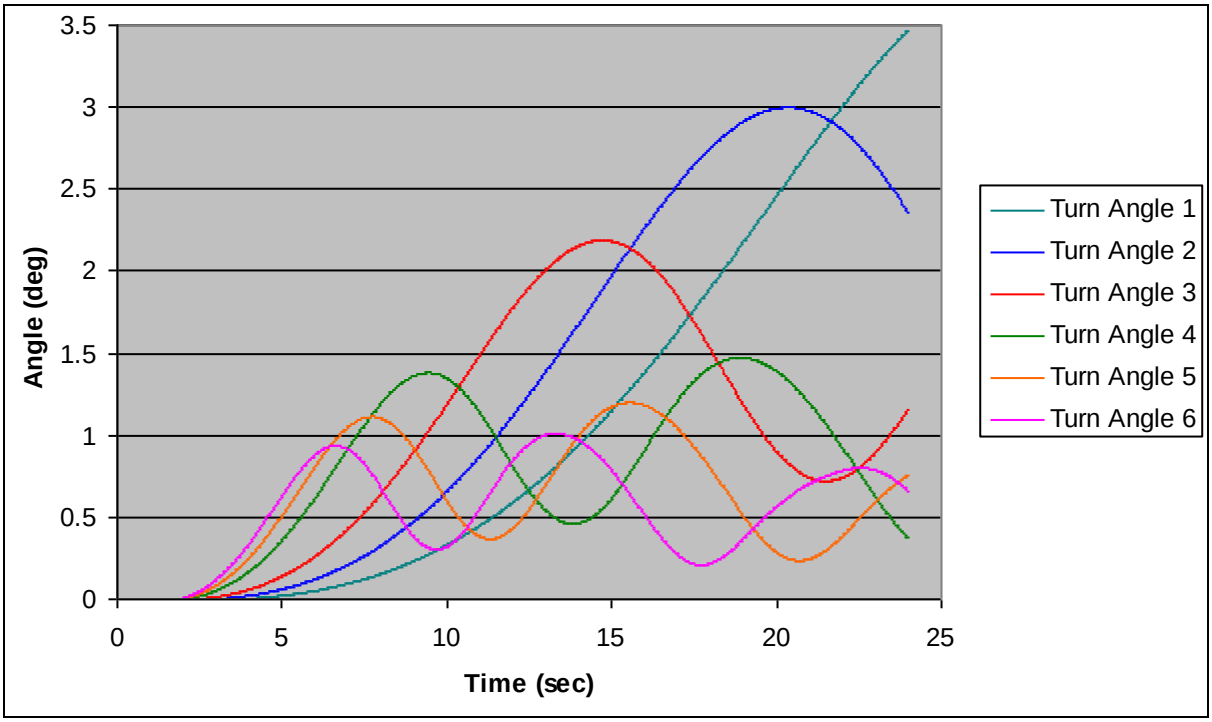

Figure 8-3. Example Turn Angle Curve

You may generate the velocity magnitude and turn angle for various failure scenarios. Generate the curves both for thrust vector offsets that will result in a pitch plane turn and for offsets that will result in a yaw plane turn. Generate the turn curves either ignoring

the force of gravity during the turn or including gravity. The purpose of generating turn curves ignoring gravity is to allow the velocity turn data to be used to estimate turns where the velocity vector is turning in a plane (containing the vehicle longitudinal axis at the start of the turn) other than that for which the turn data are generated, with the effect of gravity accounted for later in the analysis.

The major shortcoming with the velocity turn curve data is that the attitude of the vehicle and its velocity vector are not defined. Thus, you should make an assumption regarding the direction that the velocity vector turns. A common assumption used is that the velocity remains in a specified plane.

A better form of malfunction turn data are full 6-DOF malfunction trajectories giving the full state vector, including the vehicle attitude, as a function of time into a turn. Trajectory data in this form are becoming more common. Typically, you generate a family of trajectories for selected flight failure times and these apply to each of many failure scenarios covering the range of vehicle malfunction response. The attitude data provides a full state vector during a turn, and thus eliminates the need to assume the direction for the velocity. In addition, you can use the attitude data to define the orientation of the vehicle at the time of vehicle breakup or destruct. In turn you can use this to initiate free flight simulations for an inadvertently separated thrusting motor or to account for the directionality of velocities imparted to fragments at breakup (Section 10.4.6).

In addition to the malfunction turn curves or trajectories, the vehicle operator should also provide data to determine when the vehicle is expected to break up due to aerodynamic and inertial loads, or specifies that breakup will not occur. This is in the form of the time into each turn that breakup is expected to occur or, for malfunction trajectories, may be in the form of a loading condition, such as the q-alpha (dynamic pressure multiplied by the angle of attack) value, at which breakup would be expected. In some cases the time range or loading condition will be expressed as a range of values to account for uncertainty.

The relative probabilities of the malfunction turn curves or malfunction trajectories for each flight time should also be estimated to properly assess debris dispersions due to malfunction turns. These data are used to compute impact dispersion statistics from random impact points generated using the turn data.

With either form of the malfunction turn data (turn curves or turn trajectories) the analyst can choose to

1) compute the statistics of the impact dispersions from generated random impact points by fitting a probability distribution,
2) generate and use the specific impact points without fitting a probability distribution for the malfunction turn impact dispersion in risk calculations, or
3) generate a histogram of the impact point distribution to provide an accurate representation of the distribution.

EXAMPLE: Malfunction Turn Calculations

This example demonstrates the potential usefulness of three degree of freedom (3-DOF) malfunction trajectory analyses based on a fin stabilized (unguided) Talos-Castor launched without any fin cant at 80 degree elevation and 135 degree azimuth. This example used the Trajectory Analysis and Optimization Software (TAOS) and input data developed by Sandia National Laboratory and discussed in more detail elsewhere. [49]

Figure 8-4 shows impact points computed following a malfunction turn (MFT) driven by a uniform thrust angle offset between 2 and 10 degrees initiated at 40s into flight from trajectories that include nominal dispersion. Figure 8-4 contains 3000 black points based on six degree of freedom (6DOF) trajectory simulations assuming the entire vehicle remains intact to impact, and 3000 impact points marked in red points predicted based on a 3-DOF analysis used from MFT initiation until impact.

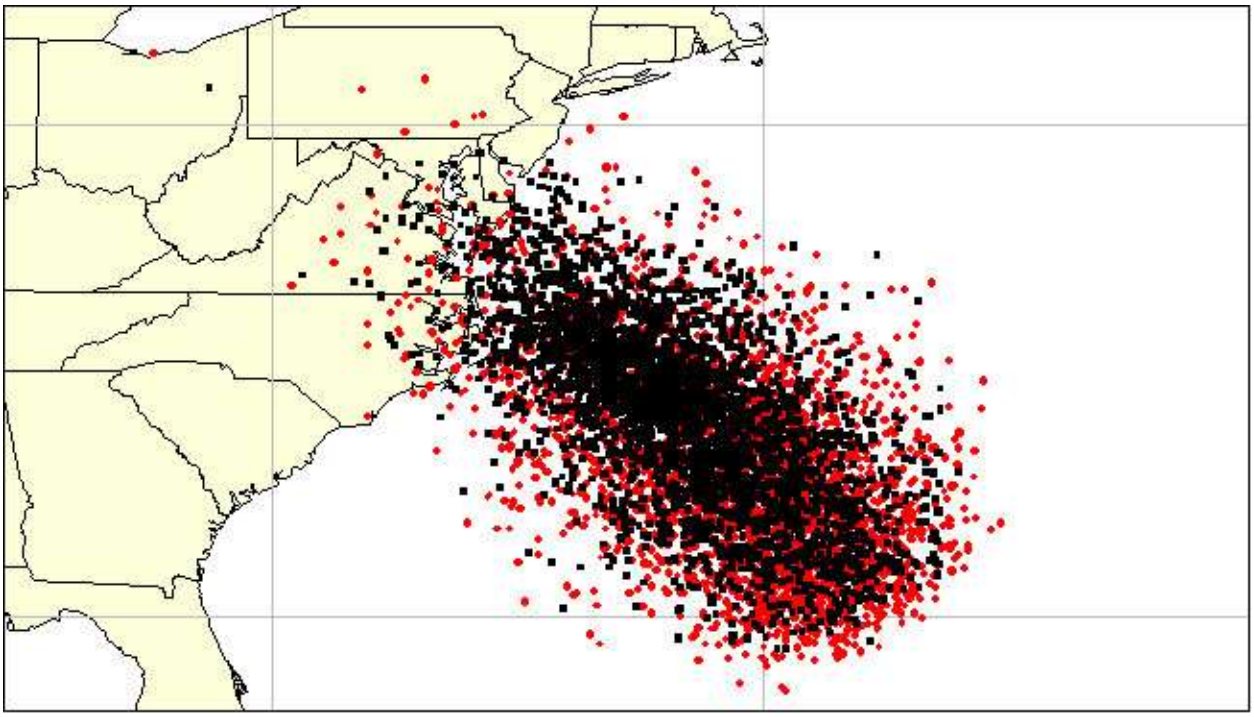

Figure 8-4. Intact Impact Points after a Malfunction Turn Initiated at 40s into Flight (Red used a 3 DOF and Black used a 6 DOF Analysis)

Figure 8-5 and Figure 8-6 show results from similar computations as in Figure 8-4, but for malfunction turns initiated earlier in flight. In this case, stage 2 ignition was scheduled at nominally 12 seconds into flight, such that only Figure 8-6 shows results from a malfunction turn initiated before staging. Notice that we predict an artificially increased maximum range of the rocket by the 3-DOF analysis.

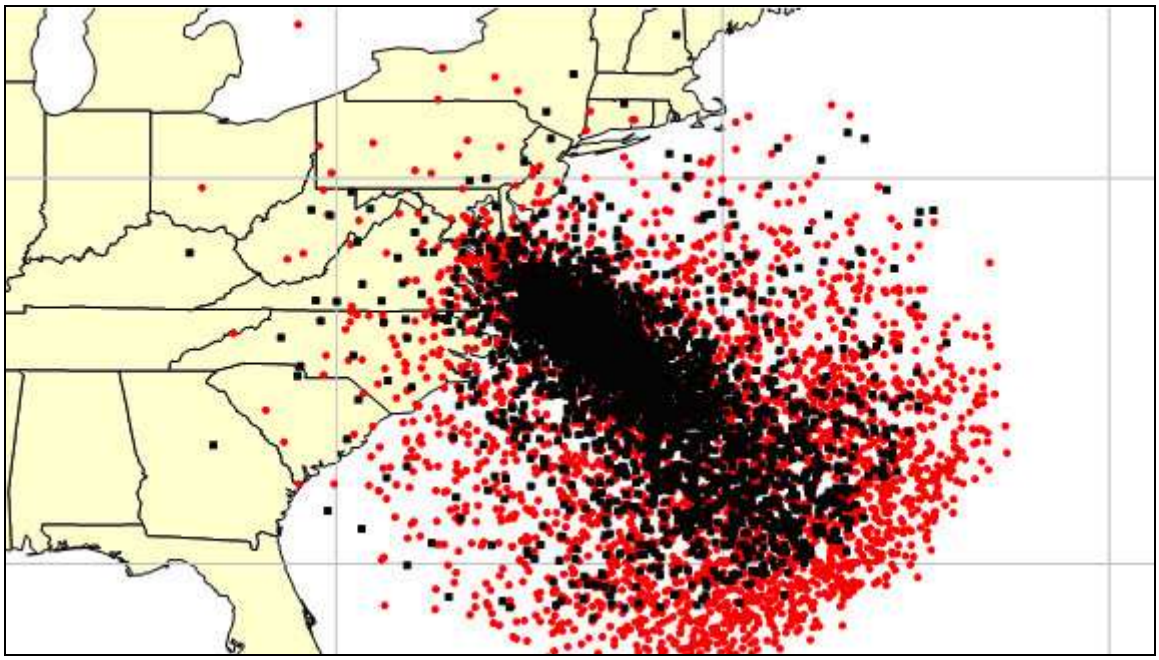

Figure 8-5. Intact Impact Points after a Malfunction Turn Initiated at 20s into Flight (Red used a 3 DOF and Black used a 6 DOF Analysis)

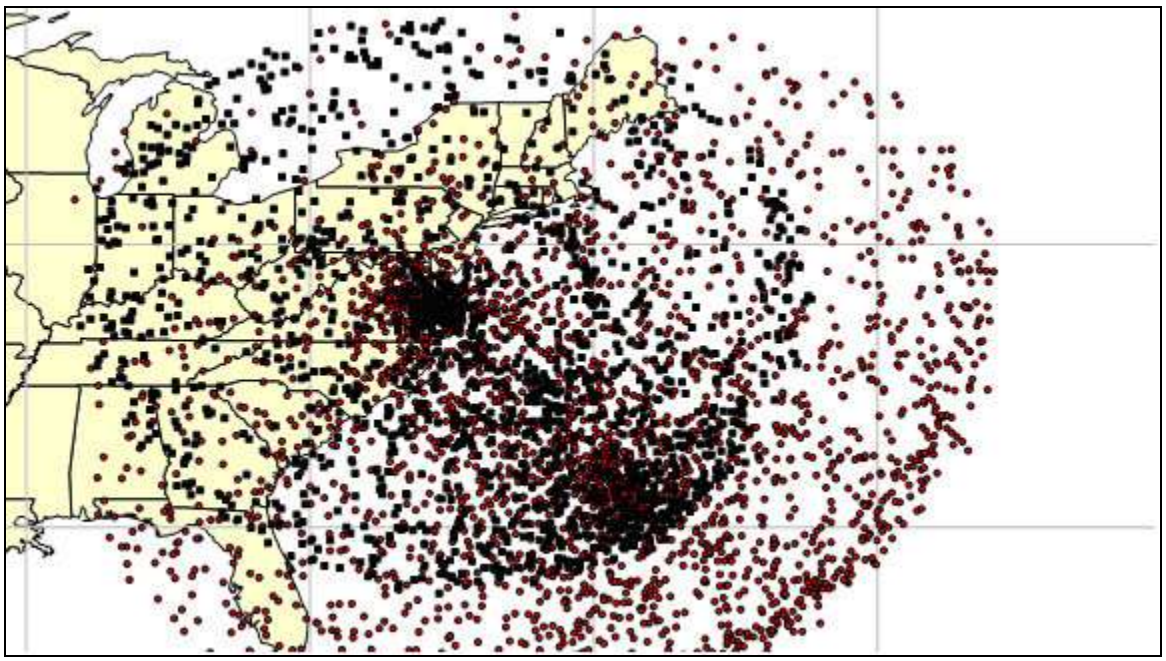

Figure 8-6. Intact Impact Points after a Malfunction Turn Initiated Soon after Rail Exit, at about 0.5s after Ignition) (Red used a 3 DOF and Black used a 6 DOF Analysis)

These results indicate that 3-DOF trajectory analyses tend to overestimate the size of the impact dispersion associated with a malfunction turn due to a constant thrust offset, at least for an unguided fin stabilized rocket. These results suggest that energy input to

angular momentum and aerodynamic forces other than drag play a significant role in determining the extent of an impact probability distribution and may be particularly important in predicting the probability of impact due to an early malfunction. These results suggest that a 3-DOF trajectory analysis may be adequate for modeling constant thrust offset malfunction trajectories, at least for unguided launch vehicles (i.e., sounding rockets) during the final stage of powered flight. However, these results also show that, very early in flight (e.g., before the final staging event), malfunction trajectories computed using a 3-DOF analysis may overestimate the dispersion and thus result in non-conservative probability of impact estimates. An artificially large impact probability distribution may or may not lead to conservative risk estimates, depending on the size and location of population centers at risk. For example, an artificially large impact probability distribution would produce a non-conservative risk estimate for a boat or aircraft located underneath the nominal trajectory, but a conservative risk estimate for a regional population located far from any point beneath the nominal trajectory (e.g., located outside a region bounded by the nominal impact distribution and the launch point). Thus, a general conclusion about the validity of 3-DOF trajectories analyses for use in a QRA is not possible. Therefore, the FAA will determine on a case-by-case basis if a 3-DOF trajectory analysis is valid for use in predicting malfunction turn trajectories as input to a QRA. Publicly available analyses have demonstrated that a full 6-DOF trajectory analysis is necessary to compute accurate nominal impact dispersions for sounding rockets with significant angular momentum. [49]

8.4.5 Random Attitude Turns

There is a failure mode that occurs upon occasion that almost instantaneously reorients the vehicle with a new reference. It happened on one occasion when the guidance computer shut down and then restarted. In such cases, the modeling requires a random attitude to be selected and the vehicle is flown along the new path until thrust termination. To perform a risk analysis, randomly compute the new attitude at the time of failure and repeat the impact prediction process thousands of times until there is a sufficient impact density to get a stable computation of impact probability and casualty expectation. The result of this analysis is a very broad impact area with possible impacts on cities and high-density populations. If it can be shown that this kind of failure can occur, the licensee should either establish a way to mitigate the failure or have a flight safety system that will limit the potentially very large cross-range dispersions.

9.0 POPULATION MODELING

9.1 Purpose

Population models are compilations of the spatial (and sometimes temporal) distribution of people (or other assets) for a geographic area of concern to the QRA. The purpose of a population model is to characterize quantitatively the exposure of people and assets of concern at an appropriate resolution with sufficient accuracy. Therefore, a population model should specify where people are located, the number of people in each location, how these people are sheltered, and the area occupied by population centers or other sensitive areas. A review of how to create a large region model is in [51]

There are five measures by which to assess the adequacy of a population model:

- Resolution: the spatial (geographic) and temporal scale,
- Completeness: inclusion of all population and assets that contribute to the risk assessment,
- Accuracy: adequacy of statistical methods to obtain data,
- Datedness: accounting for changes in population and assets, and
- Sheltering detail: number of categories and precision of structures included.

These all should be appropriate to the accuracy of other elements of the QRA.

9.2 Input Data Sources

Several products are publicly available to assist in developing a population model for QRA. These products may be divided into two groups:

- Datasets consisting of spatial data to be integrated into a model.
- Processing, Display, and GIS Applications used to integrate and analyze the datasets.

Overhead imagery, state or local development records, and US Census data are often useful sources of sheltering data. US Census data indicates where people live and often provides associated demographic data with which to distribute people among residential sheltering types. Local development records, such as the county tax assessor, often provide useful information on the nature of commercial buildings. Demographic data can be used to assign population distributions to different classes of structures (e.g., farmers, white-collar workers, and children) as a function of time-of-day (workday/evening). Reference [28] provides an example of how such data sources aided in developing a population model used in support of launches from the Eastern Range.

Information is available on potential sources of the baseline data necessary to construct a population model [52]. This handbook does not endorse any of the products described. The applicant is responsible for selecting the specific qualities and acquisition method (custom development or off-the-shelf product acquisition) of population modeling products that are most suitable for its risk analyses.

9.3 Minimum Modeling Features

Population models used as input for a QRA should characterize:

- Human population densities and distributions
- Structure locations, types, and portion of population sheltered
- Regional boundaries that separate areas with distinguishable population characteristics, or identify political boundaries, etc.
- Transportation routes and traffic descriptions

A simple population model might include a database of cells defined by a grid covering the land area subject to potential debris impacts. A common grid system used is a latitude-longitude grid where each grid cell covers an area defined by ranges of latitude and longitude. The location of a cell should be defined in terms of the coordinates (usually latitude and longitude) of the centroid of the populated area. The area of the population center is the land area used in the probability of impact calculation. For each cell the number of people and sheltering distribution should be specified over the time period subject to debris impacts. Population is then assumed to be uniformly distributed within each cell, and cell sizes should be selected to provide adequate resolution as discussed below (14 CFR C417.9(b)(9)).

Detailed population models distribute people into population centers (such as municipalities) defined by location, land area, and the distribution of people by shelter category. Population centers typically consist of small land areas, with more specific allocations of people close to a launch or landing site, and then larger and more generic as the location gets farther away. In the immediate launch area, a population center may consist of a single building or a single floor of a multi-story building. As the distance from the launch or landing site increases, the population centers may become complexes of several buildings or populated open spaces, subdivisions of cities or towns, entire cities or, at distant locations, counties, states, or even countries. Detailed population models typically include point receptors to account for high density population areas or other areas of special concern such as schools, hospitals, spectator areas, stadiums, cruise terminals, chemical or nuclear plants, etc.

A population model should account for all people present in the entire region that are significant to the calculation of total E_C. This includes population in transit (such as people in aircraft, waterborne vessels, and land vehicles) and people at recreational areas such as beaches, parks, and undeveloped land.

9.4 Modeling Discussion

A population model is produced by nine primary steps [52]:

1. Identify region and population parameters of interest.

2. Determine required population data resolution

3. Determine survey process and methods.

4. Develop or acquire baseline data sources.

5. Representation of data (use of GIS).

6. Ensuring documentation, traceability, and configuration management.

7. Data update and maintenance.

8. Modeling of shelters

9. Modeling of population transients

A discussion of the nine primary steps are found in the following sections.

Reference [53] provides detailed examples and guidelines based on the development of a population model used as input for QRAs performed in support of launches from the Eastern Range.

9.4.1 Identify Region and population parameters of Interest

The extent of the population model should include all credible impact locations from all credible failure modes. Since these failure trajectory and debris impact dispersions are often highly uncertain (especially before completing the QRA), it is often practical to begin by developing a basic population model for the entire region within maximum range of the vehicle's worst case IIP. An example of this would be the assessment process that a *winged RLV*-type vehicle would require before its flight. For example, if the vehicle is operating out of Mojave Airport, it is necessary to consider the area within the vehicle's IIP range (Kern and surrounding counties), including all credible failure modes.

9.4.2 Determine Required Population Data Resolution

In general, the size of the potential impact dispersions and the potential individual risks serve as a good guideline for the resolution of the population characteristics. For example, detailed population models are typically needed for the launch sites themselves and the immediate adjoining areas to adequately resolve individual risks, which are used to establish appropriate hazard areas where people should be evacuated or sheltered to ensure acceptable individual risk levels. However, for regions significantly downrange (e.g., Africa or Europe for U.S. launches to orbit), low resolution population models are sufficient because vehicle dispersions become much larger and individual risks are insignificant.

The degree of resolution required depends on the amount of dispersion possible from a nominal trajectory. This is illustrated in Figure 9-1, below. In Figure 9-1, a series of area-footprints within which the vehicle (or its debris) could impact are displayed along with population (data) centers of varying sizes. An adequate QRA should resolve debris impact dispersions so that the impact probability contours are smooth and continuous,

and the population model resolution should be comparable to the impact dispersions as shown in Figure 9-1.

A practical approach is to begin by acquiring data on the population density at a relatively low geographic resolution, such as the county level or equivalent. While this data alone may not be sufficient to provide final QRA results, it may facilitate identifying areas where flight is likely to meet risk criteria and where it is unlikely without extreme mitigation.

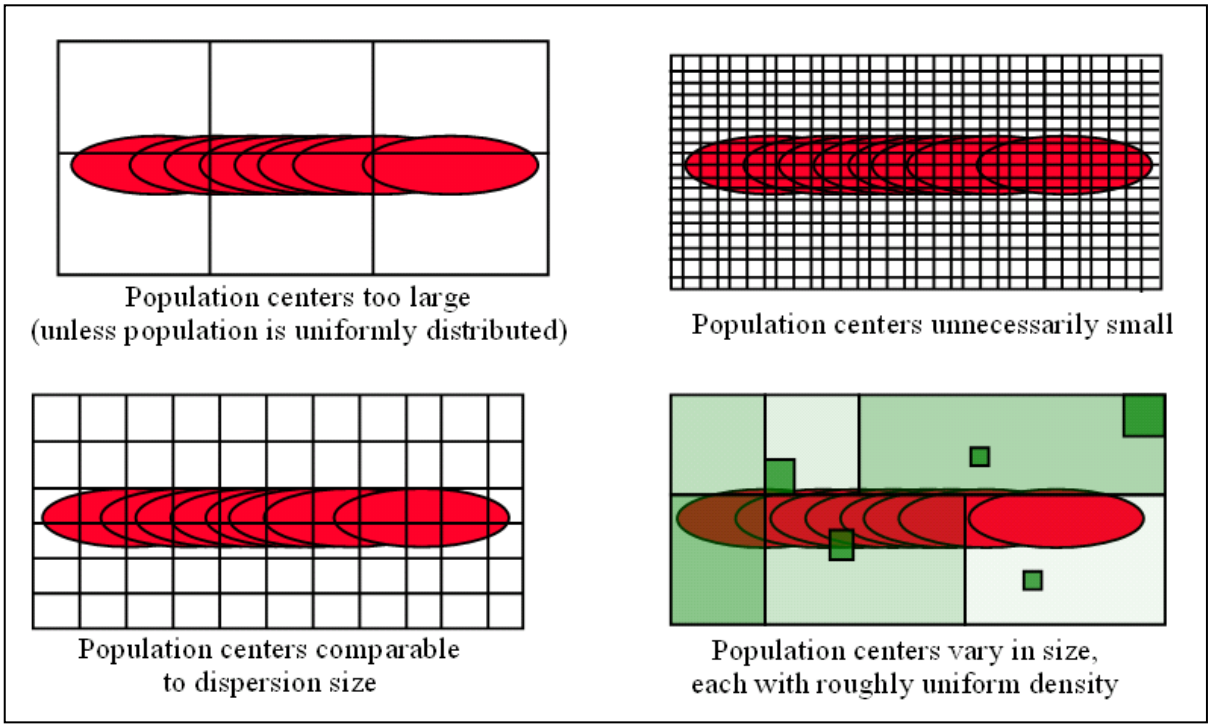

Figure 9-1. Population Data Resolution as a Function of Dispersion

9.4.3 Determine Survey Process and Methods

Most United States population models and associated applications available for acquisition use datasets derived from U.S. Census Bureau data. The US Census Bureau provides fairly detailed data on residential population characteristics. County tax assessors can be a good source of data on commercial structures. Specialized studies or ground surveys become necessary in assessing the population of a particularly high concern, based upon population density and the hazard level. This may include populated areas within the vicinity of a launch or landing site, military bases, and point receptors. For high-fidelity analysis, the means of acquiring this data include overhead imagery (identification of nighttime lighting, regional terrain, and ground activity) and physical ground surveys. Physical ground surveys to establish specific population and sheltering characteristics are necessary for high-fidelity models of areas exposed to relatively high risks; accordingly. Use this method to model the populations located at launch sites. You may require local data sources to consider the effect of specific events on the local population distribution and total in areas of interest so that you can account

for populations not normally resident, such as campers and potential crowds of observers in the vicinity of a launch or landing site.

9.4.4 Develop or Acquire Baseline Data Sources

Incorporate the survey data collected should be incorporated into a master database that serves as the baseline data source for a population model. Depending on the level of resolution required in the analysis, the baseline data source can include conditions characteristic for particular predetermined geographic areas such as districts, regions, divisions, counties, ZIP codes, point receptors. Clearly, the baseline data source should provide high resolution for areas of particularly high population density or flight risk. It is essential that the data sources taken together provide a complete picture of the population in the region of interest.

In most cases, the data sets include a spatial resolution level based on U.S. Census Bureau standards. The general hierarchy of this resolution is provided in Figure 9-2 (Geographic Resolution Levels for Census 2000 data). As indicated by Figure 9-2, the regional designations (Nation, Region, Division, etc.) are divided into a hierarchical structure to identify a scope or extent of the census area. The vertical axis of this figure represents the scale of the area units; Nation representing the largest unit of area, and Blocks representing the smallest unit of geographic resolution. The vectors indicate the dependency upon which the geographic resolution level is made; a Place is a sub-unit of a State. To further clarify this relationship, the vector indicating the sub-unit may place the sub-unit at a level along the scale lower than the next smaller area following along the main vector. This is demonstrated by the relationship between States, Counties, and Places: a Place is generally a smaller unit area than a County; however, its division is based on the State and is independent of the County's geographic borders. The vector-link relationships are not necessarily limited to those shown in Figure 9-2, but their general use-relationship and hierarchy is represented. While the figure depicts multiple types and geographic resolutions, it highlights the levels of particular consideration for launch QRAs. When circumstances require population data at the Census Block Group or individual Block level of detail, it may be useful to consider using other verifiable local sources including state and city governments. Local-source data may be better able to facilitate specialized or high detail modeling.

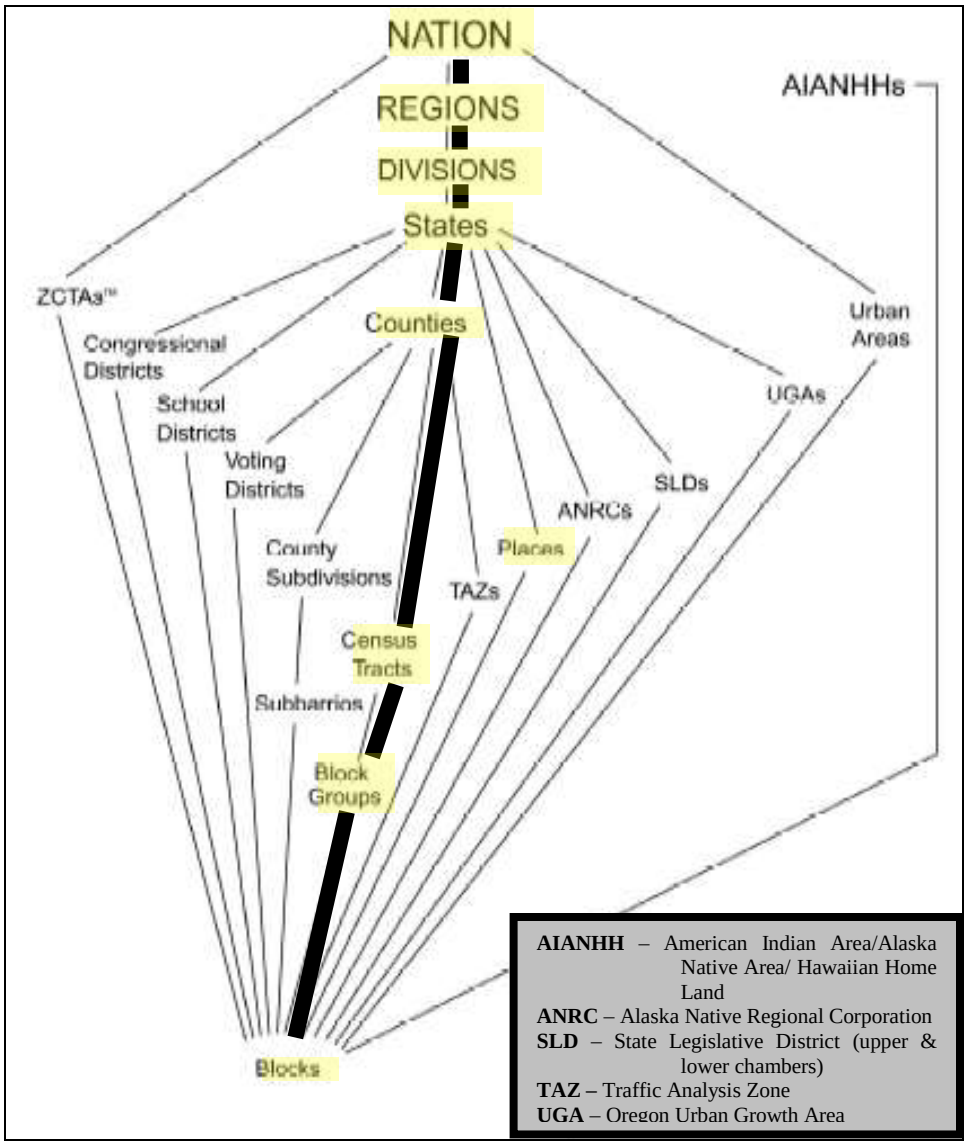

Figure 9-2. Geographic Resolution Levels for Census 2000 Data

Another approach to representing data at an appropriate resolution is using a grid-based system. This method divides the surface of the Earth into spherical grid coordinates proportionate to the minimal data resolution. This approach is used to map populations independent of political boundaries or region types. Several common datasets available are uniquely suited to this type of application and analysis.

For regions where the debris dispersion is large (outside the launch area), one approach is to develop population center data down to the smallest available size and then define open area population using the population density data with the population of the accounted for municipalities removed.

9.4.5 Representation of Data (Use of GIS)

A Geographic Information System (GIS) is typically used to present the baseline data related against a recognizable format, such as a regional map or other geographic reference. Combine the Census data and the presentation format or application so that the mutual interaction or overlay provides a useful understanding of the population in the region of concern. An example of addressing this requirement would be the assembly of a geographic representation application via a commercially-available GIS displaying the region of concern with an interface to the database containing the population information. The data should interact to meaningfully portray the population density, distribution, movement, or other datasets of concern.

9.4.6 Ensuring Documentation, Traceability, and Configuration Management

It is critical to maintain the documentation and traceability of all data used in a population model to

(1) to demonstrate due diligence if a mishap or accident occurs, and

(2) facilitate changes or updates using additional input data.

Implement a configuration management process for dataset updates to ensure that analysts use the best available data.

9.4.7 Data Update and Maintenance

Many population data services offer regular updates of their products. Data should be updated only as appropriate to meet the analysis accuracy required per mission. This does not mean that all the population modeling data should be updated for every mission – especially if there are multiple missions per year. However, an applicant needs to be aware of population growth that may affect the validity of previous analyses. Annual updates of data via annual population growth rates are usually sufficient for five to ten years. For near-launch areas (where the dispersion is smaller), the input data should be re-evaluated approximately every five years. For downrange areas, regenerating the population model on a decadal basis (following the U.S. Census) is appropriate.

9.4.8 Modeling of Shelters

Sheltering often has a significant effect on the casualty area from debris. For most missions, the effect of sheltering is to reduce risk. However, in some cases, the absence of sheltering does not constitute a conservative model. Specifically, people in a weak building or a building with windows are more vulnerable to serious injury from a nearby explosion than those outdoors. Also, a roof may protect the occupants inside from some debris impacts, but a severe debris impact may cause collapse of roof sections, leading to a larger casualty area.

Depending on the type of debris hazard, the sheltering categories may be different. For explosive debris, you need to characterize the wall type and window parameters. For inert debris, the roof type is the key consideration. Therefore, a comprehensive

population model should characterize a building type by roofing material (wood/tile, steel, etc.), overall construction type (e.g., reinforced concrete, wood frame), and window types and sizes. Certain vehicles (boats, recreational vehicles, cars) are sometimes specifically defined in a high-fidelity population model.

The number of sheltering categories depends on the level of fidelity of casualty area modeling employed. A high-fidelity population model may use a few dozen structure types, such as those used by the ER and WR [53]. A simple population model with sheltering may allocate people to only a few sheltering categories if the casualty models for people in structures are conservative, such as the four shelter classes below. This handbook provides simplified and conservative vulnerability models. Four different building classes (A, B, C, and D) have been defined here and in reference [2], that relate directly to the type of information typically available from community planning maps, Census data and similar sources:

Class A

- Mobile homes and trailers
- Temporary office trailers

Class B

- Single family dwellings
- Duplex and fourplex residential dwellings
- Small condominiums and townhouses
- Small apartment buildings

Class C

- Small retail commercial buildings (gas stations, stores, restaurants, strip malls)
- Small office and medical office buildings

Class D

- Manufacturing plants
- Warehouses
- Public buildings (large shopping malls, large office buildings, large apartment buildings, hotels, etc.)

9.4.9 Modeling of Population Transients

Transient population models characterize the fact that people may be in different places at different times of the day, week, or year. These changes can take the form of large-scale movement from one geographic region to another. Examples include seasonal agricultural workers, commuters from suburbs to city centers, and the influx or evacuation of personnel to the launch or landing facility (or other facilities) during major events. The change can also take the form of a change in the sheltering distribution. This is due to the differences between home and workplace construction practices, the

increased number of unsheltered people when the weather is conducive to outdoor activities, and other factors. In addition, consider the effects of launch-related evacuations or observers in a population model. Use transient population models to assure that the population model represents the hazarded population with sufficient accuracy.

10.0 DEBRIS DISPERSION MODELING

10.1 Purpose

The purpose of a debris dispersion analyses for a launch QRA is to compute impact probabilities for all fragments (or components) potentially produced by all debris generating events. Ultimately, a debris dispersion model should estimate the probability of impact for each debris fragment on each population center (and any other protected areas). Section 8.0 presents additional information relevant to modeling one of the primary sources of debris dispersion: vehicle trajectory dispersions.

10.2 Input Data Sources

A primary source of data to define a vehicle's state vector uncertainty are vehicle trajectory simulations performed to establish the vehicle's normal flight, as defined by the nominal trajectory and potential three-sigma trajectory dispersions about the nominal trajectory. Section 8.4.1 describes these trajectories. A vehicle trajectory analysis may also provide statistics on the state vector (versus flight time) giving the standard deviations in the state vector position and velocity components, and the correlations between the components. These provide the terms for a covariance matrix defining the state vector uncertainty statistics.

A malfunction turn analysis generally establishes the launch vehicle's turning capability in the event of a malfunction during flight, as described in Section 8.4.4. Estimate imparted velocities associated with a break-up as described in Section 10.4.6.

For some usually well defined fragments, the drag coefficient versus Mach number (along with the associated reference area) may be provided. Since a fragment's ballistic coefficient varies with Mach number, values are often subsonic because most of the fragment's fall is at subsonic speed. In some cases, ranges of ballistic coefficient values are provided for each fragment or fragment group. When drag characteristics are not provided, or the analyst wants to check the validity of the data, estimate ballistic coefficients based on a fragment shape, size and weight using standard formulas. For well defined fragments, the analyst can use standard methods to predict the drag coefficient versus Mach number (Section 6.4).

Wind data usually consists of wind statistics for a given location and given time of the year, or the measured wind taken before a launch. The wind statistics for time of year are usually provided for each month and for the entire year (annual), or they may be provided for seasons of the year. These data are generated from many wind measurements (hundreds or thousands) taken at the given location over many years. Use these time-of-year wind statistics to perform planning risk analyses (i.e., for predicting risks for a launch planned for a future time.

Common sources of wind data include:

- Range Commanders Council (RCC) Range Reference Atmosphere (RRA) data that is available for most of the test ranges.
- The Global Reference Atmospheric Model (GRAM) developed by NASA. This model can generate wind data for any given location on the Earth (latitude, longitude) using data from the Global Gridded Upper Atmosphere Statistics (GGUAS) database (distributed as the Global Upper Air Climatic Atlas) and the RCC RRA data.
- NASA developed statistical wind data.
- The Inter-Range Instrumentation Group (IRIG) wind statistics.
- The Air Force Environmental Technical Applications Center (AFETAC) wind database covering various launch ranges.
- Data published for a given range (both individual soundings and statistical) taken from historical wind measurements taken at the range using various measuring systems, such as Jimsphere, Rawinsonde, and Windsonde soundings, and Doppler Radar Profiler measurements. (These data are also used as part of the database for the other wind data sources.)
- National Oceanic and Atmospheric Administration (NOAA) data.

Uncertainty should also be addressed for statistical as well as measured winds. Sources of measured wind uncertainty include instrumentation error, the time elapsed between the wind measurement and the time of launch, and the spatial variation between where the wind is measured and where the launch vehicle flies. A statistical wind database often includes means and standard deviations of wind measurements or predictions for use in predicting uncertainty. You can also compute these statistics from raw data.

10.3 Minimum Modeling Features

A debris dispersion analysis should account for:

- Dispersions for each class of impacting debris produced by vehicle trajectories associated with normal and malfunctioning launch vehicle flight (Sections 10.4.7 and 10.4.8) (14 CFR A417.23(c)(3)),
- Drag corrected impact points for all debris classes (14 CFR A417.23(c)(3)),
- Dispersion for each debris class due to wind effects on the falling debris (Section 10.4.5),
- Dispersion for each debris class associated with aerodynamic lift and drag uncertainty (Section 10.4.4),
- Dispersion for each debris class due to potential imparted velocities produced by breakup (Section 10.4.6), and
- Any other sources of dispersion or uncertainty.

10.4 Modeling Discussion

10.4.1 Introduction

Debris impact points cannot be precisely predicted; there are too many uncertainties, some cannot be reduced even with an extremely high fidelity program. Consequently, part of the risk analysis process is developing debris dispersion models. For threats to people on the ground, the debris dispersion models are two-dimensional, e.g., a Cartesian coordinate system with latitude and longitude or, possibly, down range and cross range as the coordinates.

The significant sources of debris dispersion that a model needs to address here are (14 CFR 417.213(b)):

1. Vehicle guidance and performance uncertainty,
2. Vehicle malfunction turns off course,
3. Velocities imparted to fragments at vehicle breakup,
4. Uncertainty in the drag characteristics of a fragment,
5. Dispersion due to wind drift including the uncertainty in the wind profile,
6. Aerodynamic lift affects acting on a fragment, and
7. Free flight of inadvertently separated thrusting motors.

Other sources of dispersion could be considered, such as, uncertainty in the atmospheric density, variations in the impact altitude due to terrain, and uncertainties introduced by the earth gravitational model employed, just to name a few. However, these other sources are generally minor contributors to the overall dispersions. .

10.4.2 Mechanics of Debris Fall

The trajectory of a debris fragment is governed by the following equations demonstrated here in two dimensions, vertical (y) and horizontal (x). The forces on the fragment are gravitational (downward, parallel to the y-axis); drag (in the opposite direction of the velocity vector and lift (in a direction perpendicular to the velocity vector). In the two-dimensional model, lift is in the plane of the trajectory. In the more general model, lift can be in any direction perpendicular to the velocity vector and that direction can change with time. The density of the atmosphere is a function of the altitude, y. The gravitational constant g is also a function of altitude and, to a much lesser extent, latitude. The only exceptions to this model are cases where the fragment could have thrust (e.g., the fragment is a solid rocket motor segment and has residual burning of propellant).

$$\begin{Bmatrix}\ddot{x}\\ \ddot{y}\end{Bmatrix} = -\frac{g}{W}\begin{bmatrix}\cos\alpha & -\sin\alpha\\ \sin\alpha & \cos\alpha\end{bmatrix}\begin{Bmatrix}D\\ L\end{Bmatrix} - g\begin{Bmatrix}0\\ 1\end{Bmatrix}$$

$$\text{where } D = \frac{1}{2}\rho(\dot{x}^2+\dot{y}^2)C_D A,\ \ L = \frac{1}{2}\rho(\dot{x}^2+\dot{y}^2)C_L A$$

$$\text{and } \sin\alpha = \frac{\dot{y}}{(\dot{x}^2+\dot{y}^2)^{1/2}},\ \cos\alpha = \frac{\dot{x}}{(\dot{x}^2+\dot{y}^2)^{1/2}}$$

If there is no lift, L, the equation simplifies to

$$\begin{Bmatrix}\ddot{x}\\ \ddot{y}\end{Bmatrix} = -\frac{g\rho C_D A}{2W}\begin{Bmatrix}\cos\alpha\\ \sin\alpha\end{Bmatrix} - \begin{Bmatrix}0\\ g\end{Bmatrix} = -\frac{g\rho}{2\beta}\begin{Bmatrix}\cos\alpha\\ \sin\alpha\end{Bmatrix} - \begin{Bmatrix}0\\ g\end{Bmatrix},\ \text{where } \beta = \frac{W}{C_D A}$$

The ballistic coefficient β (with units of lb/ft^2) comes out of the equations of motion without lift. Its substitution into the equation above simplifies the numerical computation.

The initial conditions for the fragment are defined by position and velocity and time $(x, y, z, \dot{x}, \dot{y}, \dot{z}, t)$. This is also referred to as the *breakup state vector* or BUSV. The velocity components of the BUSV can also include an incremental velocity added and incremental position change due to explosion. The position and velocity can include incremental position changes and velocity changes due to vehicle motion due to a malfunction turn subsequent to the identification of the initial BUSV.

Figure 10-1 describes some of the basic mechanics in the fall of a debris fragment.

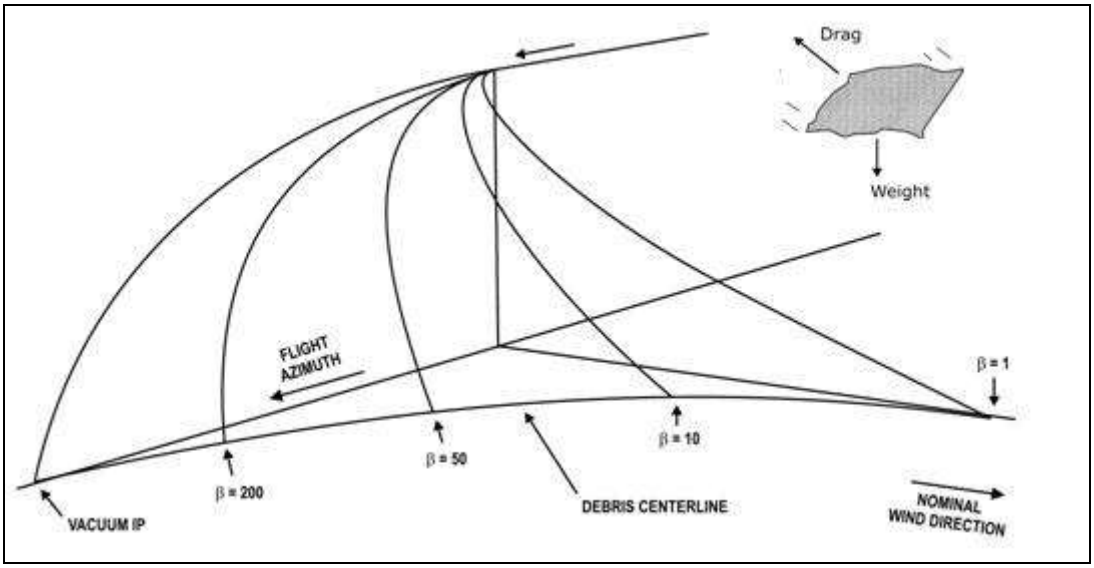

Figure 10-1. The Debris Centerline Showing the Strong Influences of Ballistic Coefficient (β) and Wind Direction and Velocity

The ballistic coefficient is indicative of the relative effects of aerodynamic drag and mass. Small dense objects will go farther than low dense objects with high drag. In addition, the wind is able to move the low density – high drag fragments off the initial trajectory and more into the direction of the wind. This is demonstrated in the debris centerline shown in Figure 10-1.

10.4.3 Discussion of Impact Dispersion Modeling

The above discussion treats the drag and lift coefficients as constants. In fact, they vary with Mach number. A fragment with an initial velocity that is supersonic (M>1) will often decelerate rapidly, with most of its fall at a subsonic speed eventually approaching terminal velocity. Subsonic drag coefficients are usually significantly less than supersonic drag coefficients and are relatively constant for all subsonic speeds. Thus assuming a constant subsonic CD (hence a constant β) is considered reasonable for most cases. The exceptions are dense stages with the roll axis aligned with the flight path and solid rockets motor segments that continue to burn and lose mass during the fall.

The dispersion relative to the debris centerline is the result of impulses and uncertainties from a number of sources. Figure 10-2 illustrates these. The distribution around the impact point in Figure 10-2 represents the impact uncertainty of debris due to the uncertainty sources. Only one debris impact uncertainty is shown, but actually there can be thousands of nominal impacts and associated impact uncertainty distributions. To simplify the modeling process, we grouped debris pieces into classes. For a typical expendable launch vehicle, there may be 50 or more classes, each containing debris pieces that have similar ballistic coefficients, explosive characteristics, or velocity perturbation characteristics. The process is to simulate the behavior and impact dispersions of each of these groups and then, in the final step, adjust the statistical results to account for the number of fragments in the group.

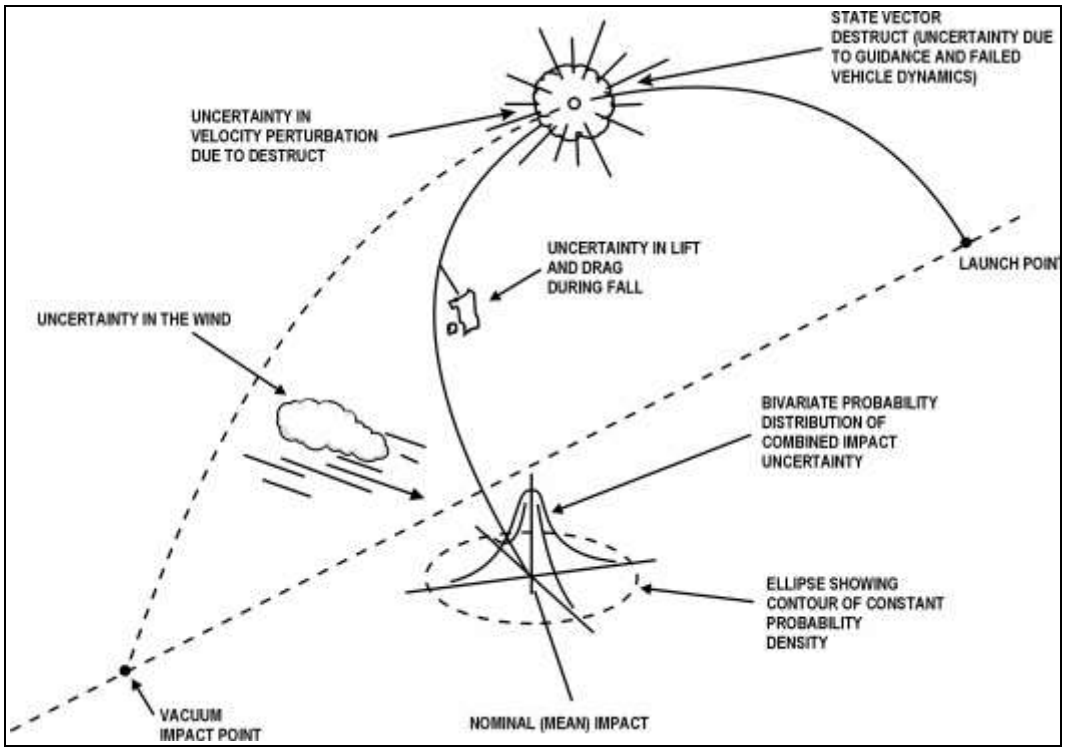

Figure 10-2. Contributions to the Impact Uncertainty Distribution of Debris

Impact distributions can be defined in various ways. One method is to fit the combined (multiple dispersion sources) dispersion statistics, or the distribution of random impact points (scatter plots from Monte Carlo simulations) that account for multiple dispersion sources, with closed form impact point distribution probability functions, such as bivariate normal distributions. A key advantage of this approach is that the closed form distributions are very computationally efficient. This expedites computing impact probabilities for a large library of locations (occupied buildings, groups of people in the open, populated regions, valuable assets, etc.) or for timely assessments of the risks during a launch countdown. The shortcoming of this method is that the distribution of impact points may have an irregular, skewed, or segmented pattern that may not be adequately represented with a closed form function. This often results from certain contributors to the impact dispersions that drive the irregularity of the impact point pattern, such as the dispersions resulting from vehicle malfunction turn behavior. Chapter 7 of the Supplement to [2] discusses develop dispersion statistics and impact distribution functions in more detail.

A second approach is to use random impact points that account for multiple sources of dispersion directly to define the impact distribution. In this case, perform debris risk calculations for each of the random impact points. Weight the resulting risk for each impact point by its relative probability and then add to get the risk given occurrence of the failure scenario. This provides an accurate representation of where a fragment can impact. However, this approach usually requires generating a very large number of impact points in order to adequately represent all of the possible impact locations for a fragment, and to get an accurate assessment of the risks. The probability of impact for a

specific population center, and the corresponding prediction of the risk, could be significantly under or over predicted because the sample of impact points within and around the location are over or under represented. For example, holes in the impact scatter of points could lead to a prediction of zero risk for a populated building where it is clear that credible deviations in the vehicle trajectory before breakup or in the fragment free fall trajectory could result in impacts on the building.

A third approach is a variation of the second. In this case, use the random impact points to generate histograms of the impact function over the region of potential impacts. This is normally done by segmenting the impact region into a two dimensional rectangular grid with an appropriately selected orthogonal grid line spacing. Then count the number of random impact points for each grid cell and compute the probability of impact in the cell. Assuming a uniform probability of impact over each cell, you can compute the probability of impact for any given location within the cell.

A fourth approach is a combination of the first and second approaches. Here treat some of the sources of impact uncertainty by generating random impact points, and treat others by generating closed form impact point uncertainty distributions about the random impact points. Then compute impact probabilities, and corresponding risks for each impact point, but now using the closed form impact distribution function to compute the impact probability for each location. Again weight the risks by the relative probabilities of occurrence of the random impact points. The advantage of this method is that the impact probability distributions about each impact point help to fill in the impact region so as to avoid under or over prediction of impact probabilities.

10.4.4 Aerodynamic Lift and Drag

Uncertainty in drag is captured in uncertainty in ballistic coefficient. The ballistic coefficient also has fragment weight and cross-sectional area, so that the effects of all three are accomplished at the same time. The uncertainty in ballistic coefficient is best modeled with a lognormal distribution (lognormal distributions generally fit products of numbers, as opposed to bivariate normal distributions, which generally fit sums of numbers).

$$\beta = \frac{W}{C_D A}$$

$$\ln \beta = \ln W - \ln C_D - \ln A$$

$$\sigma^2_{\ln \beta} = \sigma^2_{\ln W} + \sigma^2_{\ln C_D} + \sigma^2_{\ln A}$$

Thus, when developing the effect of drag uncertainty, one should also incorporate the weight and fragment area uncertainty. Estimate these from the analyst's perception of the uncertainties gained when developing the debris list.

The impact uncertainty due to ballistic coefficient uncertainty falls along the centerline shown in Figure 10-1. Compute the impact sensitivity by determining impact points from successive values of β around the reference (mean value) of β. Even though they are almost in line, the uncertainties in the impact distribution due to ballistic coefficient

uncertainty can eventually be expressed as a full covariance matrix in east-north impact coordinates. First compute the impact distribution along the centerline. Let η_β be the distance along the centerline relative to the nominal impact point for the particular β. Next, by using the perturbations of the impact point along the centerline, define the angle (δ) of the tangent to the centerline relative to east-north coordinates. The impact distance uncertainty for the uncertainty in β is log normally distributed. It should be approximated by a normal distribution. The bias and standard deviation are approximated by

$$\bar{\eta}_\beta = m e^{\frac{1}{2}\sigma^2_{\ln\beta}} \text{ and } \sigma_{\eta_\beta} = m(w^2 - w)^{1/2}$$

$$\text{where } m = e^{\mu_{\ln\alpha}} \text{ and } w = e^{\sigma^2_{\ln\beta}}$$

The final impact covariance matrix due to ballistic coefficient uncertainty is

$$\begin{bmatrix} \sigma^2_{E_\beta} & \sigma_{EN_\beta} \\ \sigma_{EN_\beta} & \sigma^2_{N_\beta} \end{bmatrix} = \sigma^2_{\eta_\beta} \begin{bmatrix} \cos\delta & -\sin\delta\cos\delta \\ -\cos\delta\sin\delta & \sin^2\delta \end{bmatrix}$$

10.4.4.1 Lift Effects

Falling debris, particularly fragments resembling flat plates, have the potential to generate lift as they fall. Lift effects on falling debris can only be approximated as it is very unlikely that a lift force on a fragment will maintain a fixed attitude, causing the fragment to tumble. For this reason, an analyst generally estimates the uncertainty in the lift-to-drag ratio of the fragment ($\sigma_{L/D}$), rather than attempting to characterize the coefficient of lift acting on it. The model generally applied assumes that the fragment lift vector is perpendicular to the flight path in the plane of the trajectory and remains oriented in a single direction. The net lift coefficient is assumed to be very small. Figure 10-3 illustrates this model. The debris impact distribution due to lift is assumed to be bivariate normal with an impact standard deviation equal to

$$\sigma_d = h \times \sigma_{L/D}.$$

where h is the initial altitude, as shown below.

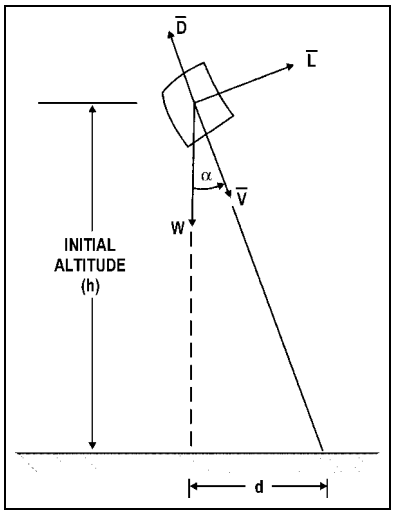

Figure 10-3. Simple L/D Impact Dispersion Model

Three object $\sigma_{L/D}$ values are generally considered.

$\sigma_{L/D} = 0.01$ for "boxy" objects

$\sigma_{L/D} = 0.03$ for objects neither flat or boxy

$\sigma_{L/D} = 0.05$ for tumbling flat objects

These values for $\sigma_{L/D}$ are based on an Apollo debris reentry lift study [54]. More recently, evaluation of the gathered debris from the *Columbia* showed that the lift effects fell within this range of $\sigma_{L/D}$. The altitudes for which the model is effective are between 0 and 60,000ft. Lift effects above 60,000 ft are ignored until the fragment falls to that altitude.

10.4.5 Wind

As noted in Figure 10-1, debris impact points can be very heavily influenced by the wind. This is particularly true of debris with small ballistic coefficients. Thus, the effect of the uncertainty in the wind should be modeled in order to develop appropriate impact distributions. For some vehicle-launch range combinations, the wind effect is the driving source of risk.

Winds are uncertain in direction and magnitude over the full range of altitude. In addition, the Cartesian components of wind velocity in east-north coordinates (v_E, v_N) are statistically correlated at each altitude and are also correlated with wind components at other altitudes. The matrix equation below represents all of the uncertainties in the east and north directions and all of the covariances between every wind component.

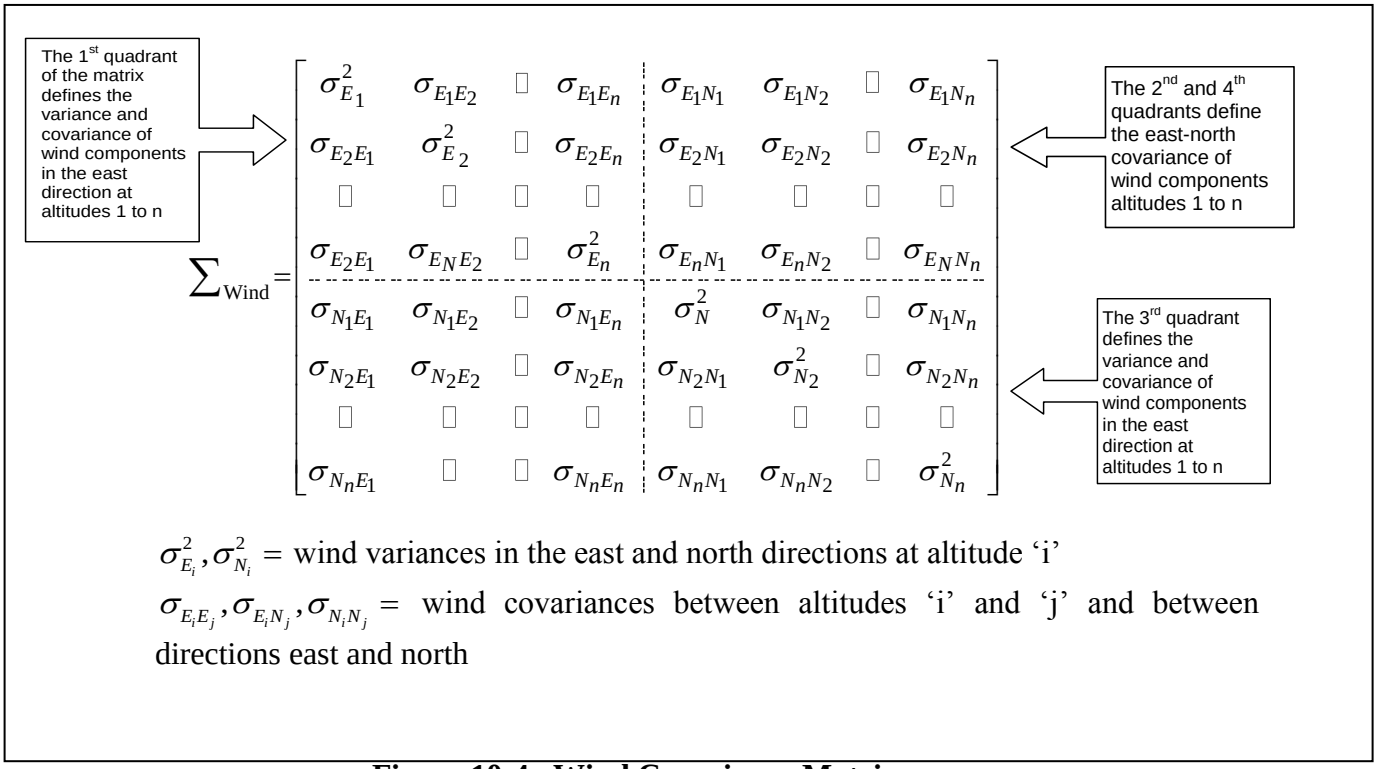

Figure 10-4. Wind Covariance Matrix

The order of rows and columns is as follows. Row 1 represents the uncertainty in the wind in the east direction at the 1st altitude. There are *n* altitudes and the first *n* rows and columns of the matrix are used to display the variances and covariance relating to wind components in the east direction to all other wind components. The $(n+1)^{th}$ row contains the 1st altitude for wind in the north direction. The dimension of the matrix is $2n \times 2n$.

Wind uncertainty results from wind variability with time and wind measurement uncertainties. For risk analyses computed for pre-launch planning, the wind covariance matrix should reflect the wind uncertainties over a period of time around the intended launch date, e.g., the wind uncertainty over a particular month. For risk analyses just before a launch, the wind covariance should reflect the uncertainty in the prediction and the time from wind measurement to the time of the launch. A detailed description of this process is beyond the current scope of this document. It will be included in a future version.

Compute debris impact dispersions by either extracting random wind profiles from the wind covariance matrix and wind mean vector, or by using a linear covariance propagation method. The first uses a decomposition of the covariance matrix and normally distributed statistically independent samples to generate random wind profiles that have the statistical properties defined by the wind covariance matrix and the associated mean wind vector.[16] The next step is to compute a drag corrected trajectory for the debris fragment or class to impact on the ground after falling through the atmosphere in the presence of wind, characterized by a wind profile. This is a Monte

[16] The general approach to generating random correlated vectors is described in *Concepts and Methods in Discrete event Digital Simulation* by George S. Fishman, John Wiley and Sons, 1973, pp 216-219.

Carlo process and is repeated until a sufficient number of impact points are available to determine an impact distribution.

The second method assumes that the piece of debris is always falling at terminal velocity. The time required to fall in an altitude band defined by h_i to h_{i+1} is called the dwell time. Compute the dwell time by dividing the differential altitude (h_i - h_{i+1}) by the average terminal velocity, V_T in that altitude range, where $V_T = \sqrt{\frac{2\beta}{\rho}}$ and ρ is the atmospheric density. Compute the atmospheric density more carefully by integrating over the altitude interval with Δt changing with altitude. Next, assume that the fragment moves horizontally exactly at the speed of the wind in the altitude interval during the time that it is falling through the altitude interval. The following linear equations express the total lateral motion due to wind from the altitude of release until impact on the ground.

$$\begin{bmatrix} E \\ N \end{bmatrix} = \begin{bmatrix} \Delta t_1 & \Delta t_2 & \ldots & \Delta t_N & 0 & 0 & \ldots & 0 \\ 0 & 0 & \ldots & 0 & \Delta t_1 & \Delta t_2 & \ldots & \Delta t_N \end{bmatrix} \begin{bmatrix} v_{E_1} \\ v_{E_2} \\ \vdots \\ v_{E_N} \\ v_{N_1} \\ v_{N_2} \\ \vdots \\ v_{N_N} \end{bmatrix}$$

$$\begin{bmatrix} E \\ N \end{bmatrix} = \begin{bmatrix} \Delta t & 0 \\ 0 & \Delta t \end{bmatrix} \begin{bmatrix} v_E \\ v_N \end{bmatrix}$$

The method overstates the lateral motion, particularly for pieces that have higher ballistic coefficient. However, the Δt terms in the equation are all proportional to the inverse of the square root of the ballistic coefficient, $1/\sqrt{\beta}$. Thus, as $\sqrt{\beta}$ increases, the effect of wind uncertainty decreases.

This method has been shown to work very well for low ballistic coefficients. As β increases, the percent error increases, but the magnitude of the dispersion due to the contribution of wind dispersion decreases.

The impact covariance matrix is expressed as the matrix product (in East, North coordinates)

$$\left[\Sigma_{Wind}^{EN}\right]_h = \begin{bmatrix} \sigma_E^2 & \sigma_{EN} \\ \sigma_{EN} & \sigma_N^2 \end{bmatrix} = \left[\begin{array}{c|c} \Delta t & 0 \\ 0 & \Delta t \end{array}\right]_h \left[\Sigma_{Wind}\right]_h \left[\begin{array}{c|c} \Delta t & 0 \\ 0 & \Delta t \end{array}\right]_h^T$$

10.4.6 Breakup Imparted Velocities

In-flight explosions or pressure vessel ruptures release energy with the potential to fracture the vehicle and disperse the resulting fragments. The amount of energy assumed to be involved in the fracture affects the number, size, and shape of the resulting fragments, and thus the casualty area. The remaining energy is assumed to impart velocity on the fragments, increasing their dispersal.

Imparted velocities associated with a breakup can be estimated using existing models based on physical principals or on velocity measurements obtained from launch vehicle accidents (usually by analyzing video recordings of an accident). Also, various models have been developed by launch vehicle vendors or the flight test ranges to predict velocities for fragments created by vehicle explosions and pressure vessel rupture. Use these models to predict imparted velocities or to check the reasonableness of velocities provided by vendors.

Fragment imparted velocities are usually defined based on a maximum expected velocity magnitude. If the velocity directions are equally likely, and if the components are assumed to be normally distributed in each of the three orthogonal directions, then the magnitude of the velocity (RSS) is represented by the Maxwell distribution shown in Figure 10-5.

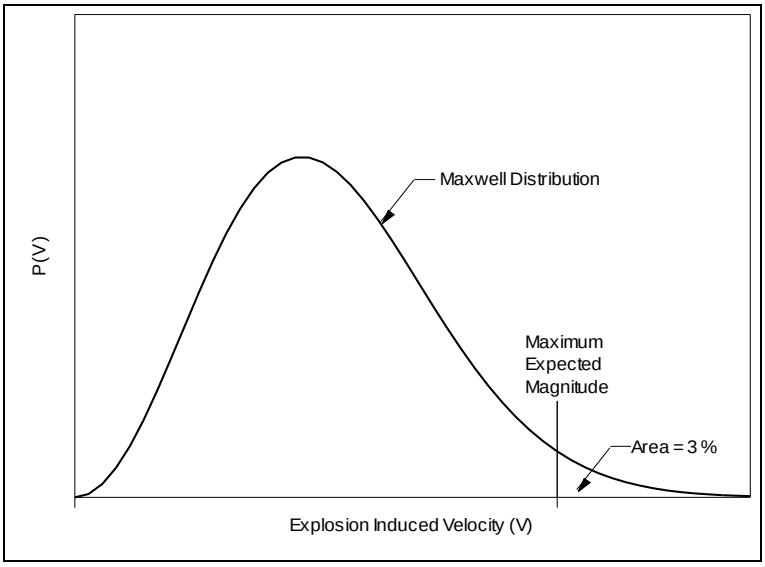

Figure 10-5. The Maxwell Distribution for Total Induced Velocity Perturbation

Figure 10-5 also shows how a maximum perturbation velocity can be interpreted as a level in the distribution for application in prediction of dispersions. A Monte Carlo process is suggested either within the debris footprint generation program or external to it. The process is as follows:

- Begin with a break-up state vector (BUSV).

- Assume a trivariate normal distribution for the velocity perturbation with equal standard deviations along all three axes and no correlation. (The Maxwellian distribution is the distribution of the imparted velocity magnitude resulting from the sampled velocity components.)
- In the Monte Carlo process, randomly select velocity perturbation magnitudes along each of three orthogonal directions and add these components to the vehicle breakup state vector

$$\vec{V}^{total}(t) = \vec{V}(t) + \Delta\vec{V}$$

- Compute a trajectory to the ground for each new state vector.
- Compile the impact points from the trajectories and compute a mean impact point and a covariance in an East-North coordinate system.

10.4.7 Impact Distributions Due to Uncertainty in Either Guidance or Vehicle Performance

Guidance and performance uncertainties are two entirely different sources that are frequently paired together because they express the impact distribution variability due to perfectly normal behavior. They are major contributors to the size of the impact distributions of jettisoned stages and other jettisoned equipment.

The guidance system reference can drift and cause the vehicle to fly to the right or to the left of the planned nominal trajectory. These dispersions are usually quite small but can be expressed in terms of miles later in the flight. Express the impact dispersions as a normal distribution cross-range. There is no measurable down-range effect from guidance uncertainty.

Rocket engines can vary in thrust and in efficiency (specific impulse, i.e., I_{sp}). These effects will cause the vehicle to gain speed faster and possibly go farther and vice versa. The dispersion effect is almost totally in an up range or down range direction, along the intended flight path and perpendicular to the dispersion due to guidance. The effect is basically getting to a point (orbital insertion) earlier or later; and, from a risk analysis perspective, that has little effect on the E_C. The problem is, that to be consistent with the impact dispersions of the jettisoned stages and other jettisoned equipment, the downrange uncertainties should be carried along so that there are no inconsistencies at the staging points.

Account for these sources of dispersion, as well as dispersions due to malfunction trajectories, using the vehicle trajectory modeling, which is discussed in Section 8.4.

10.4.8 Malfunction Turns

Malfunction turns are one of the most difficult problems to solve in performing a launch QRA because the malfunction behavior of a space vehicle is often difficult to predict. Also, the malfunction behavior is likely to be observed and aborted – thus requiring modeling of the intervention. The best approach is to work with the vehicle developer to simulate the failure modes and the subsequent behavior. This requires a detailed study of

the possible failure modes, the probability of their occurrence, the time of their occurrence and the subsequent behavior.

10.4.8.1 Full Simulation Approach

A 6-DOF flight dynamics model can incorporate the simulation of the guidance and control response into the behavior of the vehicle as it goes into the malfunction, thus more realistically simulating the behavior of a vehicle that may be making attempts to recover. The simulation approach requires:

- Aerodynamic and inertial modeling of the vehicle;
- Modeling of the vehicle control system response (if any) to the different failure modes;
- Many simulations for each of many flight times (into the thousands) that cover all of the abort modes and reasonably cover the range of each of the abort mode vehicle responses;
- Simulation of the abort response when you measure the vehicle behavior against an abort criterion (e.g., an instantaneous IIP crosses a pre-established line).

The simulation approach should produce many accidents that cover the full range of the presumed possible accidents. Each of these accidents, which have a finite probability of occurrence, may contribute to the total risk at each population center.

The simulation of abort response should consider the following:

- Simulation of what the Safety Officer sees, such as a vacuum impact prediction (VIIP).
- The VIIP is compared with an abort (or destruct) line[17] on a map and the vehicle progress (in the simulation) is stopped when the VIIP crosses the line.

Other possible abort criteria that may need to be simulated are:

- Observed obviously erratic behavior;
- The intact vehicle is falling and, if destructible, the vehicle should be broken up before impact to minimize explosive potential;
- The vehicle is erratic and tracking is diminished and, if action is not taken, communication with the vehicle may be lost.

If a vehicle has an autonomous abort system for a portion of flight, model the dispersion until abort. The dispersion will likely be smaller without a human in the loop and you may model the dispersion as an additional velocity uncertainty off the nominal trajectory.

[17] The abort line is usually a stand-off from an Impact Limit Line (ILL). The ILL represents a line on the ground behind which people are protected. The abort line is usually developed from a series of simulated failure conditions that point the trajectory toward the ILL in different ways with a prediction of impact probability of debris on a person on the ILL as the VIIP advances toward the ILL. The VIIP point is associated with a maximum allowable impact probability (e.g., 1E-6 or some other standard) on individuals standing on the ILL. The abort line is constructed from a conservative locus of points developed from these VIIP points.

10.4.8.2 Simulation Using Malfunction Turn Data

Use malfunction turn data in a risk analysis when it is not possible to perform genuine 6-DOF simulations of malfunction trajectories. The malfunction turns are often a reasonable way to simulate failure response. Assume that malfunction turns occur in a plane that contains the velocity vector at the start of the turn. Assume the angle of the plane about the velocity vector to be random (usually uniformly distributed from 0 to 360° relative to the pitch plane of the vehicle). Sample the gimbal (thrust offset) angle randomly between 0° and the maximum gimbal angle (equated to maximum thrust offset). Simulate the path of the vehicle into the turn using a 3-DOF simulation of a turn (preferably with aerodynamic forces). Figure 8-2 and Figure 8-3 are samples of typical malfunction turn data. Figure 8-2 shows the change of velocity vs. time for various gimbal angles. Figure 8-3 shows the change of direction of the velocity vector vs. time for various gimbal angles.

The time of vehicle break-up into the turn is often modeled as a probability distribution derived by the vehicle developer. Break-up will always occur if the q-α at any point in the turn exceeds the design q-α. (q is dynamic pressure and α is angle of attack.)

Each of the two methods described here, full simulation and malfunction turn data, produce footprints for each state vector. If the footprints are smaller than the spacing between them, a map of the isopleths of constant risk density in the region will have artificial islands and peninsulas. If the spacing is too wide, narrow it by adding more state vectors (more failure times and more orientations of tumble) and thus more runs. This requires more computer time. An adequate QRA should resolve malfunction state vector dispersions to produce smooth and continuous impact probability contours. (14 CFR §417.23 (c)(1)(iii))

Some methods attempt to group impact dispersions (footprints) to create larger impact dispersions. Do this with caution because the dispersions have different probabilities of occurrence and they may not be coming from the same failure mode.

In general, the detailed simulation or malfunction turn approaches are more often applied in the general launch area and corridor methods (Section 4.9.4) may be an acceptable Tier 1 approach for estimating the downrange risks.

10.4.9 Simulation of the Flight Safety System

The flight termination and abort criteria both influence the risk posed to the public and are often adjusted to ensure acceptable risks. Therefore, there is an iterative interplay between the QRA output and the flight termination criteria. An adequate QRA should account for the abort and flight termination criteria. Optimize flight termination and abort criteria by balancing the risk given a failure and termination against the risk given a failure and no flight termination or abort.

Use malfunction turn data (Section 10.4.8) during the development of the abort criteria. The objective is to determine the fastest rate that the VIIP can move cross range from the planned trajectory plane. For a very simple system, stop the VIIP when it reaches the

impact limit line. Then, back it off from this line to allow for uncertainty in the dispersions of debris and system delays. Simulate this many times with each backed off VIIP forming one point with which to develop a line that connects the most conservative VIIPs.

In the QRA, evaluate each malfunction trajectory for violation of the abort criteria. To do this, the analysis should advance incrementally through the turn and compute the VIIP. If the VIIP violates abort criteria, stop the progress and then continue Δt seconds to account for system delays. The stopping point becomes the origin of the state vector for the debris footprint associated with the vehicle break-up point. Continue the process over the entire range of failure times, tumble plane orientations, and gimbal (thrust offset) angles. Like the simulation approach, the malfunction turn approach will produce many pseudo accidents that cover the full range of all of the presumed possible accidents. Each of these accidents, which have their own probability of occurrence, will have a contribution to the total E_C on each population center and the sum of the population center E_Cs will be the total E_C associated with malfunction turns.

If an autonomous abort system is used for any portion of the flight, the turn curves need only to be used to the point in the rotation where the vehicle attitude, for instance, reaches the rotation limit in the abort system. If the system is hybrid, i.e., man in the loop early and autonomous from a hand-over time on, the simulations should acknowledge both methods of control appropriately.

10.4.10 Computation of Net Dispersion

Total impact covariance matrix (expressed in an east (E) - north (N) coordinate system)

$$\Sigma_{Total} = \Sigma_{\beta} + \Sigma_{\Delta v} + \Sigma_{state\,vector} + \Sigma_{wind} + \Sigma_{lift/drag}$$

Note that the $\Sigma_{state\ vector}$ in the equation represents the contributions of performance, guidance, and malfunction turn including the intervention of the Flight Safety System. Normally, these sources are separated.

11.0 UNCERTAINTY AND BIAS IN RISK PREDICTION

11.1 Discussion of Uncertainty Types and Sources

Launch debris risk analysis is a process that is inherently dependant on using models and model parameters to simulate the consequences of vehicle failures and the resulting hazardous events because sufficient empirical data will never exist with which to evaluate the rare events involved. The models are approximations at various levels of sophistication and the model parameters are frequently difficult to quantify very accurately. Consequently, the results of these studies can have considerable uncertainty.

There have been a few comparisons of launch risk analysis models (Tier 1 and 2) that have actually shown differences in risk predictions of up to three orders of magnitude. Comparisons between launch debris risk analysis tools used by the Air Force Eastern and Western Ranges applied to a typical commercial ELV launch using common input data found about a factor of two difference in total E_C for the public, and only about a 20% difference when random attitude risk contributions where excluded [55]. Thus, even among the most proven Tier 2 models there can be differences while still using common input data.

Of course, there is often substantial uncertainty associated with critical input data, such as the probability of failure for new vehicles especially or the debris generated by a particular failure. Thus, results from risk analysis programs have uncertainty due to both the modeling approach and the model input data. This section discusses these uncertainties for determining casualty expectation, E_C.

We define uncertainties in two general categories: aleatory and epistemic

1. *Aleatory uncertainty*, or the uncontrollable variability (or randomness) of events, is typified by the distribution of debris impacts from one accident to another because the same measurable initial conditions will not produce exactly the same consequences in sequential trials. In launch risk analysis models, the effect of aleatory uncertainty is most frequently averaged in the process of determining impact probability or E_C.

2. *Epistemic uncertainty*, i.e., the uncertainty in the model and the model parameters. The model and parameters may contain inadequacies that introduce model or systematic uncertainty. If epistemic uncertainty is accounted for, then the computed E_C is no longer a point value but represented by a probability distribution. Epistemic (or model) uncertainty should account for any bias or conservatism in the model.

Figure 4-6 provides an example of the aleatory uncertainty. The four frames in the figure represent four different randomly selected debris impact samples from a Space Shuttle breakup based on the same failure time and the same set of debris impact dispersion distributions. Each of these four scatter plots, with the distinct fragment impact points overlaid on the same set of people or structures, will produce different probabilities of exactly one, two, three, etc., casualties. This variability of results is averaged in the E_C calculation.

The first step in the uncertainty analysis is to identify key parameters and program sub-models that dominate the uncertainty. Typically, the most dominant parameters are:

1. Vehicle failure probability,
2. The debris generated in the breakup,
3. The debris impact distributions,
4. The yield from the impact of explosive debris,
5. The probability of a casualty given a hit by inert debris and the associated casualty area,
6. The probability of a casualty given exposure to the shockwave from exploding debris,
7. The probability of a casualty and the casualty area given inert debris impact on a roof that is sheltering a person,
8. The probability of a casualty given that the shockwave from exploding debris impacts a building that is sheltering a person, and
9. The number of people in each population center/area.

One option for uncertainty model architecture is the Monte Carlo method: random sampling of parameter uncertainties and numerous model executions. Another less accurate method is to apply factors/multipliers to parameters that dominate the E_C computation.

The failure probability directly affects the uncertainty in an E_C estimate. The failure probability uncertainty model is better if it accounts for uncertainty levels separately in each of the stages or flight phases and for different failure modes because that can better identify the failure scenario driving the risk or uncertainty in the risk. Uncertainty in the probability of failure distributions over time and vehicle response modes is also a major issue. Uncertainty in the conditional probabilities at various event tree nodes may be analyzed using techniques published in [13].

The debris list means and uncertainties are very difficult to model. Debris lists are difficult to develop with confidence because there are so little empirical data.

The impact distributions have uncertainties due to the appropriateness of the distributions and shifts in the midpoints of the distributions because of the difficulty in modeling vehicle behaviors prior to breakup, and changes in the size of the distribution for the same reason.

Some of these sources of uncertainty can be modeled by uncertainty factors. However, using uncertainty factors is a top down approach that has the potential of leading to an

overstatement of the effect of the uncertainty in those parameters, since many of the parameters may affect only part of the final answer.

An uncertainty analysis produces a probability distribution for E_C. The resulting E_C probability distribution typically tends to look somewhat like a normal distribution on a log-scale, i.e., a lognormal distribution, because of the Central Limit theorem [56]. Use the distribution to compute the average E_C or provide corresponding cumulative values at confidence/probability levels such as 90% or 95%. The decision maker can use these results to inform decisions regarding risk acceptability, although no formal guidelines exist on this subject to date. The RCC Risk Committee has accepted a task to investigate uncertainty methods and recommend appropriate ways to account for uncertainty in a launch risk analysis. Results of this task will be added to future versions of this handbook.

11.2 Proper Treatment of Uncertainty in Launch/Re-entry QRA

The FAA has consistently intended that the risk criteria for commercial launch[18] and reentry[19] vehicles be compared to the "best estimate" of individual and collective risks. The best estimate of the risks posed by a launch/re-entry should either (1) quantify aleatory and epistemic uncertainties to the extent necessary to understand the level of uncertainty in the final risk predictions, or (2) use only conventional approaches and demonstrably conservative assumptions to the extent necessary to conclusively demonstrate acceptable risk levels. Using such best estimates of individual and collective risk is consistent with the current practice at the Federal ranges and the larger range safety community.[20] In the past, the best estimates of launch/re-entry risks did not include a thorough treatment of aleatory or epistemic uncertainties, instead relying on conservative assumptions about input data and conservatism built into conventional approaches to demonstrate acceptable risk levels based on "best," but essentially deterministic, estimates.

Using best estimates produced by QRA appears reasonable and rational by comparison with the Nuclear Regulatory Commission (NRC) approach: "the Commission has adopted the use of mean estimates for purposes of implementing the quantitative objectives of this safety goal policy."[58] This approach recognizes, just as the NRC did, that uncertainties are inherent in risk based decision-making. Thus, the current approach taken by the FAA for risk limits and uncertainty is the same as the approach initially

[18] 14 CFR 415.35a: "Acceptable flight risk through orbital insertion for an orbital launch vehicle, and through impact for a suborbital launch vehicle, is measured in terms of the expected average number of casualties (Ec) to the collective members of the public exposed to debris hazards from any one launch." See Federal Register, Vol. 64, No. 76, April 21, 1999, page 19618. See also [57] at 14 CFR 417.107(b).

[19] 14 CFR 431.35b: "Acceptable risk for a proposed mission is measured in terms of the expected average number of casualties (Ec)." See [11]

[20] AFSPCMAN 91-710 paragraph A4.3.5: "The risk associated with the total flight to all members of the general public, excluding persons in waterborne vessels and aircraft, shall not exceed an expected average number of 0.00003 casualties (Ec < 30 x 10-6) from impacting inert and explosive debris, Ec < 30 x 10-6 for toxic release (exposure to rocket propellant effluent), and Ec < 30 x 10-6 for far field blast overpressure." See also RCC 321-07 Supplement section 5.1.3.

taken by the NRC some 20 years ago. For example, it appears that NRC references to "mean estimates" equate to the "best estimates" used by range safety, which presently do not always completely account for all sources of uncertainty; the NRC stated that the "use of mean estimates does not, however, resolve the need to quantify (to the extent reasonable) and understand those important uncertainties involved in…risk predictions." The FAA recognizes that the following statements regarding uncertainties, which were published with the NRC safety goals, also apply to risk management for launch/re-entry activities:

- "Uncertainties are not caused by use of quantitative methodology in decision-making but are merely highlighted through the use of the quantification process."
- "A number of uncertainties arise because of a direct lack of severe accident experience or knowledge of accident phenomenology along with data related to probability distributions."
- "Through the use of quantitative techniques important uncertainties have been and continue to be brought into better focus and may even be reduced compared to those that would remain with sole reliance on deterministic decision-making."
- "For this reason, sensitivity studies should be performed to determine those uncertainties most important to the probabilistic estimates. The results of sensitivity studies should be displayed showing, for example, the range of variation together with the underlying science or engineering assumptions that dominate this variation."
- "Depending on the decision needs, the probabilistic results should also be reasonably balanced and supported through the use of deterministic arguments. In this way, judgments can be made by the decision-maker about the degree of confidence to be given to these estimates and assumptions. This is a key part of the process of determining the degree of conservatism that may be warranted for particular decisions. This defense-in-depth approach is expected to continue to ensure the protection of public health and safety."

Since the primary purpose of a QRA is to demonstrate acceptable collective and individual risk levels posed by debris hazards associated with licensed launch, reentry and experimental permit activities, valid risk analyses should be based on the best available information and reasonably conservative assumptions made in each area where there are significant uncertainties or no conventional approach. Thus, a Tier 1 approach that employs only conventional approaches and demonstrably conservative assumptions may be adequate to satisfy the primary purpose of a QRA without including a formal treatment of uncertainty. However, the purposes of a QRA for launch/re-entry go beyond the demonstration of acceptable risk levels, to include providing a basis for well informed safety decisions by identifying the dominant sources of public risks and potential mitigations, and informing the MPL determination. Thus, some sensitivity or uncertainty analyses are often necessary. For example, quantify uncertainty for each element of any Tier 2 risk analysis where an unconventional approach is used, or where the underlying assumptions or input data are not demonstrably conservative. The following guidelines are intended to assist applicants in preparing QRAs that properly treat uncertainties that may affect collective and individual risk estimates.

11.3 Uncertainty Analysis Using Factors to Represent the Effects of Parameter Uncertainties

In 2004-5, the FAA and the USAF sponsored an effort involving epistemic uncertainty (i.e., model and model parameter uncertainty). The objective was to compute the risks to the public of a particular ELV on a high inclination trajectory over-flying land. Two parallel risk analyses were performed: one using the footprint method and the second using a corridor method. Using the same basic input data (no uncertainties), both approaches produced almost the same E_C. This indicated that the uncertainty in the model for this type of problem is probably quite small. In fact, the modeling for this case is fairly straight forward.

However, some of the parameters being used by the models in the study were quite uncertain (failure rate, debris list/casualty area, debris survivability). Although the basic model appeared to have a small uncertainty, there were model parameters that were uncertain and would affect the accuracy of the final computed E_C.

The uncertainty analysis was performed using factors of uncertainty, where each factor was a multiplier of the computed E_C, but represented the direct effect of variation of a selected parameter on the value of E_C. The equation can be written as follows:

$$E_C = f_1 \times f_2 \times ... E_C(\textit{computed without uncert.}) = \left(\prod_1^n f_i \right) \times E_C(\textit{computed without uncert.})$$

Taking the logarithm of both sides,

$$\ln(E_C) = \ln f_1 + \ln f_2 + \ln f_3 + ... + \ln\left(E_C(\textit{comp. without uncert.})\right)$$

$$\ln\left(\frac{E_C}{E_C(\textit{comp. without uncert.})} \right) = \sum_i^n \ln f_i$$

E_C*(comp. without uncert.)* is a point estimate of E_C and has no uncertainty. Thus, the dimensionless uncertainty in E_C is expressed by $\dfrac{E_C}{E_C(\textit{comp. without uncert.})}$ and the natural logarithm of this expression is the sum of the logarithms of the factors, f_i.

If the factors are statistically independent and the logarithms of the factors have similar standard deviations, by the Central Limit Theorem [56], the distribution of the sums of the distributions will tend toward a normal distribution. Thus the distribution of $\dfrac{E_C}{E_C(\textit{comp. without uncert.})}$ will tend toward being a lognormal distribution.

As previously mentioned, Tier 1 models often intentionally include biases to ensure conservative risk estimates. Consequently, by intent, a well-designed risk analysis will be more likely to overestimate than underestimate risk, and so the f_i's do not always have a mean value of one. When performing an uncertainty analysis, it is important to identify

the biases so that the uncertainties are about the true mean rather than about the biased computed mean. Quantifying the biases is quite difficult and often involves comparisons to empirical data or high-fidelity model results. However, ignoring sub-model biases due to intentional conservatism will cause the accompanying uncertainty analysis to overestimate the higher range of the uncertainty distribution.

Table 11-1 summarizes the dominant uncertainty sources that were used in the over-flight risk analysis. As shown, the mean values of the uncertainty factors are not necessarily equal to 1.0. The means of the factors take into account the estimated biases that were in the factors for various reasons. For instance, we performed the analysis without considering demise of debris during reentry. According to one source who had evaluated many satellite reentries, only about 54% of the debris would survive to the ground. We used this observation to estimate the bias due to ignoring demise in this study.

Table 11-1. Estimated Model Input Uncertainties in the ELV Over-Flight Risk Study

Uncertainty Source, f_i	Est. mean of the factor, f_i (the bias)	Standard Dev. of the factor, f_i	Comment
1 Failure rate	1.024	0.445	The standard deviation was based on the results of several estimates from different sources for the failure probability of the vehicle during the over-flight period.
2 Casualty area due to estimate of number of fragments	1.3 (the provided debris list was probably a low estimate)	0.4 (estimated)	The bias factor and the standard deviation are estimates based on testing the impact on E_C of having more fragments (consistent with observations of Columbia).
3 Effect of demise on casualty area	0.54 (estimated)	0.2 (estimated)	The bias factor and standard deviation are estimates based on empirical observations (*Columbia* and Aerospace Corp.).
4 Sheltering model uncertainty	1 (estimated)	0.2 (estimated)	No information was available on the uncertainty associated with the sheltering model, but it cannot be ignored. The 0.2 standard deviation was probably much too small.
The adjusted factor on E_C, considering the four factors, f_i (i = 1 to 4)	0.72	0.66	The values, multiplied by the computed E_C, will provide the new mean (adjusted for the bias) & the new standard deviation of E_C.

As mentioned above, the resulting uncertainty distribution for E_C tends to be lognormal, i.e., normal in log space, such that there appears to be skewed distribution as shown in Figure 11-1[21] in standard space. The corresponding cumulative probability distribution is shown in Figure 11-2. It is notable that even when the basic model is assumed to have a small uncertainty, the uncertainties in the model parameters still produce a significant uncertainty in the final estimate of expected average E_C.

[21] The mean results in this sample problem were scaled relative to the actual results in the FAA/USAF study.

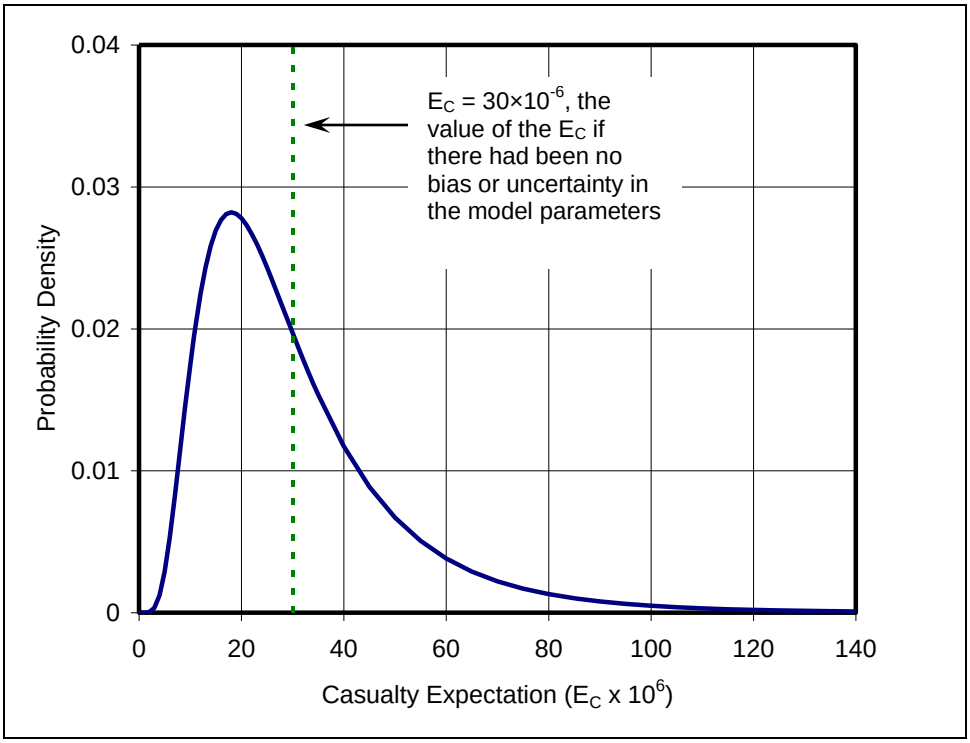

Figure 11-1. Typical Uncertainty Distribution for EC Based on Uncertainties and Biases in the Model Parameters

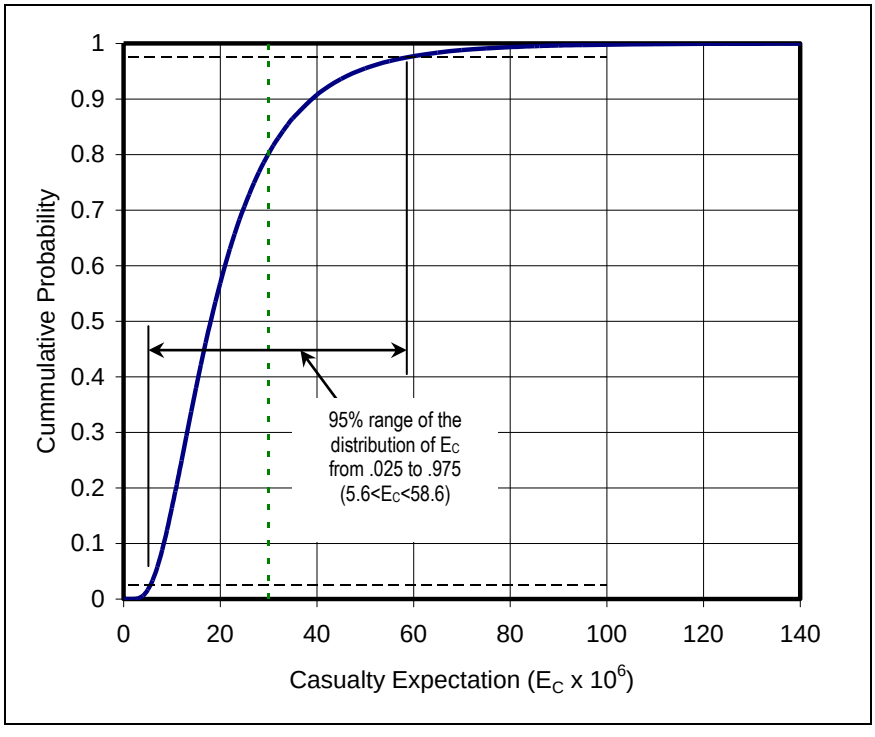

Figure 11-2. Typical Cumulative Probability Distribution for E_C Based on Uncertainties and Biases in the Model Parameters

Another acceptable approach to quantify uncertainty due to input data uncertainties uses the Monte Carlo technique. For example, you can define distributions to characterize feasible values for various input parameters (failure probability, winds, trajectories, break-up debris, etc.) and you can run the risk analysis model numerous times based on sampled input data to produce a distribution of feasible values of the E_C. The Monte Carlo technique is ideally suited for uncertainty analyses because it accounts for the potential non-linear effects of various combinations of input parameter perturbations. An appropriate uncertainty analysis using the Monte Carlo technique will also account for correlations between input parameters.

Up to this point, the discussion has focused on the effect of parameter bias and uncertainty for the case where there is little or no uncertainty in the fundamental model used to compute the E_C. Suppose that for this case, the computed E_C (which was found to be 30×10^{-6}) was actually the average obtained from several different models using the same parameter data. If the results of these calculations actually varied, but the average was 30×10^{-6}, then the variation of E_C around that average is the standard deviation of the uncertainty in the result due to model uncertainty. Assume that the variation in the results of the several models is represented by a standard deviation in the E_C of 20×10^{-6}. This uncertainty can now be combined with the effect from the parameter uncertainty effects on E_C and the resulting new probability density function and the cumulative distribution function are shown in Figure 11-3 and Figure 11-4.

In the example just discussed, the model itself had no bias, i.e., the uncertainty in the model (not the model parameters) was symmetrical about the mean. The evidence is that risk estimates of the same mission by different computer programs, and by different organizations, can vary significantly – and in the extreme as much as three orders of magnitude. The primary reasons for the wide range of results are in the varying fidelity of the models, the parameter estimates, and the structuring of the problem by individual analysts. Even considering a single program, operated by a singe user, the uncertainties in parameters and sub-models can lead to uncertainties in the E_C of between one and two orders of magnitude. In addition; always pay attention to model biases which can be very difficult to estimate in the absence of supporting empirical data.

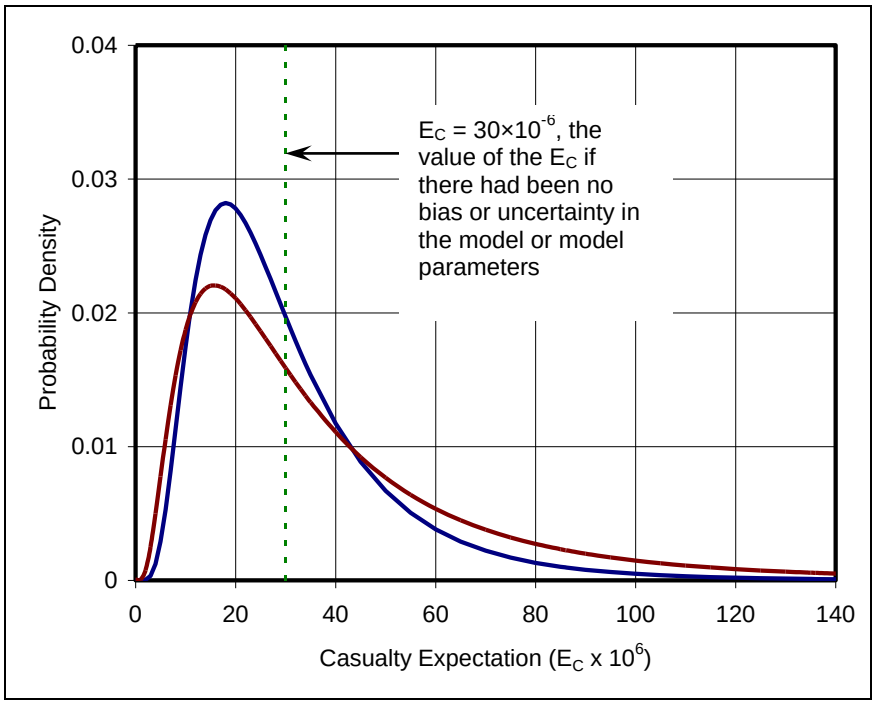

Figure 11-3. Comparison of Probability Density Functions of E_C for Cases with and without Model Uncertainty Added to the Parameter Uncertainty

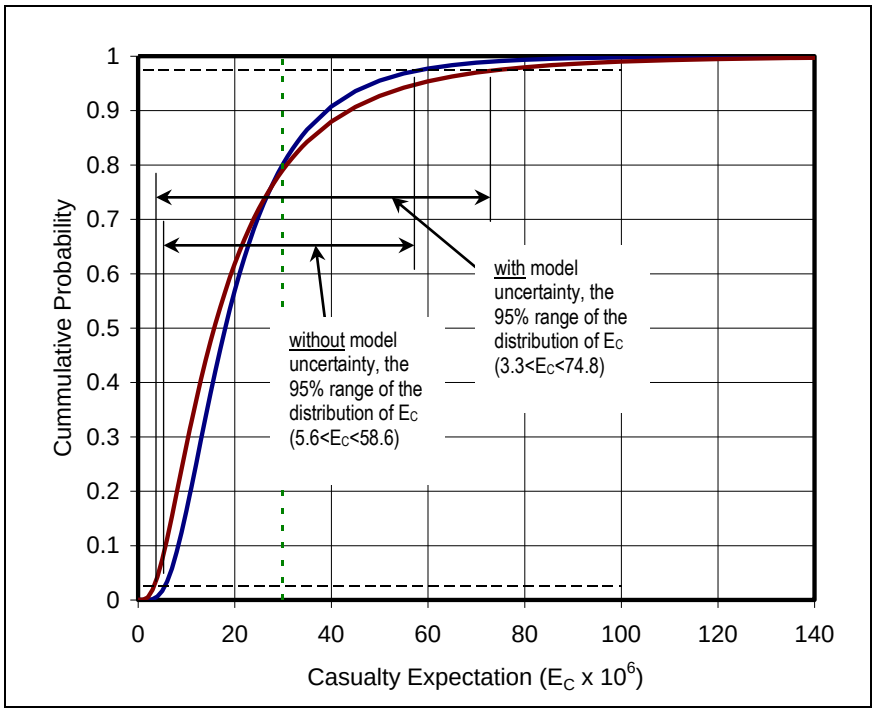

Figure 11-4. Comparison of Cumulative Probability Distributions of E_C for Cases with and without Model Uncertainty Added to the Parameter Uncertainty

There is a difference between the point estimate of E_C made by a single run of a risk analysis program and the expected average E_C resulting from averaging the results of many E_Cs from an uncertainty analysis.[22] If you use uncertainty factors (i.e., $\times f$, and $/f$), the average is always larger than the point estimate of the E_C. Consider measuring the width of the uncertainty distribution of E_C by the extent of the lower 0.025 point to the upper 0.975 point. This encompasses 95% of the distribution. In Table 11-2, the value of E_C at the upper bound, P_U is divided by the value of E_C at the lower bound to get a ratio. If there is no uncertainty, the ratio is 1. As the uncertainty gets wider, the ratio gets larger. A ratio of 100 indicates that the range from P_L (lower 0.025 point) to the P_U (upper 0.975 point) is two orders of magnitude. Next, consider the second column in the table. The corresponding value of $\frac{E_C(avg.)}{E_C(computed\ without\ uncert.)}$ is 1.99. This means that considering uncertainty (using ×factors), the point estimate of E_C computed in a standard risk analysis is one-half the value of the expected average value of E_C considering uncertainty.

Table 11-2. The Relationship Between E_C and E_C *(computed without uncertainty)* as a Function of Uncertainty

Ratio of value at P_U to the value at P_L for 95% Confidence	E_C(avg.) / E_C(computed w/o uncert.)
1	1
4	1.06
25	1.40
100	1.99
400	3.22
1000	4.72

We based this discussion on the assumption that the uncertainty distribution is lognormal, which is not necessarily the case. Hence, the ratios shown in Table 11-2 are only indicative of the ratios to be expected.

This approach, using multipliers on E_C is, at best, very approximate. First, it assumes that the multipliers apply universally, not over only a part of a flight; or for all structures uniformly, or for one class of structures, etc. Also, there is no doubt that the resulting distribution will have a central tendency, but if there is a dominating uncertainty, such as failure probability, that is not lognormal, the resulting uncertainty in E_C will not be

[22] This following discussion departs from the previous examples where both biases and uncertainties were treated. In this discussion, no biases are considered.

lognormal. Last, this approach applies very poorly to the risk profile, whose uncertainties are best represented by a collection of risk profiles that appropriately span the range of uncertainty.

In order of interest by decision makers, the highest priority is the point estimate because quantified risk acceptability limits have been defined in terms of the best point estimate. The decision maker is usually less interested in uncertainty, and even less interested in evaluating the need for a high accuracy uncertainty analysis. Thus, until risk acceptability criteria are available that include uncertainty results, the multiplier method may suffice. However, it is important to find out how far off the multiplier method may be in estimating uncertainty.

12.0 REFERENCES

[1] Murray, D., *A Tiered Approach to Flight Safety Analysis*, AIAA-2006-6499, AIAA Atmospheric Flight Mechanics Conference and Exhibit, August 2007.

[2] Risk Committee, Range Safety Group, Range Commanders Council, *Common Risk Criteria for National Test Ranges*, RCC 321-07, 2007.

[3] Federal Aviation Administration, Advisory Circular 431.35-2A, *Reusable Launch and Reentry Vehicle System Safety Process*, July 20, 2005.

[4] NASA, *Fault Tree Handbook with Aerospace Applications*, Version 1.1, August, 2002.

[5] Federal Aviation Administration, Advisory Circular 437.55-1, *Hazard Analyses for the Launch or Reentry of a Reusable Suborbital Rocket Under and Experimental Permit*, Draft March 22, 2006.

[6] Federal Aviation Administration, *Guide to Reusable Launch and Reentry Vehicle Reliability Analysis*, Version 1.0, April, 2006.

[7] Federal Aviation Administration, *Guide to Probability of Failure Analysis for New Expendable Launch Vehicles*, Version 1.0, November, 2005.

[8] NASA, *Probabilistic Risk Assessment Procedures Guide for NASA Managers and Practitioners*, Version 1.1, August, 2002.

[9] Larson, E., Stapleton, D., *Unique Considerations for Public Risk Analysis of Piloted Reusable Launch Vehicles*, AIAA-2007-6637, AIAA Atmospheric Flight Mechanics Conference and Exhibit, August 2007.

[10] NASA, *Columbia Crew Survival Investigation Report*, NASA/SP-2008-565 http://www.nasa.gov/pdf/298870main_SP-2008-565.pdf.

[11] Federal Aviation Administration, Department of Transportation, *14 CFR Parts 400, 401, 404, 405, 406, 413, 415, 431, 433, and 435 Commercial Space Transportation Reusable Launch Vehicle and Re-entry Licensing Regulations; Final Rule*, Federal Register, Vol. 65, No. 182, September 19, 2000.

[12] Columbia Accident Investigation Board (CAIB), *CAIB Report*, Vol. 2, App D.16, Government Printing Office, Washington, DC, 8/2003. (also ACTA #03-517-01)

[13] Philipson L.L. and Wilde, Paul D., *Sampling Uncertain Probabilities at Event Tree Nodes with Multiple Branches*, Journal of Reliability, Engineering, and System Safety, Vol 70, 2000, pp. 197-203.

[14] Lin, Mark Y. Y., Erik W.F. Larson and Jon D. Collins, "Determination of Debris Risk to the Public Due to the Columbia Breakup During Reentry," Report No. 03-517-01, ACTA Inc., Torrance, CA, August 2003. See also Appendix D.16 to the Columbia Accident Investigation Board Final Report, Vol. II, pp. 475-506.

[15] Futron Corporation, *Design Reliability Comparisons for SpaceX Falcon Vehicles*, November, 2004.

[16] Ward, J., *Launch and Performance Histories of US Space Launch Vehicles*, RTI/08087/008/2.5.2-01F, January, 2005.

[17] Ward, J., *Launch Vehicle Failure Probabilities for Risk Estimation*, RTI/08360/103-11F, November, 2003.

[18] Guikema S.D. and Pate-Cornell M.E., *Bayesian Analysis of Launch Vehicle Success Rates*, Journal of Spacecraft and Rockets Vol 41., No.1, 93-102, Jan-Feb 2004.

[19] Mrozinski, R., *Space Shuttle Probabilistic Risk Assessment Incorporation into Entry Public Risk Estimates*, AIAA 2005-6319, AIAA Atmospheric Flight Mechanics Conference and Exhibit, August 2005.

[20] Duffett, James R. and J. N. Thilges, "The Use of the Chance Failure Law to Evaluate Hazards on Space Vehicle Test…….," *Logistics Review and Military Logistics Journal*, Vol. 1, No. 3, 1965.

[21] "Launch Vehicle Probability of Failure Allocation," RTI International, January 2003.

[22] Wilde P., et al, "Probability of Failure Analysis: Current Approaches and Future Developments," Report No. 08-605/4.3, ACTA Inc., Houston, TX, September 2008.

[23] Klinkrad, H. et al., *On Ground Risk Assessment Software for Reentering Spacecraft*, Proceedings of the First IAASS Symposium, Nice, France, October 2005.

[24] Patera, R., *Managing Risk from Space Object Reentry*, the Aerospace Corporation 2003.

[25] Klinkrad, H. et al., *A Standardized Method for Reentry Risk Evaluation*, Proc 55th International Astronautical Congress, Vancouver, Canada, 2004.

[26] Baeker, James B., et al., *Risk Model Data Development FY96 Activities*, Report No. 96-326/89-01, ACTA Inc., Torrance, CA, September 1996.

[27] Hoerner, Sighard F., *Fluid Dynamic Drag*, Published by the Author, Midland Park, New Jersey, 1965.

[28] Wilde, Paul D. and Collins, Jon D., *Draft Revision of the Risk Analysis Advisory Circular*, Report 06-527/10.4, ACTA Inc., Torrance, CA, July 2006. Available at https://software.actainc.com/actashowreport.cgi?reportid=9465.

[29] Koppenwallner, G., "The Drag of Simple Shaped bodies in the Rarefied Hypersonic Flow Regime," AIAA-85-0998, Williamsburg, VA, 19-21 June, 1985.

[30] Montgomery and Ward, *Casualty Areas from Impacting Inert Debris for People in the Open*, RTI Report Number RTI/5180/60-31F, 13 April 1995.

[31] 31 Baeker et al, *Debris Risk Analysis Methods Development FY99 Activities*, ACTA Report 99-400/11.4-01, 30 September 1999.

[32] Kingery, C. N. and Bulmash, G., "Airblast Parameters from TNT Spherical Air Burst and Hemispherical Surface Burst," ARBRL-TR-02555, Ballistic Research Laboratory, Aberdeen Proving Ground, MD, 1984.

[33] Chrostowski J.D. and Wilde P.D., "Determination of Experimental Permit Hazard Area and Calculation of Maximum Probable Loss," Report No. 08-605/4.3, ACTA Inc., Torrance, CA, June 2008.

[34] Weals, F. H., "Titan III Solid Motor Impact Test," *Proceedings of the 6th Explosives Safety Seminar on High-Energy Solid Propellants*, Barksdale AFB, LA, 18-20 August 1964, AD456-999(64-0001) pp. 96-105.

[35] Salzman, P. K., Titan IV-SRMU Blast Risk Analysis for the Propellant Impact Risk Assessment Team (PIRAT) Titan IV-SRMU Failure Modes and Explosive Yield of Impacting Propellant, Report No. F310.PKS.98.002, TRW Strategic Systems Division, San Bernardino, CA, February 1998.

[36] Ward, J., "Implementation of Preliminary PIRAT Explosion Model, Memo for Record," dated 22 Oct 1998, Research Triangle Institute, Cocoa Beach, FL.

[37] Wilde P.D. and Anderson M, "Development of a Yield Histogram for Space Shuttle Blast Risk Analyses," *Proceedings of the 1999 JANNAF Safety and Environmental Protection Subcommittee Meeting*, San Diego.

[38] Willoughby A.B. et al, "Study of Liquid Propellant Blast Hazards," AFRPL-TR-65-144, URS Corp., Burlingame CA, June 1965.

[39] Willoughby A.B. et al, "Liquid Propellant Explosive Hazards," AFRPL-TR-68-92, Vol. 1,2,3 URS Corp., Burlingame CA, December 1968.

[40] Baeker J. et al, "Debris Risk Analysis Methods Development FY2004 Activities" ACTA Report 04-107/2.3-01, September 2004.

[41] Richmond, D.R., et al "Damage Criteria for Personnel Exposed to Repeated Blasts," Minutes of the Twentieth Explosive Safety Seminar (DDESB), August 1982.

[42] Merx, Ir. W. P. M. et al., *Methods for the Determination of Possible Damage to People and Objects from Releases of Hazardous Materials (Green Book)*, CPR 16E, Netherlands: The Netherlands Organization of Applied Scientific Research (TNO), First Edition, 1992, Chapters 2 and 3.

[43] McMunn J.C., Collins J.D., Brown B., "A Hazard Model for Exploding Solid-Propellant Rockets," J. of Spacecraft and Rockets, Vol.6, No. 12, December 1969, pp.1423-1429.

[44] Department of Defense Standard (DoD) "Ammunitions and Explosive Safety Standard 6055-9 STD," (http://www.js.pentagon.mil/whs/directives/corres/pdf/605509std.pdf) (Oct. 5, 2004).

[45] "Determination of Experimental Permit Hazard Area and Calculation of Maximum Probable Loss (Report No. 08-605/4.3)", ACTA Inc., June 2008.

[46] "Explosive Fragment Distance Research," APT Research, Inc., December 2008.

[47] Deal, Col. Duane W., *Investigation of USAF Launch Vehicle Accident, Delta II-241 / GPS IIR-1, January 1997, Cape Canaveral Air Station*, Accident Investigation Board, April 1997.

[48] Carbon, S. L. and J. D. Collins, "Real-Time Debris Footprint", *Proceedings of the JANNAF 30th Propellant Development & Characterization Subcommittee and 19th Safety and Environmental Protection Subcommittee Joint Meeting*, Colorado Springs, Colorado, 25-28 September 2001.

[49] Wilde P., "Range Safety Requirements and Methods for Unguided Suborbital Rocket Launches," 2nd IAASS Safety Conference, Chicago, IL, May 2007.

[50] Air Force Space Command Manual 91-710 Volume 2, Flight Safety Requirements.

[51] Larson, Erik. *Large Region Population Sheltering Models for Space Debris Risk Analysis.* AIAA 2005-6322, AIAA Atmospheric Flight Mechanics Conference and Exhibit, August 2005.

[52] Fudge, Michael, Sean Bain, and Erik Larson, "Population Models", submitted to FAA-AST-300, March 3, 2006.

[53] Chrostowski, Jon D. and See, A, Structure and Window Database Maintenance, ACTA Report No. 05-551/3.1, September 2005.

[54] F. Wang, O. Karatekin, J. Charbonnier, "Low-Speed Aerodynamics of a Planetary Entry Capsule", *Journal of Spacecraft and Rockets*, Vol. 36 No. 5, Sep-Oct 1999.

[55] Wilde P., et al, *Baseline Risk Analysis for Atlas V-431 Launch from Cape Canaveral*, ACTA # 06-527/9.5, Houston, TX, March 2006.

[56] Burington, Richard S. and Donald C. May, *Handbook of Probability and Statistics with Tables, 2nd Edition,"* McGraw-Hill Book Company, New York, 1970.

[57] Federal Aviation Administration, Department of Transportation, *14 CFR Parts 401, 406, 413, 415, 417 Licensing and Safety Requirements for Launch; Final Rule*, Federal Register, Vol 71, No. 165, August 25, 2006.

[58] Federal Register, Vol. 51, August 21, 1986, page 28044.

13.0 ADDITIONAL REFERENCES

[1] Federal Aviation Administration, Advisory Circular 20-128A, *Design Considerations for Minimizing Hazards Caused by Uncontained Turbine Engine and Auxiliary Power Unit Rotor Failure*, Washington, DC, March 1997. Available at http://www.airweb.faa.gov/Regulatory_and_Guidance_Library/rgAdvisoryCircular.nsf/.

[2] Federal Aviation Administration, Advisory Circular No. 39-8, *Continued Airworthiness Assessments of Powerplants and Auxiliary Power Unit Installations of Transport Category Planes*, Washington, DC, September 2003. Available at http://www.airweb.faa.gov/Regulatory_and_Guidance_Library/rgAdvisoryCircular.nsf/.

[3] American Society of Civil Engineers, *Wind Forces on Structures*, Paper 3269, Vol. 126.

[4] Baeker, James B., Jon D. Collins and Jerold M. Haber, "Launch Risk Analysis," *Journal of Spacecraft and Rockets*, Vol. 14, No. 12, December 1977, pp. 733-738.

[5] Baeker, James B., Collins, Jon D., Herndon, Mark, Larson, Erik and Philipson, Lloyd L., "Development of Flight Safety Analysis Data for RLV Launches from Harper Dry Lake," Report No. 02-463, ACTA Inc., Torrance, CA, May 2002.

[6] Bogosian, David and Brian W. Dunn, "An Analytical Model of Debris Penetration into Conventional Buildings: Hazard Area Computational Kernel (HACK), Version 1.2, TR-96-28.1, Karagozian and Case, Glendale, CA, 1996.

[7] Carbon S., and Larson E.F., *Empirical and Analytical Evaluation of ACTA Generated Fragment Impact Dispersions*, ACTA Rept. 05-527/9.1, December, 2005.

[8] Chrostowski, J.D., Wilde, P. D. and Gan, W., "Blast Damage, Serious Injury and Fatality Models for Structures," ACTA Technical Report No. 01-451/21.4-02, Revision 1, September 2002.

[9] Chrostowski, Jon D., David Bogosian, Hrire Der Avanessian and Wenshui Gan, "Methodology for Human Vulnerability Code (HuLC), Version 1.1.0," ACTA Inc., Torrance, CA, August 2004.

[10] Collins, Jon D., Moroni Jameson, Jr., and J. L. Jantz, "Real-Time Debris Patterns for Ballistic Missile launches," Journal of Spacecraft and Rockets, Vol. 13:5, May 1976.

[11] Futron Corporation, *Independent Assessment of the CSWG Proposal on Launch Vehicle Failure Probability Estimates*, April, 2003.

[12] Haber J. M. and Linn A.M., *Practical Models of Human Vulnerability to Impacting Debris*, Proceedings of the First IAASS Symposium, Nice, France, October 2005.

[13] Hasselman, Timothy K., Mark R. Legg, and Mark C. Anderson, "Casualty and Fatality Risk Models for Roof Penetration by Inert Debris." Technical Report 99-400/11.4-03, ACTA Inc., Torrance CA, September 1999.

[14] Hasselman, Timothy K. and Mark R. Legg., "Update of Casualty and Fatality Risk Models for Roof Penetration by Inert Debris," Technical Report 00-430/16.4-02, ACTA Inc., Torrance CA, September 2000.

[15] Larson E. et al., *Determination of Risk to Aircraft from Space Vehicle Debris*, Proceedings of the First IAASS Symposium, Nice, France, October 2005.

[16] Maienschein, J. L., et al, "Propellant Impact Risk Assessment Team Report: PERMS Model to Describe Propellant Energetic Response to Mechanical Stimuli," Report No. UCRL-ID-130077, Lawrence Livermore National Laboratory (Energetic Materials Section), Livermore, CA, February 1998.

[17] Marx, Michael H., "Apollo Forced Entry Debris Dispersion Study," Note No. 68-FMT-648, TRW Systems, Redondo Beach, Calif., April 1968.

[18] Nyman, Randolph L., Kenneth L. Conley, Jon D. Collins and Erik Larsen, "Titan IV B30 Over-Flight Risk Analysis," Report No. 04-531/WR01, ACTA Inc., Cape Canaveral, Florida, 27 July 04.

[19] Weaver, M et al., *Probabilistic Estimation of Reentry Debris Area*, Proc Third European Conf on Space Debris, ESOC, Darmstadt, Germany 19-21 March 2001 (ESA SP-473, October, 2001).

[20] Wilde, Paul D., and Chrostowski, Jon D, *Comparing Explosive and Inert Debris Vulnerability Model Results to Historical Event Data*, ACTA Report No. 06-527/9.2, June 2006.

[21] Haber J. et al, "Human Vulnerability to Inert Debris," Report No. 06-580/3.1-01, ACTA Inc., Torrance, CA, September 2006.

[22] Chrostowski J.D., Wilde P.D. and Gan W., "Blast Damage, Serious Injury, and Fatality Models for Structures and Windows," Report No. 00-444/16.4-03, ACTA Inc., Torrance, CA, March 2001.

[23] Chrostowski J.D., et al, "Generic Building Models for Air Blast Loading," 29th Explosives Safety Seminar, New Orleans, LA, July 18-20, 2000.

[24] Wilde P.D. and Chrostowski J.D., "Comparing Explosive Consequence Model Results to Historical Event Data," 32nd Explosives Safety Seminar, Philadelphia, PA, August 22-24, 2006.

[25] Range Commanders Council, *Common Risk Criteria for National Test Ranges*, RCC 321-07 Standard and Supplement, July 2007.

[26] Collins, Jon D., Steven L. Carbon and Jon D. Chrostowski, "Development of Quantitative Methods to Compute Maximum Probable Loss," Technical Report No. 06-527/11.6-01, ACTA Inc. Torrance, CA, December 2006.

[27] Collins, J. D., S. L. Carbon and C. P. Brinkman, "A Progress Report on Maximum Probable Loss," *Proceedings of the First IAASS Conference," 25-27 October 2005, Nice, France.*

[28] Collins, J. D., C. P. Brinkman and S. L. Carbon, Determination of Maximum Probable Loss," *Proceedings of the Second IAASS Conference," 15-17 May 2007, Chicago, Illinois.*

[29] *Means CostWorks 2004*, RS Means, Kingston, Mass, 2004.

APPENDIX A: INTEGRATED EXAMPLE

This is an example of how to compute the expected casualty for specific population centers for a nominally performing sounding rocket launched from Wallops Flight Facility in Virginia during the month of December.

A.1 Computation of a Nominal Impact Distribution

A normally performing suborbital launch vehicle is predicted to remain within the nominal impact region. The probability of impact in any location can be characterized with a statistical distribution. This, example demonstrates how a flight safety analysis can develop a nominal impact distribution for planned debris impacts.

For this example of a sounding rocket launched form Wallops Flight Facility, operators plan for the second stage and payload to impact the surface of the Earth. Figure A-1 presents 10,000 impact points computed using a 6-DOF trajectory analysis for this vehicle under normal operating conditions.

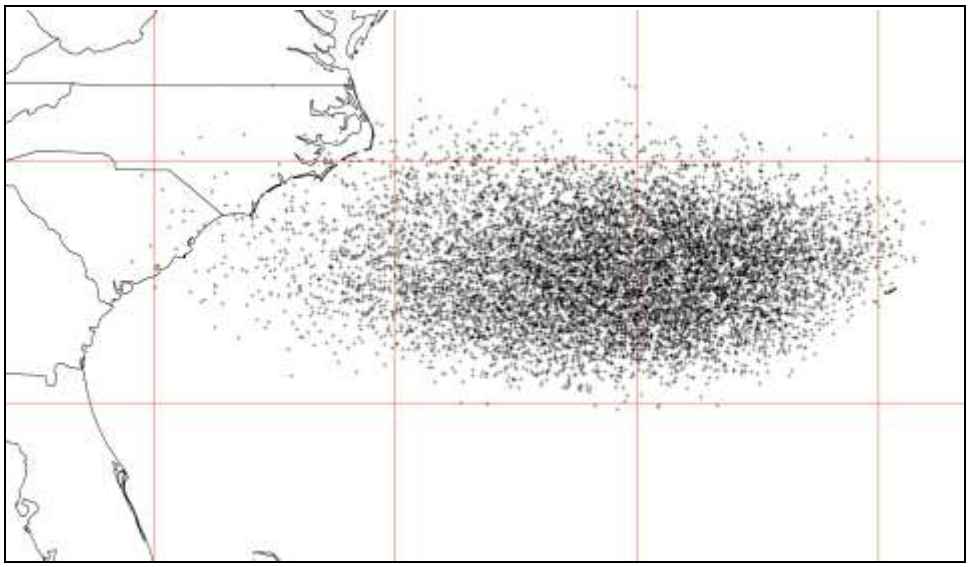

Figure A-1. Ten-thousand simulated impact points for a roll-stabilized sounding rocket launched from the Wallops Flight Facility.

The impact points identified in Figure A-1 reflect the statistical distribution described in Section A.2.

NOTE 1: 3-DOF vs. 6-DOF

Section 417.207 requires a final flight safety analysis to employ a 6-DOF model of the launch vehicle for a final analysis. As discussed earlier, a 3-DOF model may be suitable in some cases; for example, to determine conservative exclusion zones based on a set probability of containment threshold for a preliminary analysis. However, the larger dispersion associated with a 3-DOF model can result in underestimates of the probability

of impact for specific population centers, depending on their location. Therefore, the FAA will determine on a case-by-case basis if a 3-DOF trajectory analysis is valid for use as input to a QRA and provides an equivalent level of safety.

A.2 Characterize the impact dispersion as a statistical distribution

Statistical distributions are a means to characterize the outcome of random events. For example, assume wind speed in any direction (at a particular location over a given month) appears to be a random variable with an average wind speed equal 6 ft/s. If measurements of the wind speed show that 67% of the time the wind speed is between 5 ft/s and 7 ft/s, and 95% of the time the wind speed is between 4 ft/s and 8 ft/s, then you might model wind speed as a normally distributed random variable with a mean of 6 ft/s and a standard deviation of 1 ft/s.

Based on the central limit theorem, the probability of impact due to the fragments within a single debris group can often be characterized by a joint-normal (i.e., bivariate normal) distribution upon the surface of the Earth.[23] For example, you might model the probability of impact using a distribution presented in terms of longitude and latitude on a reference ellipsoid representing the non-spherical Earth. However, more generally, the probability of a fragment impact varies in two orthogonal *x* and *y*-directions that may not align with any meridian. Therefore, model the probability of a fragment impact as a function of the random variables *X* and *Y*. The joint-normal distribution density function assumes both *X* and *Y* are normally distributed (and potentially correlated) as shown in Figure A-2.

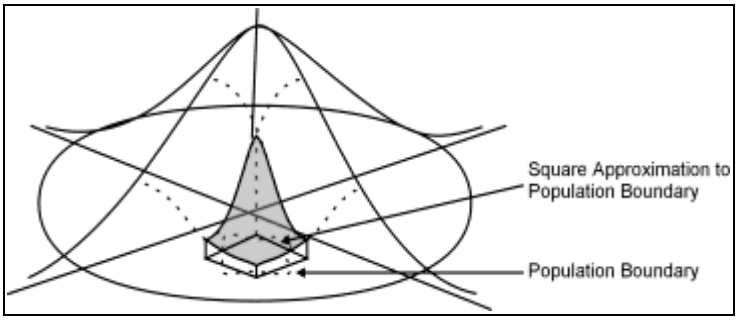

Figure A-2. Joint-normal distribution presented relative to a square population center.

Assuming a bivariate normal distribution, *x*,*y* pairs that represent random impact points can be defined as follows:

$$f(x,y) = \frac{1}{2\pi\sigma_x\sigma_y\sqrt{1-\rho^2}} e^{-\frac{G}{2}} \qquad \text{(A-1)}$$

Where *G* is defined as follows:

[23] In cases where the impact probability distribution is due to relatively few sources of dispersion, a bivariate normal impact distribution may not be a good fit.

$$G = \frac{1}{1-\rho^2}\left[\frac{(x-\mu_x)^2}{\sigma_x^2} - \frac{2\rho(x-\mu_x)(y-\mu_y)}{\sigma_x\sigma_y} + \frac{(y-\mu_y)^2}{\sigma_y^2}\right] \quad \text{(A-2)}$$

And x is the value representing the random variable X at the sampled x,y pair, μ_x and σ_x are the mean and standard deviation of all x values that the random variable X could take, and ρ is the correlation between the random variables X and Y.

The probability that an equi-probability ellipse defined by the joint-normal distribution will contain a certain percentage of x,y pairs representing the joint-normally distributed random variables X and Y is defined by the non-dimensional value c, which is equal to the square root of G. Thus, c is often used as a multiple of the standard deviation (e.g. 3-sigma, or three standard deviations from the mean) in a normal distribution to define non-dimensional bounds (or confidence levels) within which a certain percentage of outcomes will be contained. For example, Table A-1 lists non-dimensional values of sigma and c together with the probability of impacts outside the specified bounds (i.e., the probability of violation). Table A-1 shows that the probability of containment within boundaries that are 3-sigma away from the mean of a normal distribution is not the same as that within an equi-probability ellipse that is 3c from the mean x,y pair

Table A-1. Illustration of non-dimensional distances "sigma" and "c" as they related to the normal and joint-normal distributions, respectively.

Non-dimensional distance (i.e. sigma or c)	Probability of violation	
	Normal	Joint-Normal
1	0.32	0.61
2	0.05	0.14
3	2.6E-03	0.11
3.45	2.8E-04	2.6E-03
6	2.0E-09	1.5E-08

The convention in statistical analysis is to refer to a 3c ellipse as being a 3-sigma ellipse with one notable exception: in the preamble to part 431, the FAA defined a 3-sigma ellipse to be one with a probability of containment of 99.97%, which is equal to 3.45c. The 3c (i.e., conventional 3-sigma) and 3.45c ellipses for the identified impact points are presented in Figure A-3.

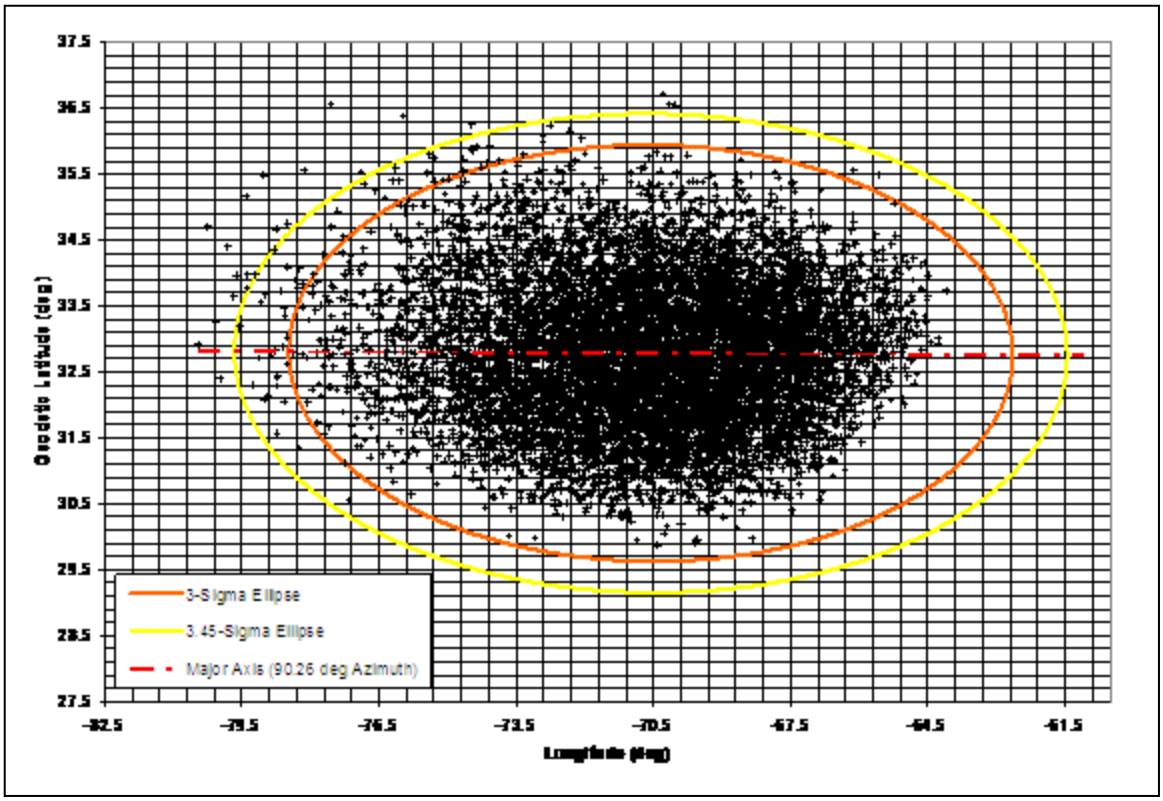

Figure A-3. The 3-sigma (i.e. 3c) and 3.45-sigma ellipses defining the simulated impact points for the examined sounding rocket assuming the impact dispersion is joint-normally distributed.

These ellipses are found by first finding the mean, standard deviation, and correlation of the latitude and longitude points representing the dispersed debris. These values are as follows:

Table A-2. Mean, standard deviation, and correlation coefficients defining the impact dispersion points, assuming they are joint-normally distributed.

	Longitude (deg)	Geodetic Latitude (deg)
Mean	-70.560	32.785
Standard Deviation	2.638	1.053
Correlation	-0.00797	

As the latitude and longitude points exhibit a slight non-zero correlation (i.e., they do not vary independently of one another), the major axis of the ellipse is not parallel to the equator. Assuming normalcy in the marginal distribution of the *Y* variable, which is a fundamental assumption of the joint-normal distribution, use a least squares fit to find the

latitude over longitude slope of the major axis. The result of this fit is a major axis whose azimuth is 90.25 degrees.

Use the orientation of the major axis to rotate the standard deviations of latitude and longitude, converted into feet from the mean impact point, to find the distance which is one-sigma along the semi-major and semi-minor axes of the equi-probability ellipse. These are found to be 808,867.2 ft and 384,210.7 ft, respectively. By making ϕ equal to the counter-clockwise rotation of the major axis, the *x* and *y* coordinates of the equi-probability ellipse centered at (*h*, *k*) can be found as a function of ϕ from the major axis given the semi-major axis length (*a*) and the semi-minor axis length (*b*) using the following equations:

$$x = h + a\cos(t)\cos(\phi) - b\sin(t)\sin(\phi) \qquad \text{(A-3)}$$

$$y = k + b\sin(t)\cos(\phi) + a\cos(t)\sin(\phi) \qquad \text{(A-4)}$$

Given these characteristics of the joint-normal distribution assumed to represent the identified debris dispersion from the normal impact case, the probability of impacting any identified population center can be found.

NOTE 2: Multiple fragments in a group

This example is for the attached second stage and payload impacting as planned. Therefore, for any given impact, there is only one debris fragment in each debris group. The previously cited probability of containment values for a given sigma level are only valid if there is only one fragment per group. If there are *N* fragments within a debris group, the probability that an equi-probability ellipse defined as a multiple of *c* is found using the following equation:

$$\Pr(containment) = \left[1 - e^{-\frac{c^2}{2}}\right]^N \qquad \text{(A-5)}$$

While this example will calculate the probability of one debris piece impacting a particular population center, Equation 12.0-5 should be used if multiple debris pieces are present within a single debris class.

NOTE 3: Skewness

Examination of Figure A-3 indicates that the identified debris impacts are not entirely joint-normally distributed. While there are only 22 impacts outside of the 3.45-sigma ellipse when 26 are allowed, these impacts are not evenly distributed outside of the probability of containment ellipse as one would expect. Instead of being evenly distributed about the identified ellipses, the density of impacts on the upper left hand corner of the plot is greater than any other quadrant. This variation in density can be characterized by the skewness of the distribution. It is important to note that, if the

highest density population centers are located in the upper left hand corner, the joint-normal distribution assumption will arrive at non-conservative risk estimates.

NOTE 4: Dispersion Reference

If the debris is so widely dispersed at the planned impact point that there is a significant variation in the distance between each longitudinal line over the relevant latitudes or significant variation in impact time for all debris within the debris group as a result of the Earth's curvature, an analyst should be careful. Ensure any analyses based on standard deviations in latitude and longitude are suitable for all fragments within the debris group. This is rarely an issue for conventional launches from ranges near the equator.

A.3 Compute the casualty area associated with impact

This example assumes the vehicle operates normally so that the second stage remains intact with the payload when impacting the surface of the earth. Therefore, the debris characteristics at each impact location are as follows:

Table A-3. Debris characteristics associated with the impacting stage.

Weight (lbs)	2,718
Projected Area (ft^2)	118
Median Ballistic Coefficient (lbs/ft^2)	275
Radius of fragment (r_F) (ft)	6.13

Given this information, the basic and secondary casualty areas can be computed with the following equation (11) from section 6.5:

$$A_c = \pi\left(r_P + r_F\sqrt{F_A}\right)^2 \qquad \text{(A-6)}$$

For all cases, the radius of a person (r_P) is assumed equal to 1 ft. The basic casualty area is found when F_A is equal to one, resulting in an area of 159.6 ft^2. From Table 6-5, the median F_A for the typical impact location is 4.36, which is based on a 20/80 mix of hard and soft ground. Using this F_A value, the secondary casualty area without elongation due to wind effects is about 600 ft^2, giving a ratio of secondary casualty area to the basic casualty of 3.75. A check of whether there will be any significant elongation of the casualty area due to direct debris impacts (i.e., whether there is a non-zero A_c') can be made using the following equation to find the minimum wind threshold, where h represents the assumed height of a standing person (6 ft):

$$v_{wind} > \frac{30 r_F\sqrt{\beta}}{h}\left(\sqrt{F_A} - 1\right) \qquad \text{(A-7)}$$

From this equation, the wind threshold that would cause a non-zero A_c' is 327 knots (552 ft/s). As this wind level is outside the typical allowable launch day wind parameters, it is safe to assume there will be no A_c' contribution to this casualty area. Therefore, the ratio of the secondary casualty area to the basic casualty area in this case remains at 3.75.

As discussed in Section 6.5, this secondary casualty area is conservative for people in the open. The effect that this impacting debris may have on people in the open or in structures should account for casualty producing events secondary to the direct impact that may be estimated using valid human and structural vulnerability models. As an example of this, the casualty areas for the four structure classes listed in Table 6-13 were determined using the weight of 2,718 lbs, the median ballistic coefficient of 275 lb/ft^2, and Figure 6-17 through Figure 6-20. The results are listed in Table A-4.

Table A-4. Casualty Area for as a Function of Sheltering Type.

Type Number	Structure Type	A_C (ft^2)
	Open	600
A	Light Metal Roof	500
B	Wood Roof	500
C	Composite Roof	500
D	Concrete/Steel Roof	500

The results indicate that sheltering can play a significant part in determining the effective casualty area of individuals in structures. For this example, any form of sheltering will provide protection. This is not always the case, as some fragments are capable of impacting with such energy that they collapse entire structures, creating a much larger casualty area than would be expected for a similar fragment impacting in the open.

A.4 Identify and characterize population centers of interest

A risk analysis should account for any population center whose exclusion would significantly affect the results of the analysis. Because a population center can vary in terms of size, density, location, and sheltering distribution, there is no simple rule of thumb for determining whether including a population center will significantly affect the resulting expected number of casualties. However, a risk analysis must account for no less than every population center within the 5-sigma debris dispersion (14 CFR A417.25(b)(2)(ii)) or 1E-12 probability of impact.

This example examines four counties across North Carolina and South Carolina and the island of Bermuda. The basic features of these counties are as follows:

Table A-5. Characteristics for Five Selected Population Centers

Population Center Name	Population	Longitude (deg)	Latitude (deg)	Area (nm^2)
Bermuda	66,163	-64.78	32.29	15.56
Brunswick County, NC	87,516	-78.23	34.00	645.47
Bladen County, NC	33,197	-78.59	34.60	660.68
Marion County, SC	34,992	-79.34	34.16	369.30
Chesterfield County, SC	43,383	-80.16	34.65	603.04

Figure A-4 identifies these population centers.

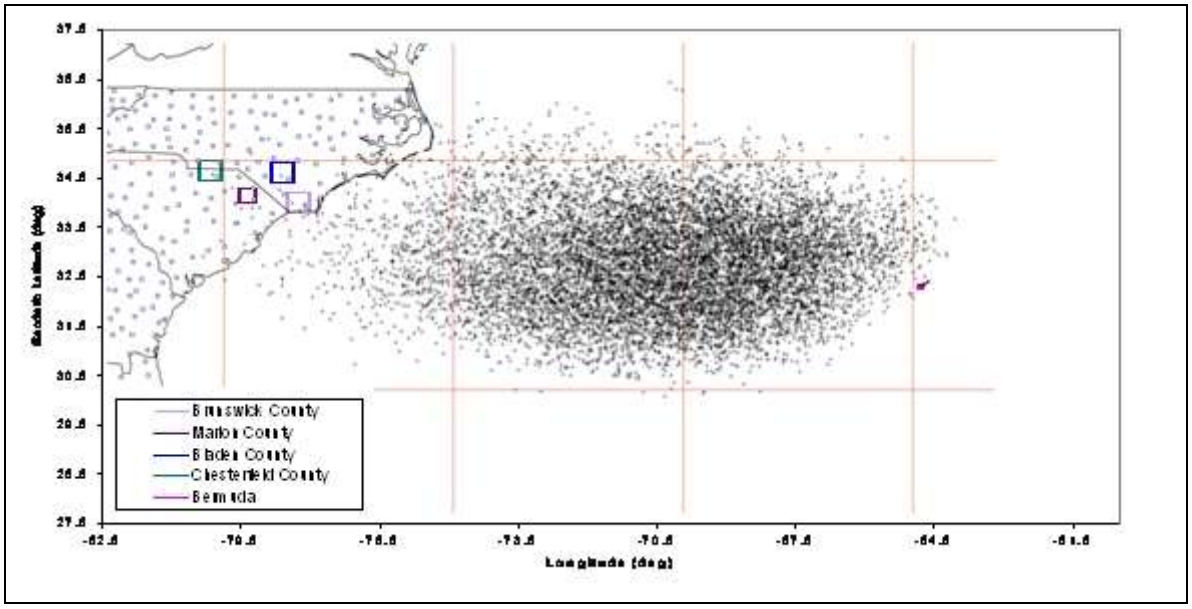

Figure A-4. Location of Five Selected Population Centers and Simulated Debris Impacts

Within these population centers, we determined the estimated distributions of sheltering type for a winter week day using population counts, demographic data, and site surveys. The site surveys provide information as to the relative number of the four types of structures present. The demographic data (e.g., ages, occupations, and incomes) provides a basis with which to assign population counts to each structure type based on the specifics of the geographical area being analyzed. As the launch is set to occur in December, expect fewer people to be outdoors (in the open) than in the summer months.

For the purposes of this example, assume the data for Bermuda to suggest that 10% of its population will be in the open, 10% will be in light metal roofed structures, 25% will be

in wood roofed structures, 15% will be in composite roofed structures, and 40% will be in concrete roofed structures. Data for the other locations provides percentages for those areas as well. The result is as follows:

Table A-6. Number of people in each population center under each type of sheltering.

Type Number	Structure Type	Bermuda	Brunswick County, NC	Bladen County, NC	Marion County, SC	Chesterfield County, SC
	Open	6,616	8,752	3,320	3,499	4,338
A	Light Metal	6,616	8,752	3,320	3,499	4,338
B	Wood	16,541	21,879	8,299	8,748	10,846
C	Composite	9,924	13,127	4,980	5,249	6,507
D	Concrete/Steel	26,465	35,006	13,279	13,997	17,353
	TOTAL	**66,163**	**87,516**	**33,197**	**34,992**	**43,383**

Using the location and area of each population center, it is possible to calculate the probability of impact.

NOTE 4: Population clustering

For each shelter type, assume the populations within each population center to be uniformly distributed. If the probability of impact within a population center varies significantly over the population center (e.g., the population center occupies a large area relative to the size of the impact probability distribution), then refine the size of the population center. Also, break out population clusters such as towns within a large regional population center out into more refined population centers. In all cases, size population centers so that the assumption of uniform population distribution remains valid.

A.5 Compute the probability of impact on each population center

Find the probability of impacting a population center by integrating the probability density function representing the debris dispersion within each debris group over the area of the population center. This is presented mathematically as follows:

$$\Pr(impact) = \int_{A_{pop}} f(x, y) dA \qquad \text{(A-8)}$$

As this integral can be difficult to solve for an irregularly sized population center, it is easier to calculate the probability of impacting a population center as the geometric probability of impacting the population center within an equi-probability ring as explained below.

Figure A-5 identifies the five examined population centers as representative squares. Each square is centered on the population center coordinates and has sides equal to the square root of the population center area.

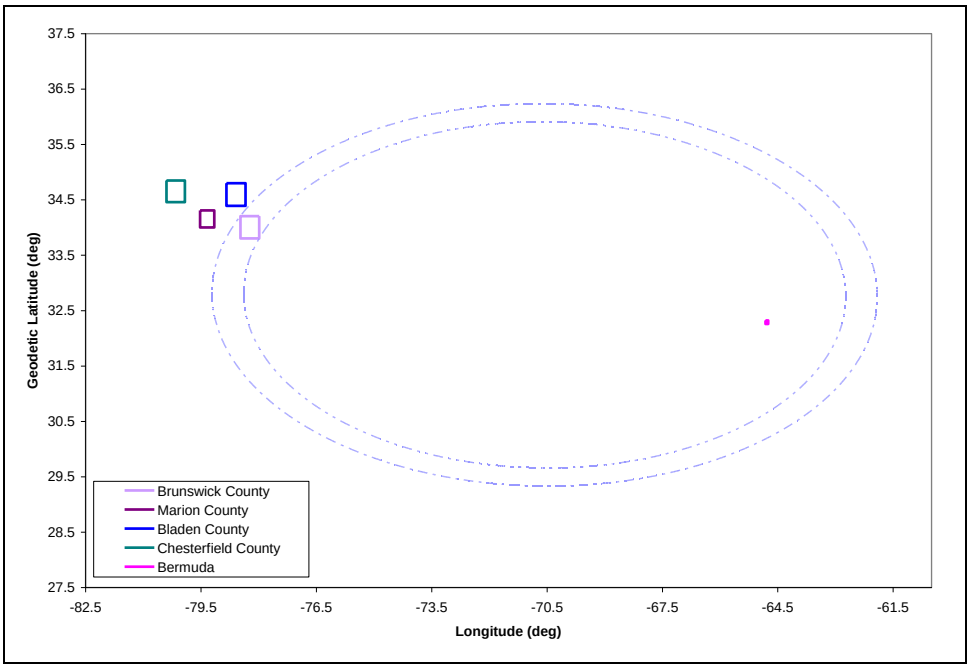

Figure A-5. Five population centers and two equi-probability ellipses for maximum and minimum corner of the Brunswick County population center.

Also identified in Figure A-5 are two equi-probability ellipses. These ellipses touch the corners of the Brunswick County population center that are nearest and farthest from the center of the ellipses. These two ellipses, defined by the values c_1 and c_2, respectively, form a ring within which the probability of impact for the single debris fragment under investigation is found as follows:

$$\Pr\left(impact_{ring}\right) = e^{-\frac{c_1^2}{2}} - e^{-\frac{c_2^2}{2}} \qquad \text{(A-9)}$$

With the probability of impacting in the ring known, the probability of the single debris piece impacting within the population center is found using the ratio of the population center area to the ring area as follows:

$$\Pr\left(impact_{pop}\right) = \frac{A_{pop}}{A_{ring}}\left(e^{-\frac{c_1^2}{2}} - e^{-\frac{c_2^2}{2}}\right) \qquad \text{(A-10)}$$

Table A-7 contains the probability of impact for each population center.

Table A-7. Population center and Impact Probability Distribution Characteristics.

Population Center Name	Area (nm^2)	Min "sigma"	Max "sigma"	Pi(pop)
Bermuda	15.56	2.22	2.26	2.21E-05
Brunswick County, NC	645.47	2.97	3.28	8.73E-05
Bladen County, NC	660.68	3.31	3.66	2.75E-05
Marion County, SC	369.30	3.45	3.68	1.14E-05
Chesterfield County, SC	603.04	3.88	4.20	3.19E-06

NOTE 6: Distance is not the only factor

It may be counter-intuitive to observe that the closest population center, Bermuda, does not exhibit the greatest probability of impact. This is because the area of the population center is directly related to the probability of impact. For example, while Brunswick County is much farther away from the nominal impact point, the probability of impacting Brunswick County is four times greater than impacting within the area representing Bermuda because the area of Bermuda is more than 40 times smaller.

NOTE 7: Multiple fragments, same concept

It is important to again note that the probability of multiple debris fragments impacting within each population center cannot be found by just using Equation 14.0-10. However, it is still valid to take the probability of containment associated with the far ellipse and subtract the probability of containment associated with the inner ellipse.

NOTE 8: Is the joint-normal best?

As identified earlier, the debris impacts are not joint-normally distributed as assumed. The impact dispersion is skewed towards the North-West quadrant. Therefore, the 6-DOF analysis results showed more simulated impacts within the examined counties than would be predicted based on the joint normal distribution. Table A-8 summarizes this.

Table A-8. Expected and Actual Number of Simulated Impacts

Population Center Name	Expected Number of Impacts	Actual Number of Impacts	Difference Between Actual and Expected Pi
Bermuda	0.221	0	-1
Brunswick County, NC	0.873	3	2.4
Bladen County, NC	0.275	2	6.3
Marion County, SC	0.114	0	-1
Chesterfield County, SC	0.032	1	30.4

The population centers to the North-West exhibit far higher number of impacts than expected if the debris were truly joint-normally distributed. For example, even though Bermuda is far closer to the ellipse center, the probability of impacting within the area defined by Bermuda is just less than that of impacting within Bladen County, NC. However, there are 2 out of 10,000 impacts within Bladen County and none within the area of Bermuda. As identified by the final column, when using only a straight ratio of the number of impacts observed over the total number of simulated trajectories to compute the actual probability of impact for each location, the actual probability of impact in this example is up to 30 times higher than that predicted with the joint-normal approximation. This example shows that skewness may be important to account for to produce valid risk results. Therefore, a flight safety analysis should evaluate the validity of any assumptions made in each case, including ones as basic as the joint-normal distribution of debris.

A.6 Compute the collective risk for all population centers

As identified previously, the expected casualty for a single shelter category population center due to a single debris class is as follows:

$$E_{C_{ij}} = P_{I_{ij}} \left(\frac{N_{P_j}}{A_{P_j}} \right) \left(N_{F_i} A_{C_i} \right) \quad (3.6\text{-}11)$$

1. P_{Iij}, the probability of impact of a piece of debris on a population center;

2. N_{Pj}/A_{Pj}, the population density in the population center; and

3. $N_{Fi} \times A_{Ci}$, the total effective casualty area of the N_{Fi} fragments in fragment category "i." A_{Ci} is the casualty area of a single fragment.

This equation is used for the data associated with Bermuda to produce the following expected casualty estimate enumerated in Table A-9. Population density for each shelter type was computed by dividing the population in each shelter type by the population center area (524,714,700 ft^2).

Table A-9. Intermediate Results for the E_C Contribution from Bermuda Population Center

Pr(Imp)	Population in each Shelter Type (#)	Pop Density (# per ft^2)	Casualty Area (ft^2)	Product of Population Density and Casualty Area
Open	6,616	1.34E-05	600	0.008
Wood Roof	16,541	2.62E-05	500	0.013
Light Metal	6,616	3.16E-06	500	0.016
Composite	9,924	4.44E-06	500	0.002
Concrete/Steel	26,465	1.03E-05	500	0.005
TOTAL	**66,163**			**0.044**

Compute an E_C value of 9.72E-07 by summing the products of the population density and casualty area in Table A-9 and multiplying by the probability of impact within the populated area (2.21E-05 for Bermuda from Table A-7). Doing this for each population center produces the estimates given in Table A-10:

Table A-10. E_C Contribution from Each of the Five Population Centers

Population Center	Expected Casualties
Bermuda	9.72E-07
Brunswick County, NC	5.27E-06
Bladen County, NC	6.39E-07
Marion County, SC	2.86E-07
Chesterfield County, SC	9.90E-08

With just these five population centers, the expected number of casualties for a nominal flight of this sounding rocket mission is over 7 in a million, based on a joint-normal impact distribution. Accounting for the fact that the probability of impact could be as much as four times higher for the population centers in the North-West due to skewness

in the simulated impacts, result in a potential aggregate E_C over these same population centers of about 26 in a million. This example demonstrates the potential importance of accurate nominal impact distributions, as noted in previously published documents. [49]

NOTE: Probability of failure

In this case, assume the probability of impact for each planned impact to be one since safety should be assured if the mission is successful. If the E_C contribution is due to a malfunction, multiply the computations above by the probability of the malfunction occurring.